



Services du Premier Ministre  
Programmation de la Politique scientifique  
Rue de la Science 8  
1040 BRUXELLES  
BELGIQUE



Diensten van de Eerste Minister  
Programmatie van het Wetenschapsbeleid  
Wetenschapsstraat 8  
1040 BRUSSEL  
BELGIE

**ACTIONS DE  
RECHERCHE CONCERTÉES**

**GECONCERTEERDE  
ONDERZOEKSACTIES**

**ACTION INTERUNIVERSITAIRE**

**INTERUNIVERSITAIRE ACTIE**

**OCEANOLOGIE**

**OCEANOLOGIE**

Rapport final

Eindverslag

Volume 1

Boekdeel 1

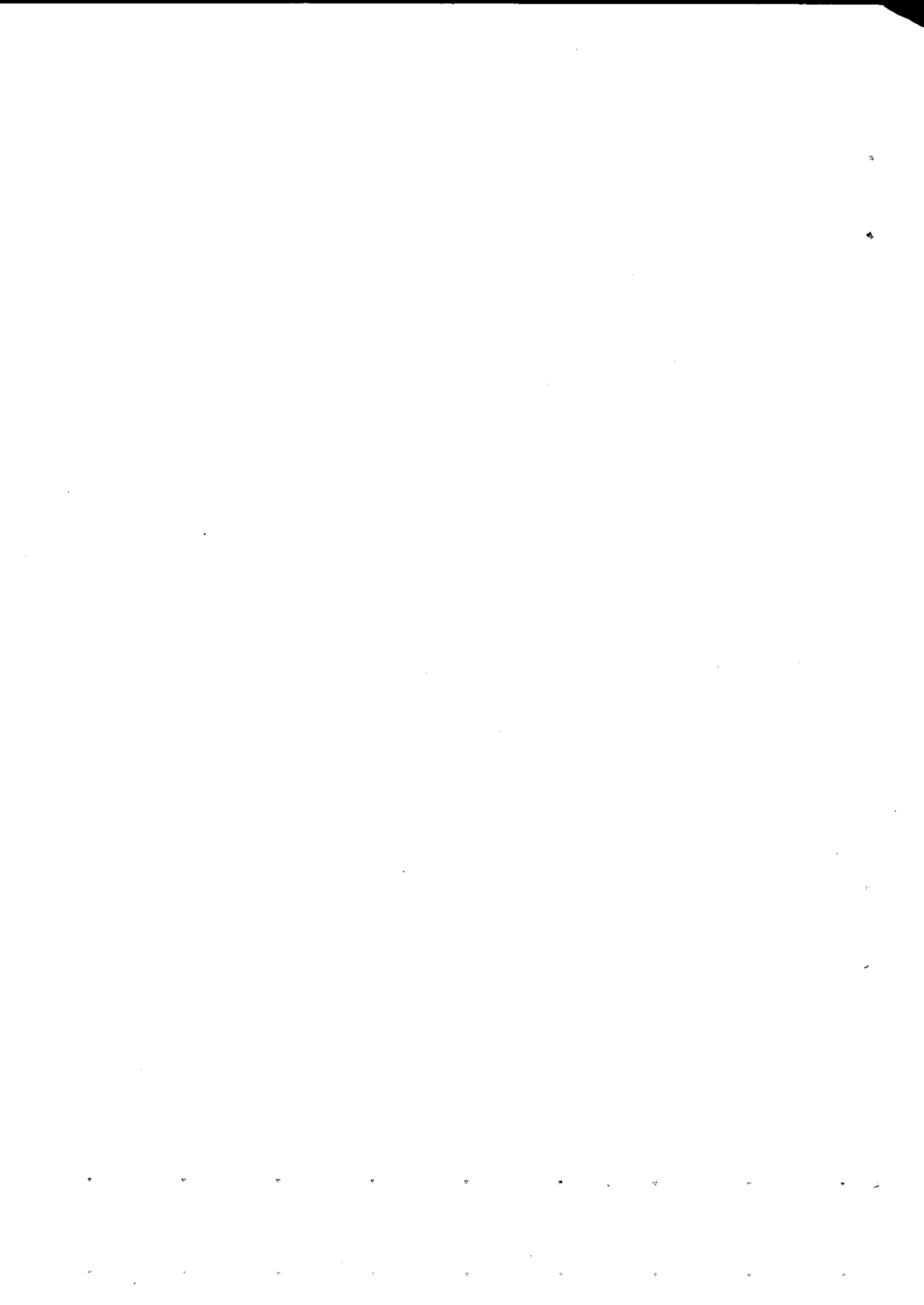
**HYDRODYNAMIC AND DISPERSION MODELS  
BOUNDARY FLUXES AND BOUNDARY CONDITIONS**


edited by  
J.C.J. NIHOUL and R. WOLLAST




**HYDRODYNAMIC AND DISPERSION MODELS  
BOUNDARY FLUXES AND BOUNDARY CONDITIONS**

edited by  
J.C.J. NIHOUL and R. WOLLAST





Services du Premier Ministre  
Programmation de la Politique scientifique  
Rue de la Science 8  
1040 BRUXELLES  
BELGIQUE



Diensten van de Eerste Minister  
Programmatie van het Wetenschapsbeleid  
Wetenschapsstraat 8  
1040 BRUSSEL  
BELGIE

**ACTIONS DE  
RECHERCHE CONCERTÉES**

**GECONCERTEERDE  
ONDERZOEKSACTIES**

**ACTION INTERUNIVERSITAIRE**

**INTERUNIVERSITAIRE ACTIE**

**OCEANOLOGIE**

**OCEANOLOGIE**

Rapport final

Eindverslag

Volume 1

Boekdeel 1

**HYDRODYNAMIC AND DISPERSION MODELS  
BOUNDARY FLUXES AND BOUNDARY CONDITIONS**

edited by  
J.C.J. NIHOUL and R. WOLLAST

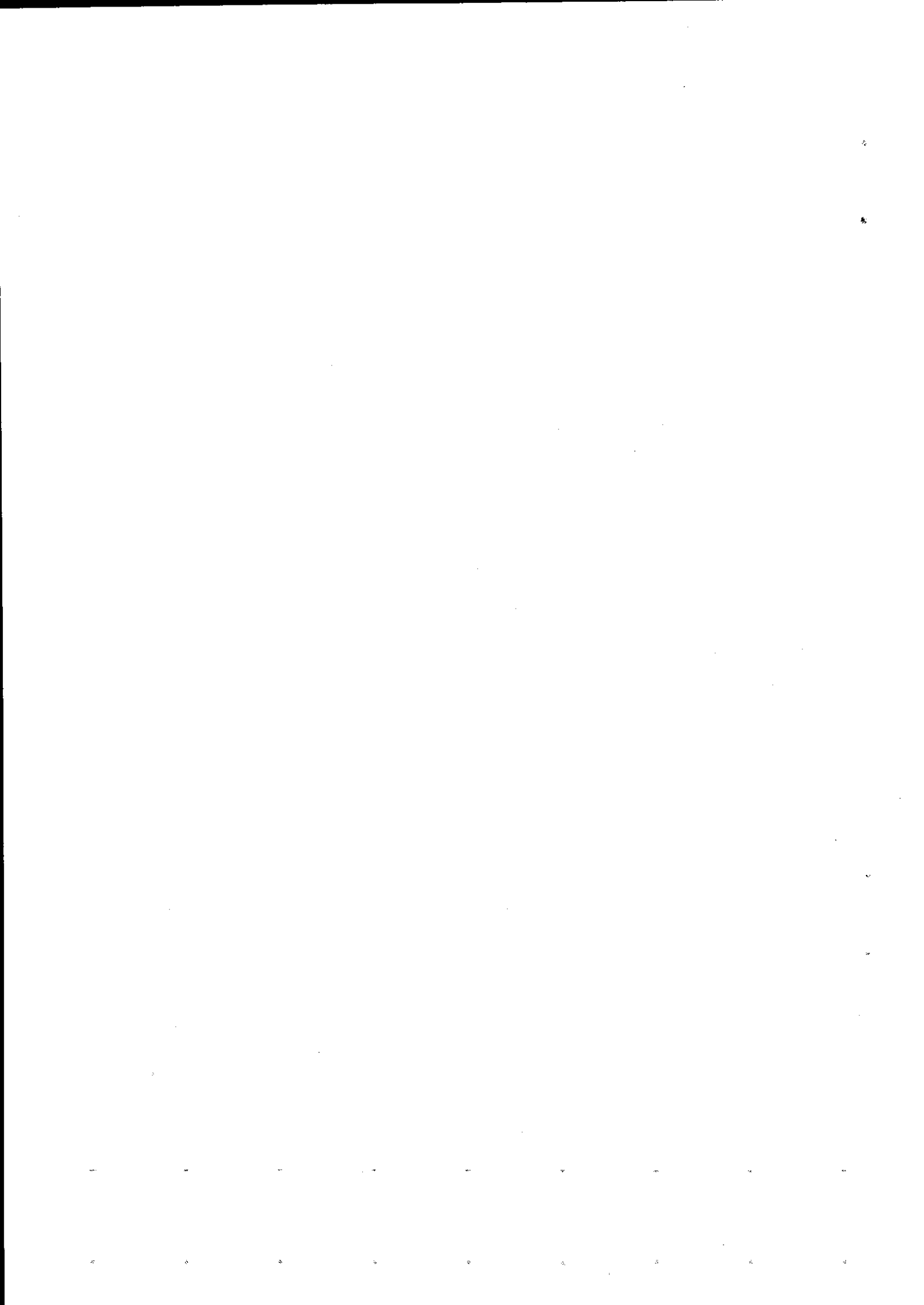
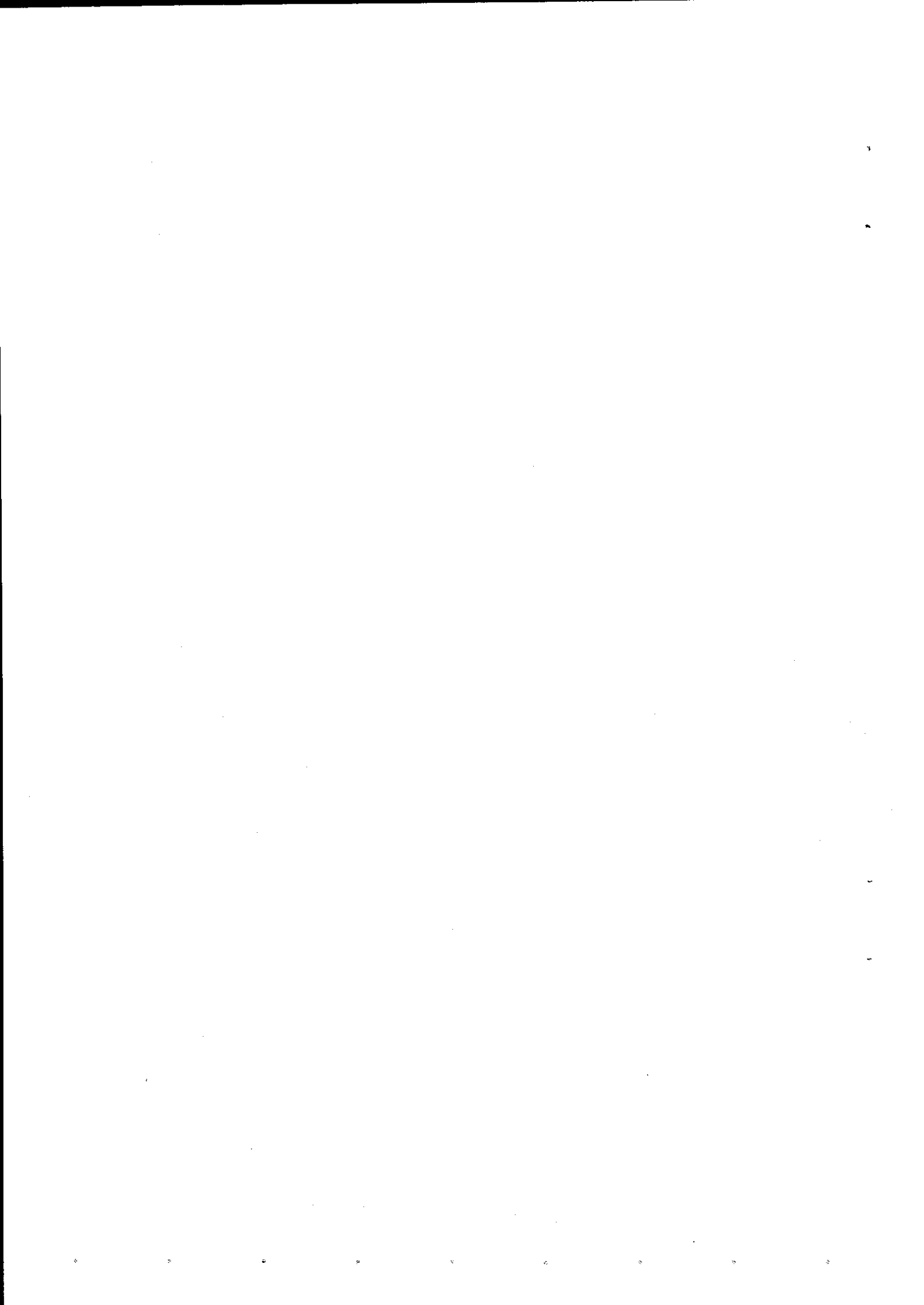


## TABLE OF CONTENTS

Hydrodynamic models of shallow continental seas .....	7
Jacques C.J. Nihoul	
Behaviour of organic carbon, nitrogen and phosphorous in the Scheldt estuary and the adjacent coastal zone .....	199
Roland Wollast	
Boundary conditions for heavy metals at the air-sea interface .....	223
F. Dehairs, H. Dedeurwaerder, M. Dejonghe, G. Decadt, G. Gillain, W. Baeyens and I. Elskens	
Mathematical modelling for evaluating water quality of aquatic environments .....	243
Martine Somville	





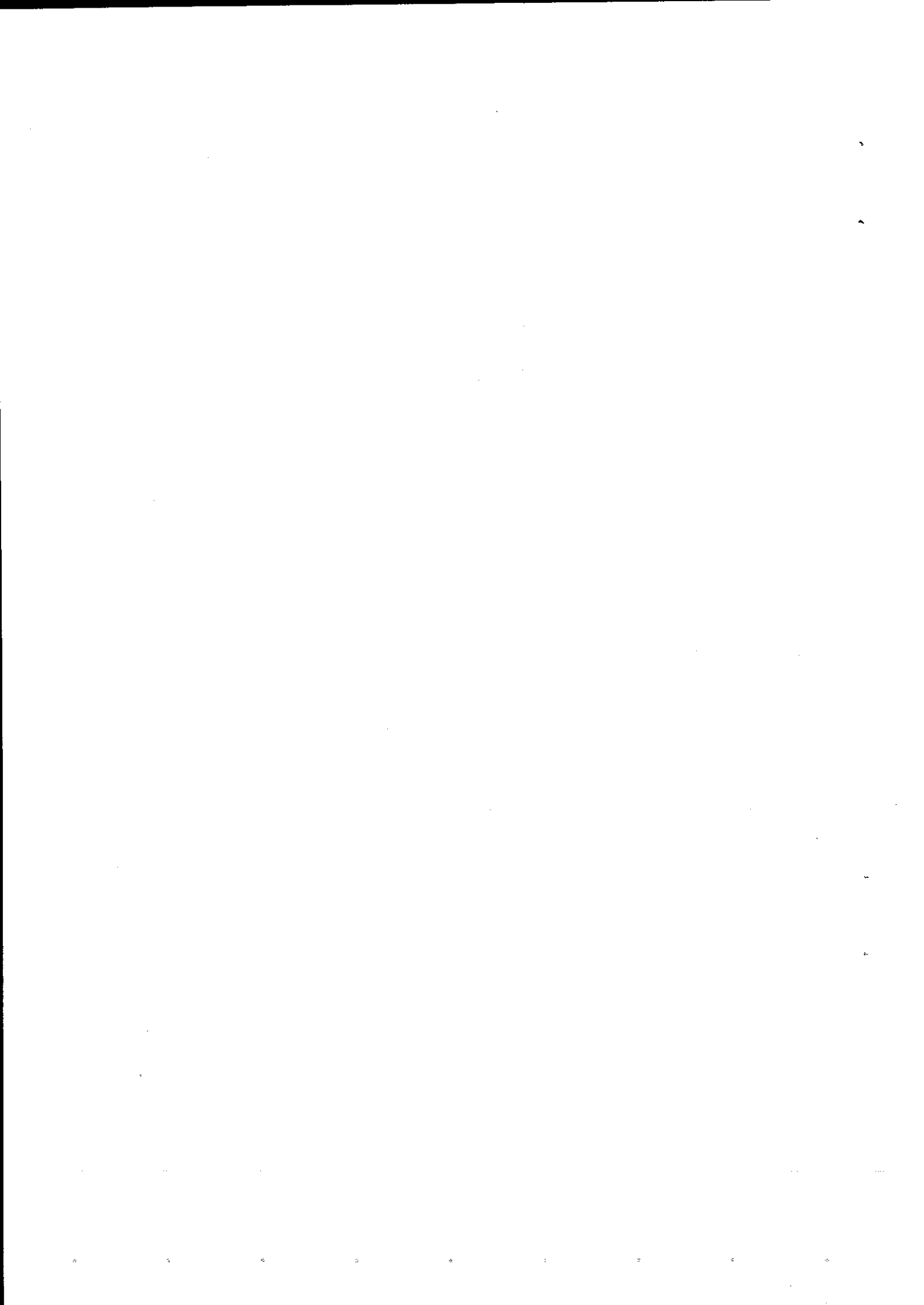
**HYDRODYNAMIC MODELS  
OF SHALLOW CONTINENTAL SEAS**

**Application to the North Sea**

Jacques C.J. NIHOUL

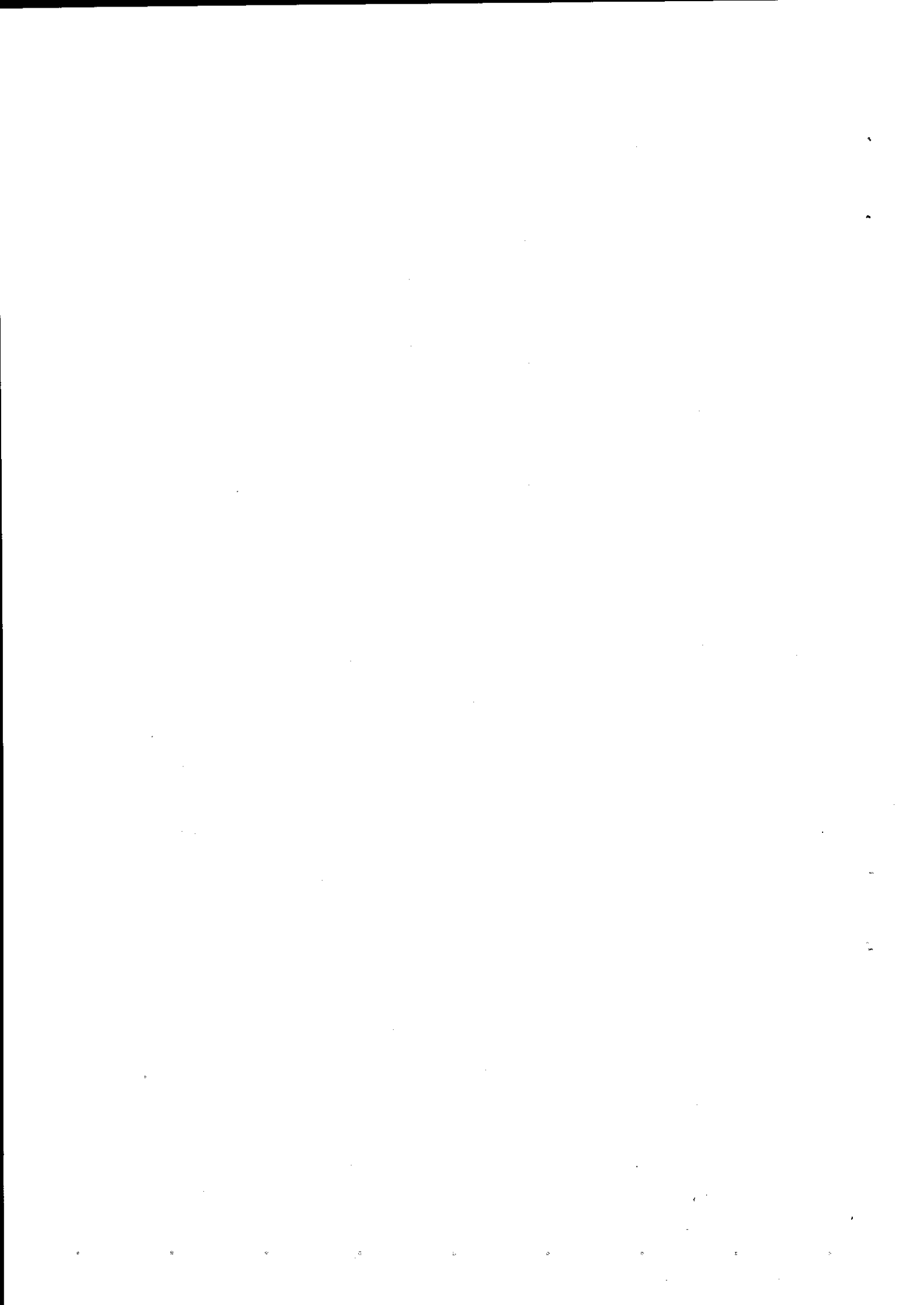
---

Université de Liège.



## SUMMARY

1.— Introduction .....	11
2.— Hydrodynamic equations .....	13
3.— Initial and boundary conditions .....	16
4.— Two-dimensional depth-averaged models .....	20
<i>Shear effect</i> .....	22
<i>Surface fluxes</i> .....	24
<i>Depth-averaged equations</i> .....	25
5.— Two-dimensional models of tides and storm surges .....	26
6.— A comparison between two-dimensional models of tides and storm surges in the North Sea .....	35
<i>Model equations</i> .....	35
<i>Model boundary conditions</i> .....	38
<i>Non-linear interactions between tides and storm surges</i> .....	46
<i>Numerical techniques</i> .....	47
7.— Recent developments in two-dimensional mesoscale modelling .....	60
8.— Three-dimensional models of tides and storm surges .....	68
<i>Mesoscale three-dimensional hydrodynamic equations</i> .....	70
<i>Depth-integrated and multi-layer models</i> .....	71
<i>Vertical shear models</i> .....	72
<i>Analytical models</i> .....	73
<i>Multi-mode models</i> .....	74
<i>Variable eddy viscosity multi-mode model</i> .....	75
9.— Three-dimensional (2D + 1D) model of tides and storm surges in a well-mixed shallow sea .....	77
<i>Locally one-dimensional model of the vertical variations of the horizontal current</i> .....	81
<i>Vertical profile of the horizontal current</i> .....	82
<i>Application of the model to the North Sea</i> .....	85
10.— Non-linear three-dimensional model of tides and storm surges in a well-mixed continental sea .....	91
11.— Three-dimensional and two-dimensional models of the residual circulation .....	102
<i>The governing equations</i> .....	105
<i>The mesoscale Reynolds stress tensor</i> .....	108
<i>The equation for the horizontal transport</i> .....	109
12.— Energy transfers between residual flows and mesoscale motions .....	117
<i>The contribution of the residual stress <math>\tau_0</math> to the energy budget</i> .....	118
<i>The exchange of energy between scales of motion</i> .....	121
13.— Application of the residual model to the North Sea .....	123
<i>Tidal residuals</i> .....	123
<i>Wind residuals</i> .....	134
14.— Three-dimensional dispersion models for passive constituents .....	154
15.— Two-dimensional models of horizontal dispersion .....	161
16.— Depth-integrated models of horizontal dispersion .....	169
<i>Parameterization of the shear effect</i> .....	170
<i>Application to the North Sea</i> .....	173
<i>Vertical concentration profile</i> .....	176
<i>Influence of the wind on the shear effect diffusivity tensor</i> .....	178
<i>A case study: dispersion and sedimentation around a waste disposal point in the Southern Bight of the North Sea</i> .....	187
References .....	191



## 1.- Introduction.

Marine hydrodynamics is obviously an important subject by itself. Prediction of storm surges and tides, surface elevation, current patterns are all essential factors of navigation, fishing, coastal engineering, etc.

In addition, the whole dynamics of the marine system is driven by the sea motion. Dispersion of nutrients or pollutants, migrations, sedimentation and bottom erosion are conditioned by the mixing and circulation of the water masses. The determination of the velocity field and the associated turbulence is the first step in any effort to model a marine system.

From the point of view of modelling, hydrodynamic processes, in a shallow continental sea like the North Sea, can be separated in three main categories according to their time scales.

*Macroscale* processes are represented by the "quasi-steady" residual circulation (time scale : from weeks to months) and the associated frontal structures; *mesoscale* processes comprise tides, storm surges and wind-induced currents (time scale : from hours to days); *microscale* processes comprehend all scales of random motions composing three-dimensional turbulence (time scale : from seconds to minutes).

The study of turbulent fluctuations is not the primary objective of hydrodynamic models, concerned with *organized* circulations at macroscales and mesoscales. (The detailed description of the random turbulent velocity field would, in any case, be beyond any model's capacity.) The state variables of the hydrodynamic models are then not the instantaneous erratic velocity, pressure, temperature, ... but their mean values over a time  $T$  sufficiently large for microscale fluctuations and oscillations to roughly cancel over a time of that order, but sufficiently small for mesoscale and macroscale processes to "pass through" the averaging unaffected.

The hydrodynamic equations describing the "mean" variables are then obtained by averaging over the chosen time  $T$  ( $T \sim 10^3$  s, say) the basic equations of Fluid Mechanics. Since, these equations are non-linear, microscale fluctuations are not entirely eliminated by the averaging. Non-linear terms give two contributions, one containing the product of the means and the other one the mean product of the fluctuations.

The extra terms in the evolution equations can be parameterized on the model of the molecular diffusion terms.

Microscale fluctuations appear indeed to play qualitatively the same role as molecular fluctuations. They contribute to a "turbulent" or "eddy" diffusion analogous to molecular diffusion but many times more efficient.

The eddy diffusion coefficients can be determined (eventually parameterized in terms of characteristics of the mean flow) using classical results of turbulence theory.

In shallow continental seas like the North Sea, the eddy coefficients are found several orders of magnitude larger than their molecular counterparts and one generally neglects the molecular effects, considering that they are implicitly included in the turbulence.

The equations governing mesoscale and macroscale flows have then the same form as the original Fluid Mechanics equations with, simply, molecular diffusivities replaced by turbulent ones.

One emphasizes here that the basic equations describe the large scale flow; a superposition of macroscale and mesoscale motions. With appropriate boundary conditions, the solution represents the sum of macroscale and mesoscale processes, characterized, as pointed out before, by distinct time scales. In principle, the residual (macroscale) circulation could be obtained from this solution by a second time average; the averaging period  $T$  being now chosen to filter out mesoscale oscillations and leave quasi-steady macroscale flows essentially unperturbed.

A problem arises here from the completely different orders of magnitude of the two types of flow. While the currents associated with tides and storm surges may reach velocities of more than  $1 \text{ m s}^{-1}$  in shallow continental seas like the North Sea, the residual circulation is often only of the order of a few  $\text{cm s}^{-1}$  and actually of the same order as the error the model makes on the total (macroscale + mesoscale) flow.

The errors being non-linear, one cannot expect them to cancel in the averaging process, the result of which could be a residual flow obtained with a 100 % error.

It has been shown that this difficulty can be avoided if, instead of averaging the *solution*, one derives average *equations* and solve them for the residual flow, taking explicitly into account the additional forcing due to the non-linear interactions of mesoscale motions, the so-called "*mesoscale Reynolds stress*" (e.g. Nihoul, 1975a, 1980; Nihoul and Ronday, 1975, 1976; Nihoul and Runfola, 1981).

Hydrodynamic models divide then into two sub-sets : (i) long-wave models for tides and storm surges, (ii) quasi-steady state models for the residual circulation.

In both cases, two different approaches have been used : (i) depth-integrated two-dimensional models predicting the surface elevation and the depth-mean velocity vector and (ii) three-dimensional models taking into account the variations along the vertical of such parameters as the eddy diffusivities, ...

In the following, the techniques of two-dimensional and three-dimensional models of marine hydrodynamics are presented and discussed. Taking the North Sea as an illustrative case study, existing models are compared, emphasizing the different approximations made in each case and the corresponding forecasting efficiency.

## 2.- Hydrodynamic equations.

Restricting attention to well-mixed continental seas, for which the specific mass of sea water  $\rho$  can be considered as a constant\*, one can write the hydrodynamic equations in the form (e.g. Nihoul, 1975a, 1976, 1977a) :

$$(1) \quad \nabla \cdot \mathbf{v} = 0$$

$$(2) \quad \frac{\partial \mathbf{v}}{\partial t} + \nabla \cdot (\mathbf{v}\mathbf{v}) + 2 \boldsymbol{\Omega} \wedge \mathbf{v} = - \nabla q + \nabla \cdot \mathcal{R}$$

where  $\mathbf{v}$  is the velocity vector,  $\boldsymbol{\Omega}$  the earth's rotation vector,

$$q = \frac{p}{\rho} + gx_3 + \xi ,$$

$p$  is the pressure,  $\rho$  the specific mass of sea water,  $x_3$  the vertical coordinate (the  $x_3$ -axis pointing upwards),  $\xi$  the tidal potential and  $\mathcal{R}$  the Reynolds stress tensor (the stress is here per unit mass of sea water) resulting from the non-linear interactions of three-dimensional turbulent fluctuations and implicitly including the "negligible" viscous stress tensor.

The equation for the concentration of a "passive constituent" (i.e. a constituent which does not interact with others and is simply carried along by sea movements of all scales) can be written

$$(3) \quad \frac{\partial c}{\partial t} + \nabla \cdot (\mathbf{v}c) = Q + \nabla \cdot \boldsymbol{\gamma}$$

where  $Q$  is the rate of production (or destruction) of the constituent and  $\boldsymbol{\gamma}$  the turbulent flux.

Temperature and salinity obey an equation of type (3).

The tidal potential can be neglected in the case of continental seas where the main tidal oscillations are not directly produced by astronomical forces but result from ocean waves propagating into the seas through the open-sea boundaries (e.g. Nihoul, 1975a).

---

\* The extension to stratified waters can be made easily in the scope of Boussinesq's approximation (e.g. Nihoul, 1977a). This aspect will be reexamined later in relation with three-dimensional modelling.

The Reynolds stress tensor  $\mathcal{R}$  and the turbulent flux  $\mathbf{y}$  can be parameterized in terms of eddy diffusivity coefficients. In microscale three-dimensional turbulence, these coefficients are of the same order of magnitude in the horizontal and vertical directions. Then, horizontal length scales being much larger than the depth, the last terms in the right-hand sides of eqs (2) and (3) can be written simply, with a good approximation

$$(4) \quad \nabla \cdot \mathcal{R} = \frac{\partial \boldsymbol{\tau}}{\partial x_3} = \frac{\partial}{\partial x_3} \left( \tilde{\nu} \frac{\partial \mathbf{v}}{\partial x_3} \right)$$

$$(5) \quad \nabla \cdot \mathbf{y} = \frac{\partial}{\partial x_3} \left( \tilde{\lambda} \frac{\partial c}{\partial x_3} \right)$$

where  $\boldsymbol{\tau}$  is the Reynolds stress vector,  $\tilde{\nu}$  the eddy viscosity and  $\tilde{\lambda}$  the eddy diffusivity.

Neglecting horizontal turbulent (and molecular) diffusion makes advection the essential mechanism in the horizontal plane. This does not exclude horizontal *dispersion* since the velocity  $\mathbf{v}$  in eqs (2) and (3) still contains variable, irregular currents which will act on a patch of contaminant in more or less the same way as three-dimensional fluctuations at smaller scales (e.g. Nihoul, 1976, 1977a).

The vertical component of eq. (2) can be written, using eq.

(4)

$$\frac{\partial v_3}{\partial t} + \nabla \cdot (\mathbf{v} v_3) + 2(\Omega_1 v_2 - \Omega_2 v_1) - \frac{\partial}{\partial x_3} \left( \tilde{\nu} \frac{\partial v_3}{\partial x_3} \right)$$

(6)

$$= - \frac{\partial q}{\partial x_3} = - \frac{\partial}{\partial x_3} \left( \frac{p}{\rho} + g x_3 \right)$$

All terms in the left-hand side of eq. (6) are very small compared to the acceleration of gravity  $g \sim 10 \text{ m s}^{-2}$ . If we take, for instance, the example of tidal motion in the North Sea, one has typically (e.g. Nihoul, 1975a) :

$$v_3 \sim 10^{-4} \text{ m s}^{-1}$$

$$\frac{\partial v_3}{\partial t} \sim 10^{-8} \text{ m s}^{-2}$$

$$v_1 \sim v_2 \sim 1 \text{ m s}^{-1}$$

$$\nabla \cdot (\mathbf{v} v_3) \sim 10^{-9} \text{ m s}^{-2}$$

$$2 \Omega_1 \sim 2 \Omega_2 \sim 10^{-4} \text{ s}^{-1}$$

$$2(\Omega_1 v_2 - \Omega_2 v_1) \sim 10^{-4} \text{ m s}^{-2}$$

$$\tilde{\nu} \sim 10^{-1} \text{ m}^2 \text{ s}^{-1}$$

$$\frac{\partial}{\partial x_3} \left( \tilde{\nu} \frac{\partial v_3}{\partial x_3} \right) \sim 10^{-8} \text{ m s}^{-2}$$



One can thus neglect the left-hand side of eq. (6) and write, with a good approximation

$$(7) \quad \frac{\partial q}{\partial x_3} = \frac{\partial}{\partial x_3} \left( \frac{p}{\rho} + gx_3 \right) = 0$$

At equilibrium, eq. (2) reduces to the hydrostatic balance of force

$$(8) \quad \nabla q = 0$$

Eq. (7) shows that, in a dynamic situation, the hydrostatic balance of force remains valid in the vertical direction. This is the so-called "quasi-hydrostatic approximation".

Integrating eq. (7) over  $x_3$ , one obtains

$$(9) \quad p = -\rho gx_3 + f(t, x_1, x_2)$$

At the free-surface,  $x_3 = \zeta$ , the pressure must be equal to the atmospheric pressure  $p_a$ . Hence

$$(10) \quad p_a = -\rho g\zeta + f$$

This determines the so-far arbitrary function  $f$ . Combining eqs (9) and (10), one gets

$$(11) \quad q = \frac{p_a}{\rho} + g\zeta$$

The horizontal components of the Coriolis acceleration are

$$\begin{aligned} & 2 \Omega_2 v_3 - 2 \Omega_3 v_2 \\ & - 2 \Omega_1 v_3 + 2 \Omega_3 v_1 \end{aligned}$$

In mid-latitude continental seas, the first terms, proportional to the vertical velocity, may be neglected. Setting

$$2 \Omega_3 = f,$$

to conform to usual notations, the Coriolis acceleration can be written

$$(12) \quad -fv_2 \mathbf{e}_1 + fv_1 \mathbf{e}_2 = f \mathbf{e}_3 \wedge \mathbf{v}$$

taking into account that the vertical component has previously been found negligible.

If, from now on,  $\mathbf{u}$  denotes the horizontal velocity vector

$$(\mathbf{v} = \mathbf{u} + v_3 \mathbf{e}_3),$$

the basic hydrodynamic equations can be written, using eqs (1), (2), (4), (11) and (12)

$$(13) \quad \frac{\partial \mathbf{u}}{\partial t} + \nabla \cdot (\mathbf{u}\mathbf{u}) + f \mathbf{e}_3 \wedge \mathbf{u} + \frac{\partial}{\partial x_3} (\mathbf{u} v_3) = - \nabla \left( \frac{p_a}{\rho} + g\zeta \right) + \frac{\partial}{\partial x_3} \left( \tilde{v} \frac{\partial \mathbf{u}}{\partial x_3} \right)$$

$$(14) \quad \nabla \cdot \mathbf{u} + \frac{\partial v_3}{\partial x_3} = 0$$

The evolution equation of a passive constituent becomes, combining eqs (3) and (5)

$$(15) \quad \frac{\partial c}{\partial t} + \nabla \cdot (\mathbf{u} c) + \frac{\partial}{\partial x_3} (v_3 c) = \frac{\partial}{\partial x_3} \left( \tilde{\lambda} \frac{\partial c}{\partial x_3} \right) + Q$$

This equation holds also for temperature and salinity with the appropriate values of  $Q$  and  $\tilde{\lambda}$ .

### 3.- Initial and boundary conditions.

The hydrodynamic equations must be solved subject to given initial and boundary conditions.

Major problems are :

- (i) the reliability of data given at open-sea boundaries,
- (ii) the formulation of boundary conditions at the bottom and at the air-sea interface.

The specification of boundary conditions at the air-sea interface and at the sea floor illustrates a typical difficulty of modelling.

As mentioned before, models deal with mean variables (over some characteristic time of interest) and summarize the non-linear effects of the fluctuations in suitably defined "dispersion terms" where several control parameters are introduced. Obviously, the demarcation of the system and, in particular, the definition of its support must conform to this simplification, and the boundaries delimiting the system for a given model are idealized boundaries where most of the intricacy of the real frontiers have been smoothed out by the averaging.

Thus, if  $x_3 = \zeta$  and  $x_3 = -h$  are the equations of the air-sea interface and the bottom, respectively, one has

$$(16) \quad \frac{\partial \zeta}{\partial t} + \mathbf{u} \cdot \nabla \zeta = v_3 \quad \text{at} \quad x_3 = \zeta$$

$$(17) \quad \frac{\partial h}{\partial t} + \mathbf{u} \cdot \nabla h = -v_3 \quad \text{at} \quad x_3 = -h$$

Eqs (16) and (17) express that the "model" boundaries are material surfaces of an idealized fluid moving with the mean velocity

$$\mathbf{v} = \mathbf{u} + v_3 \mathbf{e}_3$$

They thus differ from the complicated real frontiers which are jagged material surfaces following the real stirring velocity.

(A particular inference is that problems with different time scales require different model boundaries as, for example, "surface elevation" has a different meaning in tidal models and in residual current models.)

Schematically, one might say that each model has its particular conception of the sea surface and of the bottom. Interpreting in mathematical terms the interactions at the sea boundaries is a difficult task. It is complicated, in modelling, by the obligation to comply with the model's refinement and formulate the boundary conditions with just the right degree of sophistication.

A few examples may serve to illustrate the difficulty.

Waves at the sea surface create a first problem. They influence the instantaneous local wind and the subsequent air-sea interactions but they are themselves (their speed, form and height) function of the wind stress *in the past*. Waves break frequently as a result of interactions between waves of different wave numbers. Wave breaking, which can occur at low wind speed, is more frequent and efficient under strong wind conditions. In the process, spray is produced.

Depending on the relative velocities of wind and waves, the disruption of wave crests into spindrifts can also produce spray. [At winds above 8 m/s, there is apparently a sudden increase in the spray load which could be attributed to this mechanism (Krauss, 1967).] Bubbles of air are entrained by the breaking waves. When bubbles burst on reaching the surface, drops are ejected into the air.

An irregular mixing of air and water results on both sides of a jagged interface which one finds difficult to position practically within a complicated zone of transition between the atmosphere and the sea.

The situation is similar at the bottom. Sea water contains suspended sediments. Whether the mean turbidity is low (open sea) or high (coastal area), there is inevitably a marked increase in the concentration of sediments as one approaches the sea floor which itself can be permeated with water to some depth. It is almost impossible to draw a line through the solid-water mixture at the bottom of the sea and the so-called bottom boundary is often nothing more than a conventional limit corresponding to

some chosen concentration of the sediments. Moreover, the shear stress exerted by the sea on the bottom may recirculate deposited sediments and erode the sea floor.

Blowing sand (like flying spray at the air-sea boundary) contributes to shade off the border between sea and soil.

A further difficulty, in specifying boundary conditions at the sea surface, occurs evidently when some alien substance is interposed between air and water. Organic surface-active films are frequently formed on the sea surface. Damping capillary waves, they produce anomalies in the reflection of light which one calls "slicks". Natural sea slicks constituted by monomolecular films of adsorbed organic molecules have been known for a long time. As a result of pollution, contaminant films or layers such as slicks of petroleum products or other chemicals are now more and more often observed.

Surface films modify air-sea interactions, in general in an assuaging way, attenuating small waves, hindering wave formation, reducing air drag, inhibiting gas exchange ... (e.g. Garrett, 1967, 1972).

Momentum is presumably transferred from wind to waves and, for a substantial part, passed over to the water column by combining waves or other mechanisms (Stewart, 1967; Krauss, 1967). The detailed machinery of this transfer is rather complicated because the wind profile is itself affected by the state of the sea surface, the nature and the shape of the waves and, both wind and waves, are largely influenced by the stratification. The complicated interplay between air stability, sea state and wind field reflects on the resulting stress exerted by the wind. Heavy rainfall and wave breaking will increase it. [Momentum transfer is presumably enhanced by the agitation of air caused near the interface by the interpenetration of air and water layers (Hidy, 1972; Krauss, 1972).] Oil slicks decrease the stress. In unstable conditions, a definite augmentation of momentum transfer seems to occur when the wind speed exceeds some 7 m/s, associated with the onset of foaming (De Leonibus, 1971). Acceleration of spray drops (and deceleration of bubbles) produce an additional shear stress which is presumably small at low wind speed but may become relatively more important at higher wind speeds (Krauss, 1967).

The situation is evidently similar for the transport of heat and material across the air-sea interface. Intricated surface mechanisms ensure the transmission of fluxes with variable efficiency. Infrared radiations, for instance, are absorbed at the interface, producing a discontinuity in the heat flux (Krauss, 1967).

Wave generation can improve significantly the rates of evaporation and aeration. According to Hidy (1972), this must be attributed to the disturbance of the diffusional sublayer near the water boundary, which plays a key role in the material transfer across the interface.

A similar situation prevails at the bottom. When a viscous layer can be maintained on the sea floor, the flux of material is simply due to the slow sedimentation of particles. When the layer is disrupted by turbulence, the material concentrated in the viscous layer can be recirculated. For still higher values of the turbulent shear, the flow is able to erode the bottom and blow solid sediments into the water column and its turbulent dynamics (Mc Cave, 1970; Cormault, 1971).

A few examples suffice to demonstrate the complexity of the interactions at the upper and lower sea boundaries. One understands the difficulty of specifying judicious boundary conditions appropriate to a model. The uncertainties in the boundary conditions however deeply reflect on the model's predictions and the inaccuracy of boundary data is often the more severe handicap to modelling.

Once microscale turbulent fluctuations have been parameterized in the hydrodynamic equations, the boundary conditions which must be provided to solve these equations are likewise the conditions which apply to macroscale and mesoscale processes.

At the air-sea interface, it is generally assumed that the fluxes are proportional to the magnitude of the wind velocity at some reference height (10 m, say). If  $V$ ,  $\Theta$ ,  $q$  denote the velocity, the temperature and the moisture (or perhaps the concentration of some contaminant) at the height of reference and  $\Theta_0$ ,  $q_0$  the corresponding surface values, one writes (Krauss, 1972)

(i) momentum flux (divided by the density of sea water)

$$(18) \quad \tau_s = V C^* \|V\|$$

(ii) heat flux (divided by the specific heat and the density of sea water)

$$(19) \quad h_s = (\Theta_0 - \Theta) C^* \|V\|$$

(iii) moisture flux (divided by the density of sea water)

$$(20) \quad \omega_s = (q_0 - q) C^* \|V\|$$

where the "drag coefficient"  $C^*$  is a control parameter (e.g. Nihoul, 1975a, 1976, 1977a).

According to Krauss (1972), "the preceding expressions, applied to good meteorological data, probably can yield flux estimates over the open ocean with a mean expected error of less than 30 %". Hidy (1972) anticipate a "more realistic error" as large as 50 %. This would seem to be the range in which the data from various observations scatter under comparable wind conditions.

In addition, observations from the Bomex experiment reported by Pond et al (1971) cast doubt on the validity of (19) for the heat transport which is significantly affected by radiation. One may also question the extension of (20) to the flux of chemical species which may dissolve or interact preferentially in organic surface films.

At a rigid bottom boundary, the velocity must be zero. Ignoring slow deformation of the sea floor, this requirement would seem to provide the simplest boundary condition at the bottom.

However, as discussed later, it is not always the most convenient and, in particular, two-dimensional (depth-averaged) models need boundary conditions expressed in terms of the depth-averaged velocity.

It is generally assumed that the momentum flux (and the related "bottom stress") is given by an equation similar to eq. (18), i.e. (e.g. Nihoul, 1975a)

$$(21) \quad \tau_b = D \bar{u} \|\bar{u}\| - m \tau_s$$

where  $D$  is a suitable drag coefficient and where the last term in the right-hand side is a small correction introduced to account for the fact that, in case of negligible volume transport of water, there is still a stress exerted by the bottom (Groen and Groves, 1966).

The limitations of this type of parameterization will be discussed later in relation with three-dimensional models.

#### 4.- Two-dimensional depth-averaged models.

The depth-averaged motion is described in terms of the mean velocity  $\bar{u}$  or the total flow-rate  $U$  defined by

$$(22) \quad U = U_1 e_1 + U_2 e_2 = H \bar{u} = \int_{-h}^{\zeta} u \, dx_3$$

where  $H$  is the total depth, i.e.

$$(23) \quad H = h + \zeta$$

Deviations from the vertical mean are indicated by  $\hat{u}$ . Thus

$$(24) \quad u = \bar{u} + \hat{u}$$

with

$$(25) \quad \int_{-h}^{\zeta} \hat{u} \, dx_3 = 0$$

Integrals over  $x_3$  of partial derivatives with respect to  $t$ ,  $x_1$  or  $x_2$  can be expressed in terms of the derivatives of the integrals by the formula

$$(26) \quad \int_{-h}^{\zeta} \frac{\partial f}{\partial \eta} dx_3 = \frac{\partial}{\partial \eta} \int_{-h}^{\zeta} f dx_3 - f(\zeta) \frac{\partial \zeta}{\partial \eta} - f(-h) \frac{\partial h}{\partial \eta}$$

where  $\eta$  stands for any of the variables  $t$ ,  $x_1$  and  $x_2$  and where  $f$  is any function of  $t$ ,  $x_1$ ,  $x_2$  and  $x_3$ ,

$$f(\zeta) \equiv f(t, x_1, x_2, \zeta)$$

and  $f(-h) \equiv f(t, x_1, x_2, -h)$

its values at the sea surface and at the sea floor respectively.

Integrating eq. (14) over depth, one obtains

$$(27) \quad \int_{-h}^{\zeta} (\nabla \cdot \mathbf{u}) dx_3 + v_3(\zeta) - v_3(-h) = 0$$

Commuting the integration and derivation signs according to eq. (26) and eliminating  $v_3(\zeta)$  and  $v_3(-h)$  by eqs (16) and (17), one can write eq. (27) in the form

$$(28) \quad \frac{\partial H}{\partial t} + \nabla \cdot \mathbf{U} = 0$$

where  $H$  is given by eq. (23) and

$$(29) \quad \frac{\partial H}{\partial t} \sim \frac{\partial \zeta}{\partial t}$$

(neglecting slow deformations of the bottom).

In term of the depth-averaged velocity  $\bar{\mathbf{u}}$ , eq. (28) reads

$$(30) \quad \frac{\partial H}{\partial t} + \bar{\mathbf{u}} \cdot \nabla H + H \nabla \cdot \bar{\mathbf{u}} = 0$$

[Note that  $\nabla$  reduces to

$$\mathbf{e}_1 \frac{\partial}{\partial x_1} + \mathbf{e}_2 \frac{\partial}{\partial x_2}$$

in eqs (28) and (30) since the functions  $H$ ,  $U$  and  $\bar{\mathbf{u}}$  do not depend on  $x_3$ .]

Although the divergence of the three-dimensional velocity  $\mathbf{v}$  is zero, the divergence of the two-dimensional mean velocity  $\bar{\mathbf{u}}$  is not zero.

However if  $\zeta$  is everywhere negligible with respect to  $h$  and if  $h$  varies slowly in space as compared to  $\bar{\mathbf{u}}$  and  $\zeta$ , eq. (30) can be approximated by

$$(31) \quad \nabla \cdot \bar{\mathbf{u}} = 0$$

Indeed if  $L$  is the characteristic length of variation of  $h$  and  $\ell$  the characteristic length of variation of  $\zeta$  and  $\bar{\mathbf{u}}$ ,

the first two terms of eq. (30) can be estimated as

$$\frac{\partial H}{\partial t} \sim \frac{\partial \zeta}{\partial t} \sim 0\left(\frac{\zeta \bar{u}}{\ell}\right)$$

$$\bar{\mathbf{u}} \cdot \nabla H \sim \bar{\mathbf{u}} \cdot \nabla \zeta + \bar{\mathbf{u}} \cdot \nabla h \sim 0\left(\frac{\zeta \bar{u}}{\ell}\right) + 0\left(\frac{\bar{u} h}{L}\right)$$

while the third term is the sum of two parts, each one of the order

$$H \frac{\partial \bar{u}_i}{\partial x_j} \sim 0\left(\frac{h \bar{u}}{\ell}\right)$$

If one can assume

$$\ell \ll L \quad ; \quad \zeta \ll h$$

the contributions from the first two terms are all negligible as compared to the contributions from the third term. These must consequently balance each other and eq. (31) holds.

#### **Shear effect.**

The integration of eq. (14) presented no difficulty. The equation being linear, all terms containing deviations  $\hat{u}$  from the mean field disappeared in the integration process by virtue of eq. (25). The same is not true for the momentum equation which contains products of the velocity vector components. Indeed, one finds

$$(32) \quad H^{-1} \int_{-h}^{\zeta} u_i u_j \, dx_3 = \bar{u}_i \bar{u}_j + H^{-1} \int_{-h}^{\zeta} \hat{u}_i \hat{u}_j \, dx_3$$

Thus the average of a product gives two contributions. The first one is the product of the means, the second one the mean product of the deviations.

This is similar to the situation discussed earlier when the actual velocity vector was separated into a mean part (over a characteristic time  $T$ ) and a fluctuation around the mean. Although the average then was a time average while, in eq. (32), it is a depth average, the same difficulty occurs: when averaging the evolution equations, all terms cannot be expressed in terms of average quantities, the non-linear terms also contain average products of fluctuations or deviations.

These non-linear contributions must somehow be expressed in terms of the mean variables if one wishes to proceed with the model without undertaking a detailed study of the fluctuations or deviations.



Acknowledging the essentially dispersive action of the turbulent fluctuations, their general effect on the mean motion has been shown previously to be equivalent to a diffusion term similar to the molecular diffusion term but with much larger diffusion coefficients.

One may argue that the mean product of deviations occurring in eq. (32) has a similar effect; differences in local velocities contributing to the spreading of momentum and, as discussed later, to the dispersion of temperature, nutrients, pollutants, etc. (e.g. Nihoul, 1975a; Benqué et al., 1981).

This effect has been called the *shear effect* because deviations would be zero if the velocity were uniform over the depth and terms like the second term in the right hand side of eq. (32) only exist because there is a vertical gradient of velocity or "shear".

The shear effect will be discussed in detail later. It will be shown that it plays an essential part in the dispersion of passive constituents and it will be necessary to find appropriate formulas to express it in terms of the depth-mean variables.

In hydrodynamic models, one usually makes crude approximations which amount more or less to including the shear effect in a horizontal dispersion term -- which also includes the small contribution from three-dimensional turbulence -- and adjusting the coefficient of dispersion accordingly.

Indeed, one can argue that hydrodynamic models of large sea regions can be less delicate in this respect than dispersion models concerned with the spreading of a contaminant over an area of a few kilometers around the point of release. The coarseness of the grid imposed to the simulation model by the extent of the modelled region and the subsequent approximations associated with the numerical viscosity coefficients suggest that the formulation is sufficiently rudimentary, hence flexible, to incorporate the shear effect.

It is important to note, however that including the shear effect may notably change the magnitude of the dispersion coefficients.

Indeed, if a shear effect diffusivity  $a$  is introduced such that

$$(33) \quad H^{-1} \int_{-h}^{\xi} \hat{u}_i \hat{u}_j \, dx_3 = - a \frac{\partial \bar{u}_i}{\partial x_j}$$

comparing the orders of magnitude of the two sides of the equation, one finds that  $a$  must be of the order

$$(33') \quad a \sim \frac{\ell \hat{u}^2}{\bar{u}}$$

where  $\bar{u}$  and  $\hat{u}$  are typical values of the mean and deviation velocities and  $\ell$  the characteristic length of horizontal variations.

The ratio  $\hat{u}^2/\bar{u}$  depends on the vertical distribution of  $u$ . It would be very small if the velocity was nearly uniform over the depth. One can argue however that this cannot be the case because the velocity must be maximum at the surface and zero at the bottom and  $\hat{u}$  which is necessarily of order  $\bar{u}$  at the bottom remains reasonably important over a large part of the water column. Thus  $\hat{u}^2/\bar{u}$  is an appreciable fraction of  $\bar{u}$ .

If this is the case, the coefficient  $a$  can be one or two orders of magnitude larger than the eddy viscosity  $\tilde{\nu}$  which can be estimated by

$$\tilde{\nu} \sim \ell v_\ell$$

where the characteristic velocity

$$v_\ell \sim \varepsilon^{1/3} \ell^{1/3}$$

associated with the eddies of size  $\ell$  is considerably smaller than  $\bar{u}$ .

### Surface fluxes.

In eqs (13) and (15),

$$\frac{\partial}{\partial x_3} \left( \tilde{\nu} \frac{\partial \mathbf{u}}{\partial x_3} \right)$$

and

$$\frac{\partial}{\partial x_3} \left( \tilde{\lambda} \frac{\partial c}{\partial x_3} \right)$$

are exact differentials.

Integrating over depth, one finds

$$(34) \quad \int_{-h}^{\zeta} \frac{\partial}{\partial x_3} \left( \tilde{\nu} \frac{\partial \mathbf{u}}{\partial x_3} \right) dx_3 = \left[ \tilde{\nu} \frac{\partial \mathbf{u}}{\partial x_3} \right]_{x_3=\zeta} - \left[ \tilde{\nu} \frac{\partial \mathbf{u}}{\partial x_3} \right]_{x_3=-h} \\ = \tau_s - \tau_b$$

$$(35) \quad \int_{-h}^{\zeta} \frac{\partial}{\partial x_3} \left( \tilde{\lambda} \frac{\partial c}{\partial x_3} \right) dx_3 = \left[ \tilde{\lambda} \frac{\partial c}{\partial x_3} \right]_{x_3=\zeta} - \left[ \tilde{\lambda} \frac{\partial c}{\partial x_3} \right]_{x_3=-h}$$

Hence, using eqs (18) and (21) and setting

$$C = C^*(1 + m)$$

for brevity, one can write

$$(36) \quad \int_{-h}^{\zeta} \frac{\partial}{\partial x_3} \left( \tilde{\nu} \frac{\partial \mathbf{u}}{\partial x_3} \right) dx_3 = C \mathbf{V} \|\mathbf{V}\| - D \bar{\mathbf{u}} \|\bar{\mathbf{u}}\|$$

**Depth-averaged equations.**

Integrating the momentum equation (13) over depth, using eqs (26), (28) and (36), one obtains (e.g. Nihoul, 1975a; Benqué et al., 1981)\*

$$(37) \quad \begin{aligned} \frac{\partial \mathbf{U}}{\partial t} + \nabla \cdot (H^{-1} \mathbf{U} \mathbf{U}) + f \mathbf{e}_3 \wedge \mathbf{U} \\ = - H \nabla \left( \frac{P_a}{\rho} + g\zeta \right) + a \nabla^2 \mathbf{U} - \frac{D}{H^2} \mathbf{U} \|\mathbf{U}\| + C \mathbf{V} \|\mathbf{V}\| \end{aligned}$$

or, for the mean velocity  $\bar{\mathbf{u}}$ , using eq. (28),

$$(38) \quad \begin{aligned} \frac{\partial \bar{\mathbf{u}}}{\partial t} + \bar{\mathbf{u}} \cdot \nabla \bar{\mathbf{u}} + f \mathbf{e}_3 \wedge \bar{\mathbf{u}} \\ = - \nabla \left( \frac{P_a}{\rho} + g\zeta \right) + a \nabla^2 \bar{\mathbf{u}} - \frac{D}{H} \bar{\mathbf{u}} \|\bar{\mathbf{u}}\| + \frac{C}{H} \mathbf{V} \|\mathbf{V}\| \end{aligned}$$

Similarly, integrating eq. (15) over depth, one finds

$$(39) \quad \frac{\partial \bar{c}}{\partial t} + \bar{\mathbf{u}} \cdot \nabla \bar{c} = \Lambda + \Sigma$$

where

$$(40) \quad \Lambda = \bar{Q} + H^{-1} \left( \left[ \tilde{\lambda} \frac{\partial c}{\partial x_3} \right]_{x_3=\zeta} - \left[ \tilde{\lambda} \frac{\partial c}{\partial x_3} \right]_{x_3=-h} \right)$$

and

$$(41) \quad \Sigma = H^{-1} \nabla \cdot \int_{-h}^{\zeta} (-\hat{c} \hat{\mathbf{u}}) dx_3$$

$H\Lambda$  is the total input per unit time in a water column of unit cross section. It includes the contributions from the volume sources  $Q$  and the turbulent fluxes through the air-sea interface and the bottom.  $\Sigma$  is the shear effect diffusion term.

\* The diffusion coefficient  $a$  has obviously not exactly the same meaning in eqs (37) and (38), as the passage from one to the other would involve space derivatives of  $H$ . However, in view of the approximate character of such formulations, one generally agrees that refinements would be illusory and that, according to the terminology of the problem, one will use formula (37) or (38), considering  $a$  as a control parameter to be determined empirically.

## 5. - Two-dimensional models of tides and storm surges.

Eqs (28) and (37) describe both macroscale and mesoscale flows. However, in shallow continental seas like the North Sea, the latter is one or two orders of magnitude larger than the former. If the boundary conditions are restricted to the mesoscale signal, one substantial part of the macroscale residual flow - in the case of the North Sea, the North Atlantic current - is lost and what remains of the residual motion, due to wind forcing and non-linear interactions of mesoscale processes, is very small indeed and, at most, comparable with the error on the solution.

One may thus regard the solution of eqs (28) and (37), subject to mesoscale boundary conditions, as representing essentially the mesoscale motion, ignoring a negligible coupling with macroscale processes.

The first hydrodynamic models of the North Sea were concerned with the calculation of tides and storm surges (e.g. Hansen, 1956; Fisher, 1959; Leendertse, 1967; Heaps, 1967, 1969, 1972; Nihoul, 1973a; Runday, 1973; Duun-Christensen, 1971).

This is obviously justified by the predominance of mesoscale processes. An additional advantage is the relative reliability of open-sea boundary conditions which, for long waves, are comparatively easy to assess.

Indeed, as mentioned before, one of the main problems in hydrodynamic modelling is the specification of boundary conditions on open-sea frontiers (e.g. Nihoul, 1973a, 1975a). The lack of reliable experimental data and the necessity to interpolate from incomplete - often obsolete - observations is a source of errors and misapprehension which can be propagated by the model through the entire system.

In some of the mesoscale models, the basic equations (28) and (37) are further simplified by neglecting the surface elevation  $\zeta$  with respect to the depth  $h$ . This approximation limits the applicability of the models to reasonably deep regions of the sea and the results of the simulation in shallow areas and near the coasts may be significantly affected and differ appreciably from the observations.

The existing models of tides and storm surges also suffer from the lack of sufficiently detailed atmospheric data over the sea. One cannot do much more than estimate the wind stress to the best of one's ability, especially as the value of the drag coefficient  $C$  is uncertain and may vary considerably, as pointed out before.

Two other control parameters  $a$  and  $D$  appear in the equations. They are also difficult to determine with precision and very often the success of a model depends on a more or less skillful estimate of them.

The approximation of the boundary conditions on open sea frontiers may finally be responsible for other limitations of the models.

In the case of internal surges for instance, it is generally accepted that, if the sea basin is relatively shallow and its open boundary is contiguous with a deep ocean, the surface elevation may be put equal to zero along that boundary for all time. One may fear that this produces erroneous reflections at the open boundary after a time. It seems unlikely that the prediction of the sea behaviour after the first transit of the storm surge can be very accurate. For external surges, the open sea boundary conditions are either measured - in which case they suffer from the general lack of accuracy of experimental data on open sea boundaries - or approximated by known periodic conditions. This amounts really to replacing a travelling wave by a standing one and again creates the same problems.

By the standards of other fields of simulation, however, it is fair to say that the storm surge and tidal models are at present the most advanced and best prepared for practical applications. To illustrate the art and limitations of these models, it is profitable to discuss briefly one example. It will serve to exemplify the classical approximations and methods and it will give an idea of the typical results such models can achieve.

Figure 1 shows the numerical grid used by Runday (1973) to study the circulation induced in the North Sea by external tides originating from the Atlantic Ocean.

As shown by Defant (1961), external tides are largely dominant in coastal seas like the North Sea and the astronomical tide may be neglected. This amounts to setting  $\xi = 0$  in the governing equation (2) and considering only tidal oscillations induced by incoming tidal waves at the open sea boundary. Attention is furthermore restricted to the semi-diurnal tide  $M_2$  which is by far the main component in the North Sea.

The horizontal mesh size is  $21.7 \times 10^3$  m and the associated time step, based on numerical stability criteria, is  $1/360$  of the  $M_2$  tidal period, i.e. about one minute.

Following Brettschneider (1967), Runday (1973) takes

$$a \sim 10^4 \text{ m}^2 \text{ s}^{-1}$$

which is consistent with a length scale of some 20 kilometers [eq. (33')].

Showing that the finally established oscillatory regime is practically independent of the initial conditions, Runday (1973) assumes zero fluid transport and zero elevation at the initial time.

The boundary conditions along the open-sea frontiers are approximated by simple harmonic functions

$$(42) \quad H = A \cos(\omega t + \varphi)$$

where the amplitude  $A$  and the phase  $\varphi$  are functions of position. The values of  $A$  and  $\varphi$  at the coastal extremities of the

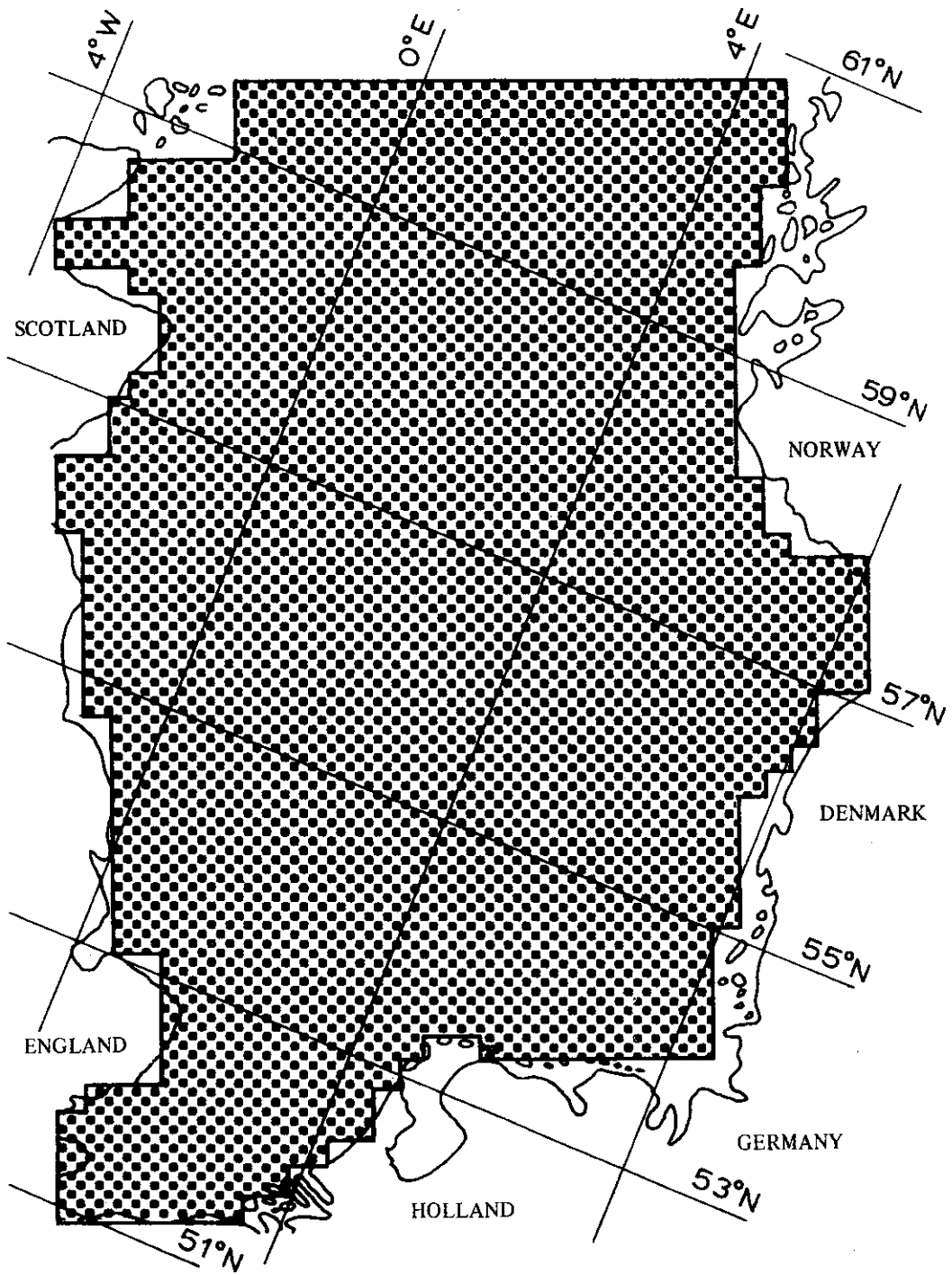


fig. 1.

Numerical grid in Røndal's model of the tidal circulation in the North Sea

open sea frontiers are given in table 1. The values of  $A$  and  $\phi$  at boundary points out at sea being unknown, they are calculated by linear interpolation.

Table 1

	A (m)	$\phi$ (degrees)
Straight of Dover		
Northern side	2.45	330
Southern side	2.70	325
Northern boundary		
Western side	0.632	306
Eastern side	0.439	241
Baltic Sea		
Northern side	0.083	80
Southern side	0.108	95

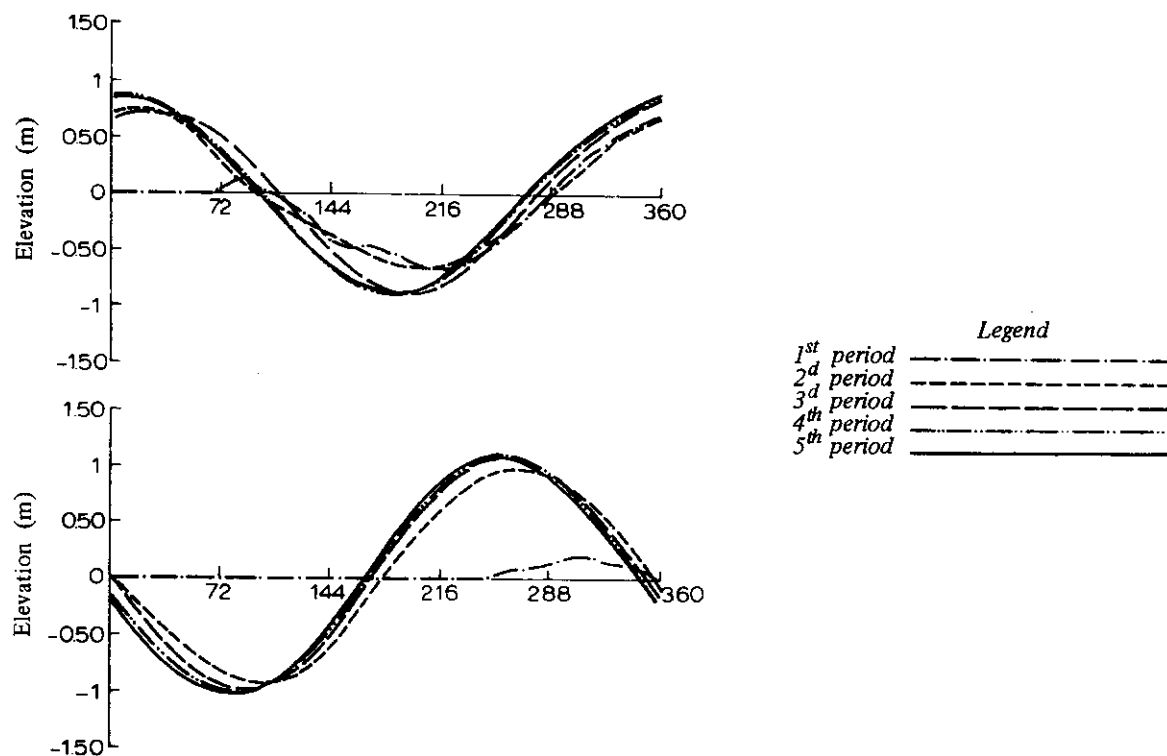


fig. 2.

Influence of the number of iterations on the surface elevations at two points respectively at small and large distance from the boundary excitation (after Runday, 1973).

Running the simulation program shows that the regime is attained after three tidal periods even for grid points far away from the boundary excitation and situated in shallow areas. This confirms that the solution of the fundamental equations which corresponds to forced oscillations, is fairly insensitive to the initial conditions. Figure 2 shows the influence of the number of iterations on the elevation of the sea surface for two points situated respectively at small and large distance from the exciting forces.

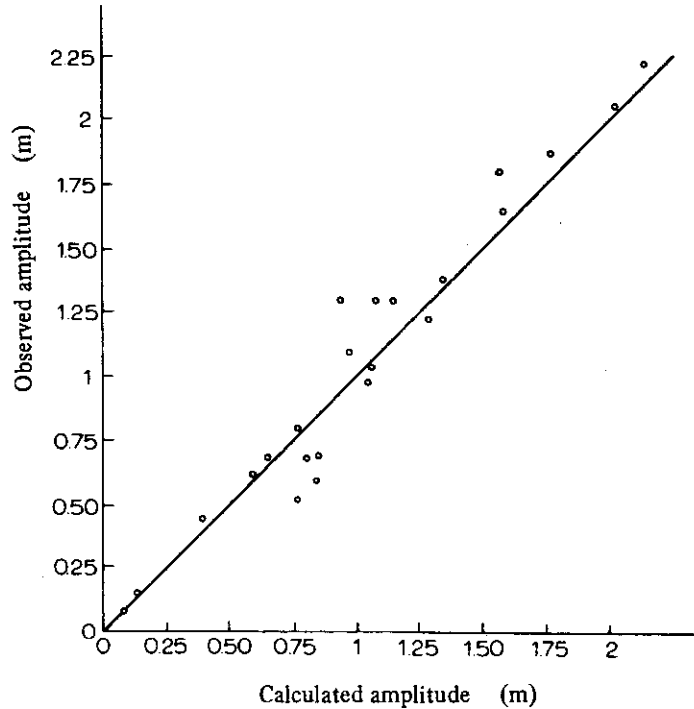


fig. 3.

Correlation between calculated and observed amplitudes of the  $M_2$  tide in the North Sea (after Røndal, 1973).

Figures 3 and 4 show a comparison between observed and calculated values of the tidal amplitude and phase at different coastal stations. There is a generally good agreement except at some points which fall a little beside the ideal line at  $45^\circ$ . These points correspond to places near the English and Danish coasts where the depth is small and the bottom very irregular.

The discrepancy here illustrates the general lack of precision of tidal models in shallow areas where non-linear terms are important.



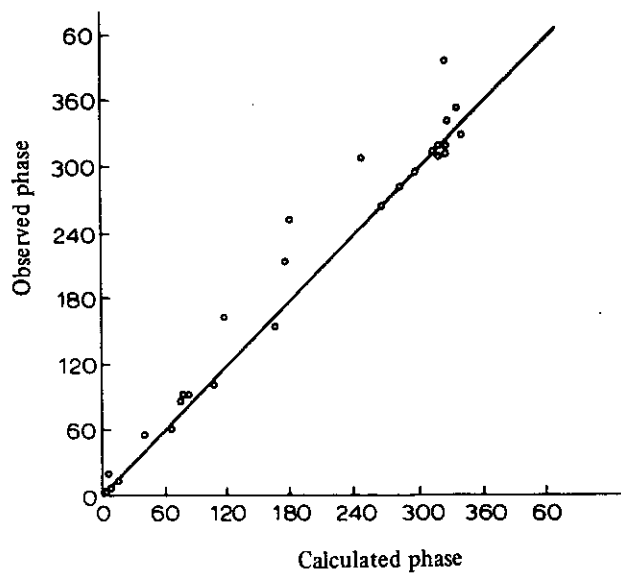


fig. 4.

Correlation between calculated and observed values of the phase of the  $M_2$  tide in the North Sea (after Runday, 1973).

A comparison between observed and calculated lines of equal amplitudes and phases (figures 5 and 6\*) also shows an excellent agreement; with again some differences in the German Bight and along the coast of England where the small water depth is responsible for the effect of non-linear terms.

Runday (1973) also calculated the tidal currents in the North Sea and compared them with the observations. He found a variance of 5 % to 20 % between the calculated and observed currents, the maximum difference occurring at reversing tide when the slightest phase displacement is enough to modify significantly the current pattern because of the marked anisotropy of the tidal "ellipses" (fig. 7).

The differences may be attributed to the approximations of the mathematical and simulation models (discretization, linear interpolation of boundary conditions, ...) but they cannot be regarded as really significant, considering the relatively rare and indeterminate experimental data.

\* Note that figures 5 and 6 are rotated with respect to one another of some 30°.

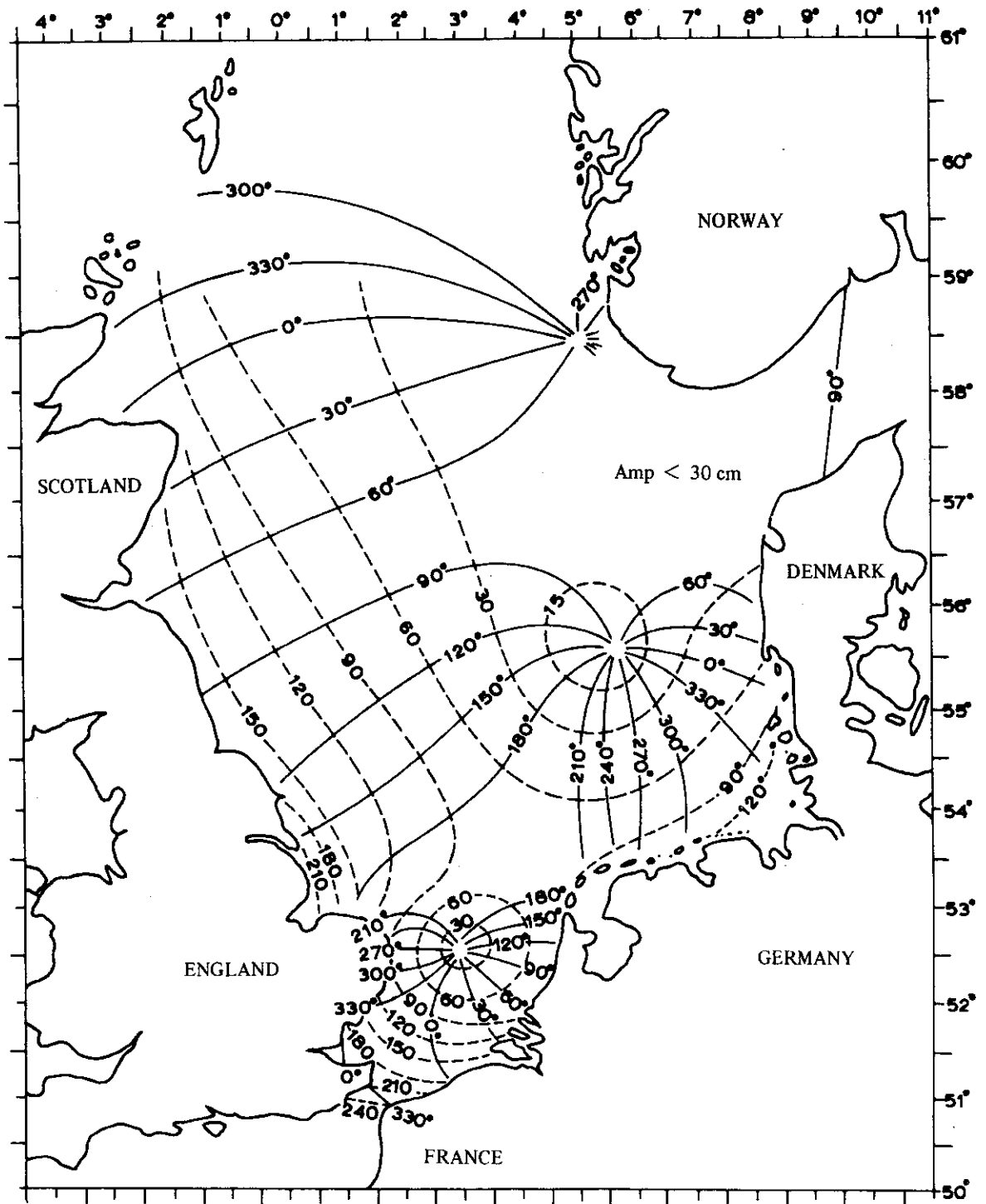


fig. 5.

Lines of equal tidal phases and amplitudes in the North Sea according to observations (after Proudman and Doodson, 1924).

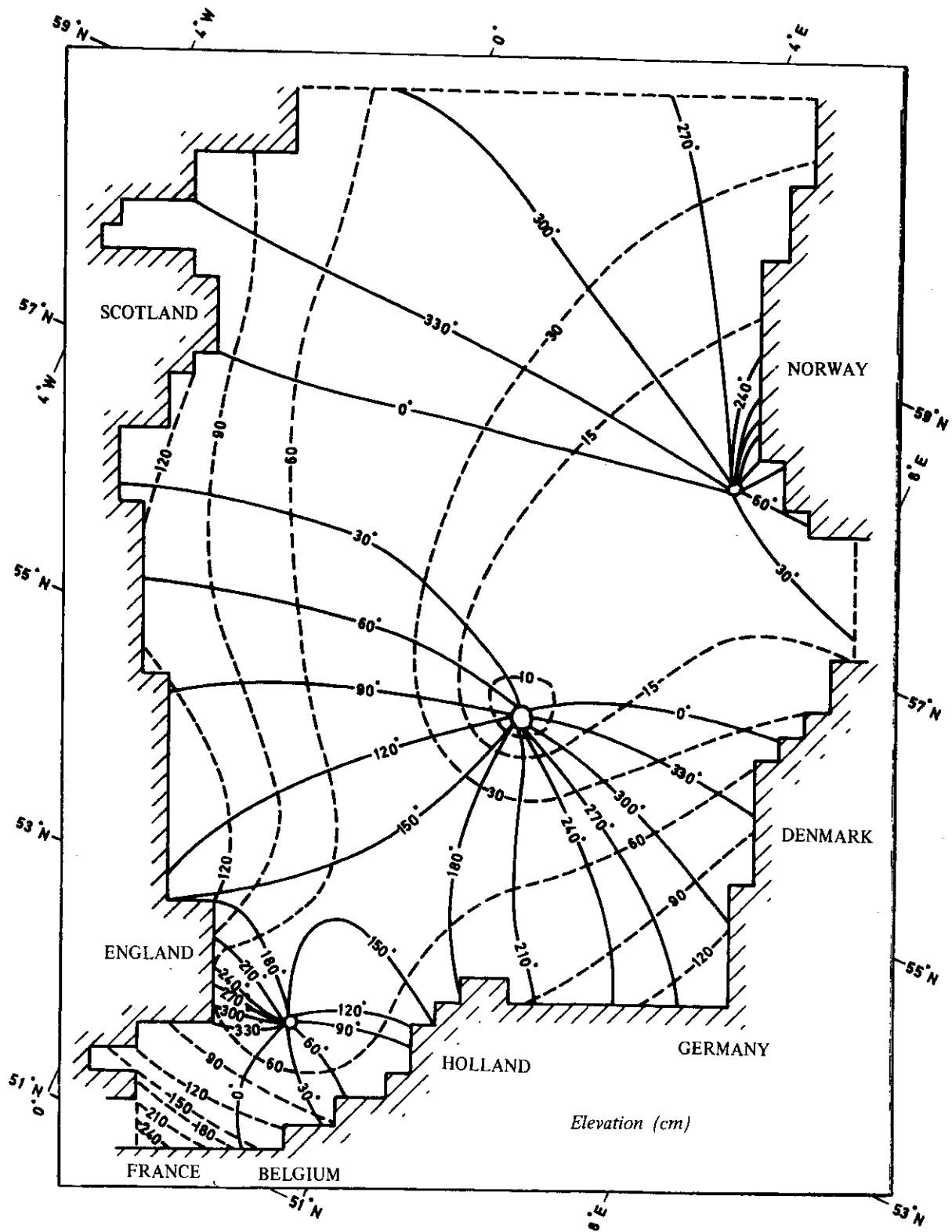


fig. 6.

Lines of equal tidal phases and amplitudes in the North Sea according to the mathematical model (after Runday, 1973).

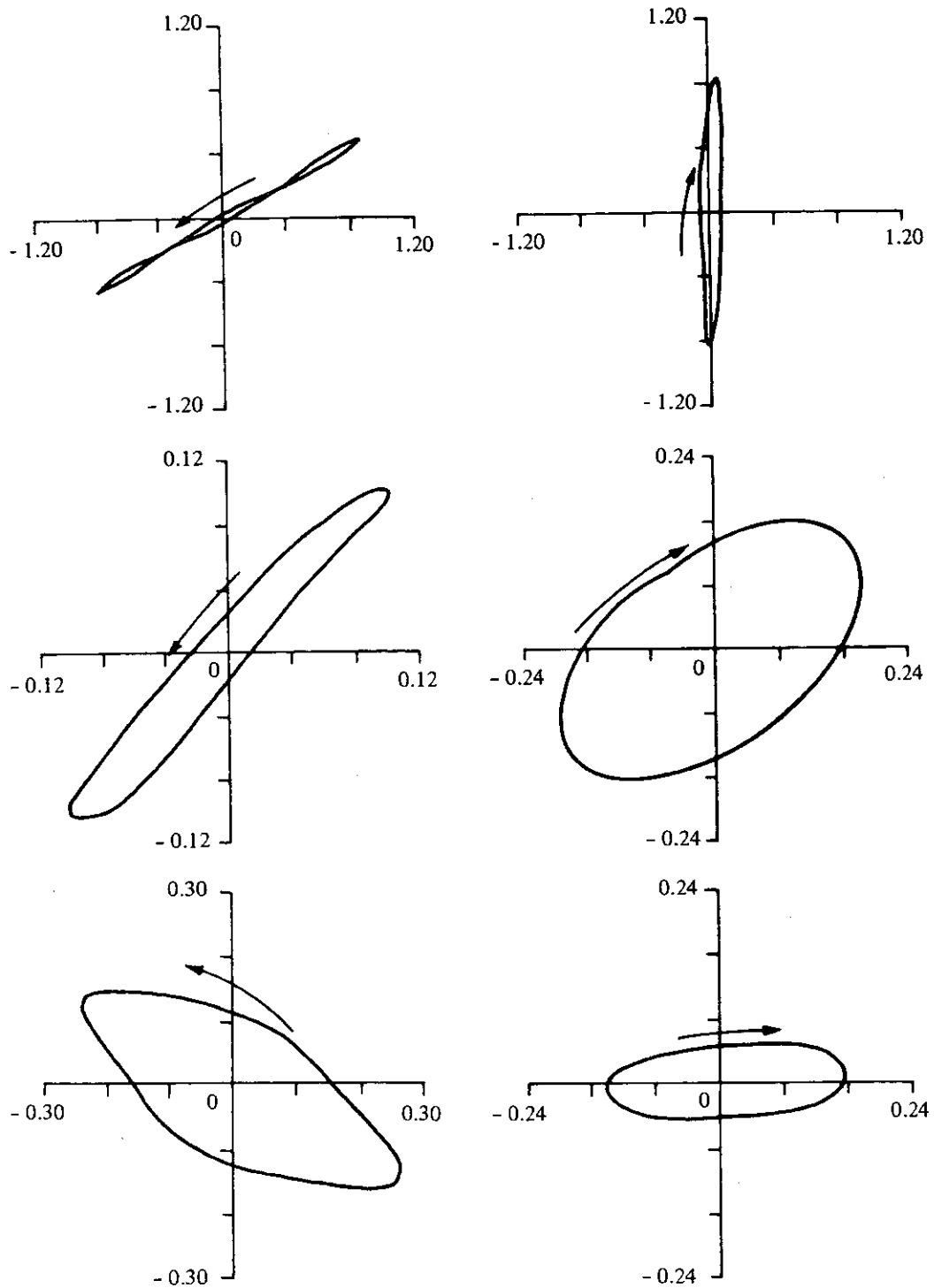


fig. 7.

Tidal "ellipses" at some typical points of the North Sea (after Røndal, 1973)

## 6.- A comparison between two-dimensional models of tides and storm surges in the North Sea.

If, for the sake of the following discussion, one leaves the surface and bottom stresses unspecified, one can write the fundamental equations governing tides and storm surges in the form

$$(43) \quad \frac{\partial \mathbf{U}}{\partial t} + \nabla \cdot (H^{-1} \mathbf{U} \mathbf{U}) + f \mathbf{e}_3 \wedge \mathbf{U} = -H \nabla \left( \frac{p_a}{\rho} + g\zeta \right) + a \nabla^2 \mathbf{U} - \boldsymbol{\tau}_b + \boldsymbol{\tau}_s$$

$$(44) \quad \frac{\partial H}{\partial t} + \nabla \cdot \mathbf{U} = 0$$

$\boldsymbol{\tau}_s$  and  $\boldsymbol{\tau}_b$  are here defined by unit mass of sea water.

### Model equations.

① The advection term  $\nabla \cdot (H^{-1} \mathbf{U} \mathbf{U})$  has generally been neglected. Brettschneider (1967) claims an error of 1 % on the predictions of his model neglecting the advection term. His subsequent estimates do not however support his claim.

According to Brettschneider (1967) [MKS units]

U	0.2	1
Mesh size	$5 \cdot 10^4$	$10^4$
$\frac{\text{Advection}}{\text{Coriolis}}$	$5 \cdot 10^{-2}$	1.3

Typical tidal velocities being of the order of 1 m/s, it seems thus that the advection term cannot be neglected. Advection is taken into account by Leenderste (1967) and Ronday (1976).

② The Coriolis term  $f \wedge \mathbf{U}$  is obviously essential, although, according to Heaps (1975), it affects more the surface elevation than the water transport.

Fig. 8 shows the results of an elementary model ( $H = 80$  m constant) taking the Coriolis effect into account and neglecting it (Hansen, 1966).

Not only is the Coriolis term important, but also the variations of  $f$  with latitude must be taken into account. This is done automatically in modern models which use spherical coordinates to define the numerical grid (e.g. Ronday, 1976).

③ The tidal forcing  $\boldsymbol{\epsilon}$  is usually put equal to zero as internal tides are small in the North Sea compared to incoming waves.

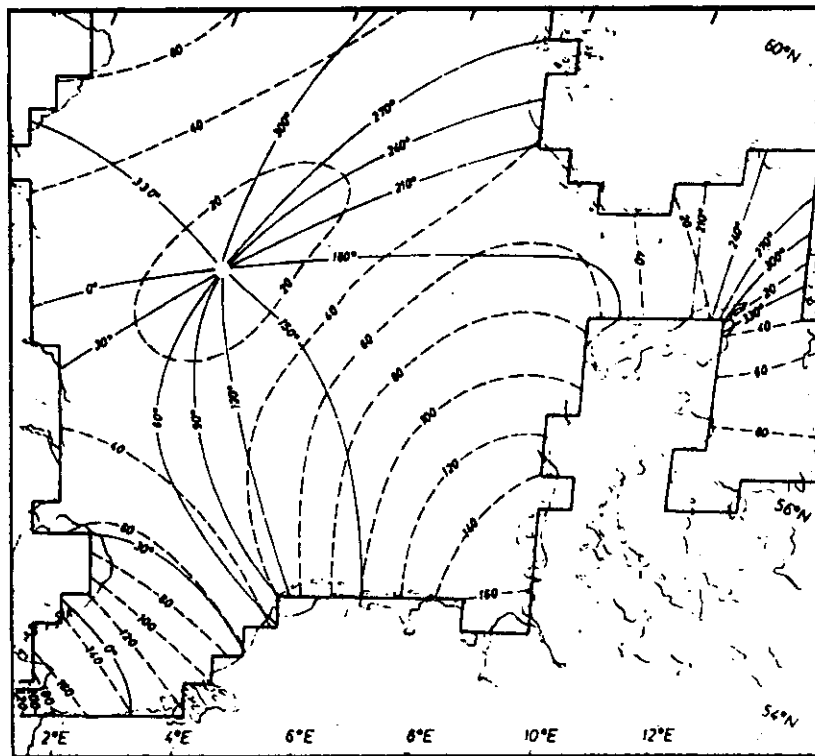
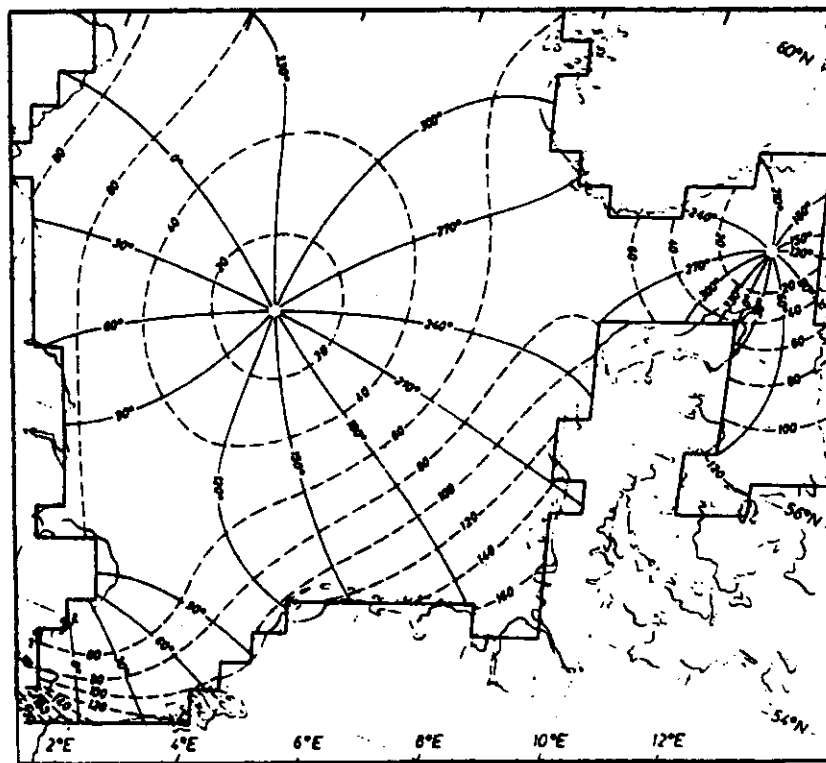


fig. 8.

Lines of equal phases and amplitudes of the  $M_2$  tide in the North Sea, taking the Coriolis effect into account (above) and neglecting it (below). (Hansen, 1966).  
 $H = 80$  m constant.

④ The dispersion term  $a \nabla^2 U$  is found negligible in the mathematical model. Many authors have kept this term in the numerical model with often an artificially high value of  $a$  for numerical stability (this is in fact not required if advection is properly included). This point will be discussed later.

⑤ Bottom friction is another important effect. Although several authors (e.g. Heaps, 1969, 1972, 1975; Durance, 1976) have attempted to represent the bottom stress by a linear law in the water transport, it is now commonly admitted that a quadratic law must be used, i.e.

$$(45) \quad \tau_b = \Gamma U \|U\| - m \tau_s$$

where  $\Gamma$  is a function of  $H$ .

When the simple assumption is made that the bottom stress is a quadratic function of the depth-averaged velocity,  $\Gamma$  is of the form

$$(46) \quad \Gamma = D H^{-2}$$

where  $D$  is a constant [Hansen and his school take  $D = 3 \cdot 10^{-3}$ ; Banks (1974) takes  $D = 2.5 \cdot 10^{-3}$ ]

More sophisticated models assume the bottom stress proportional to the square of the velocity at some reference height above the bottom. Using vertical velocity profiles adjusted to the observations, the reference velocity can be expressed in terms of  $U$ . The final result for  $\Gamma$  is of the same form as eq. (46) but  $D$  is no longer a constant. According to Leenderste (1967)

$$(47) \quad D = \frac{\alpha}{[19.4 \ln(0.9 H)]^2}$$

According to Ronday (1976)

$$(48) \quad D = \frac{\alpha}{(1.23 + \ln \frac{0.14 H}{z_0})^2}$$

where  $z_0$  is the rugosity length and  $\alpha$  a constant. With Ronday's formula, one finds

$$\alpha \sim 2.5 \cdot 10^{-3} \quad \text{for } H \sim 10 \text{ m}$$

$$\alpha \sim 1.4 \cdot 10^{-3} \quad \text{for } H \sim 80 \text{ m}$$

The bottom friction used by Hansen and Banks would thus seem appropriate for shallow areas but overestimated for deeper seas.

⑥ The wind stress is a quadratic function of the wind speed at some reference height (10 m, say). Thus

$$(49) \quad \tau_s = C^* V \|V\|$$

where  $C^*$  is the drag coefficient divided by the specific mass  $\rho$  of sea water.

According to Roll (1965), typical values of  $C^*$  would be comprised between  $10^{-6}$  and  $3 \cdot 10^{-6}$ . Hansen (1966) and Jensen and Weywardt (1966) take  $C^*$  constant and equal to  $3.2 \cdot 10^{-6}$ . Nihoul (1976) considers  $C^*$  as a function of the wind velocity and, following Sheppard (1958), writes

$$(50) \quad C^* = (0.98 + 0.14 V) 10^{-6}$$

The velocity  $V$  introduced in eqs (49) and (50) is the actual wind velocity calculated from the geostrophic wind field and the available observations. Similar corrections of the geostrophic wind velocity are made by Heaps (1969) and Banks (1974).

Dunn-Christensen (1974, 1975) takes  $C^*$  constant equal to  $3.2 \cdot 10^{-6}$  while he assumes that  $V$  in eq. (49) can be derived from the geostrophic wind velocity  $V_g$  by the following formula

$$(51) \quad V = a \sqrt{f_1 V_g + f_2} + b$$

where  $a$  and  $b$  are two experimental constants and where  $f_1$  and  $f_2$  are functions of the difference of temperature between air and water.

#### ***Model boundary conditions.***

Mathematical models may differ considerably according to the position of the open-sea boundaries and the approximation of the boundary conditions.

① The Southern boundary has traditionally be set at the Straits of Dover. The increasing difficulty to make field measurements in the Straits has recently lead to the choice of a new boundary line from Cherbourg to St. Alban's Head, thus including the Eastern part of the English Channel in the model (see fig. 9).

In the early stages, the assumption was made that for tides and storm surges - which, in the North Sea, are basically long waves incoming through the Northern entrance - one could impose zero flow through the Straits.

It was shown later that closing the Straits introduces an error which affects the results as far North as  $54^\circ$  N. Figures 10 and 11 show the lines of equal phase and amplitude of the  $M_2$  tide. In fig. 10 (Brettschneider, 1967), the Straits is closed. In fig. 11 (Ronday, 1976), water flow is allowed through the Straits.



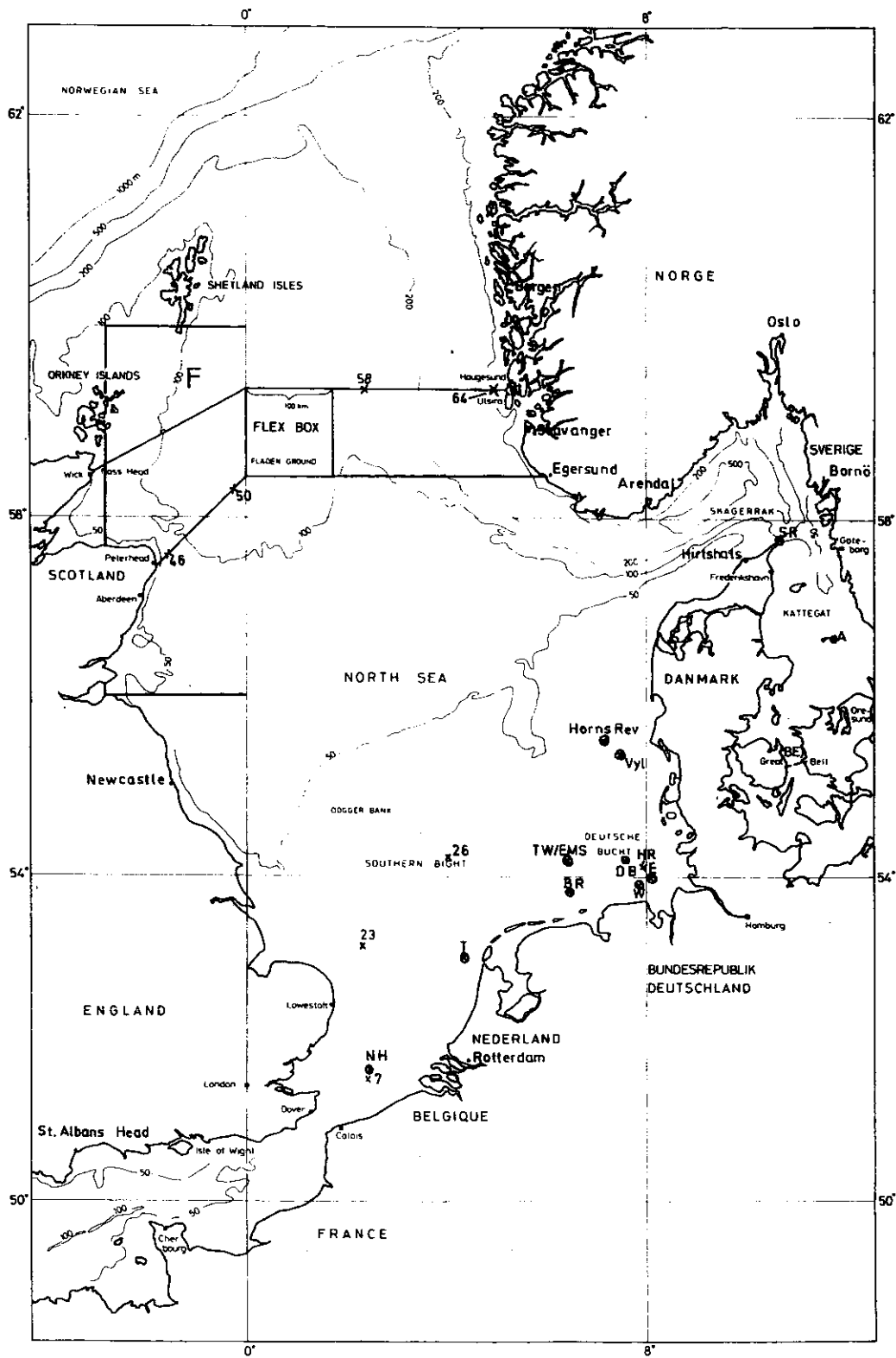


fig. 9.

The North Sea showing the boundaries of the Jonsdap '76 survey

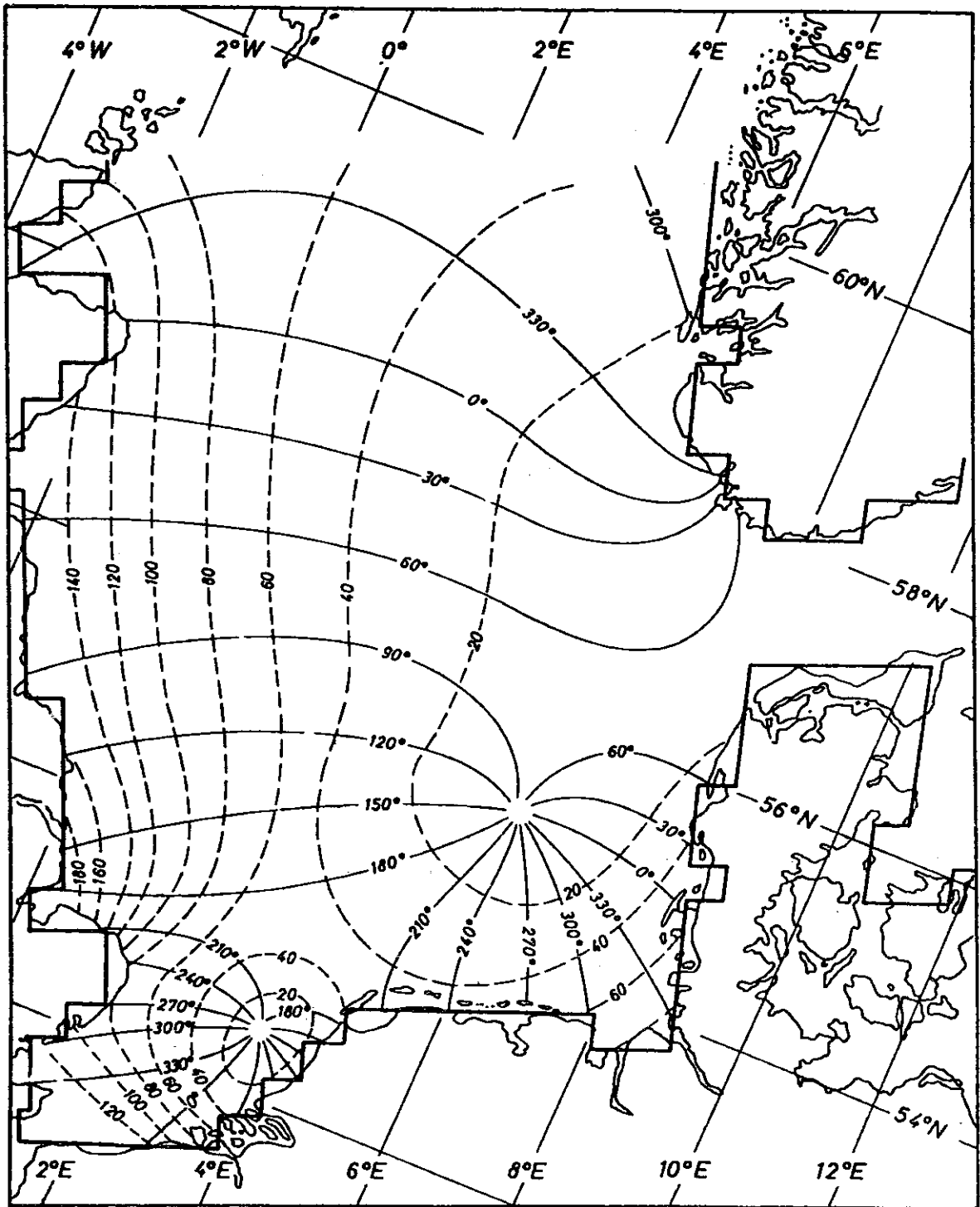


fig. 10.

Lines of equal phase and amplitude of the  $M_2$  tide with the assumption of zero flow through the Straits of Dover. (Brettschneider, 1967)

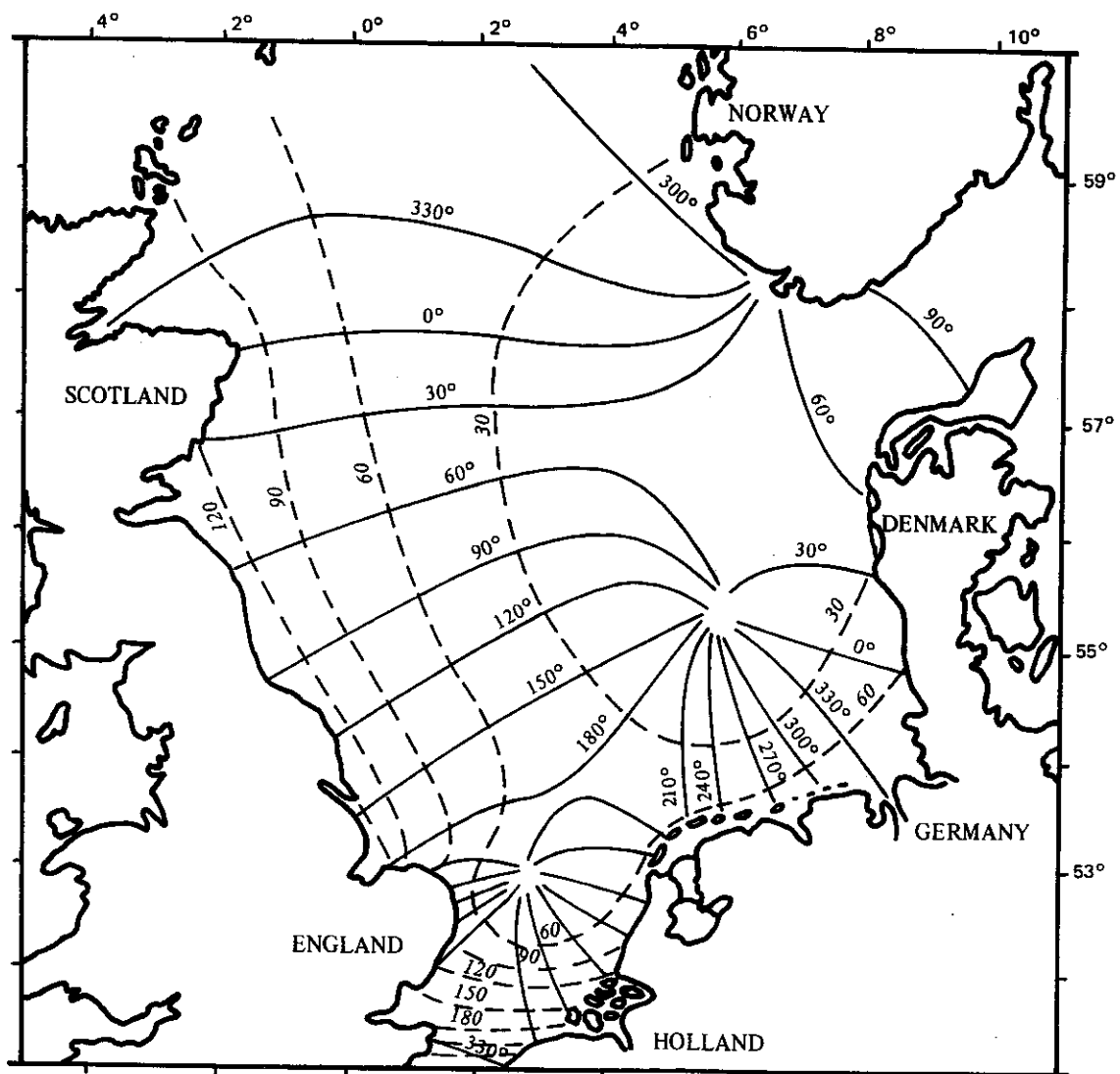


fig. 11.

Lines of equal phase and amplitude of the  $M_2$  tide allowing flow through the Straits of Dover. (Ronday, 1976)

In the case of storm surges, Jensen and Weywardt (1966) have shown that closing the Straits may alter the model's predictions as far as Cuxhaven. Fig. 12 (Heaps, 1969) shows the surface elevation at different coastal stations computed for the storm surge of 13 to 15 September 1956, (a) with the Straits of Dover closed, (b) with the Straits of Dover open (surface elevation is decreased at all stations in the Southern part).

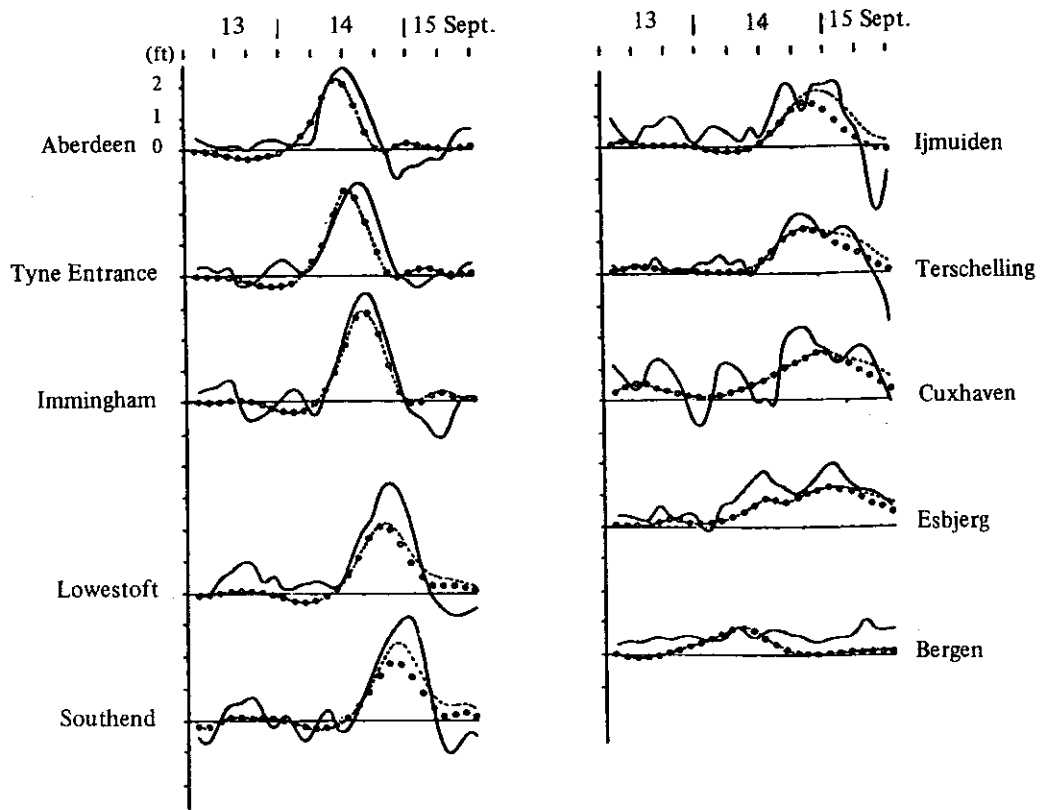
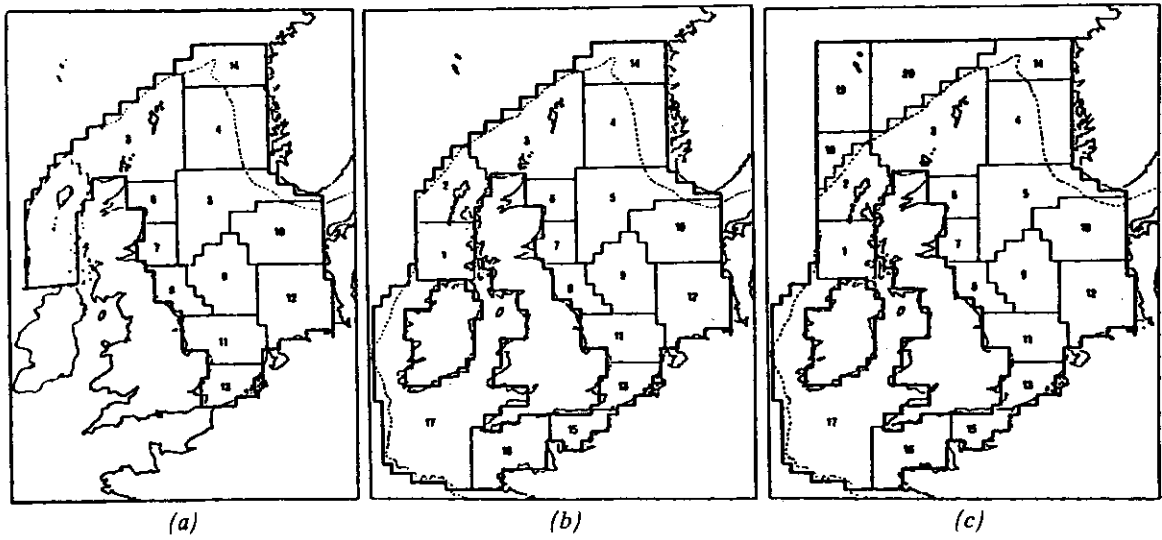


fig. 12.

Storm surge of 13 to 15 September 1956

— Residuals after removal of the barometric surge;

- - - - - wind surge from model (a);

..... wind surge from model (b).

(Heaps, 1969)

② The position of the Eastern boundary affects very little the tides in the North Sea. Fig. 13 shows the lines of equal phase and amplitude of the  $M_2$  tide computed with a model including the Skagerrak (Ronday, 1976). Comparison with fig. 11 computed with the same model limited at the Mandal Meridian line shows little difference.

In the case of storm surges, however, the Skagerrak must be included in view of the very strong currents generated along the coast of Jutland [fig. 14 (Fisher, 1959)].

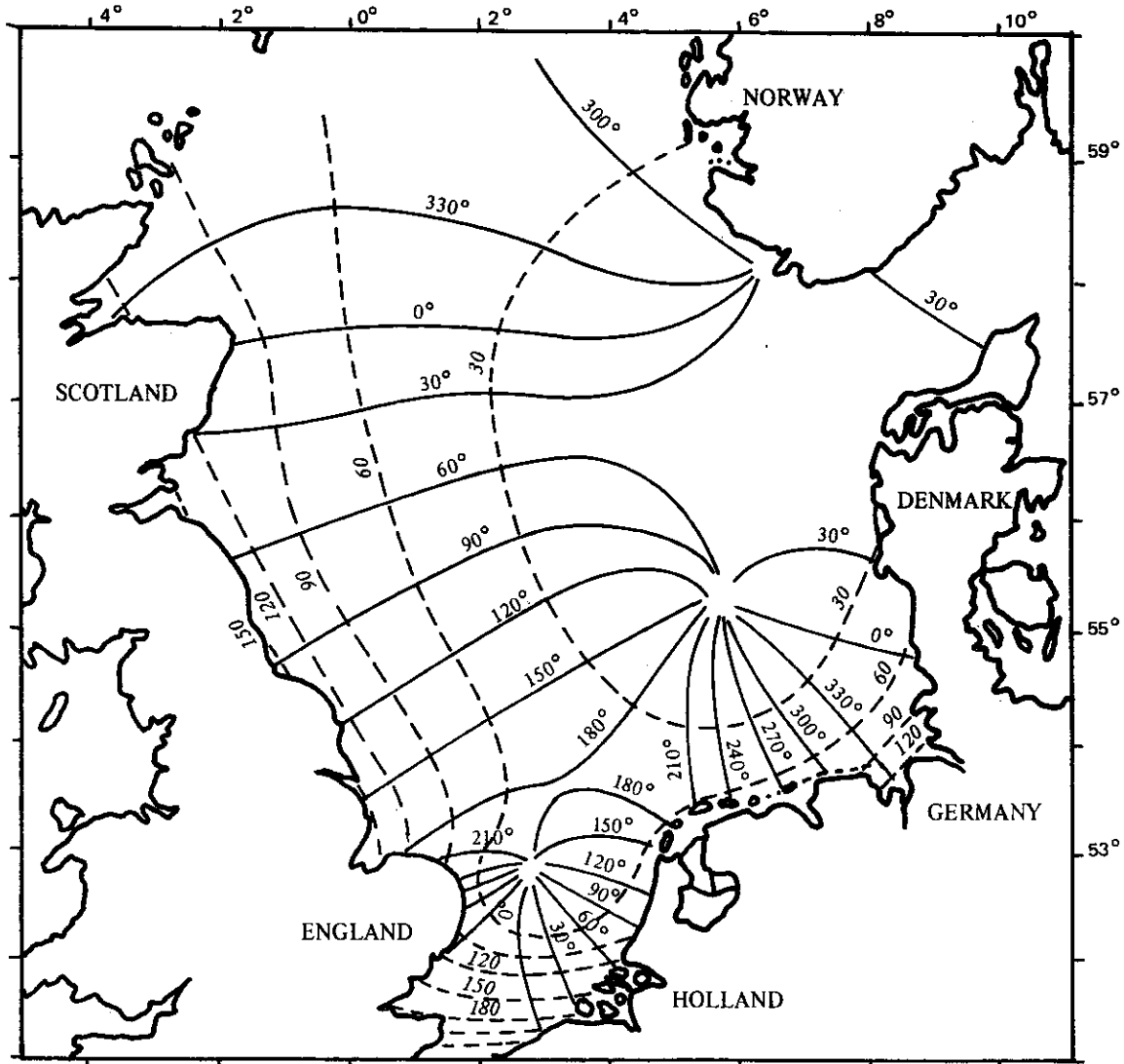


fig. 13.

Lines of equal phase and amplitude of the  $M_2$  tide computed with a model including the Skagerrak. (Ronday, 1976).

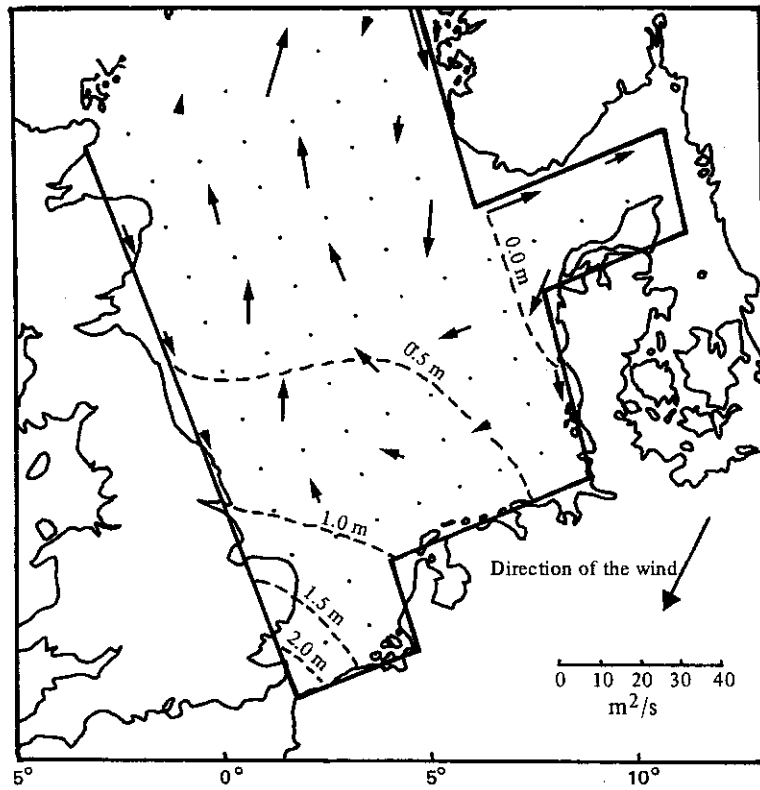
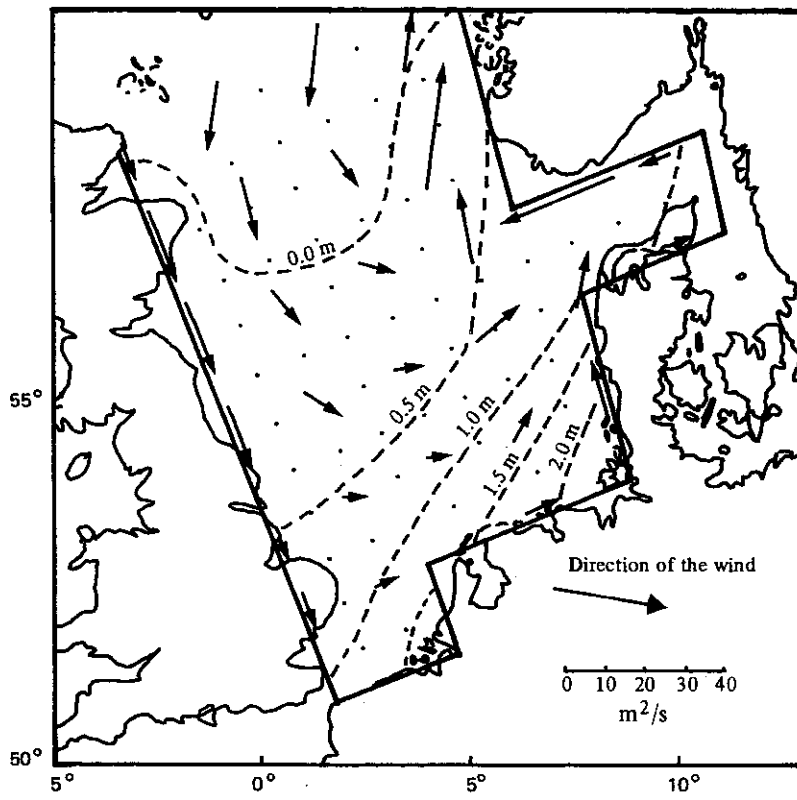


fig. 14.

Storm currents in the North Sea. (Fisher, 1959).

③ For storm surges, one generally assumes zero surface elevation along a line which follows the edge of the continental shelf, although this presumably induces spurious reflections at the Northern boundary and may limit the predictions to the first transit of the waves (Nihoul, 1973a). Extending the model further into the ocean does not seem to provide significant improvement as shown in fig. 15 where surge predictions obtained by Heaps (1969) with models (b) and (c) of fig. 12 (upper part) are compared.

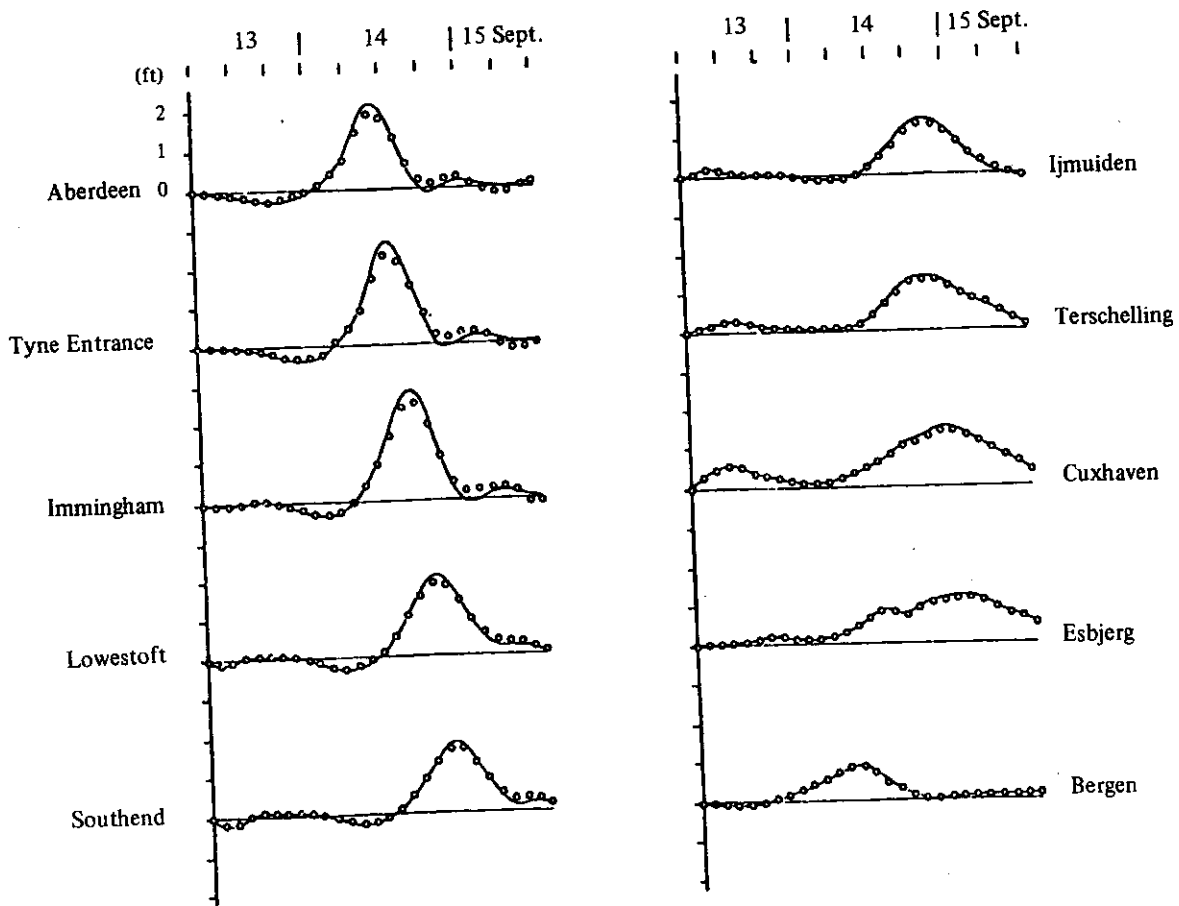


fig. 15.

Storm surge of 13 to 15 September 1956.  
 — Wind surge from model (b) [fig. 12];  
 ..... wind surge from model (c) [fig. 12].  
 (Heaps, 1969)

For tides, the Northern boundary must be chosen where the most realistic boundary conditions can be imposed. Its position is otherwise rather irrelevant.

**Non-linear interactions between tides and storm surges.**

The non-linear interaction between tides and storm surges is enhanced in shallow areas because of friction and more rapid spatial variations of  $U$ .

Fig. 16 shows the superposition of tidal and wind produced water elevations at Cuxhaven according to Hansen (1966).

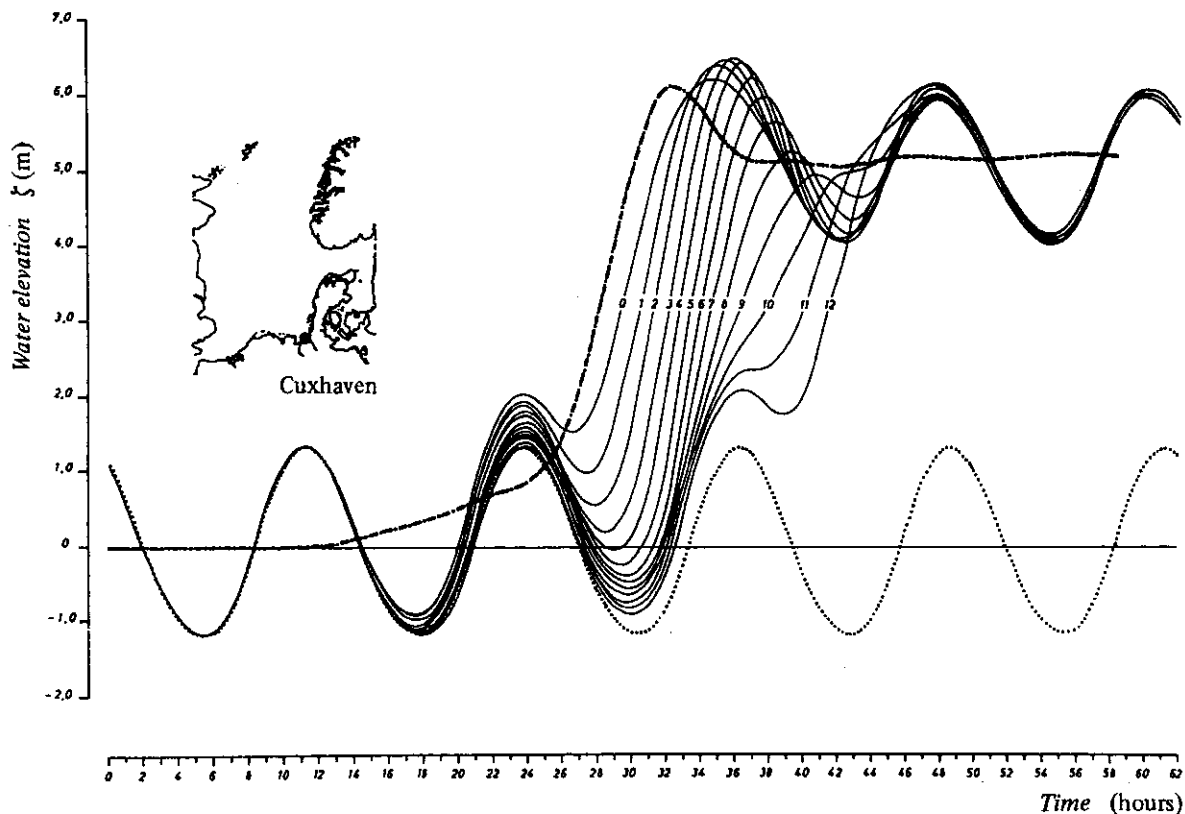


fig. 16.

The superposition of tidal and wind-produced water elevations. (Hansen, 1966).

(1) - - - - - Wind only.

(2) .....  $M_2$  tide only.

(3) ——— Non-linear superposition of curves (1) and (2) for phase differences of 0 - 12 hours.

A very interesting feature is the amplification of the surge at low tide as predicted by Proudman (1955). This effect which is associated with a reduction of the bottom friction is shown on fig. 17 (Banks, 1974).



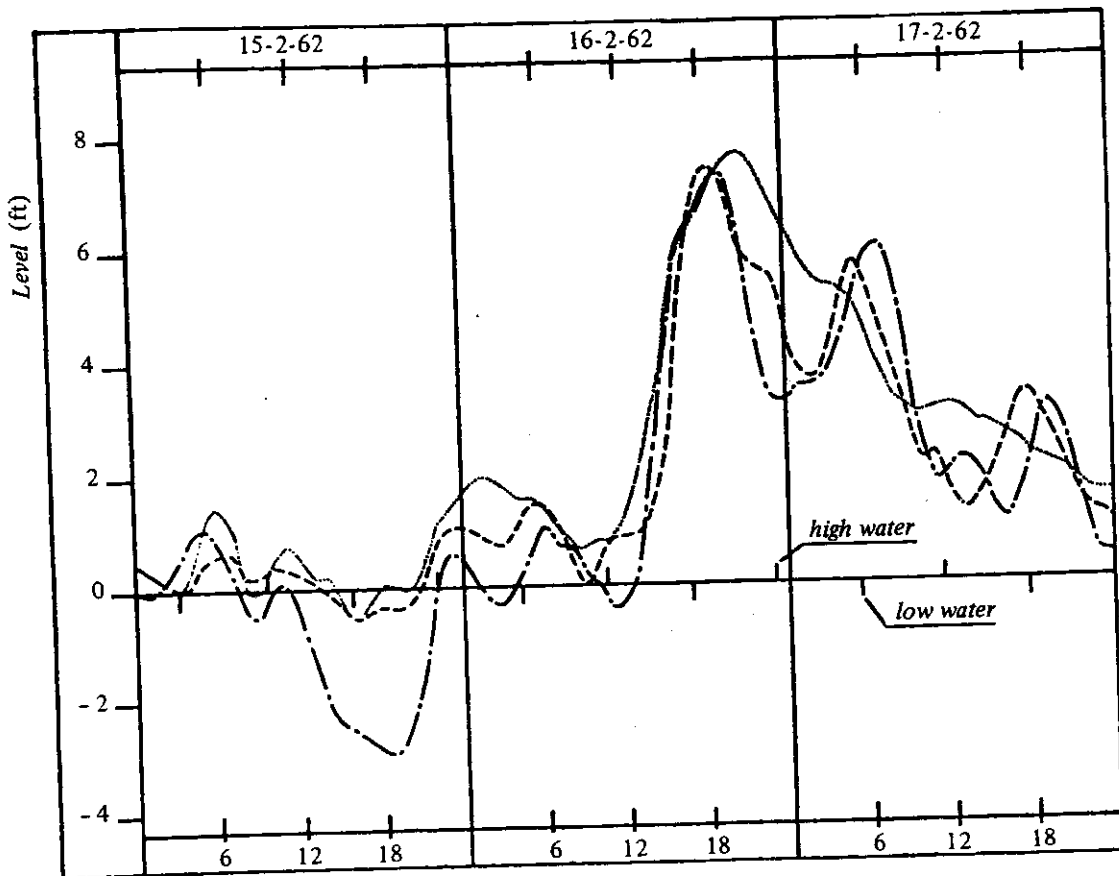


fig. 17.

Wind-induced surge levels at Southend during the period of the Hamburg surge. (Banks, 1974).

- Observed residual elevation after removal of the barometric surge.
- Surge level  $\zeta_{s.1}$  computed on the basis of wind and tide.
- ..... Wind surge  $\zeta_s$  computed in the absence of tide.

**Numerical techniques.**

Eqs (28) and (37) constitute a system of non-linear partial differential equations which must be solved for an arbitrary spatial geometry (irregular coasts and bathymetry). One cannot expect to find an analytical solution unless drastic simplifications are made.

Taylor (1920) studied the propagation of tidal waves in a narrow rotating gulf. In order to simplify the model and find an analytical solution, he neglected the friction term and all the non-linear terms. Lauwerier (1960) developed a linear depth-averaged model to investigate the highest sea elevation produced by an uniform wind field at the Dutch coast.

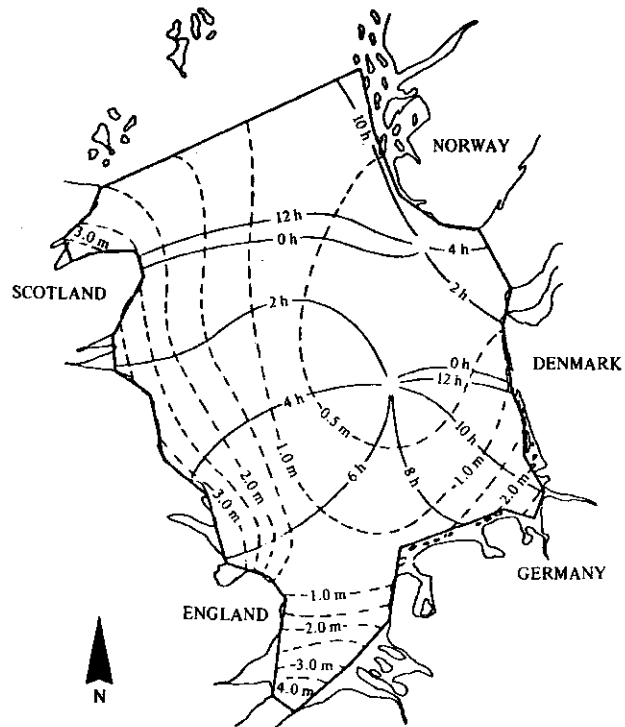
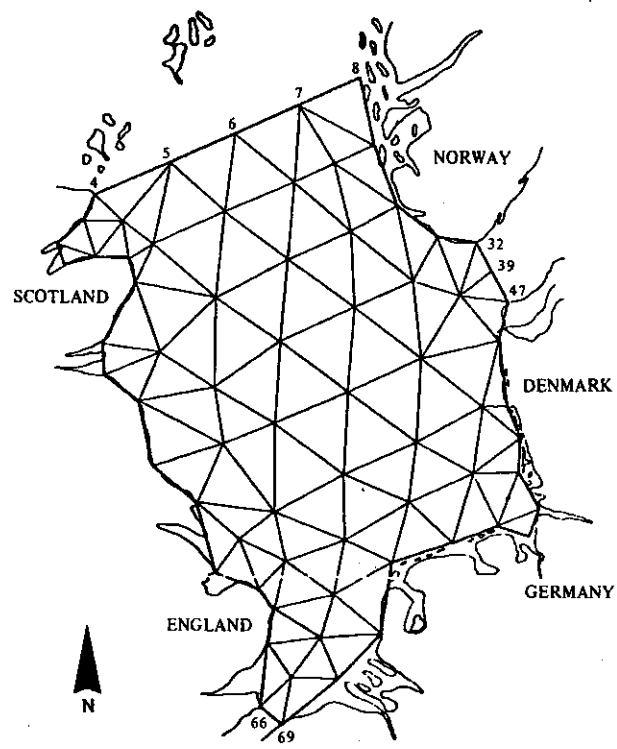


fig. 18.

Lines of equal phase and amplitude for the  $M_2$  tide calculated with a numerical model based on the finite elements method. (Grotkop, 1973).

These simple models provide interesting qualitative information but they are not precise enough to be an instrument of prediction of storm surges, tides, and drift of pollutants and nutrients. For these reasons, fully non-linear depth-averaged models must be used and numerical techniques are required.

① Finite elements.

In the field of solid mechanics, the finite elements method has been successfully used in the last decade. The problem of non-uniform meshes and complex boundary conditions is resolved with this technique. The usual way to formulate the finite elements method is by developing a variational principle. For solid mechanics, it is not difficult to find a true variational principle for stationary problems.

Hydrodynamic equations are more complicated than stationary equations of elasticity, moreover there is no true variational principle for non-linear motions of viscous fluids. Applications of the finite elements method to problems of wave propagations are rare. Fig. 18 shows the lines of equal phase and amplitude for the  $M_2$  tides obtained by Grotkop (1973) with a finite elements method in space and in time and an algorithm of resolution based on the Galerkin method.

- With the finite elements methods,
- α) there is no stability condition on the time step when the algorithm of resolution is implicit in space and in time;
  - β) the problem of non-uniform meshes is resolved.
- However,
- γ) as the algorithm is implicit in time and in space, a set of 18 algebraic equations must be solved for each elementary cell;
  - δ) the running time is very important. Grotkop (1973) showed that his method is slower than a classical finite differences method using an explicit scheme.

② Finite differences.

α) *Implicit schemes.*

An implicit scheme has often the advantage of imposing no condition on the time step in the integration of the equations of the model. However the ratio  $\Delta t/T$  has to be taken sufficiently small to reduce the error between the solution of the differential equations and that of the finite difference equations. The resolution of an initial boundary value problem with two spatial dimensions is quasi impossible with a fully implicit scheme because a too large system of algebraic equations must be solved at each time step. A semi-implicit method (alternative directions method) leads to good results, and is efficient when the geometry of the sea is simple. However the computer programme is very heavy and the time of computation becomes very long when the coastal line is irregular.

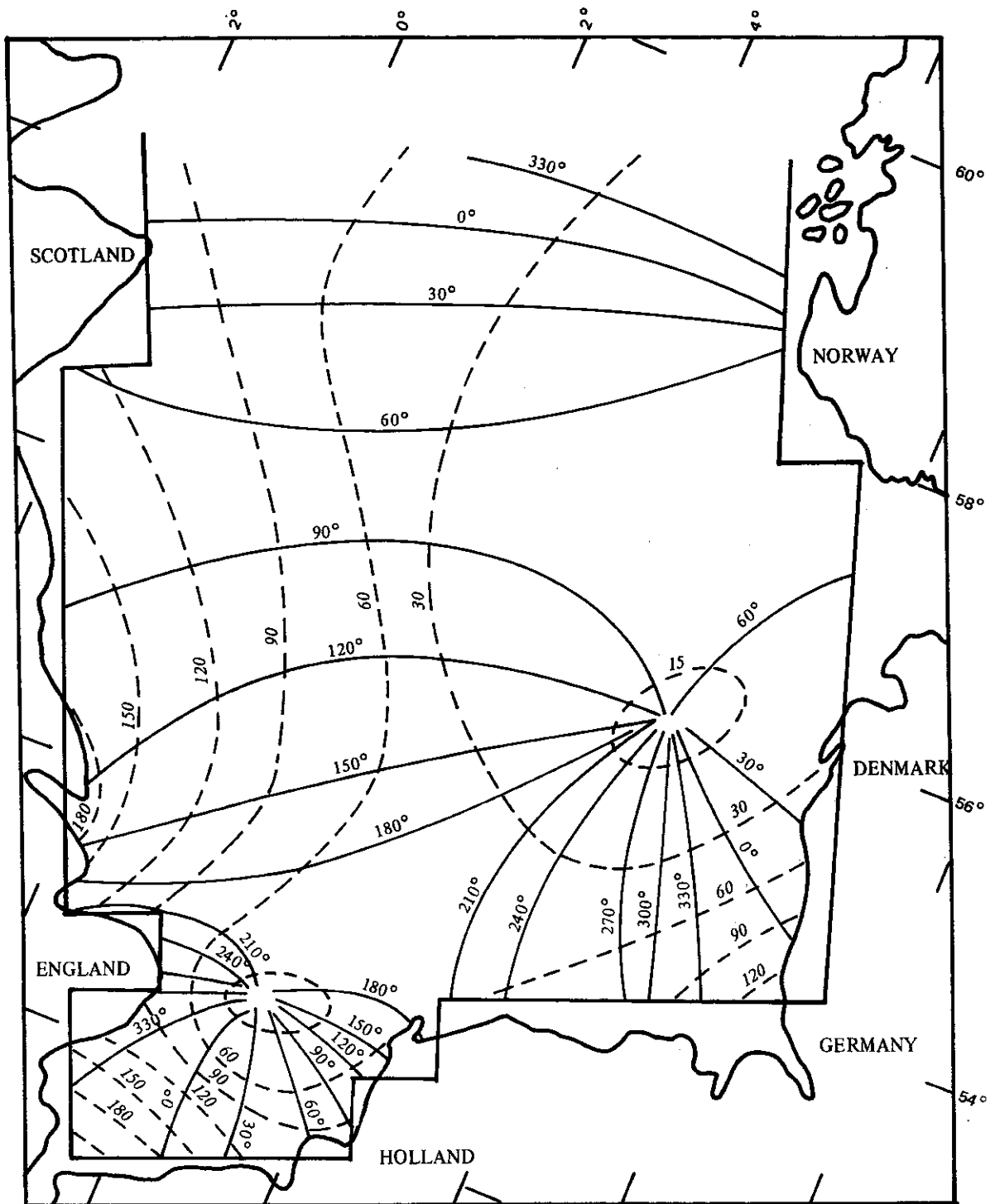


fig. 19.

Lines of equal phase and amplitude calculated with a numerical model based on the alternative directions method. The two components of the velocity and the sea elevation are calculated at the same grid point. (Marchuk et al., 1973).

Marchuk et al. (1973) developed an alternative directions method to solve tidal wave problems where the two components of the velocity and the sea elevation are calculated at the same grid point. Unfortunately there is a stability condition given in the linear case by :

$$(52) \quad \beta < \frac{1}{\sqrt{2}}$$

with

$$(53) \quad \beta = \sqrt{gh} \frac{\Delta t}{\Delta s}$$

(one assumes  $\Delta x_1 = \Delta x_2 = \Delta s$ )  $\Delta t$  and  $\Delta s$  are respectively the time and space intervals.

Fig. 19 shows the lines of equal phase and amplitude for the  $M_2$  tide obtained by Marchuk et al.

Leenderste (1967) applied an alternative directions method to study the tide in the Southern North Sea. Fig. 20 shows the lines of equal phase and equal amplitude for the tide in the Southern Bight. The three state variables ( $\bar{u}_1$ ,  $\bar{u}_2$  and  $\zeta$ ) are calculated at three different grid points. This scheme has no condition of stability on  $\Delta t$ , but  $\Delta t/T$  must remain small for consistency and to limit phase and amplitude deformations of the solutions. Ronday (1976) showed that the solution of the linearized model has no amplitude deformation and that the phase shift for the physical modes is given by

$$(54) \quad \Delta\Phi \sim A \operatorname{tg} \beta \sqrt{\vartheta_1^2 + \vartheta_2^2}$$

$$\text{with} \quad \vartheta_1 = 2\pi \frac{\Delta s}{L_1} \quad ; \quad \vartheta_2 = 2\pi \frac{\Delta s}{L_2}$$

$L_1$  and  $L_2$  represent the wave lengths in the  $x_1$  and  $x_2$  directions.

From the relation (54), one understands that the time step must remain small when a small phase deformation is imposed. The advantage of having no condition on  $\Delta t$  for the stability of the scheme cannot be exploited when a limited phase shift is imposed.

### $\beta$ ) *Explicit schemes.*

All the explicit schemes have a condition of stability : the critical time step is a function of the maximum depth, of the maximum velocity of the current and of the spatial step. According to the discretization in space and time, one gets different stability conditions.

The physical space is covered with a numerical grid. Most of hydrodynamic models are based on the staggered grid given in fig. 21. Jensen et al. (1966), Hansen (1966), Brettschneider (1967), Leendertse (1967), Ronday (1973, 1976), Durance (1976), Dunn-

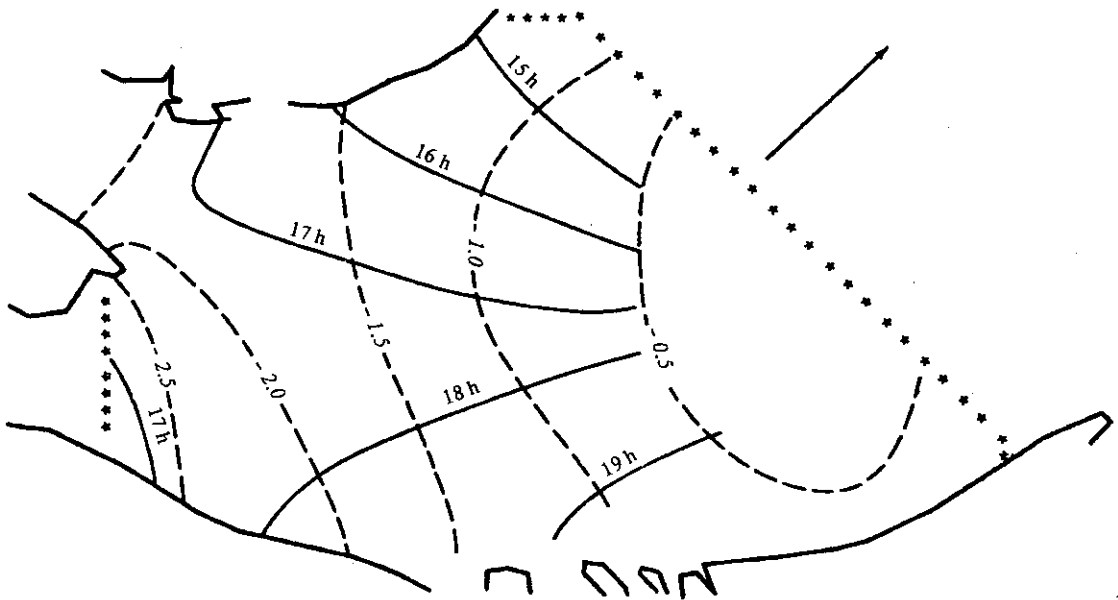
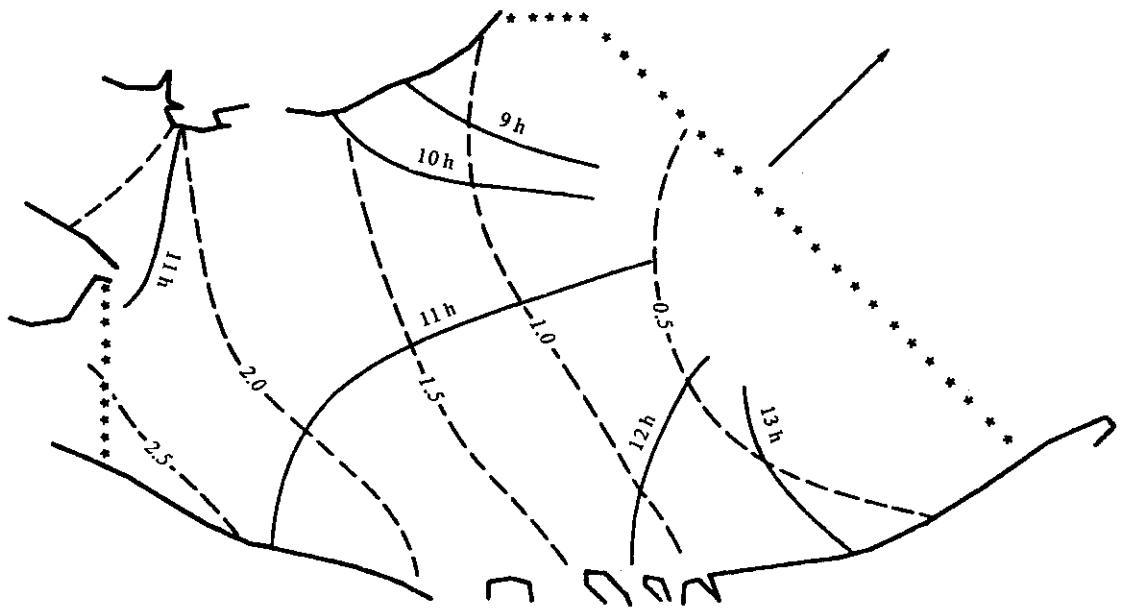


fig. 20.

Lines of equal phase and amplitude calculated with a semi-implicit scheme.  
 The sea elevation and the two components of the velocity are not calculated  
 at the same grid points. (Leendertse, 1967).

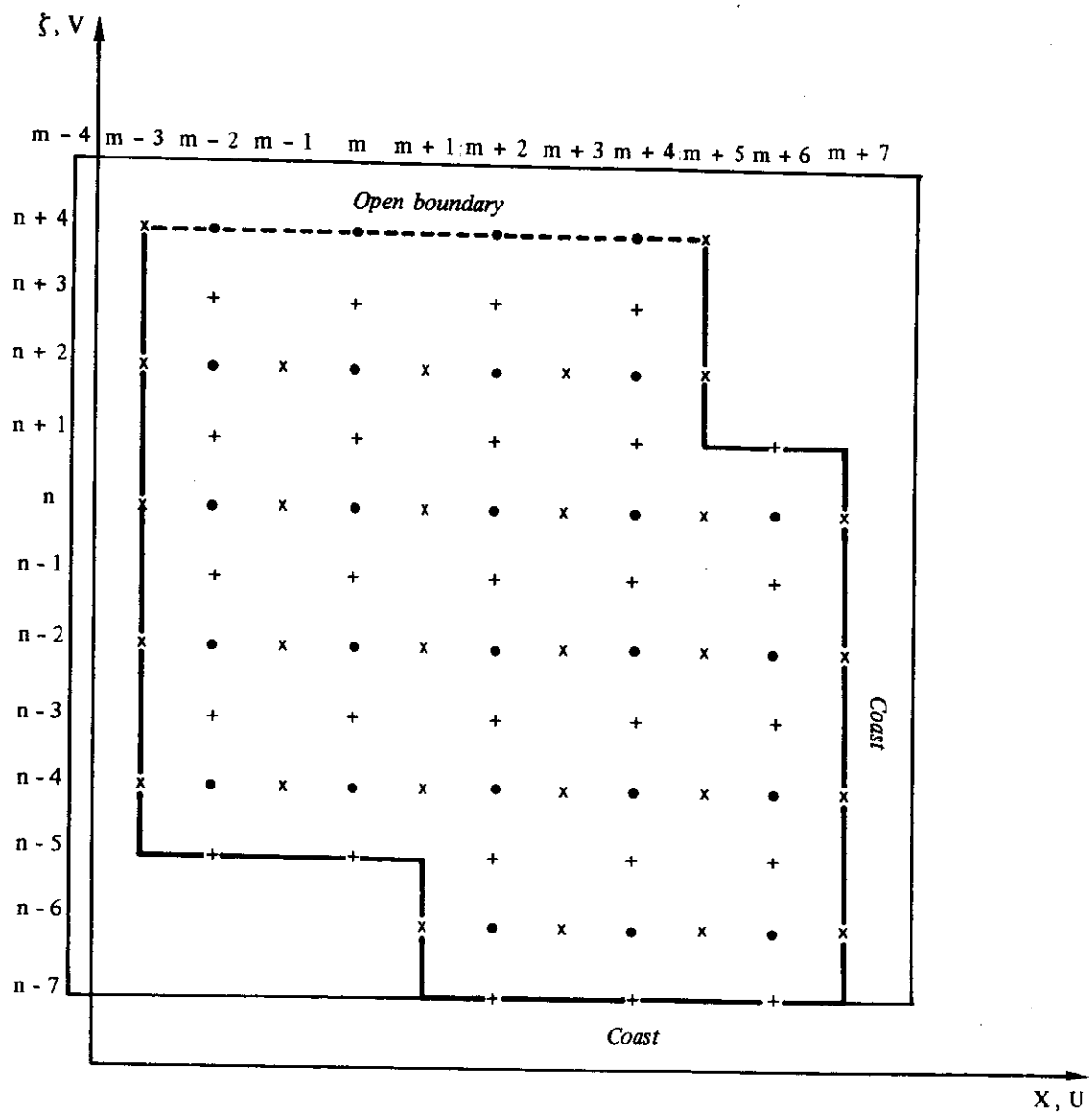


fig. 21.

The classical staggered grid used for depth-averaged models (Ronday, 1973)  
 • Point  $\xi$     + Point  $V$     x Point  $U$

Christensen (1974) and others have used this grid because the expression of the coastal boundary conditions is very simple.

Ronday (1976) established the following stability criterion :

$$(55) \quad 2 \beta^2 + 2 (\alpha + \delta) \leq 1$$

with

$$\alpha = u_0 \frac{\Delta t}{\Delta s} \quad ; \quad \delta = v_0 \frac{\Delta t}{\Delta s}$$

$u_0$  and  $v_0$  are the two components of the maximum current.

For the physical modes, Ronday (1976) showed that the wave deformation is, in amplitude :

$$(56) \quad A \sim 1 - \frac{1}{2} \left\{ \pm \beta \sqrt{\vartheta_1^2 + \vartheta_2^2} (\alpha \vartheta_1 + \delta \vartheta_2) + \vartheta_1^2 (\alpha - \alpha^2) + \vartheta_2^2 (\delta - \delta^2) - 2 \alpha \delta \vartheta_1 \vartheta_2 \right\}$$

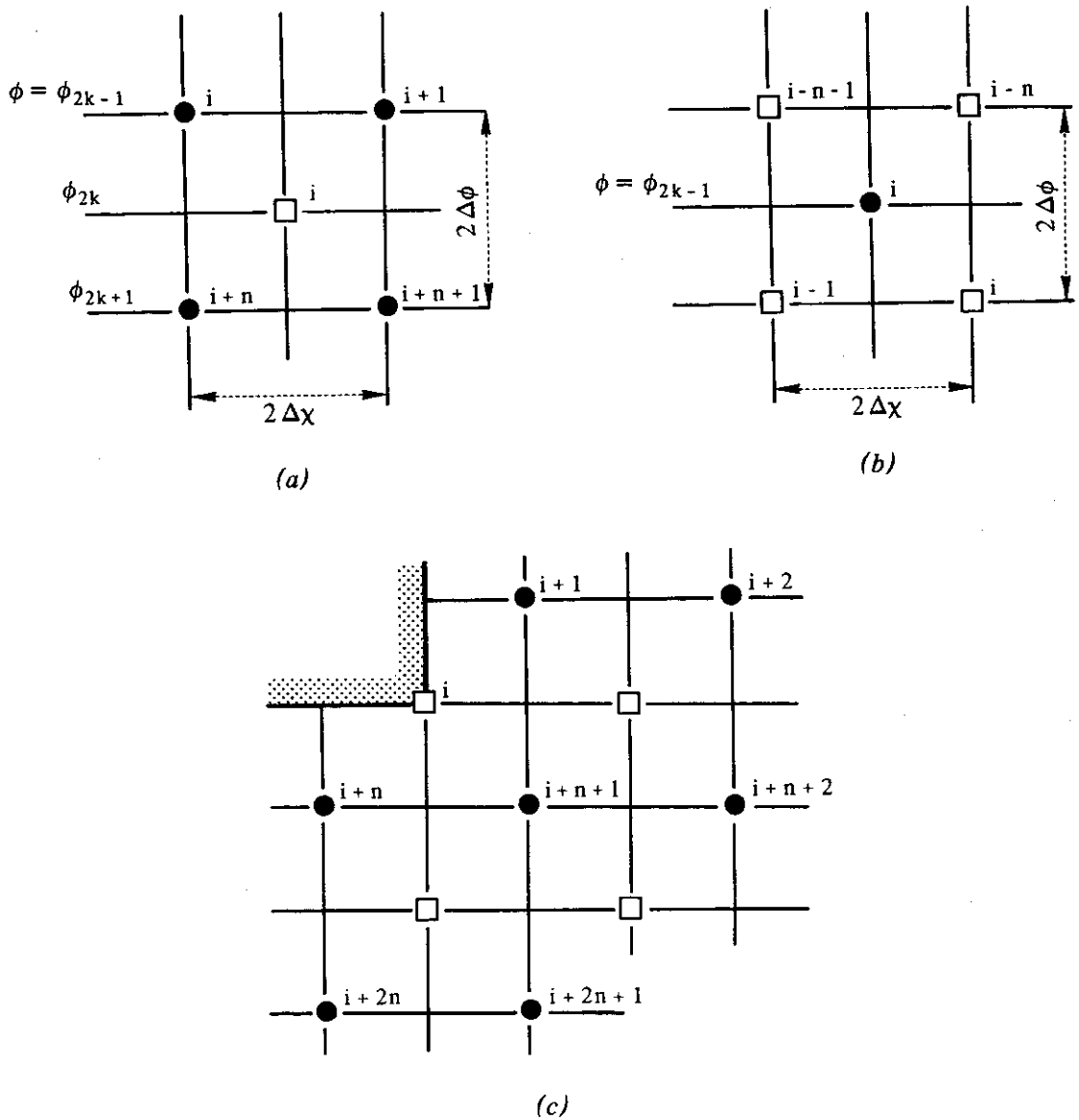


fig. 22.

Interior grid points.

- (a) Elevation points surrounding stream point  $i$ ;
- (b) Stream points surrounding elevation point  $i$ ;
- (c) Stream point  $i$  at a corner formed by a  $90^\circ$  sector of land in the quadrant North to West.



in phase :

$$(57) \quad \Delta\Phi \sim \pm A \operatorname{tg} [\beta \sqrt{\vartheta_1^2 + \vartheta_2^2} \mp (\alpha\vartheta_1 + \delta\vartheta_2)]$$

In the linear case there is no deformation in amplitude because  $\alpha$  and  $\delta$  are equal to zero. The phase shift is in this case :

$$\Delta\Phi \sim \pm A \operatorname{tg} \beta \sqrt{\vartheta_1^2 + \vartheta_2^2}$$

The phase deformations given in eqs (54) and (57) are thus the same. The limitation of the phase deformation to an acceptable value determines the choice of the time step. (A small  $\Delta\Phi$  leads to a small time step). In most cases,  $\beta^2$  must be smaller than  $1/2$ ; for this reason, an unconditionally semi-implicit scheme does not benefit from the advantage of no condition on  $\Delta t$ .

Heaps (1969) and Banks (1974) used another spatial grid where the two components of the velocity are calculated at the same grid point. [The grid used by Heaps (1969) is given in fig. 22.] Runday (1976) showed that the wave deformations obtained using Heap's or Hansen's grid were equal. Moreover the formulation of the boundary conditions with Heap's grid have compelled Heaps and Bank to introduce a parameter of identification.

#### *$\gamma$ ) Influence of the geometry of the basin.*

The principle of finite differences or finite elements method is to cover the area of interest with a numerical grid. In many problems, sea elevations and depth averaged currents are required along or near the coastal line. For this reason, the numerical grid must fit the coast as well as possible.

Fig. 23 shows that the results for the inner part of the basin strongly depend on the global shape of the grid. Better the grid fits the coasts, more precise the results are.

#### *$\delta$ ) Influence of the choice of the spatial step.*

Most of the hydrodynamic models of the North Sea (e.g. Hansen, 1966) used a fixed space interval. Runday (1976) showed that the error on the first derivative with a fixed space interval (of about 30 km) is of the order of 5%. In order to reduce this error, one has to introduce spherical coordinates when the dimensions of the basin are of the order of 1000 km and when the area of investigation lies at high latitude ( $50^\circ$  and more).

Eqs (54) and (57) show that the error on the amplitude and on the phase is very sensitive to the choice of  $\Delta s$ . Moreover it is difficult to interpolate between grid points and especially near the coast for large space intervals.

Figures 24 and 25 show the lines of equal phase and amplitude for the  $M_2$  tides in the cases  $\Delta s \sim 148$  km (Brettschneider, 1967) and  $\Delta s \sim 20$  km (Runday, 1976).

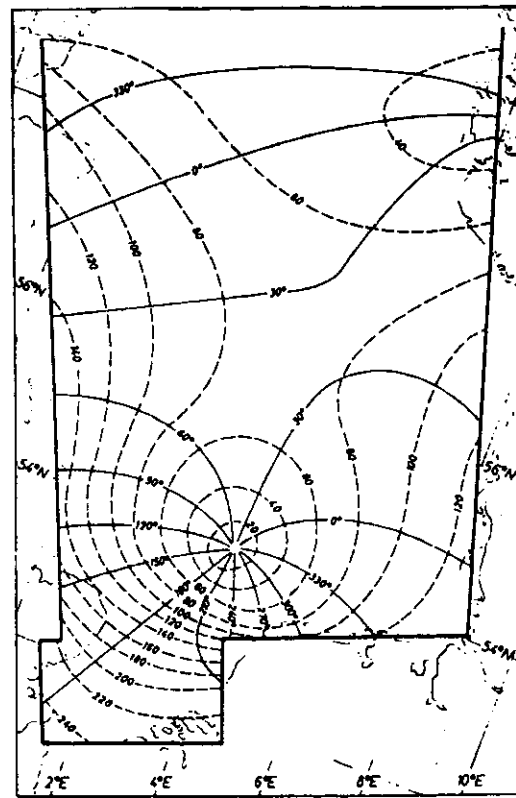
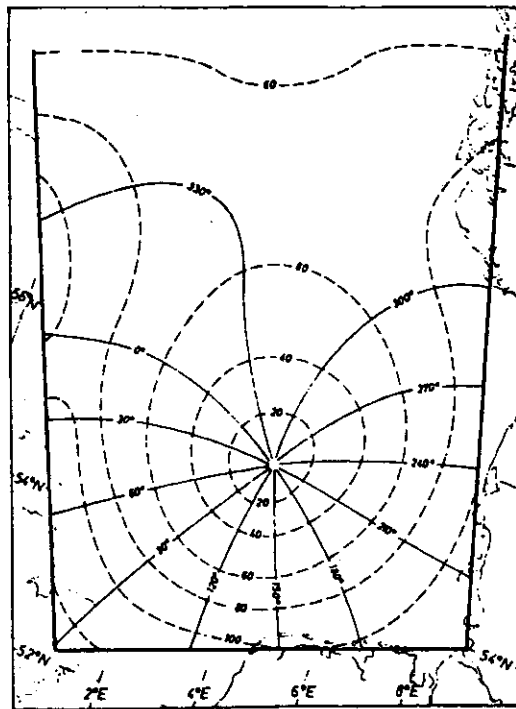


fig. 23.

Influence of the geometry of the basin. (Hansen, 1966).

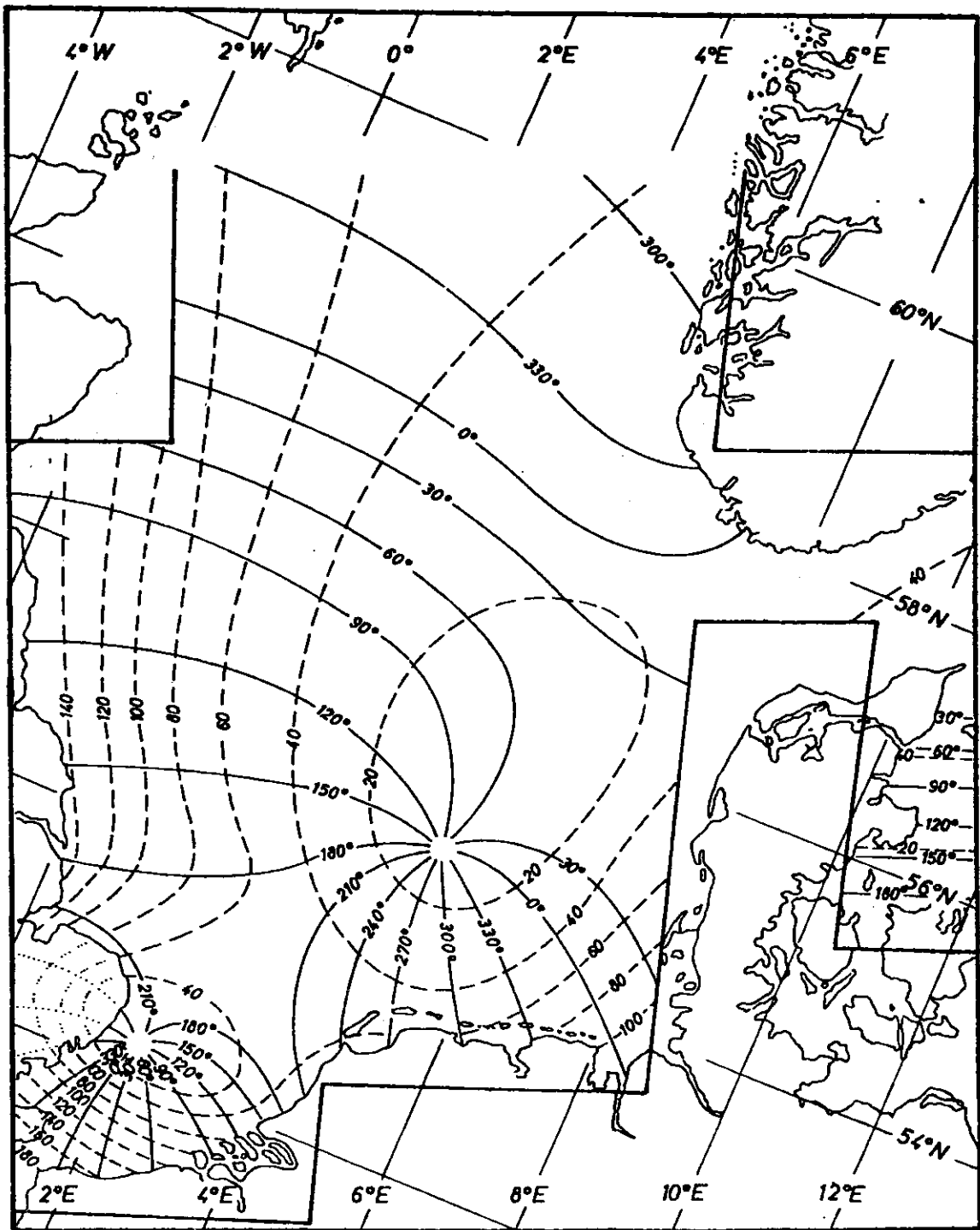


fig. 24.

Lines of equal phase and amplitude calculated with a numerical model based on cartesian coordinates. (Brettschneider, 1967).

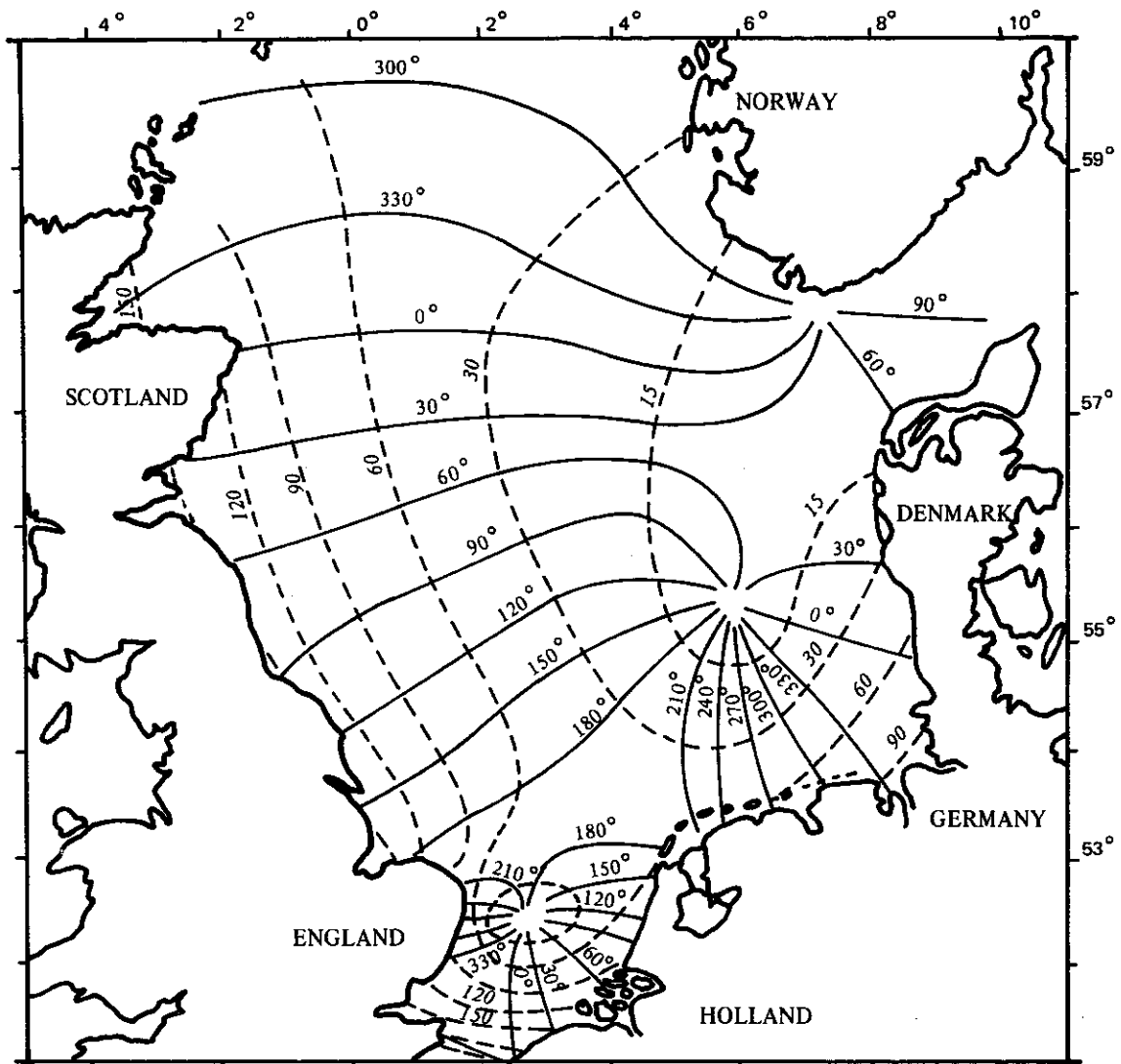


fig. 25.

Lines of equal phase and amplitude calculated with a numerical model based on spherical coordinates ( $\Delta\lambda = \Delta\Phi = 10^\circ$ ). (Ronday, 1976).

In the North Sea, the observations (fig. 26a) show a phase variation for the  $M_2$  tide of  $120^\circ$  on a distance of 100 km along the East Anglia coast. To reduce the phase error on the current and on the sea elevation, one must use a small space step. A model for the whole North Sea based on a space interval of about 5 to 10 km would require an important memory occupation and a small time step. One avoids such a problem by using two models : one for the whole North Sea with a coarse grid which provides data at the Northern boundary of another model characterized by a small space interval (figures 25 and 26b).

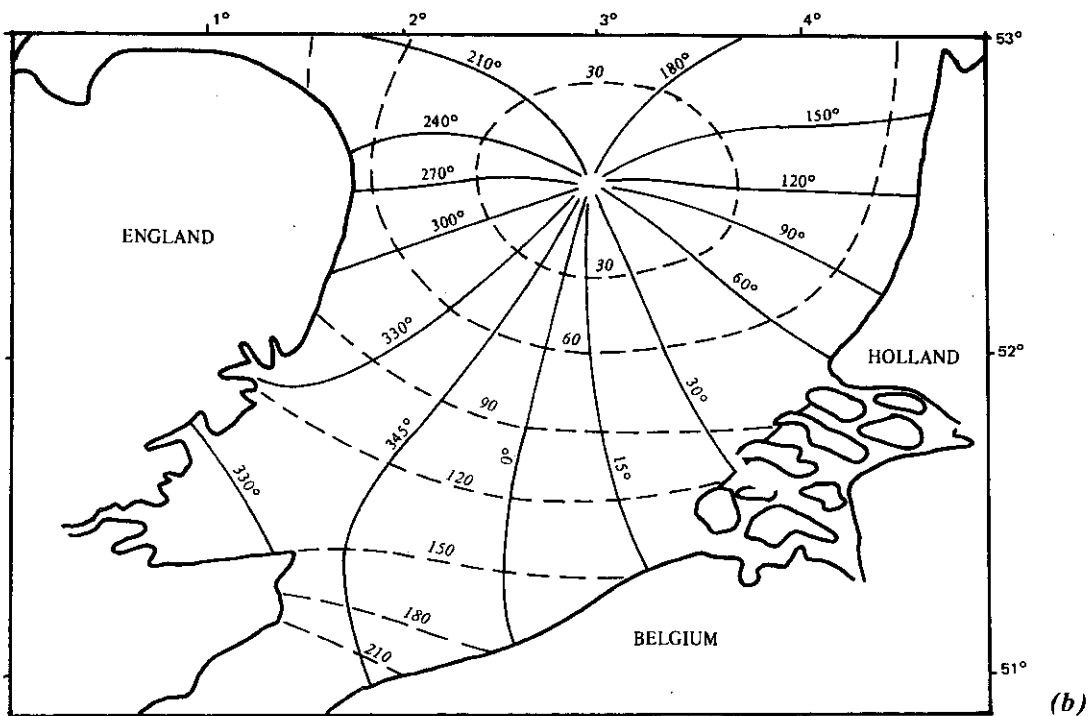
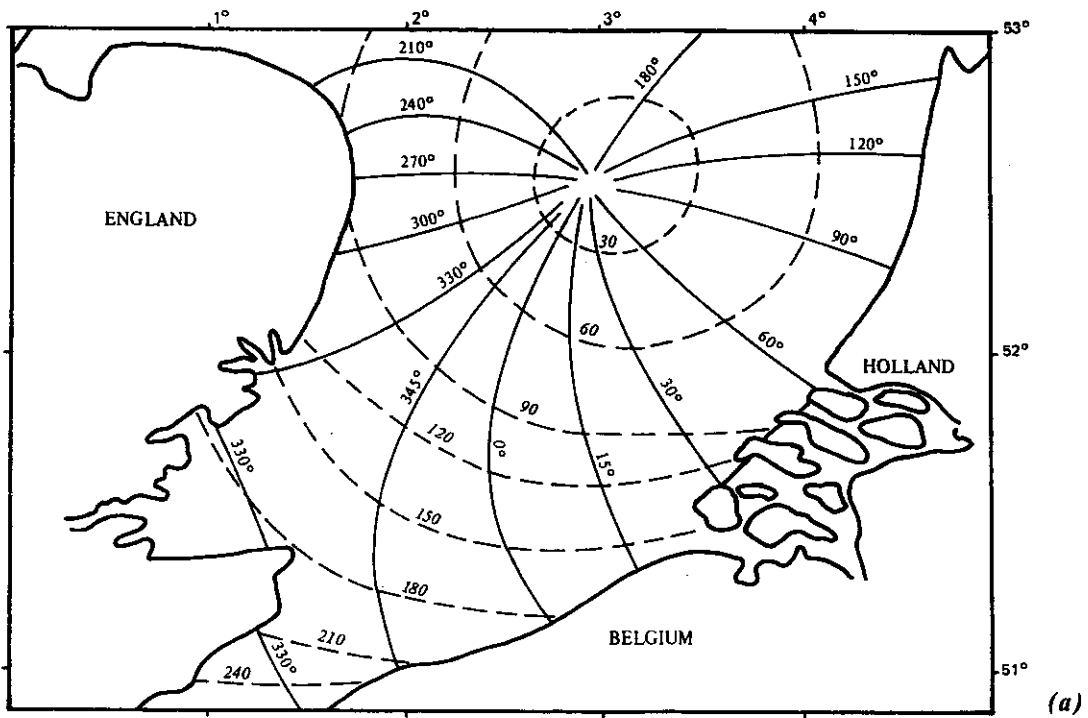


fig. 26.

Lines of equal phase and amplitude for the  $M_2$  tide  
 (a) deduced from the observations (Admiralty Chart 301);  
 (b) calculated with a numerical model (Ronday, 1976).

## 7.- Recent developments in two-dimensional mesoscale modelling.

The discussion, in the last section, has been, on purpose, limited to the first generation of operational depth-averaged models of tides and storm surges in the North Sea.

The achievements and limitations of these models have been emphasized, showing both a solid mathematical foundation and weaknesses related to such problems as coastal irregularities (geometry of the coast and bathymetry), inadequate open-sea boundary conditions and coarse meteorological data.

The models which have developed in the line of the pioneers were thus, in a first stage, essentially concerned with specific improvements, increasing the forecasting ability of the models rather than revising their structures and substructures.

Prandle's model of storm surges in the southern North Sea and River Thames (Prandle, 1975) consists of two parts dynamically interfaced, a one-dimensional representation of the River Thames together with a two-dimensional representation of that part of the North Sea south of latitude  $53^{\circ} 20'$ . The model is used to simulate the surge of January-February 1953. It is shown that the major surge component along the east coast of England is that propagating from the northern North Sea, whereas along the Dutch coast the major component was due to the wind effect over the southern North Sea. The effect of deploying a storm barrier on the Thames is examined and it is shown that the amplitude of the reflected wave from the barrier is negligible at Southend.

Observations of storm surges in the River Thames show that surge peaks tend to occur on the rising tide and seldom, if ever, occur on high tide. This tendency has been attributed to the interaction between tide and surge propagation as described by the non-linear terms in the associated hydrodynamic equations.

Prandle and Wolf (1978) show that an important component of interaction originates outside of the river and they develop a method of identifying interaction in the southern North Sea involving the use of two hydrodynamic numerical models, one simulating tidal propagation and the other surge propagation. Operating these models concurrently, the coupling between tide and surge is introduced by perturbation terms which represent the influence in either model of sea levels and velocities computed by the other. This approach is used to simulate the pattern of interaction which occurred during the storm surge of 30 January to 2 February 1953. It is shown that interaction in the southern North Sea results primarily from the quadratic friction term, developing significantly in the coastal region off Lowestoft as far south as the Thames estuary due to the high velocities associated with both tide and surge propagation in that area. Changes in the surface elevation of tide and surge due to the effects of interaction may develop rapidly in certain localised regions such as the Thames estuary. They may also be longer period changes of the order of the duration of the storm due to a systematic displacement of the  $M_2$  tidal regime.

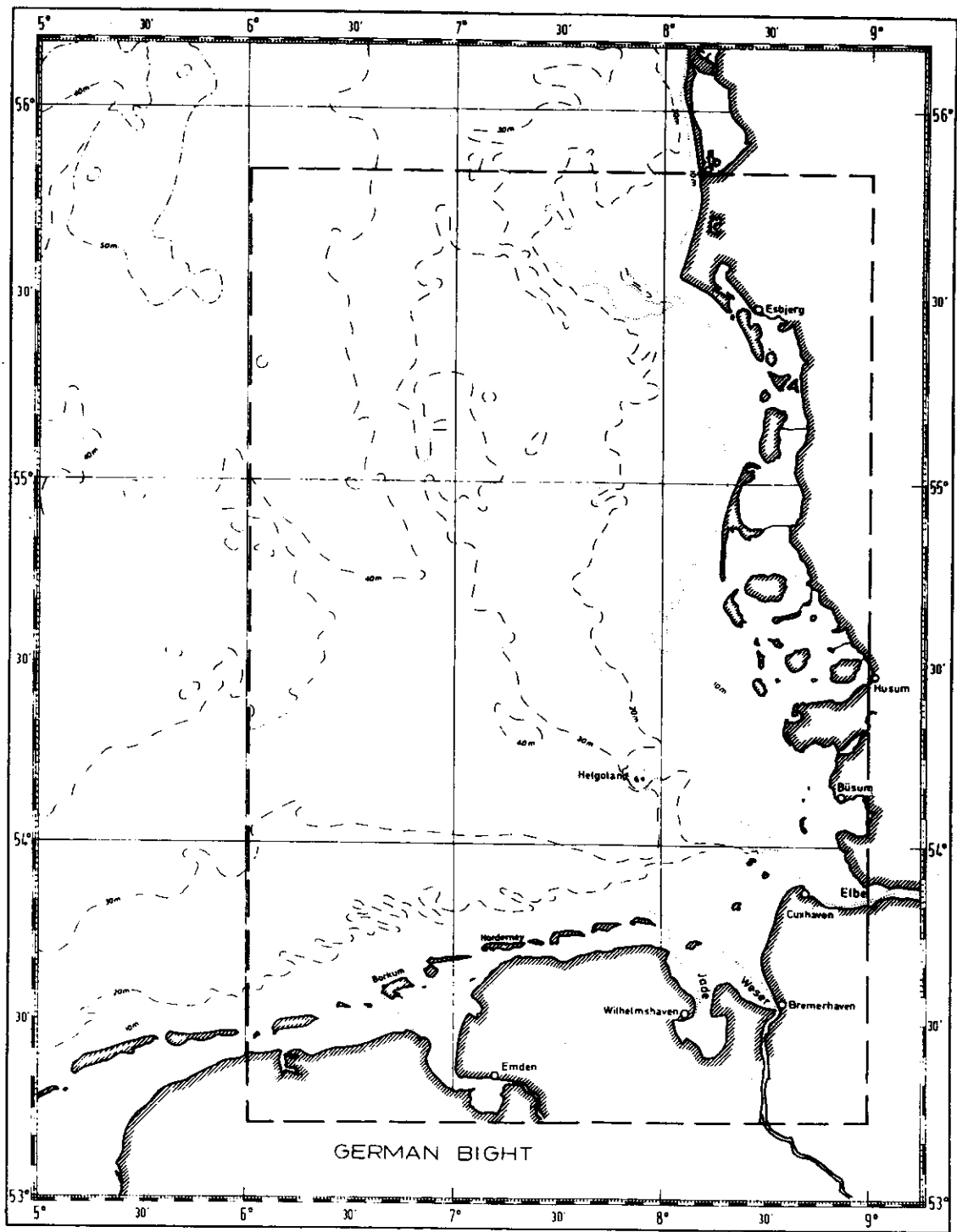


fig. 27.

Map of the German Bight, indicating the area covered by Backhaus' three-layer model. (Backhaus, 1979).

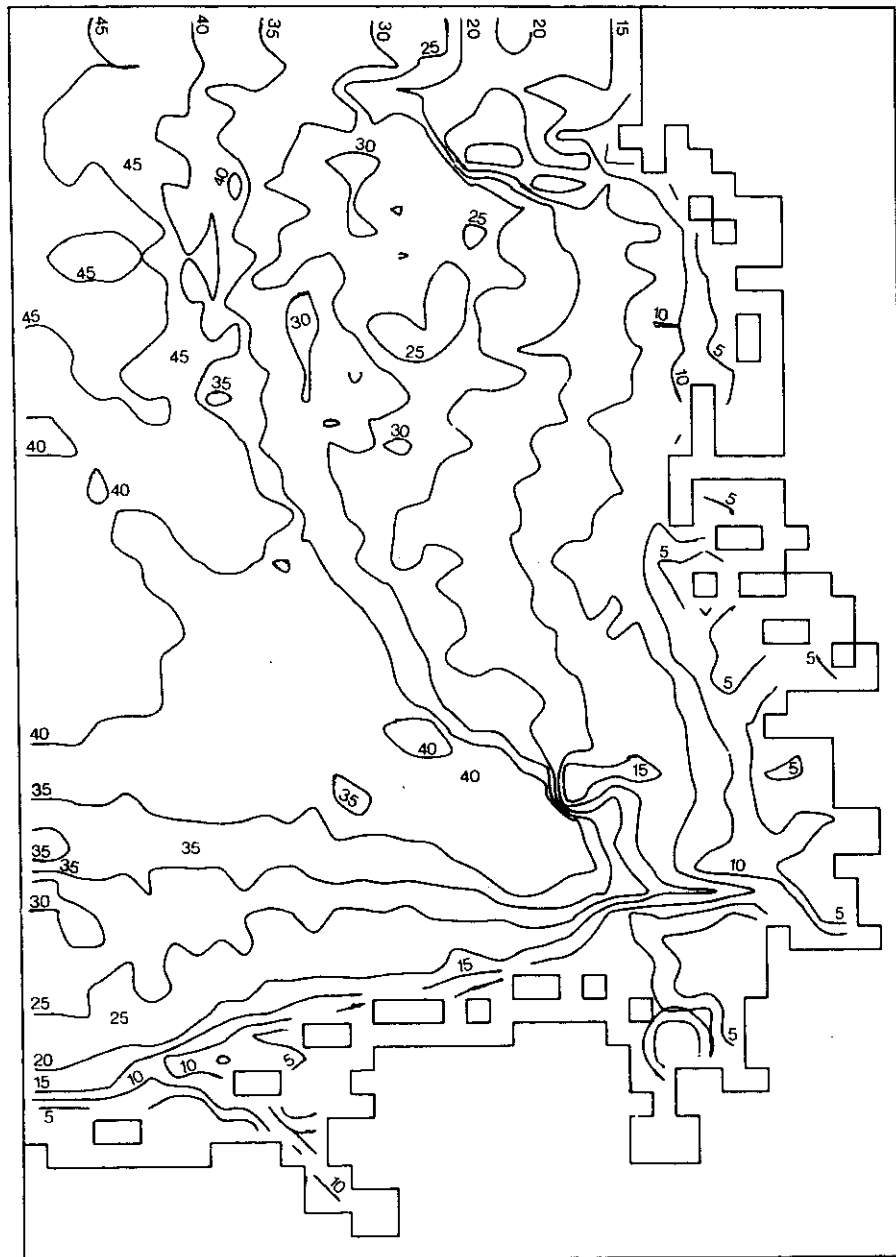


fig. 28.

Depth (m) contours of discretized bottom topography. (Backhaus, 1979).

In coastal areas, models must have a high resolution to take into account the marked variations of depth and the geometry of the coast. The cost of operating fine mesh models however restrict their applications to limited regions with inevitably a large portion of open-sea boundary.



Backhaus' three-layer model of the German Bight (Backhaus, 1979) [fig. 27] has a horizontal grid resolution of three nautical miles to approximate the complex bottom topography (fig. 28). [The largest system of coastal drying banks, which exists in the entire North Sea region, in combination with small islands, is to be found along the coast of the German Bight. Water depths vary between 45 m below mean sea level and 2 m above mean sea level (drying banks) in coastal waters.]

In this case, *water levels are prescribed on the open-sea boundary* (fig. 27) and, for all layers, the gradient of the flux normal to the boundary is assumed to be zero.

The lack of reliable open-sea boundary data is, in many cases, a severe handicap for high resolution coastal models. Several authors have thus attempted to determine the appropriate boundary conditions by running one or several larger scale, larger mesh models extending finally to the whole North Sea or even the whole continental shelf (e.g. Ramming, 1976, 1978; Ronday and Nihoul, 1978, 1979; Clément et al., 1981).

This method, however, is not beyond reproach. Whether one deals with a single nested model or with superimposed models of different grid sizes, the regions of transition from one mesh to another are sources of numerical errors which may spoil the advantages of the higher resolution in the coastal area.

An interesting, rather different, approach to coastal problems is the irregular-grid finite-difference technique proposed by Thacker (1979). Finite-difference computations on irregular grids offer the advantages of resolving the coastal curvature and of allowing for an explicit time step of optimal size. A further advantage is the flexibility associated with editing the grid, which allows for improvements in its design. The techniques are based on the approximation of partial derivatives with slopes of planar surfaces associated with triangular components of the irregular grid.

The sensitivity of hydrodynamic models to open-sea boundary conditions was studied by Davies (1976a), using a two-dimensional numerical model of the North Sea, including the Skagerrak, the Kattegat and the eastern part of the English Channel. This model has a resolution of  $1/9^\circ$  in latitude and  $1/6^\circ$  in longitude. The open boundaries correspond to those monitored during JONSDAP '76 (Joint North Sea Data Acquisition Program 1976). Thus, the open boundary in the north runs along the line between Wick and position  $59^\circ 20' N$ ,  $0^\circ 0' W$ , and then along latitude  $59^\circ 20' N$  between this point and the Norwegian coast. The southern open boundary is the line of longitude crossing the English Channel at  $2^\circ W$ . The southern end of the Kattegat is a very shallow region, and has been considered as closed (fig. 29).

The model is used to determine the amplitude and phase of the  $M_2$  component of tide over the whole sea region and the results are compared with values of amplitude and phase for  $M_2$  derived from the tidal analysis of observations at a number of coastal stations and off-shore points. Good agreement between observed

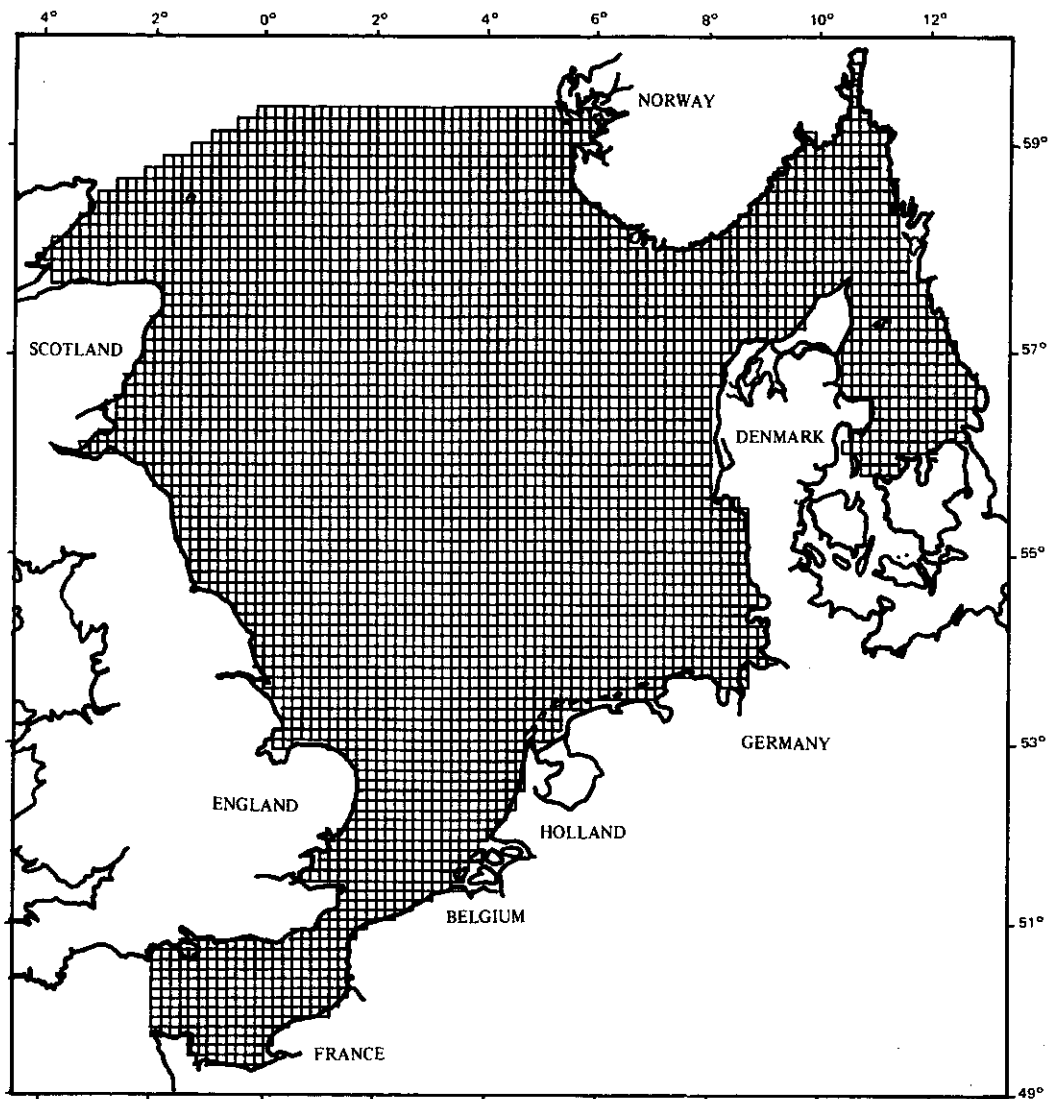


fig. 29.

North Sea model finite difference grid. (Davies, 1976a).

and calculated results is obtained throughout the whole region, with some deterioration, however, in areas where bottom topography is known to be very complex – particularly near Cuxhaven where there are a large number of drying banks and deeper channels unresolved by the numerical grid. Since observational tidal data is not yet available along the open boundaries of the model, with the exception of one record from an off-shore tide gauge at  $59^{\circ} 18' N$ ,  $0^{\circ} 3' W$ , required boundary values of  $M_2$  amplitude and phase are obtained from an examination of cotidal charts (Hydrographic Department, Admiralty, England : chart n<sup>o</sup> 5058 and the German chart, Oberkommando der Kriegsmarine [1942] : Karten der

harmonischen Gezeitenkonstanten für das Gebiet der Noordsee) and from consideration of the output derived from a larger numerical tidal model of the entire north-western European shelf (Flather, 1976a).

The model is also used to examine the sensitivity of its tides to changes in boundary input. The main purpose here is to find out if any particular sections of the boundary play a more important role than others in determining the tidal distribution within the model, and to use this information to decide where to concentrate the off-shore measurements of sea surface elevation in the JONSDAP '76 experiment. The sensitivity analysis also helps to understand some of the discrepancies between the observed North Sea tides and those produced by the numerical model. It turns out that the tides prescribed along the section of northern open boundary close to the Norwegian coast are quite important in determining the overall tidal distribution in the North Sea and certainly have a large influence on the tidal regime within the Skagerrak and Kattegat. The tides specified along the section of open boundary close to Wick are of special importance in determining the amplitude and phase of the tide down the east coast of Great Britain.

Extending their tidal models to the calculation of storm surge elevations and currents, Davies (1976b) and Flather (1976b) undertook a series of hindcasting exercises, running the two models simultaneously to simulate the same surges and comparing the results. These exercises helped to clarify several aspects of storm surge modelling and, in particular, the influence of the location of open-sea boundaries and of the associated boundary conditions and the effect of reducing the mesh size, with a subsequent better representation of depth variations, in shallow coastal regions.

The boundary conditions imposed at the sea surface (air pressure, wind stress) were first deduced from meteorological observations. A different scheme, employing numerical finite difference models of the atmosphere and of the sea, was presented by Flather and Davies (Flather and Davies, 1975, 1976; Flather, 1979 [fig. 30]).

The atmospheric model, the Bushby-Timpson 10-level model on a fine mesh, used in operational weather prediction at the British Meteorological Office (Benwell et al., 1971) provides the essential forecasts of meteorological data which are then used in sea model calculations to compute the associated storm surge. The basic sea model, having a coarse mesh, covers the whole of the north-west European continental shelf.

A similar procedure, based on the hydrodynamic model developed by Nihoul and Ronday (Ronday, 1976), is followed by Adam for the "Belgian Real-Time System for the Forecasting of Currents and Elevations in the North Sea" (Adam, 1979 [figs 31a,b]).

Recent two-dimensional mesoscale models differ essentially from earlier models by a better representation of boundary conditions, on open-sea boundaries, at the coast, at the sea surface and also at the bottom. A better parameterization of bottom friction and other non-linear effects has led to more realistic models able to forecast together tides and storm surges or different tidal components (e.g. Flather, 1979; Adam, 1979; Ronday, 1979; Pingree and Griffiths, 1978, 1981a,b).

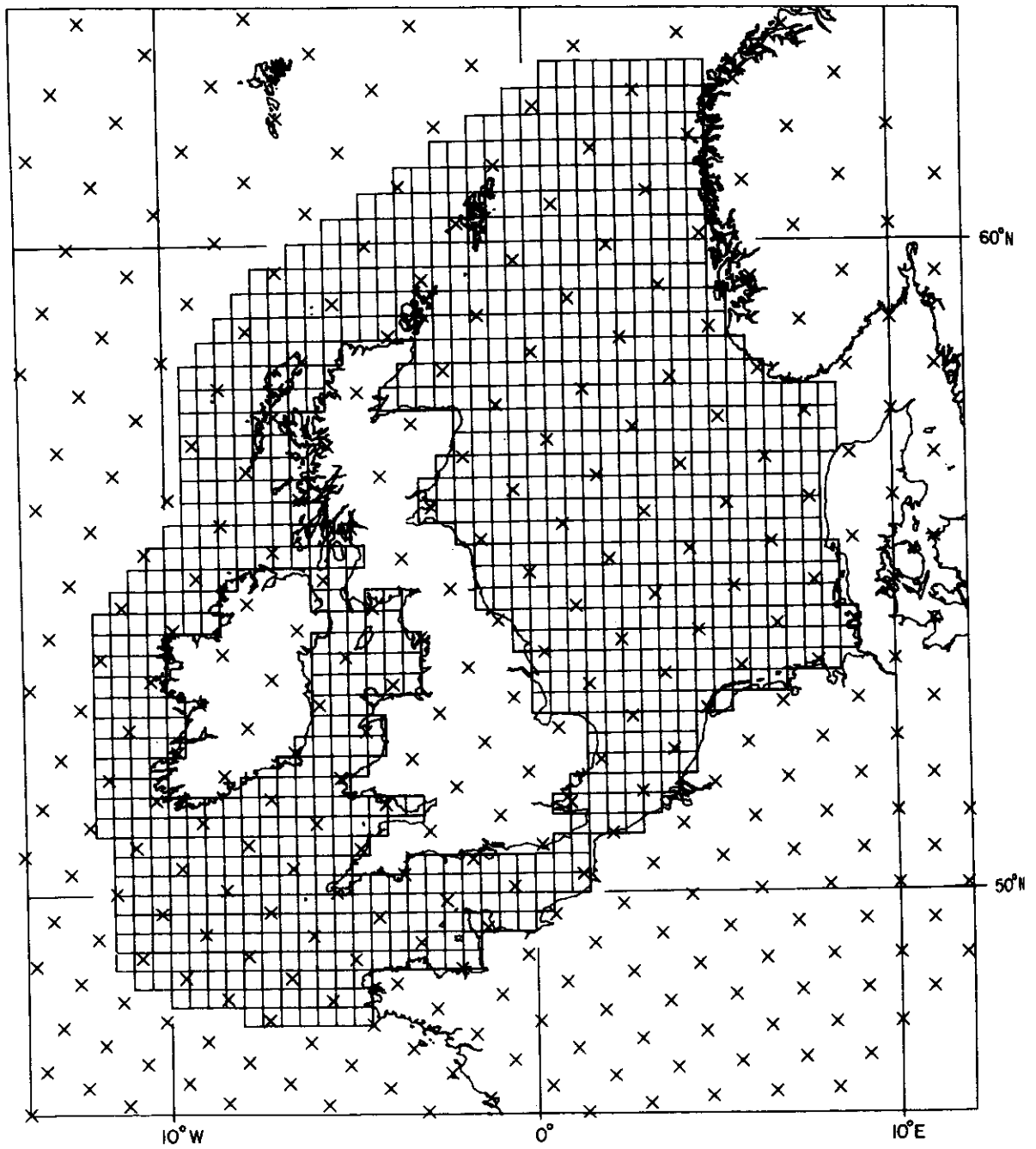


fig. 30.

Finite difference mesh of the continental shelf sea model with grid points (x) of the 10-level model of the atmosphere. (Flather, 1979).

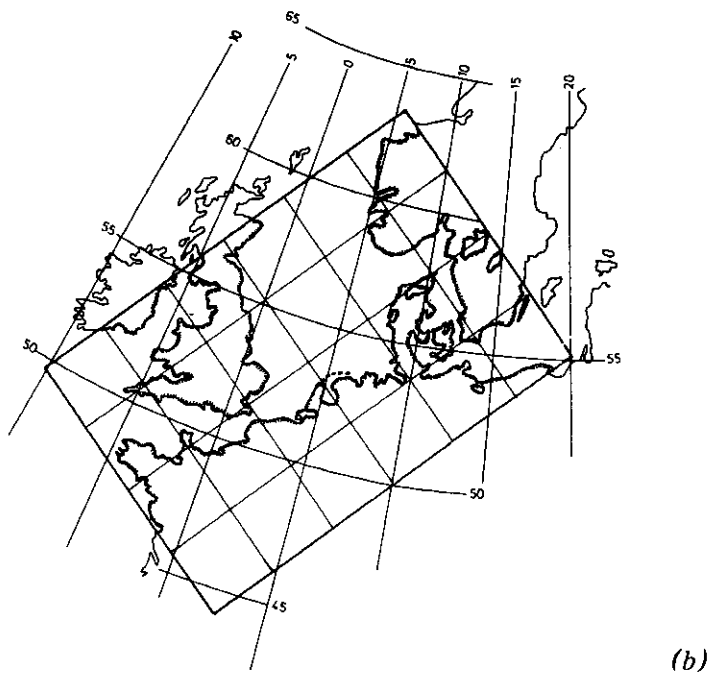
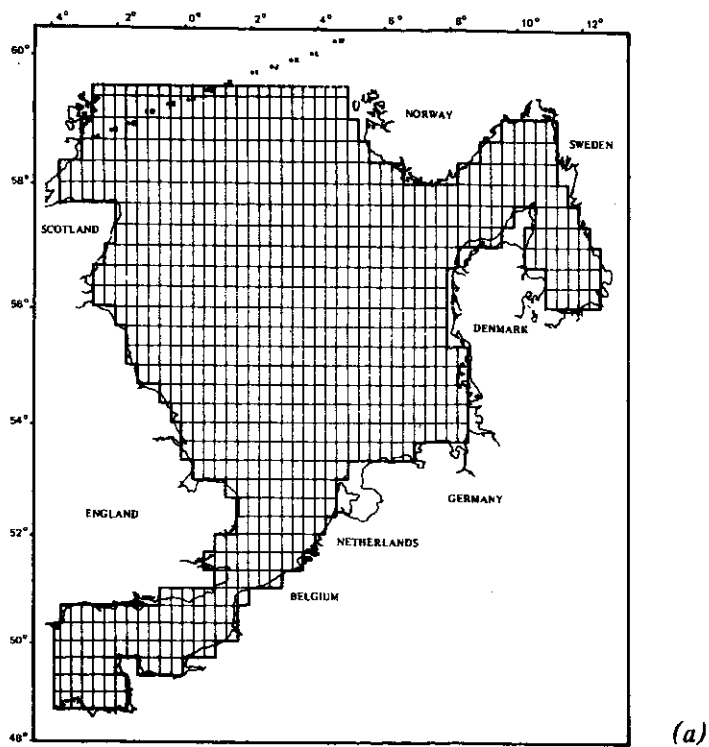


fig. 31.

- (a) The finite difference grid used for the computations with the mathematical model.
- (b) The meteorological grid covering the North Sea.

(Adam, 1979).

## 8.— Three-dimensional models of tides and storm surges.

Mesoscale phenomena in seas and great lakes are characterized by time scales ranging from hours to days. They encompass inertial oscillations, tides, wind induced currents, storm surges and diurnal thermally induced fluctuations.

With well-mixed continental seas like the North Sea in mind, attention is focused here on tides and storm surges. Their governing equations are obtained from the general Navier-Stokes equations by application of the Boussinesq approximation and the quasi-hydrostatic approximation (e.g. Nihoul, 1977). In this context, as shown in section 2, taking into account the different orders of magnitude of the horizontal and vertical velocity and length scales, one can generally neglect also the components of the Coriolis force where the horizontal component of the Earth's rotation vector appears, and the terms of horizontal turbulent diffusion as compared with the vertical turbulent diffusion.

The Boussinesq approximation is tantamount to assuming that the specific mass of sea water is a constant while its specific weight may be variable; small deviations of specific mass being there multiplied by the acceleration of gravity  $g$ , much larger than typical accelerations of the fluid.

The variations of the specific weight appear, in the hydrodynamic equations, as a vertical force, the "buoyancy", the magnitude of which must be regarded as an additional variable for which a supplementary equation is required.

In the scope of the Boussinesq approximation, one can relate buoyancy to temperature, salinity and turbidity variations and it is generally assumed that the three governing equations for temperature, salinity and turbidity can be combined in a single equation for buoyancy. Although this is obviously feasible when only one of the three variables (usually temperature) plays a significant role in the density variations; in the general case, it constitutes an additional approximation requiring further assumptions on the turbulent diffusion coefficients and the possibility of expressing volume sources of buoyancy (like the effect of radiation) in terms of buoyancy alone.

The system of equations governing mesoscale circulations, even in the simplest case of a single equation for buoyancy, is still a formidable problem. It is a system of five *non-linear* partial differential equations. In real situations, the boundaries may be very irregular (coasts, sea floor, ...) and the boundary conditions are often partly inadequate (in particular, along open sea boundaries). The equations contain eddy diffusion coefficients which are unknown functions of space and time (and, possibly, of the velocity and buoyancy fields) and one of the first problem is to establish an adequate parameterization for them.

The solution of the three-dimensional time dependent equations of the mesoscale circulation does not seem to be possible, at this stage, without rather severe simplifications. If one takes, for instance, the paper by Freeman et al. (1972) — one of the very few

attempting to solve the complete three-dimensional model-, one finds dangerously restrictive hypotheses such as constant eddy viscosity, zero bottom stress, uniform depth (when buoyancy is taken into account), zero buoyancy (when depth's variations are included) and a constant wind stress whose relation with the wind velocity, incidently, is not correct.

Confronted with the complexity of the three-dimensional model, one naturally tries to reduce its size and one turns to situations which can be described by two-dimensional or one-dimensional models.

With their main interest in the vertical structure of currents and density, several authors, advocating the small value of the Rosby number in mesoscale flows [ $0(10^{-4})$ ], have neglected the non-linear advection terms. Since the horizontal diffusion terms are also negligible, the resulting equations known as the Ekman equations contain no derivative with respect to the horizontal coordinates  $x_1$  and  $x_2$ , except for the pressure gradient which appears as an unknown forcing term related essentially to the atmospheric pressure gradient and the sea surface slope.

Some authors (e.g. Welander, 1957) have attempted to find an analytical solution of the Ekman equations where forcing functions like pressure gradient and wind stress appear as kernels of convolution integrals.

Others have tried to eliminate the pressure gradient by considering not the horizontal current, but its deviation from either a geostrophic current (defined as to be driven by the pressure gradient) or a depth-averaged current. Most of the models of the diurnal thermocline fall in this category (e.g. Niiler and Kraus, 1977; Phillips, 1977; Kitaigorodskii, 1979).

Along a rather similar line, one can also differentiate with respect to the vertical coordinate  $x_3$  and derive, from the Ekman equations, a complete set of three equations for the vertical shear

$$\omega = \frac{du}{dx_3}$$

(where  $u$  is the horizontal current vector) and buoyancy.

More interested in the general circulation pattern of a continental sea or a lake, many authors have restricted their attention to the horizontal distribution of surface slope and depth-averaged currents. When the water column is well mixed and buoyancy can be ignored, integration is carried from the bottom to the surface. In more complicated cases, several layers are treated separately and characterized by their depth-averaged properties. Depth-averaged models have been extensively applied in the recent years and detailed references can be found in numerous reviews and books (e.g. Nihoul, 1975a; Cheng et al., 1976; Nihoul and Roday, 1976).

The two kinds of models, local one-dimensional models and depth-averaged two-dimensional models, have their obvious limitations. The one-dimensional Ekman models are not applicable in

certain regions (like the vicinity of tidal amphidromic points or in coastal zones) where the non-linear advection terms are not negligible (e.g. Ronday, 1976). One can also show that these terms must be retained everywhere if the mesoscale circulation model is to be exploited to compute the residual macroscale circulation in tidal seas like the North Sea (Nihoul and Ronday, 1975).

The depth-averaged models allow only for a crude representation of stratification and give no information on the vertical profile of the horizontal current which may be rather essential in such fields as sediments transport, off-shore engineering, current meter data interpretation, ...

Moreover, neither the Ekman equations nor the depth-averaged equations constitute a closed system. At one stage or another, one-dimensional Ekman models cannot be pursued without a knowledge of surface elevation, geostrophic or mean current, bottom stress, ... to materialize the results of an analytical solution or to formulate the boundary conditions, at the bottom for instance. Two-dimensional depth-averaged models, on the other hand, require a parameterization of the bottom stress (introduced in the equations by the vertical integration) and classical empirical formulas in terms of the depth-averaged velocity may not be entirely satisfactory, especially in particular situations like the reversal of tides in weak wind conditions (Nihoul, 1977).

In fact, it is obvious that the two types of models are complementary and should be run in parallel, following some appropriate iteration procedure.

#### *Mesoscale three-dimensional hydrodynamic equations.*

In the scope of Boussinesq's approximation, eqs (7), (13), (14), (16) and (17) become (e.g. Nihoul, 1977a) :

$$(58) \quad \frac{\partial \mathbf{u}}{\partial t} + \nabla \cdot \mathbf{u}\mathbf{u} + \frac{\partial}{\partial x_3} (v_3 \mathbf{u}) + f \mathbf{e}_3 \wedge \mathbf{u} = - \nabla q + \frac{\partial}{\partial x_3} (\tilde{\nu} \frac{\partial \mathbf{u}}{\partial x_3})$$

$$(59) \quad \nabla \cdot \mathbf{u} + \frac{\partial v_3}{\partial x_3} = 0$$

$$(60) \quad \frac{\partial q}{\partial x_3} = - b$$

$$(61) \quad \frac{\partial b}{\partial t} + \nabla \cdot (\mathbf{u}b) + \frac{\partial}{\partial x_3} (v_3 b) = Q_b + \frac{\partial}{\partial x_3} (\tilde{\lambda} \frac{\partial b}{\partial x_3})$$

$$(62) \quad \frac{\partial \zeta}{\partial t} + \mathbf{u} \cdot \nabla \zeta = v_3 \quad \text{at} \quad x_3 = \zeta$$

$$(63) \quad \mathbf{u} = \mathbf{0} \quad , \quad \left( \frac{\partial h}{\partial t} + \mathbf{u} \cdot \nabla h = - v_3 \right) \quad \text{at} \quad x_3 = - h$$

where the  $\mathbf{e}_3$ -axis is vertical, pointing upwards with its origin



at the reference sea level and where

$$\mathbf{u} = u_1 \mathbf{e}_1 + u_2 \mathbf{e}_2$$

is the horizontal velocity vector,  $v_3$  is the vertical component of the three-dimensional velocity vector,

$$\nabla = \mathbf{e}_1 \frac{\partial}{\partial x_1} + \mathbf{e}_2 \frac{\partial}{\partial x_2} + \mathbf{e}_3 \frac{\partial}{\partial x_3}$$

reducing to

$$\nabla = \mathbf{e}_1 \frac{\partial}{\partial x_1} + \mathbf{e}_2 \frac{\partial}{\partial x_2}$$

in this case,  $f$  is the Coriolis parameter, twice the vertical component of the earth's rotation vector,

$$q = \frac{p}{\rho_0} + g x_3$$

(where  $p$  is the pressure,  $\rho_0$  the constant reference density and  $g$  the acceleration of gravity),  $\tilde{\nu}$  is the vertical eddy viscosity,  $b$  is the buoyancy

$$(b = -g \frac{\rho - \rho_0}{\rho_0}),$$

$Q_b$  is the rate of buoyancy production,  $\tilde{\lambda}$  is the vertical eddy diffusivity for buoyancy,  $\zeta$  is the surface elevation,  $h$  is the depth,

$$h + \zeta = H$$

is the water height.

#### ***Depth-integrated and multi-layer models.***

The difficulty of solving the three-dimensional system of equations (58) to (63) has already been pointed out.

In the case of shallow well-mixed seas and lakes, assuming negligible buoyancy and renouncing the determination of the vertical variations, one usually integrates the equations over depth and restricts attention to the computation of the surface elevation and of the depth-averaged velocity field  $\bar{\mathbf{u}}$ . Integration over depth, however, introduces the bottom stress into the equations.

The bottom stress (per unit mass of sea water) is defined as

$$(64) \quad \boldsymbol{\tau}_b = \left[ \tilde{\nu} \frac{\partial \mathbf{u}}{\partial x_3} \right]_{x_3 = -h}$$

and must be parameterized in terms of the mean velocity  $\bar{\mathbf{u}}$  although, from a physical point of view, it should really be expressed in terms of bottom currents.

Two-dimensional depth-integrated models can be improved to give some indications of vertical variations by considering different layers. Multi-layer models determine the depth-mean velocity of each layer and thus provide a staircase approximation of the velocity profile. They allow a parameterization of the bottom stress in terms of the mean current in the bottom layer but they introduce additional approximations such as interfacial friction coefficients in the boundary conditions at the interface between layers (e.g. Leendertse et al., 1973).

Moreover the volume of computation involved, when the number of layers increases, severely limits this number (or equivalently the number of vertical grid points in a three-dimensional attempt) and the variations in the vertical are very crudely represented. Being limited in the number of layers, it seems reasonable to define them in relation with the vertical buoyancy structure (for instance a well-mixed layer above the diurnal thermocline and a stratified layer below). Unfortunately, with this definition, the interfaces between layers are not fixed and how they vary in time is very often poorly known and, in any case, very difficult to take into account (e.g. Cheng et al., 1976).

*In most mesoscale phenomena, one can regard the non-linear advection terms as small except, probably, in localized regions where exceptionally high velocities or rapid spatial variations significantly increase their order of magnitude. If these terms are neglected, the mesoscale hydrodynamic equations can be transformed in many different ways into a one-dimensional system.*

*Some typical one-dimensional models are briefly discussed in the following with particular emphasis on the possibility of combining such models with two-dimensional ones to obtain the full three-dimensional picture.*

#### **Vertical shear models.**

Differentiating eq. (58) with respect to  $x_3$  and neglecting the non-linear advection terms, one obtains

$$(65) \quad \frac{\partial \omega}{\partial t} + f e_3 \wedge \omega = \nabla b + \frac{\partial^2}{\partial x_3^2} (\tilde{v} \omega)$$

where

$$(66) \quad \omega = \frac{\partial u}{\partial x_3}$$

is the vertical shear vector.

Eq. (65) and eq. (61) [linearized] constitute a closed system for  $\omega$  and  $b$ .

If one excepts estuarine and similar regions where horizontal gradients of buoyancy (related to horizontal salinity gradients, for instance) may play an important part, it is customary to neglect the horizontal gradient of  $b$ , regarding locally the marine

system as "horizontally homogeneous". In that case, eq. (65) can usually be solved for  $\omega$  and eq. (61) for  $b$ , the eddy diffusivity  $\tilde{\lambda}$  being eventually a function of  $\|\omega\|$ .

The velocity field  $u$  can then be derived from  $\omega$  within a "constant of integration" (actually a function of  $x_1, x_2$  and  $t$ ) which depends on the general circulation in the area.

The same result can be obtained by considering a "geostrophic current"  $u_g$  independent of depth and solution of the equation

$$(67) \quad \frac{\partial u_g}{\partial t} + f e_3 \wedge u_g = - \nabla q$$

where  $\nabla q$ , in the hypothesis of horizontal homogeneity and after integration of eq. (60), is given by

$$(68) \quad \nabla q = \nabla \left( \frac{p_a}{\rho_0} + g\zeta \right)$$

where  $p_a$  is the atmospheric pressure. The unknown forcing term  $\nabla q$  can then be eliminated by studying the velocity difference  $u - u_g$ . Obviously the geostrophic current plays the same role as the "constant of integration" mentioned above.

This type of approach has been used extensively in thermocline models (e.g. Niiler, 1977; Phillips, 1977; Kitaigorodskii, 1979). The difficulty here resides in the expression of the boundary conditions. For instance, the value of  $\omega$  at the bottom is related to the bottom stress which is either unknown or parameterized in terms of the depth-averaged velocity  $\bar{u}$ . The no-slip condition at the bottom will require that  $u$  be zero, i.e.  $u - u_g = -u_g$ . Apart from writing a formal analytical solution, in both cases, there is an unknown function of  $x_1, x_2$  and  $t$  ( $\bar{u}$  or  $u_g$ ) to determine separately.

#### **Analytical models.**

Assuming pseudo-horizontal homogeneity and neglecting the non-linear advection terms, one can, with more or less reasonable assumptions on the expression of the eddy viscosity  $\tilde{\nu}$ , derive an analytical solution of eq. (58) in terms of the unknown forcing term  $q$ . Eq. (58) takes, in these conditions, the simple form

$$(69) \quad \frac{\partial u}{\partial t} + f e_3 \wedge u = - \nabla \left( \frac{p_a}{\rho_0} + g\zeta \right) + \frac{\partial}{\partial x_3} \left( \tilde{\nu} \frac{\partial u}{\partial x_3} \right)$$

where eq. (68) has been used. Eq. (69) is known as the Ekman equation.

A well-known solution of this type is the model of Welander (1957). Neglecting the spatial variations of  $b$  and assuming constant vertical eddy viscosity  $\tilde{\nu}$ , Welander seeks an analytical solution of eq. (69), with the initial conditions  $u = 0$  for  $t = 0$  and the boundary conditions

$$(70) \quad \tilde{\nu} \frac{du}{dx_3} = \tau_s \quad \text{at the surface}$$

$$(71) \quad u = 0 \quad \text{at the bottom}$$

where  $\tau_s$  is the wind stress (per unit mass of sea water).

Obtained by superposition of elementary solutions corresponding to Heaviside step functions forcing terms (e.g. Hidaka, 1933), the final solution of Welander appears as the sum of two convolution integrals with respective kernels  $q(t)$  and  $\tau_s(t)$ .

The velocity profile determined by Welander depends thus on the time history of the atmospheric pressure, the wind stress and the surface elevation. Obviously, the latter must be determined, some way or another, before one can exploit the result in practical applications.

In reality, the analytical solution of the Eckman equation must be regarded as a first step, paving the way to accurate two-dimensional modelling. Jelesnianski (1970), for instance, obtains the same solution as Welander by application of the Laplace transform. From the velocity profile, he derives expressions for the mean velocity  $\bar{u}$  and the bottom stress  $\tau_b$ . Eliminating the convolution integral with unknown kernel  $q$ , one can derive an expression for  $\tau_b$  in terms of  $\bar{u}$  and  $\tau_s$ , which can be used in a subsequent depth-averaged model.

As shown by Foristall (1974), using a simplified version of Jelesnianski's integrals, the two-dimensional depth-averaged model gives  $\bar{u}$  and  $q$  and the latter can be substituted in Jelesnianski's formula to determine the velocity profile  $u(x_3)$ .

The main shortcoming of the Welander-Jelesnianski-Foristall approach is the severe hypothesis made on the vertical eddy viscosity ( $\tilde{\nu} = \text{constant}$ ) to obtain an analytical solution. This hypothesis is in contradiction with the observations and indeed the models fail to reproduce correctly the bottom boundary layer characteristics and the bottom stress turns out to be a linear function of the mean velocity and not a quadratic one, as it should.

The same objection can be made to all models constructed along the same line: too severe hypotheses, made at the beginning, handicap the whole model and the exploitation of the results in realistic situations. One can refer here to the model of Gedney and Lick (1972) [constant eddy viscosity, steady state, no atmospheric pressure gradient], Witten and Thomas (1976) [steady state, no atmospheric pressure gradient and an unrealistic and rather unfortunate exponential form for the eddy viscosity].

#### **Multi-mode models.**

Generalizing the concept of vertical integration, Heaps (1972) suggested that the vertical variations could be elegantly taken into account by expanding the velocity  $u$  in series of eigenfunctions of the turbulent operator

$$(72) \quad \frac{d}{dx_3} \left( \tilde{\nu} \frac{d}{dx_3} \right)$$

The philosophy of this approach can be summarized as follows: substituting the series expansion in the Ekman equation, one gets a system of equations for the coefficients, each of which is a function of  $x_1$ ,  $x_2$  and  $t$  and satisfies a two-dimensional equation, in many ways similar to the two-dimensional equation of a depth-averaged model.

The final result is obtained by superposing the solutions of two-dimensional models, each of which corresponds to a different vertical mode (as compared with the multi-layer model where several two-dimensional models are solved simultaneously, each of them corresponding to a different vertical layer).

This method was applied to the Irish Sea by Heaps and Jones (1975). A slightly more sophisticated version was used by Davies (1977) in a numerical experiment (rectangular sea basin of constant depth) with the object of testing the sensitivity of the results to various parameters.

The difficulty here resides in the parameterization of the eddy viscosity  $\tilde{\nu}$  and the determination of the corresponding eigenfunctions. Heaps and his co-workers were forced to introduce several simplifications regarding especially the eddy viscosity  $\tilde{\nu}$  (assumed independent of  $x_3$  and a function of  $x_1$ ,  $x_2$  and  $t$  such that the ratio  $\tilde{\nu}/h$  is a constant) and the bottom stress (taken as a linear function of the bottom velocity assumed different from zero, in contradiction with the obvious no-slip condition)\*.

#### *Variable eddy viscosity multi-mode model.*

Most models described so far can be labelled "1D + 2D" in the sense that they seek, by a preliminary one-dimensional model, some appropriate formulation of the vertical dependence of the velocity field to use subsequently in a complementary two-dimensional model. The almost inevitable hypothesis of constant eddy viscosity, in the preliminary analytical calculations, turns out to be a terrible embarrassment when exploiting the results of the one-dimensional model in two-dimensional modelling as, with an initially incorrect representation of the bottom boundary layer and of the bottom stress, one may doubt whether there will be, ultimately, real improvements in the two-dimensional forecast.

Nihoul (1977) approached the problem in a contrary direction and recognizing that two-dimensional depth-integrated models, carefully calibrated, have been successfully applied to many lakes

---

\* In his numerical experiment, Davies (1977) was able to reduce the severity of some of the assumptions but then, even with a simple piece-wise linear eddy viscosity, his solution is entirely numerical and the physical insight of the eigenfunction expansions is somewhat obscured.

and seas and that the results are available, he suggested a locally one-dimensional multi-mode model using the predictions of the preexisting two-dimensional depth-integrated model to provide the local values of the forcing terms and of the boundary conditions.

Indeed, a depth-integrated model provides, at any point where one might desire the vertical current profile, the local surface elevation, mean velocity and associated bottom stress.

The only difficulty here is that, in two-dimensional models, the bottom stress is parameterized by a quadratic formula assuming that the stress is (except for a small wind stress correction) in the direction of the mean velocity. This type of parameterization is one of the things one would like to verify by a three-dimensional model. Although the quadratic law may be generally applicable, one suspects that it could be faulty in certain situations, such as tide reversals, when the mean current becomes very small.

However, it is readily seen that, the local wind stress being known, the two-dimensional model provides two additional boundary conditions instead of one for the second order Ekman equation (the velocity and the stress at the bottom). Nihoul (1977) thus derives an analytical solution of the local Ekman equation as a series of eigenfunctions of the turbulent operator (72) using the surface stress  $\tau_s$  and the bottom stress  $\tau_b$  as boundary conditions. The velocity deviation

$$\hat{u} = u - \bar{u}$$

is obtained as a functional of  $\tau_s$  and  $\tau_b$  and the additional boundary condition ( $\hat{u} = -\bar{u}$  at the bottom) is used to determine the relationship between  $\tau_b$  and  $\bar{u}$  and to verify the two-dimensional parameterization. In this model, which could be labelled "2D + 1D", the necessary matching of the one-dimensional and the two-dimensional models requires a more realistic parameterization of the eddy viscosity which is taken as a function of  $t$ ,  $x_1$ ,  $x_2$  and  $x_3$  and, in particular, respects the observed asymptotic form of the eddy coefficient in the bottom boundary layer.

The application of the model to the North Sea shows that, for typical values of tides and storm surges, the classical bottom friction law is valid over most of the tidal cycle but fails, in magnitude and in direction, during a comparatively short period of time, at tide reversal. This may be regarded as a validation of the depth-integrated model, the result of which can be used to determine the velocity profile at any grid point where the information might be requested (off-shore structure, current-meters mooring, sediment transport problem, ...).

There is however, in principle, no difficulty in setting, for improved numerical forecasting, an iteration process by which the corrected relationship between  $\bar{u}$  and  $\tau_b$  is introduced in the two-dimensional model; the two-dimensional model being run a second time to feed back better values of  $\zeta$ ,  $\bar{u}$  and  $\tau_b$  into the one-dimensional model, etc.

One can go a step further and include the non-linear advection terms in the iteration process. In this way, the combined 2D + 1D model is applicable everywhere and results in a truly non-linear three-dimensional model of mesoscale circulation.

This model is described in the next sections.

### 9.- Three-dimensional (2D + 1D) model of tides and storm surges in a well-mixed shallow sea.

For simplicity, one shall restrict attention to well-mixed shallow seas like the North Sea and assume that buoyancy is negligible\*.

The governing equations are eqs (13) and (14). It is convenient to rewrite these equations in a slightly different form, changing variables from  $(x_1, x_2, x_3, t)$  to  $(x_1, x_2, \xi, t)$  where

$$(73) \quad \xi = \frac{x_3 + h}{H}$$

The definition of the auxiliary variable  $\xi$  is reminiscent of the well-known  $\sigma$ -transformation used by several authors (e.g. Freeman et al., 1972; Durance, 1976) but it is, in reality, only one part of it, as, for instance, one does not make use, in the following, of the  $\sigma$ -vertical velocity which, in the present notation, would be given by  $d\xi/dt$ .

The purpose of eq. (73) is to transform the variable range of vertical variations  $(-h \leq x_3 \leq \zeta)$  into the fixed range  $(0 \leq \xi \leq 1)$  which is better adapted to the determination of the eigenfunctions of the vertical turbulent diffusion operator which will be needed later.

Strictly speaking, the new variable  $\xi$  varies from some very small value

$$\xi_0 = \frac{z_0}{H}$$

to 1, where  $z_0$  is the so-called "rugosity length".  $z_0$  can be visualized as the distance above the bottom where the velocity is conventionally set equal to zero, ignoring the intricate flow situation which occurs near the sea floor and willing to parameterize its effect on the turbulent boundary layer as simply as possible (e.g. Nihoul, 1977a,b). In the North Sea, the value of  $z_0$ , which varies according to the nature of the bottom, is of the order of  $10^{-3}$  m ( $\ln \xi_0 \sim -10$ ) [Ronday, 1976].

---

\* The extension of the model to stratified seas is now under investigation. It requires a more subtle parameterization of the eddy viscosity which must be allowed to vary with the Richardson number and, at least, one more iteration loop introducing the effect of buoyancy in the pressure gradient and in the two-dimensional model.

In the North Sea, in typical weather conditions, the observations indicate that the vertical eddy viscosity is a function of the depth, increasing first linearly with height over the bottom and then flattening out in the upper layers following some form of parabolic curve (e.g. Bowden, 1965; Runday, 1976). This is obviously in relation with the existence near the sea floor of a logarithmic bottom boundary layer of which there is now ample experimental evidence (e.g. Weatherly, 1977).

Although  $\xi_0 \ll 1$ , it cannot be set equal to zero because the logarithmic velocity profile is singular at  $\xi = 0$ . However, one shall see in the following that the singular part of the profile can be sorted out by an appropriate change of variables, and that the new variables can be expanded in series of eigenfunctions of the vertical turbulent diffusion operator in the range  $0 \leq \xi \leq 1$ .

In brief, the lower limit of  $\xi$  will be taken equal to zero as long as it does not create a singularity.

Changing variables from  $(x_1, x_2, x_3, t)$  to  $(x_1, x_2, \xi, t)$  the first two terms of the left-hand side of eq. (13) become :

$$(74) \quad \frac{\partial \mathbf{u}}{\partial t} + \mathbf{A} + \mathbf{B} + \mathbf{S}$$

where

$$(75) \quad \mathbf{A} = \mathbf{u} \cdot \nabla \mathbf{u}$$

$$(76) \quad \mathbf{B} = H^{-1} \frac{\partial \mathbf{u}}{\partial \xi} (1 - \xi) (\mathbf{u} \cdot \nabla h + v_3)$$

$$(77) \quad \mathbf{S} = H^{-1} \frac{\partial \mathbf{u}}{\partial \xi} \xi [(\mathbf{u}_s - \mathbf{u}) \cdot \nabla \zeta - (v_{3_s} - v_3)]$$

and where the relation

$$(78) \quad \frac{\partial \zeta}{\partial t} + \mathbf{u}_s \cdot \nabla \zeta = v_{3_s} \quad \text{at} \quad x_3 = \zeta$$

has been used, the subscript <sub>s</sub> denoting surface values.

The conditions under which the terms  $\mathbf{A}$ ,  $\mathbf{B}$  and  $\mathbf{S}$  - which are generated by the time derivative as well as by the non-linear advection terms - can be neglected in the case of the North Sea, are not obvious.

[The situation here is different from the studies of Jelesnianski (1970) and Foristall (1974), for instance, where the equations being linearized to begin with, a  $\sigma$ -type transformation cannot generate any term of importance.]

To estimate the orders of magnitude of the non-linear terms  $\mathbf{A}$ ,  $\mathbf{B}$  and  $\mathbf{S}$ , one must have some, even rough, idea of the vertical profile of the velocity and, for that purpose, one can presumably take Van Veen's profile



$$[u = u_s \xi^{0.2} ; \text{Van Veen (1938)}],$$

which is probably not too good in the immediate vicinity of the bottom but appears to reproduce satisfactorily the observations in many cases (e.g. Bowden, 1965; Nihoul, 1975a).

Estimating the orders of magnitude of the different terms of  $B$ , one finds that they vanish at the surface and reach the greatest values, as expected, near the bottom.  $S$  is more evenly distributed over the water column but it remains everywhere much smaller.

Comparing  $A$  and  $S$  (noting that  $u$  and  $\zeta$  have the same characteristic length of horizontal variations) one finds :

$$\frac{S}{A} \lesssim 0.1 \frac{\zeta}{H}$$

Even in very shallow coastal zones, this can only be a few percents and one may reasonably neglect  $S$  as compared to  $A$ .

Dealing with long waves, one may associate to the time variations and the horizontal space variations of the velocity field a typical frequency  $\omega$  ( $\omega \sim 10^{-4} \sim f$ ) and a typical wavelength  $c/\omega$  where  $c$  is the phase velocity.

Observed values of the phase velocity exceed 10 m/s even in shallow coastal areas (note that  $\sqrt{gH}$  gives 10 m/s for  $H$  only 10 m). Maximum values of the flow velocity  $u$  are of the order of 1 m/s (e.g. Runday, 1976). The non-linear advection term  $A$  (and *a fortiori*  $S$ ) is thus generally negligible as compared to the time derivative; the two terms being in the ratio  $u/c$ .

This might not be true in some places, near amphidromic points, for instance where the characteristic length of horizontal variations of the velocity field could be smaller than the wavelength. Its smallest value however is the grid size, because one cannot introduce in the model variations at scales which are meant to be smoothed out. Still, with a grid size of, say, 10 km,  $A$  could be one order of magnitude larger, comparable with the time derivative. There are thus localized areas, where the non-linear advection terms cannot be neglected. Depth-integrated two-dimensional models cannot reproduce correctly the tide and storm surge characteristics over the whole North Sea without retaining the non-linear terms. [It can be shown that these terms are also necessary if one wants to model the residual circulation (Nihoul, 1975a; Nihoul and Runday, 1976).] However, if one excepts "singular" regions like amphidromic points, it seems reasonable to neglect  $A$  in the determination of the local vertical profile of the velocity.

The characteristic length of variations of the bottom topography  $h(x_1, x_2)$  is not related to the wavelength  $c/\omega$ . It cannot, however, be smaller than the grid size for the same obvious reason as before. For a 10-km grid size, each term composing  $B$  can be comparable to the time derivative. However, as

shown previously,  $B$  is essentially important near the bottom where one may expect the streamlines to follow the bottom topography fairly closely. In that case, the three terms may be expected to nearly cancel each other, i.e.:

$$(79) \quad u_1 \frac{\partial h}{\partial x_1} + u_2 \frac{\partial h}{\partial x_2} + u_3 \sim 0 \quad \text{near the bottom.}$$

In the following, counting on a grid size of some 10 km and assuming that the departure of the left-hand side of eq. (79) does not exceed 10 % of the value of the individual terms, one shall neglect  $B$  as compared to  $\partial u / \partial t$ . One should be aware, however, that, in finer-grid models, for coastal studies for instance,  $B$  might be more important and, indeed, turn out to be the essential contribution of the non-linear terms to include by priority in the models. More details about numerical values and orders of magnitude characteristic of the North Sea can be found, for instance, in Ronday (1976).

Changing variables from  $x_3$  to  $\xi$ , the last term in the right-hand side of eq. (13) becomes

$$H^{-2} \frac{\partial}{\partial \xi} \left( \tilde{\nu} \frac{\partial}{\partial \xi} \right)$$

Observations indicate that the eddy viscosity  $\tilde{\nu}$  can be expressed as the product of a function of  $t$ ,  $x_1$  and  $x_2$  and a function of  $\xi$  (Bowden, 1965). If one sets :

$$(80) \quad \tilde{\nu} H^{-2} = \sigma(t, x_1, x_2) \lambda(\xi)$$

and neglects the non-linear terms according to the discussion above, one can write the components of eq. (13) in the form

$$(81) \quad \frac{\partial u_1}{\partial t} - f u_2 = - \frac{\partial}{\partial x_1} \left( \frac{p_a}{\rho} + g\zeta \right) + \sigma \frac{\partial}{\partial \xi} \left( \lambda \frac{\partial u_1}{\partial \xi} \right)$$

$$(82) \quad \frac{\partial u_2}{\partial t} + f u_1 = - \frac{\partial}{\partial x_2} \left( \frac{p_a}{\rho} + g\zeta \right) + \sigma \frac{\partial}{\partial \xi} \left( \lambda \frac{\partial u_2}{\partial \xi} \right)$$

One emphasizes that these equations, although valid for the greater part of the North Sea, are not applicable in localized areas where the non-linear terms are important. In such "singular" regions, however, their solution can be used as described in the next section, to initiate an iteration process in which the non-linear terms are regarded as driving forces. The combination of eqs. (81) and (82) (or higher iteration forms of them) with a depth-integrated two-dimensional model will provide the elements of a three-dimensional model by which, at each grid point, surface elevation, vertical mean current and vertical profile of the velocity can be predicted.

**Locally one-dimensional model of the vertical variations of the horizontal current.**

Let :

$$(83) \quad u = u_1 + i u_2$$

$$(84) \quad \tau = \tilde{\nu} \frac{\partial u}{\partial x_3} = \sigma H \lambda \frac{\partial u}{\partial \xi}$$

$$(85) \quad \Phi = - \frac{\partial}{\partial x_1} \left( \frac{P_a}{\rho} + g \zeta \right) - i \frac{\partial}{\partial x_2} \left( \frac{P_a}{\rho} + g \zeta \right)$$

Eqs. (81) and (82) can be combined into the single equation :

$$(86) \quad \frac{\partial u}{\partial t} + i f u = \Phi + \sigma \frac{\partial}{\partial \xi} \left( \lambda \frac{\partial u}{\partial \xi} \right)$$

The forcing term  $\Phi$  is a function of  $t$ ,  $x_1$  and  $x_2$ . Hence, although the dependence does not appear explicitly in eq. (86),  $u$  must be regarded as a function of  $\xi$ ,  $t$ ,  $x_1$  and  $x_2$ . At any given point  $(x_1, x_2)$ , eq. (86) provides a locally one-dimensional model of the vertical distribution of  $u$  as a function of time.

If  $\tau_s$  and  $\tau_b$  denote the values of  $\tau$  at the surface and at the bottom respectively, the depth-averaged velocity  $\bar{u}$  is given by the equation :

$$(87) \quad \frac{\partial \bar{u}}{\partial t} + i f \bar{u} = \Phi + (\tau_s - \tau_b) H^{-1}$$

and the deviation  $\hat{u} = u - \bar{u}$  is given by :

$$(88) \quad \frac{\partial \hat{u}}{\partial t} + i f \hat{u} = \sigma \left[ \frac{\partial}{\partial \xi} \left( \lambda \frac{\partial \hat{u}}{\partial \xi} \right) - \frac{\tau_s - \tau_b}{\sigma H} \right]$$

The vertical profile of the eddy viscosity  $\tilde{\nu}$  may be different in different circumstances but it is generally admitted that, in any case, its asymptotic behaviour for small  $\xi$  is given by :

$$(89) \quad \tilde{\nu} = k |\tau_b|^{1/2} (x_3 + h)$$

where  $k$  is an appropriate constant which, according to observations in the North Sea, may be taken as the classical Von Karman constant of turbulent boundary layer theory (e.g. Roday, 1976).

Combining eqs. (80) and (89), one can see that  $\sigma H$  must be proportional to  $k |\tau_b|^{1/2}$ . There is no lack of generality in taking the constant of proportionality equal to 1 (the functions  $\sigma$  and  $\lambda$  are only defined by their product). Hence :

$$(90) \quad \sigma H = k |\tau_b|^{1/2}$$

and

$$(91) \quad \lambda(\xi) \sim \xi \quad \text{for small } \xi$$

Changing variables to  $w$  and  $y$  defined by :

$$(92) \quad \hat{u} = w e^{-ift} + \frac{\tau_s}{\sigma H} s(\xi) + \frac{\tau_b}{\sigma H} b(\xi)$$

$$(93) \quad y = \int_0^t \sigma(v) dv$$

where

$$(94) \quad s(\xi) = \int_{\xi_0}^{\xi} \frac{\eta}{\lambda(\eta)} d\eta$$

$$(95) \quad b(\xi) = \int_{\xi_0}^{\xi} \frac{1 - \eta}{\lambda(\eta)} d\eta$$

eq. (88) can be written :

$$(96) \quad \frac{\partial w}{\partial y} + \theta_s s(\xi) + \theta_b b(\xi) = \frac{\partial}{\partial \xi} \left( \lambda \frac{\partial w}{\partial \xi} \right)$$

where

$$(97) \quad \theta_a = \frac{e^{ift}}{\sigma} \left( \frac{\partial}{\partial t} + if \right) \left( \frac{\tau_a}{\sigma H} \right) = \frac{\partial}{\partial y} \left( e^{ift} \frac{\tau_a}{\sigma H} \right) \quad a = s, b$$

with the boundary conditions :

$$(98) \quad \lambda \frac{\partial w}{\partial \xi} = 0 \quad \text{at} \quad \xi = 0 \quad \text{and} \quad \xi = 1$$

If the vertical profile of the eddy viscosity is known,  $s$  and  $b$  are known functions of  $\xi$ . Eq. (96) allows then the determination of the vertical profile of the velocity in terms of  $\sigma$ ,  $H$ ,  $\theta_s$  and  $\theta_b$  which - at any given point  $(x_1, x_2)$  - are functions of  $t$  and thus of  $y$ .

#### *Vertical profile of the horizontal current.*

Introducing the Laplace transforms :

$$(99) \quad W(a, \xi) = \int_0^{\infty} e^{-ay} w(y, \xi) dy$$

$$(100) \quad \Theta_a(a) = \int_0^{\infty} e^{-ay} \theta_a(y) dy \quad a = s, b$$

eq. (96) can be transformed into :

$$(101) \quad aW + \Theta_s s(\xi) + \Theta_b b(\xi) - w_0(\xi) = \frac{d}{d\xi} \left( \lambda \frac{dW}{d\xi} \right)$$

with the boundary conditions :

$$(102) \quad \lambda \frac{dW}{d\xi} = 0 \quad \text{at} \quad \xi = 0 \quad \text{and} \quad \xi = 1$$

Let now a series of functions  $f_n(\xi)$  ( $n = 0, 1, \dots$ ) such that :

$$(103) \quad \frac{d}{d\xi} \left( \lambda \frac{df_n}{d\xi} \right) = -\alpha_n f_n \quad n = 0, 1, 2, \dots$$

$$(104) \quad \lambda \frac{df_n}{d\xi} = 0 \quad \text{at} \quad \xi = 0 \quad \text{and} \quad \xi = 1$$

the  $\alpha_n$ 's being appropriate eigenvalues with  $\alpha_0 = 0$ .

It is readily seen that these functions are orthogonal on  $(0, 1)$ . They can be further normalized by imposing :

$$(105) \quad \int_0^1 f_n^2 d\xi = 1$$

It is tempting to seek a solution of eq. (101) in the form of a series expansion in  $f_n(\xi)$ .

Let thus :

$$(106) \quad W = \sum_0^{\infty} c_n f_n(\xi)$$

$$(107) \quad w_0 = \sum_0^{\infty} \omega_n f_n(\xi)$$

$$(108) \quad s_n = \int_0^1 s f_n d\xi$$

$$(109) \quad b_n = \int_0^1 b f_n d\xi$$

The coefficients  $\omega_n, s_n, b_n$  are known if  $\lambda(\xi)$  and thus  $s(\xi)$  and  $b(\xi)$  are known. The coefficients  $c_n$  are determined by eq. (101). One finds :

$$(110) \quad c_n = \frac{\omega_n - s_n \Theta_s - b_n \Theta_b}{a + \alpha_n}$$

Hence

$$(111) \quad w = \mathcal{L}^{-1} W = \sum_0^{\infty} (\omega_n e^{-\alpha_n y} - s_n R_n^s - b_n R_n^b) f_n(\xi)$$

where

$$(112) \quad R_n^a = \int_0^y \theta_a(y') e^{-\alpha_n(y-y')} dy', \quad a = s, b$$

From eqs. (103) and (104), it is readily seen that :

$$(113) \quad \int_0^1 f_n(\xi) d\xi = 0 \quad n > 0$$

and that  $f_0$  is a constant so that the first terms in the series expansions (106), (107), (108) and (109) represent the depth-mean values of the corresponding functions.

Combining eqs. (92), (97) and (112), one then obtains :

$$(114) \quad \hat{u} = \frac{\tau_s}{\sigma H} [s(\xi) - \bar{s}] + \frac{\tau_b}{\sigma H} [b(\xi) - \bar{b}] + \sum_1^{\infty} (\omega_n e^{-\alpha_n y} - s_n R_n^s - b_n R_n^b) f_n(\xi) e^{-ift}$$

Here  $\bar{s}$  and  $\bar{b}$  represent the depth-averaged values of  $s$  and  $b$  and the condition that the depth-averaged value of  $\hat{u}$  must be zero has been used to eliminate  $\omega_0$ .

By successive integrations by parts, one can write, using eq. (97) :

$$(115) \quad R_n^a = \sum_{p=0}^{\infty} \left[ \frac{d^p \theta_a}{dy^p} \frac{e^{\alpha_n y}}{\alpha_n^{p+1}} \right]_0^y e^{-\alpha_n y} \quad \begin{array}{l} a = s, p \\ n = 1, 2, \dots \end{array}$$

$$= \sum_{q=1}^{\infty} \left\{ \alpha_n^{-q} \left[ \frac{d^q}{dy^q} \left( \frac{e^{ift} \tau_a}{\sigma H} \right) \right]_y - \alpha_n^{-q} e^{-\alpha_n y} \left[ \frac{d^q}{dy^q} \left( \frac{e^{ift} \tau_a}{\sigma H} \right) \right]_0 \right\}$$

Using eq. (90) and typical values for the North Sea (e.g. Ronday, 1976), one finds that  $\sigma$  may vary from  $10^{-4} \text{ s}^{-1}$ , in cases of small currents almost reduced to residuals at turning tides and weak winds, to  $10^{-2} \text{ s}^{-1}$  in cases of large tidal currents and strong winds. The time variations of the stress and velocity fields may be characterized by a typical "frequency"

$$\omega \sim 10^{-4} \text{ s}^{-1} \sim f$$

Thus :

$$(116) \quad \frac{d}{dy} = \frac{1}{\sigma} \frac{d}{dt} \sim \frac{\omega}{\sigma} \lesssim 1$$

Successive differentiations with respect to  $y$  should thus, if anything, reduce the order of magnitude. The eigenvalues  $\alpha_n$  being increasing functions of  $n$ , the factor  $\alpha_n^{-q}$  in eq. (114) will rapidly become negligibly small as  $n$  and  $q$  increase and one can foresee that in eqs. (114) and (115), only a few terms of the sums will have to be retained.

With the observed values of  $\sigma$ , the variable  $y$  reaches values of order 10 in less than a tidal period. One can see then that the influence of the initial conditions rapidly vanishes;

the factor  $e^{-\alpha_n y}$  [in eqs. (114) and (115)] becoming exceedingly small.

Thus, after a short time, the essential contribution to the velocity deviation will be :

$$(117) \quad \hat{u} = \frac{\tau_s}{\sigma H} [s(\xi) - \bar{s}] + \frac{\tau_b}{\sigma H} [b(\xi) - \bar{b}] - \sigma^{-1} \frac{\partial}{\partial t} \left[ \frac{e^{ift}}{\sigma H} \left( \frac{s_1 \tau_s + b_1 \tau_b}{\alpha_1} \right) \right] f_1(\xi) e^{-ift}$$

One can see that Ekman veering affects only the third term (and the other smaller terms of the sum) and is most effective when  $\sigma$  is the smallest (low current velocities, weak winds) as one would normally expect.

The velocity deviation given by eq. (117) must satisfy the additional requirement that the velocity be zero at the bottom, i.e.:

$$(118) \quad \hat{u} = -\bar{u} \quad \text{at} \quad \xi = \xi_0$$

Eq. (118) provides a relationship between  $\tau_b$ ,  $\bar{u}$  and  $\tau_s$ . Thus the bottom stress can be parameterized in terms of the depth-mean velocity and the wind stress and it can be substituted in the depth-integrated two-dimensional model. The two-dimensional model can compute the mean velocity, the surface elevation and subsequently  $\tau_b$  and  $\sigma$ . These in terms can be substituted in eq. (117) to yield the vertical profile of the velocity.

#### ***Application of the model to the North Sea.***

As pointed out before, depth-integrated two-dimensional models of tides and storm surges in the North Sea have been successfully operated for many years (e.g. Nihoul and Ronday, 1976). Before considering undertaking a complete new simulation using the two-dimensional model in parallel with eqs. (117) and (118), it has seemed interesting to apply the locally one-dimensional model at a certain number of grid points of the two-dimensional grid where one knew, from the depth-integrated model, the mean velocity, the surface elevation and the order of magnitude of the non-linear terms and where sufficient experimental data were available to determine the functional dependence of the eddy viscosity on depth.

In this first application, the selected grid points where the calculation was made were chosen in regions where the non-linear terms were negligible and the depth-variation of the eddy viscosity could satisfactorily be represented by a function of the type

$$(119) \quad \lambda = \xi \left( 1 - \frac{\xi}{2} \right)$$

which has the advantage of allowing the solution of eqs. (103) and (104) in analytical form.

As, in the existing depth-integrated models, eq. (21) is used to parameterize the bottom stress, eq. (118) is exploited in this approach as a test of consistency between the two-dimensional model at any grid point and the one-dimensional depth-dependent model at the same grid point.

The eigenfunctions and the eigenvalues corresponding to eqs. (103) and (104) are found to be :

$$(120) \quad f_n = (4n + 1)^{1/2} P_{2n}(\xi - 1)$$

$$(121) \quad \alpha_n = n(2n + 1)$$

where  $P_{2n}$  denotes the Legendre polynomials of even order.

Eq. (117) becomes :

$$(122) \quad \hat{u} = \frac{\tau_s}{\sigma H} [4 \ln 2 - 2 - 2 \ln(2 - \xi)] \\ + \frac{\tau_b}{\sigma H} [2 - 2 \ln 2 + \ln(2 - \xi) + \ln \xi] \\ + \sigma^{-1} \frac{\partial}{\partial t} \left( e^{ift} \frac{\tau_s + 2 \tau_b}{\sigma H} \right) \left( \frac{5 \xi^2}{12} - \frac{5 \xi}{6} + \frac{5}{18} \right) e^{-ift}$$

where it is understood that  $\xi$  runs from 0 to 1 everywhere except in  $\ln \xi$  where its lower limit must be specifically set at  $\xi_0$ .

At  $\xi = \xi_0 \sim 0$ , eq. (118) gives :

$$(123) \quad \bar{u} = \frac{\tau_s}{\sigma H} (2 - 2 \ln 2) + \frac{\tau_b}{\sigma H} (-\ln \xi_0 + \ln 2 - 2) \\ - \frac{5}{18} \sigma^{-1} \frac{\partial}{\partial t} \left( e^{ift} \frac{\tau_s + 2 \tau_b}{\sigma H} \right) e^{-ift}$$

Hence :

$$(124) \quad u = \frac{\tau_s}{\sigma H} 2 \ln \frac{2}{2 - \xi} + \frac{\tau_b}{\sigma H} \left( \ln \frac{\xi}{\xi_0} + \ln \frac{2 - \xi}{2} \right) \\ - \sigma^{-1} \frac{\partial}{\partial t} \left( e^{ift} \frac{\tau_s + 2 \tau_b}{\sigma H} \right) \frac{5}{12} \xi(2 - \xi) e^{-ift}$$

Eq. (124) shows that the vertical profile of the velocity  $u$  is the result of three contributions which may be related to the wind stress, the bottom stress and the effect of the Coriolis force combined with the action of wind or bottom friction.

Taking  $\ln \xi_0 = -10$  as a typical value (e.g. Ronday, 1976), one estimates :

$$\frac{\frac{\tau_s}{\sigma H} 2 \ln \frac{2}{2 - \xi}}{\frac{\tau_b}{\sigma H} \left( \ln \frac{\xi}{\xi_0} + \ln \frac{2 - \xi}{2} \right)} \sim 0.1 \frac{\tau_s}{\tau_b}$$



$$\frac{\sigma^{-1} \frac{\partial}{\partial t} (e^{ift} \frac{\tau_s}{\sigma H}) \frac{5}{12} \xi(2 - \xi)}{\frac{\tau_s}{\sigma H} 2 \ln \frac{2}{2 - \xi}} \sim 0.3 \frac{\omega}{\sigma}$$

$$\frac{\sigma^{-1} \frac{\partial}{\partial t} (e^{ift} \frac{\tau_b}{\sigma H}) \frac{5}{12} \xi(2 - \xi)}{\frac{\tau_b}{\sigma H} (\ln \frac{\xi}{\xi_0} + \ln \frac{2 - \xi}{2})} \lesssim 0.1 \frac{\omega}{\sigma}$$

where  $\omega$  is, as before, a typical frequency of time variations ( $\omega \sim 10^{-4} \text{ s}^{-1} \sim f$ ).

① In the case of strong winds ( $> 10 \text{ m/s}$ ) and strong currents ( $\geq 1 \text{ m/s}$ ),  $\tau_s$  and  $\tau_b$  are comparable ( $\geq 10^{-3} \text{ m}^2/\text{s}^2$ ),  $\sigma$  can be one order of magnitude larger than  $\omega$ , the essential contribution is due to bottom friction, the direct effect of the wind stress does not exceed some 10% of the former and there is no noticeable Ekman veering. This will be *a fortiori* true in the case of strong (tidal) currents and weak winds.

② In the case of strong winds but relatively moderate currents related to residual and wind-induced circulations at slack tide, the effects of wind and bottom friction may become comparable. The Ekman veering will however remain rather limited as the ratio  $\omega/\sigma$  will presumably still be smaller than 1.

③ In the case of weak wind and small currents (almost reduced to residuals at slack tide), ( $\tau_s \sim \tau_b \sim 10^{-5}$ ) the essential contribution remains related to the bottom stress,  $\sigma$  may be comparable to  $\omega$  and both the wind stress and the Coriolis force can produce a 10% deviation of the vertical profile of the velocity.

Thus, in shallow continental sea like the North Sea where tides are omnipresent and can reach velocities of the order of 1 m/s or more, one expects that, during a substantial fraction of the tidal period, Coriolis effects may be neglected and eq. (123) can be written, in first approximation:

$$(125) \quad \bar{u} \sim \frac{\tau_s}{\sigma H} (2 - 2 \ln 2) + \frac{\tau_b}{\sigma H} (-\ln \xi_0 + \ln 2 - 2)$$

Moreover, the numerical coefficient of the first term being approximately 0.1 of the coefficient of the second term, eq. (90) may be written:

$$(126) \quad (\sigma H)^2 = k^2 |\tau_b| \sim \frac{\sigma H |\bar{u}| k^2}{-\ln \xi_0 + \ln 2 - 2}$$

or

$$(127) \quad \sigma H \sim \frac{|\bar{u}| k^2}{-\ln \xi_0 + \ln 2 - 2}$$

Combining with eq. (125), one gets :

$$(128) \quad \tau_b \sim -m \tau_s + D \bar{u} |\bar{u}|$$

or, equivalently,

$$(129) \quad \tau_b \sim -m \tau_s + D \bar{u} \|\bar{u}\|$$

where

$$(130) \quad m = \frac{2 - 2 \ln 2}{-\ln \xi_0 + \ln 2 - 2} \sim 0.07$$

$$(131) \quad D = \frac{k^2}{(-\ln \xi_0 + \ln 2 - 2)^2} \sim 2.11 \times 10^{-3}$$

for  $\ln \xi_0 \sim -10$ .

Eq. (129) is identical with the empirical formula (21). Moreover the numerical values of the coefficients  $m$  and  $D$  predicted by the model appear in close agreement with the empirical coefficients used in success in practice ( $m \sim 0.1$ ,  $D \sim 2 \times 10^{-3}$ ; Roday, 1976).

The empirical bottom friction law (21) would thus seem to be valid except perhaps for a fraction of time at tide reversal. Whether this is sufficient to affect significantly the predictions of a depth-integrated model can be judged by the test of consistency: the mean velocity  $\bar{u}$  calculated by the depth-integrated model, using eq. (21), must be the same as the mean velocity  $\bar{u}$  given by eq. (125).

This proved to be the case at all points where the calculation was made. Only a slight difference was observed and this occurred, as expected at tide reversal.

Figs. 32-36 give, in illustration, the results of the computation at the point  $52^\circ 30' N$   $3^\circ 50' E$  under strong wind conditions where the depth-integrated model provided the following estimates:

$$\|\bar{u}\| \lesssim 0.7 \text{ m s}^{-1} \quad ; \quad H \sim 28 \text{ m}$$

$$z_0 \sim 1.8 \times 10^{-3} \text{ m} \quad ; \quad D \sim 2.2 \times 10^{-3}$$

$$\|\tau_s\| \lesssim 2 \times 10^{-4} \text{ m}^2 \text{ s}^{-2}$$

Figs. 32 and 33 show the time evolution over half a tidal period of the vertical profiles of, respectively, the northern and the eastern components of the horizontal velocity vector. The curves from left to right are vertical profiles computed at one hour interval.

Figs. 34 and 35 show the same components at tide reversal. The curves from left to right are vertical profiles computed at a 20 minutes interval. One can see, on fig. 34, the indication of a reverse flow in the bottom layer.

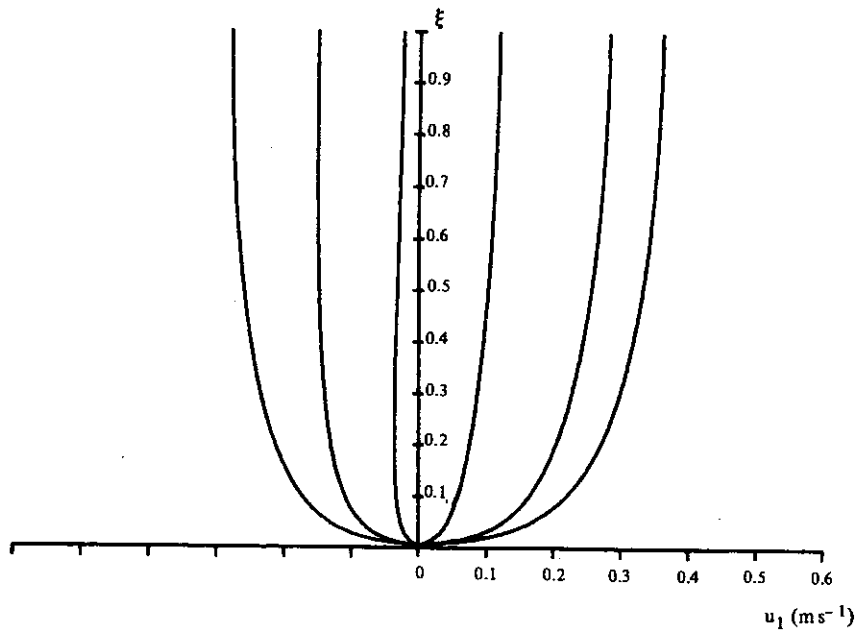


fig. 32.

Time evolution over half a tidal period of the vertical profile of the northern component of the horizontal velocity vector at point  $52^{\circ}30'N$   $3^{\circ}50'E$ . The curves from left to right are vertical profiles computed at one hour interval.

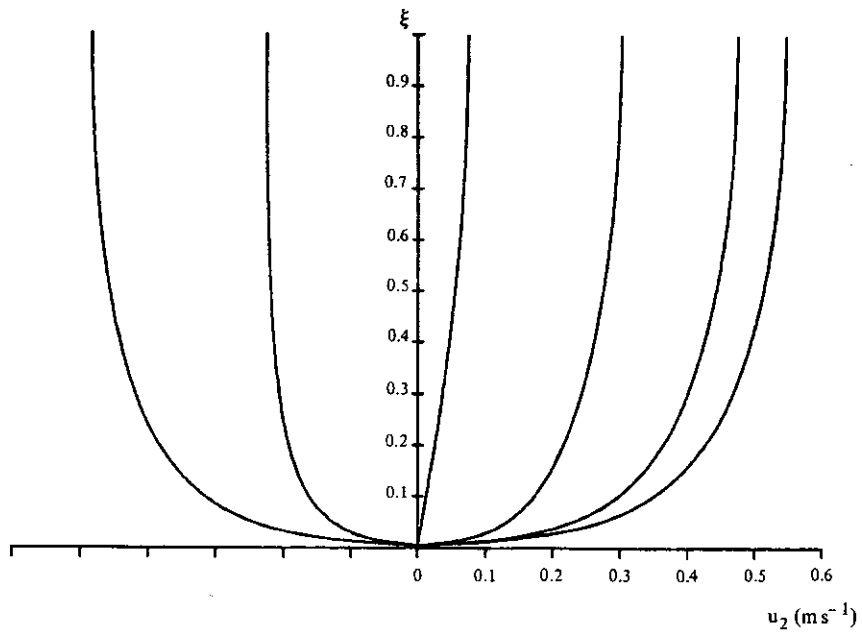


fig. 33.

Time evolution over half a tidal period of the vertical profile of the eastern component of the horizontal velocity vector at point  $52^{\circ}30'N$   $3^{\circ}50'E$ . The curves from left to right are vertical profiles computed at one hour interval.

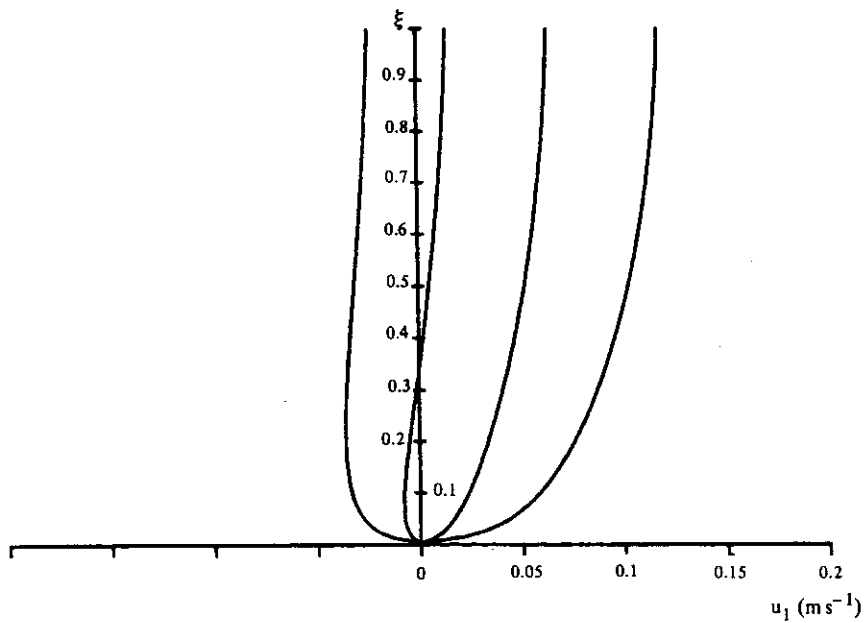


fig. 34.

Vertical profile of the northern component of the horizontal velocity vector at tide reversal. The curves from left to right are vertical profiles computed at a 20-minute interval.

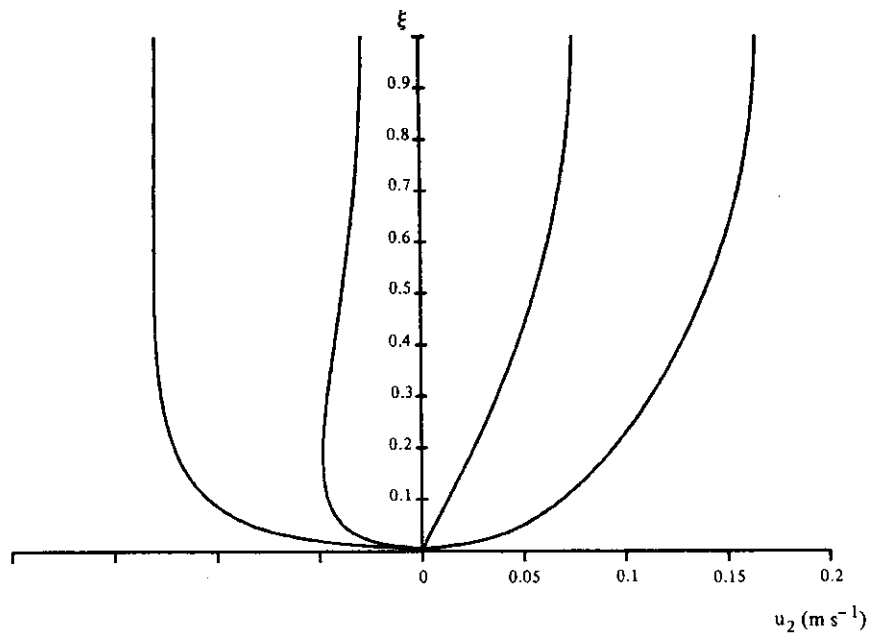


fig. 35.

Vertical profile of the eastern component of the horizontal velocity vector at tide reversal. The curves from left to right are vertical profiles computed at a 20-minute interval.

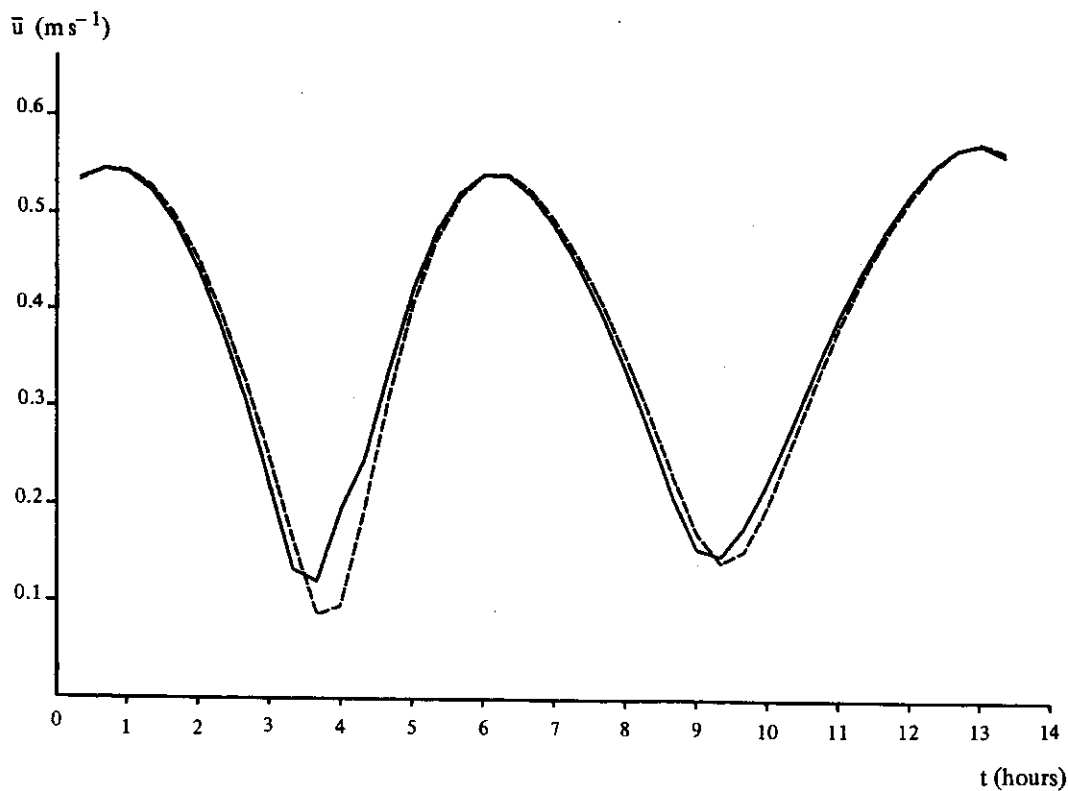


fig. 36.

Comparison between the mean velocity computed by the depth-integrated two-dimensional model (dashed line) and by the locally one-dimensional depth-dependent model subject to the condition of zero velocity at the bottom (full line).

Fig. 36 shows a comparison between the mean velocity computed by eq. (125) and by the two-dimensional depth-integrated model. A very good agreement is found except perhaps at minimum flow velocity associated with tide reversal.

#### 10.-- Non-linear three-dimensional model of tides and storm surges in a well-mixed continental sea.

Using the results of the two-dimensional depth-integrated model of the North Sea (Ronday, 1976), Nihoul (1977) computed the evolution with time of the velocity profile  $u(t, x_1, x_2, x_3)$  at a series of representative horizontal grid points in the Southern Bight. The extra condition

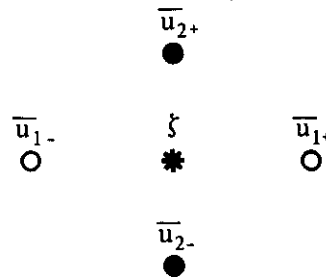
$$\bar{u} = -\hat{u}(\xi_0)$$

was used as a test of consistency; a significant discrepancy indicating a local influence of the non-linear terms or a temporary failure of the parameterization of  $\tau_b$  in the depth-integrated model (memory effects for small  $\bar{u}$ ).

At all the grid points where the study was conducted, Nihoul (1977) found very little difference between the mean velocity calculated by the depth-integrated model and calculated by the local multi-mode solution.

However, no point was taken in danger zones near coasts or tidal amphidromic points and the model was not tested for other regions than the Southern Bight and the North Sea or for different types of mesoscale circulations or climatic conditions. The necessity was thus felt of a generalization of the model based on an iteration procedure by which the non-linear terms could be included in the one-dimensional local Ekman model while the parameterization of the bottom stress could be revised in the two-dimensional model according to the calculated vertical structure.

The two-dimensional model gives the components  $\bar{u}_1$  and  $\bar{u}_2$  of the mean velocity and the surface elevation  $\zeta$  at the points of a staggered horizontal grid



The integration of the equation for the velocity deviation  $\hat{u}$  is made at the  $\zeta$ -point. At that point, the two components of the mean velocity  $\bar{u}$  are calculated by linear interpolation [the error is in  $(\Delta x)^2$  and consistent with the order of the two-dimensional scheme]. To compute the non-linear terms which contain horizontal derivatives of  $\hat{u}$ , the velocity deviation must be calculated simultaneously at nine  $\zeta$ -points of the two-dimensional grid. (In the application to the North Sea, these points form a rectangle of 20 km  $\times$  26 km.)

At each time step  $t + \Delta t$ , a first approximation  $\hat{u}^1$  is calculated numerically, setting  $\mathbf{n} = \mathbf{n}^1(t)$  where  $\mathbf{n}$  stands in brief for the sum of the non-linear terms.

This approximation, combined with the results of the two-dimensional model, is then used to compute  $\mathbf{n}^1(t + \Delta t)$ . A second approximation  $\hat{u}^2$  is then calculated setting

$$\mathbf{n} = \frac{1}{2} [\mathbf{n}^1(t + \Delta t) + \mathbf{n}^1(t)]$$

With the second approximation,  $\mathbf{n}^2(t + \Delta t)$  is computed and the iteration continues.

At the initial time, the first approximation is obtained taking  $\mathbf{n} = \mathbf{0}$  and the result of the analytical model can be used.

The numerical method is an extension of the compact hermitian method developed by Adam (1977).

As boundary conditions for the determination of  $\hat{u}$ , one imposes the surface stress and the bottom stress (the latter obtained from the two-dimensional model). The consistency condition

$$\bar{u} = -\hat{u} \quad \text{at the bottom}$$

indicates if the model can proceed to the next time step or if a preliminary iteration must be performed on the parameterization of the bottom stress.

As shown above, the classical bottom friction law constitutes the algebraic part of a differential relation where the additional terms (containing derivatives with respect to the time) are negligible as long as the mean velocity  $\bar{u}$  and the associated bottom friction are sufficiently large. At small values of the mean velocity however the correction may become comparatively important and, for instance, the resulting bottom stress may have a different direction from the mean velocity vector, even in the absence of wind.

At small velocities, the correction for the non-linear terms  $n$  is not necessary and the result of the analytical multi-mode model can be used to correct for the bottom stress parameterization.

The relationship between  $\bar{u}$  and  $\tau_b$  given by the multi-mode model is rather complicated but Roisin (1977) has shown that it could be written in much more convenient and simple forms and that, with a good approximation, one could take

$$(132) \quad \tau_b = D^{1/2} \|\tau_b\|^{1/2} \bar{u} - m \tau_s + \gamma H \left( \frac{\partial \bar{u}}{\partial t} + f e_3 \wedge u \right)$$

where  $D$  and  $m$  are the coefficients of the classical bottom friction law ( $D$  is the drag coefficient) and where  $\gamma$  is a numerical factor.

If the consistency condition,  $\bar{u} = -\hat{u}$  at the bottom, is not satisfied at a given time step  $t$ , eq. (132) can be introduced in an iteration scheme where the corrected value of  $\tau_b$  at time  $t$  is computed in terms of the simultaneous value of  $\bar{u}$  and  $\tau_s$  and the immediate past history of  $\bar{u}$  [ $\bar{u}(t - \Delta t)$ ].

The non-linear three-dimensional model was applied to the calculation of tides and storm surges in the North Sea (Nihoul, 1979). The two-dimensional depth-integrated model was run for the whole North Sea with the horizontal grid used by Roday (1976). The vertical profile of the velocity vector was calculated at a series of points in the Southern Bight. The test points were selected for their role in the existing management program of the North Sea and corresponded to places where current meters were to be moored or where the vertical variations of the current were desired to study the deposition of silt, the distribution of eggs and larvæ, etc.

Although some of these points were close to the coast or in relatively shallow irregular depths, very few iteration stages were found necessary in most cases.

In many places, there is no significant improvement in taking the non-linear advection terms into account in the calculation of  $\bar{u}$  and the variable eddy viscosity multi-mode model (Nihoul, 1977) appears to give very satisfactory results. This is illustrated, in the following, by the results of the computation at the point  $52^{\circ} 30' N$   $3^{\circ} 50' E$ .

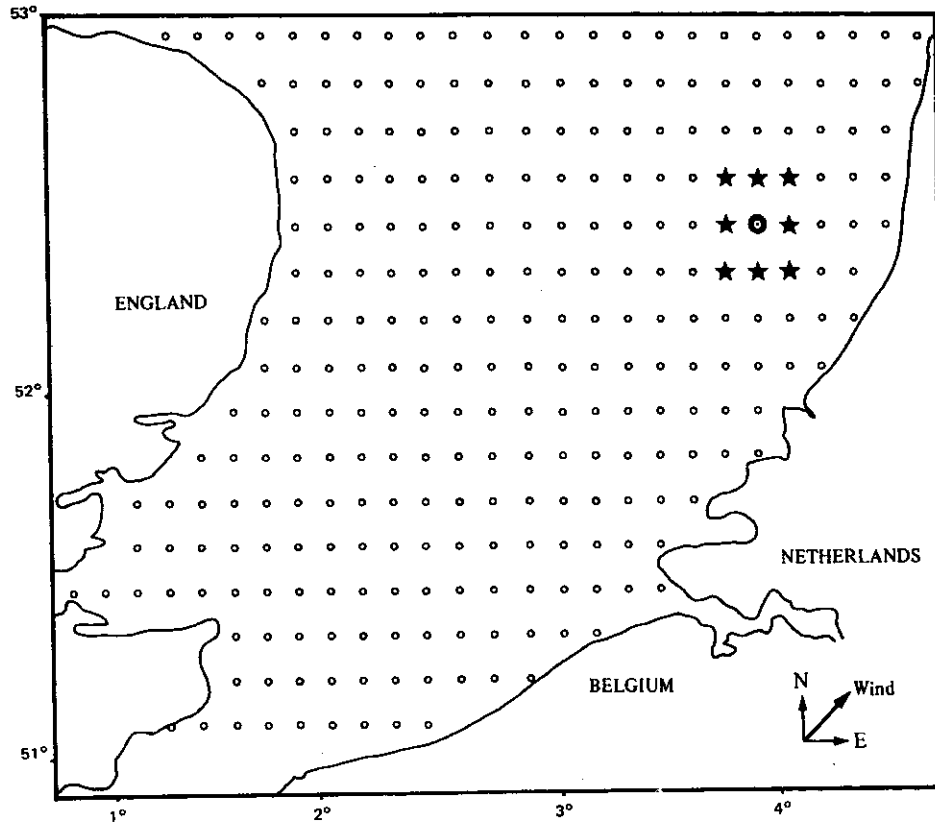


fig. 37.

Numerical grid for the two-dimensional depth-integrated model showing the test point and the wind direction.

Fig. 37 shows the numerical grid for the two-dimensional model of the Southern Bight of the North Sea ( $\Delta x_1 = 10^4$  m;  $\Delta x_2 = 1.395 \times 10^4$  m). The test point is indicated by  $\odot$ . The depth there is 22 m, the rugosity length  $10^{-3}$  m ( $\xi_0 \sim 5 \times 10^{-5}$ ). The wind stress is oriented to the North-East as indicated in the lower right-hand corner of the figure and it has a maximum magnitude of  $2 \times 10^{-4} \text{ m}^2 \text{ s}^{-2}$ .

In this exercise, the iteration was restricted to the introduction of the non-linear advection terms. No correction was made on  $\tau_b$  to emphasize the comparison with the analytical multi-mode model (Nihoul, 1977).



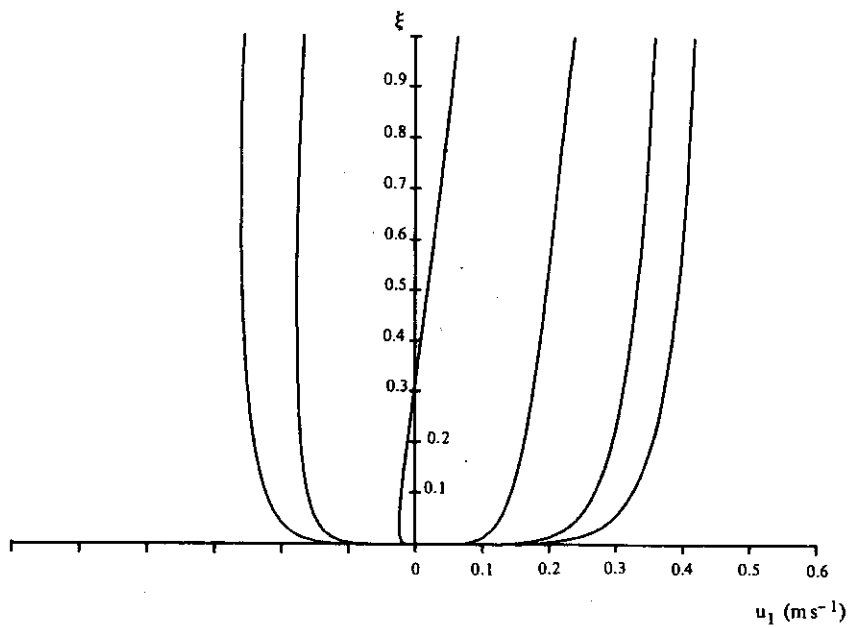


fig. 38.

Evolution with time, over the first half tidal period, of the eastern component of the horizontal velocity vector  $u_1$ . The curves from right to left are vertical profiles computed at 54' interval.

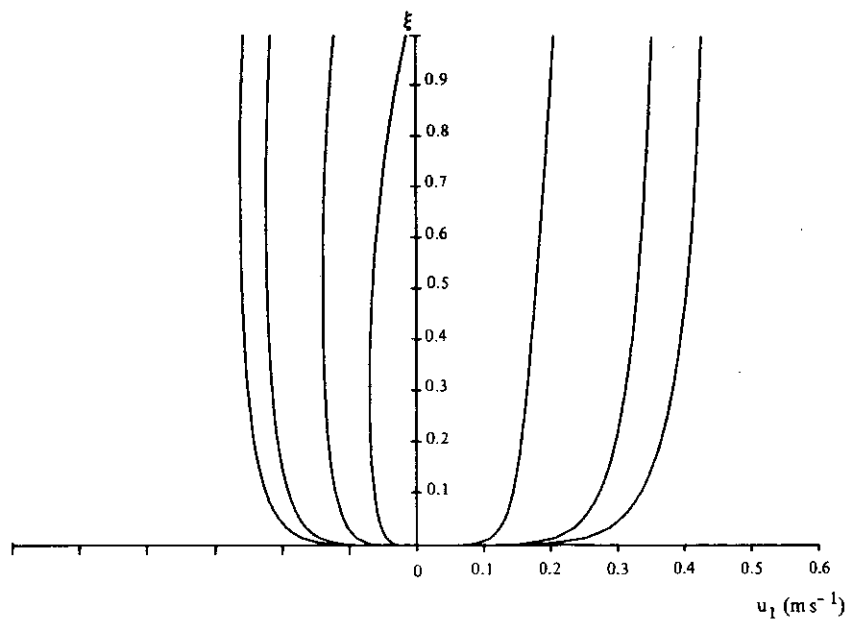


fig. 39.

Evolution with time, over the second half tidal period, of the eastern component of the horizontal velocity vector  $u_1$ . The curves from right to left are vertical profiles computed at 54' interval.

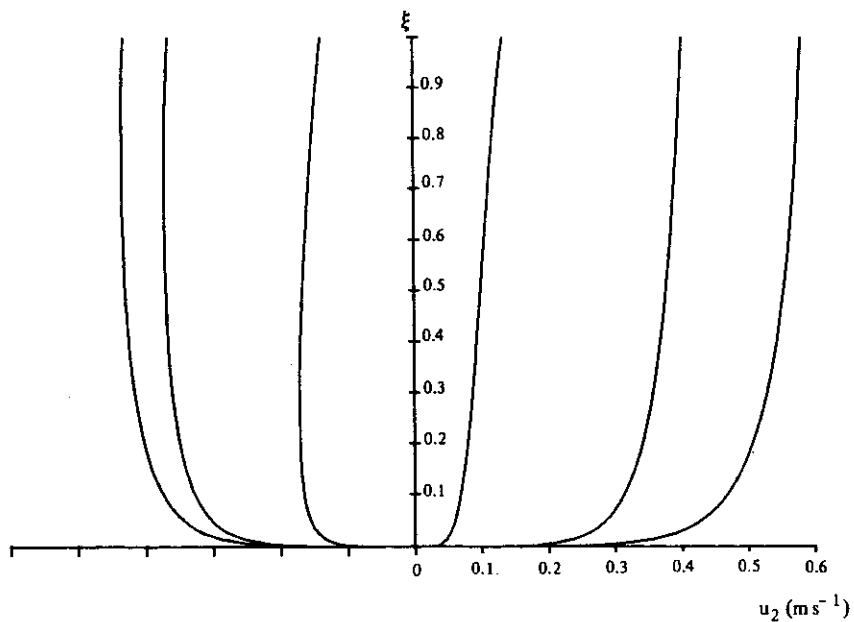


fig. 40.

Evolution with time, over the first half tidal period, of the northern component of the horizontal velocity vector  $u_2$ . The curves from right to left are vertical profiles computed at 54' interval.

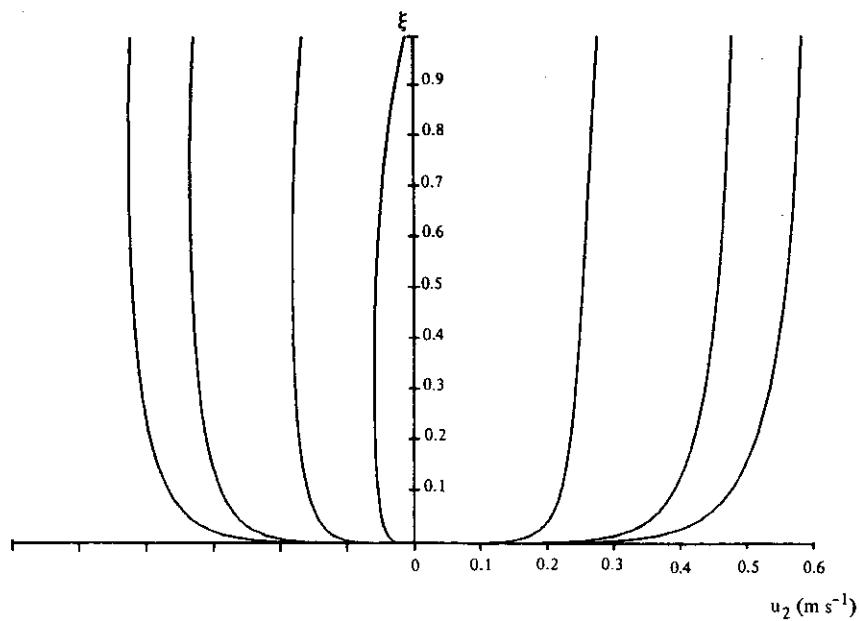


fig. 41.

Evolution with time, over the second half tidal period, of the northern component of the horizontal velocity vector  $u_2$ . The curves from right to left are vertical profiles computed at 54' interval.

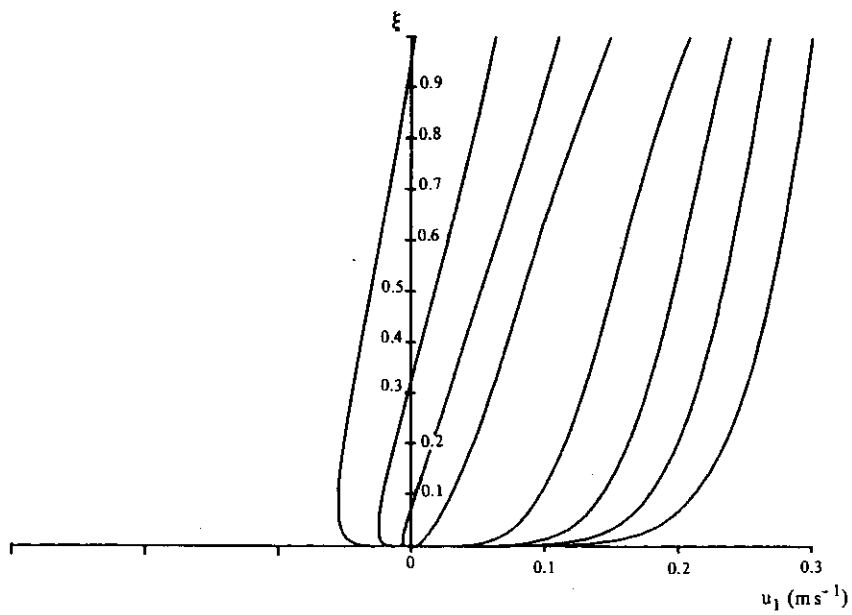


fig. 42.

Evolution with time, at tide reversal, of the eastern component of the horizontal velocity vector  $u_1$ . The curves from right to left are vertical profiles computed at 18' interval.

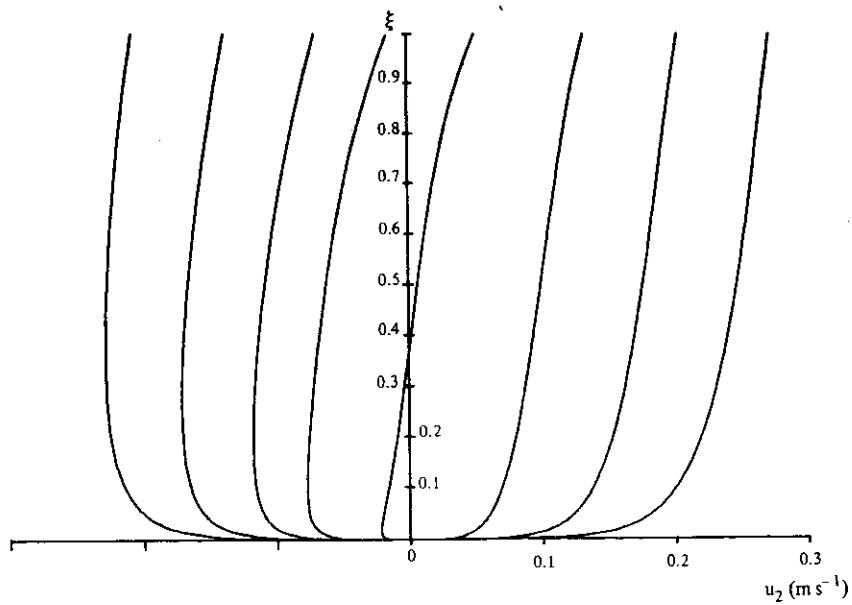


fig. 43.

Evolution with time, at tide reversal, of the northern component of the horizontal velocity vector  $u_2$ . The curves from right to left are vertical profiles computed at 18' interval.

Figs. 38 - 43 show the results of the model in which the non-linear advection terms were included by successive iterations at each time step. One notices on figs. 42 and 43 that, near tide reversal, bottom currents may flow in opposite directions and that the bottom stress maintained by the current in the bottom layer is then difficult to relate to the mean current which may become very small.

Figs. 44 and 45 show the difference in magnitude and direction between the mean velocity  $\bar{u}$  computed by the uncorrected two-dimensional depth-integrated model and by the non-linear three-dimensional model, respectively.

Figs. 46 and 47 show the veering of the horizontal velocity vector over the water column. It must be noted here that most of the veering occurs above  $\xi \sim 0.1$ . This is not obvious on the figures because there is about the same number of points in the lower layer  $\xi \leq 0.1$  and the upper layer  $0.1 \leq \xi \leq 1$ . This is actually an artifice of the numerical method which, for increased accuracy, introduces the change of variable

$$y = \ln \frac{\xi}{\xi_0}$$

in the bottom layer ( $\xi_0 \leq \xi \leq 0.15$ ) where the vertical gradients are large. The same remark applies to fig. 48.

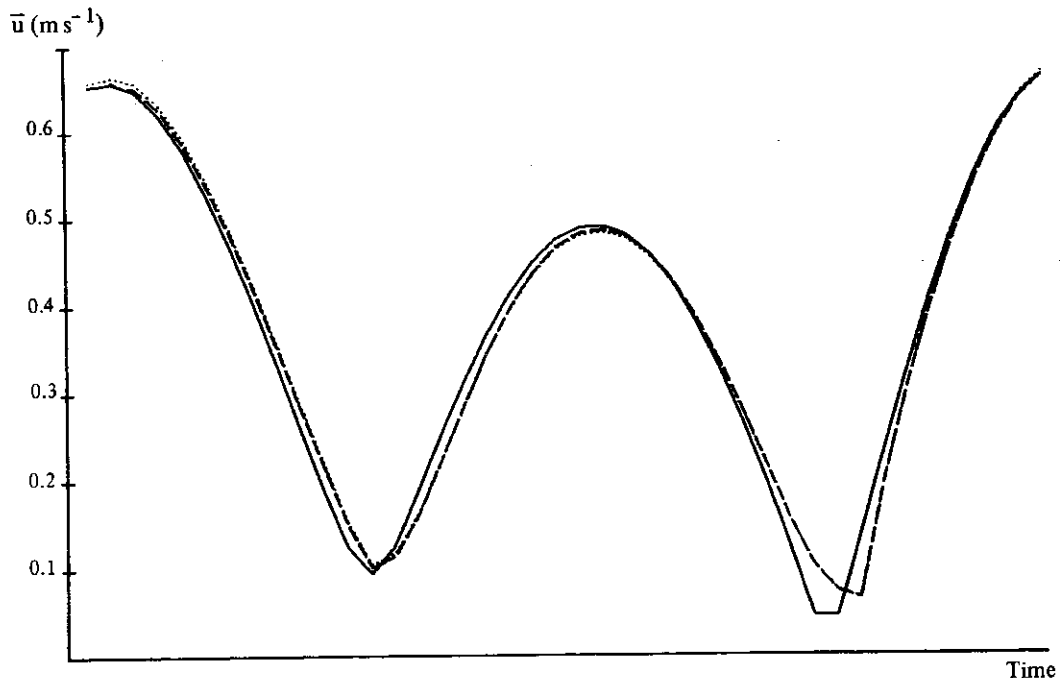


fig. 44.

Evolution with time over one tidal period of the magnitude of the mean velocity  $\bar{u}$  computed respectively by the uncorrected two-dimensional depth-integrated model (full line —), the linear local model (dash line ---) and the non-linear local model (dots .....).

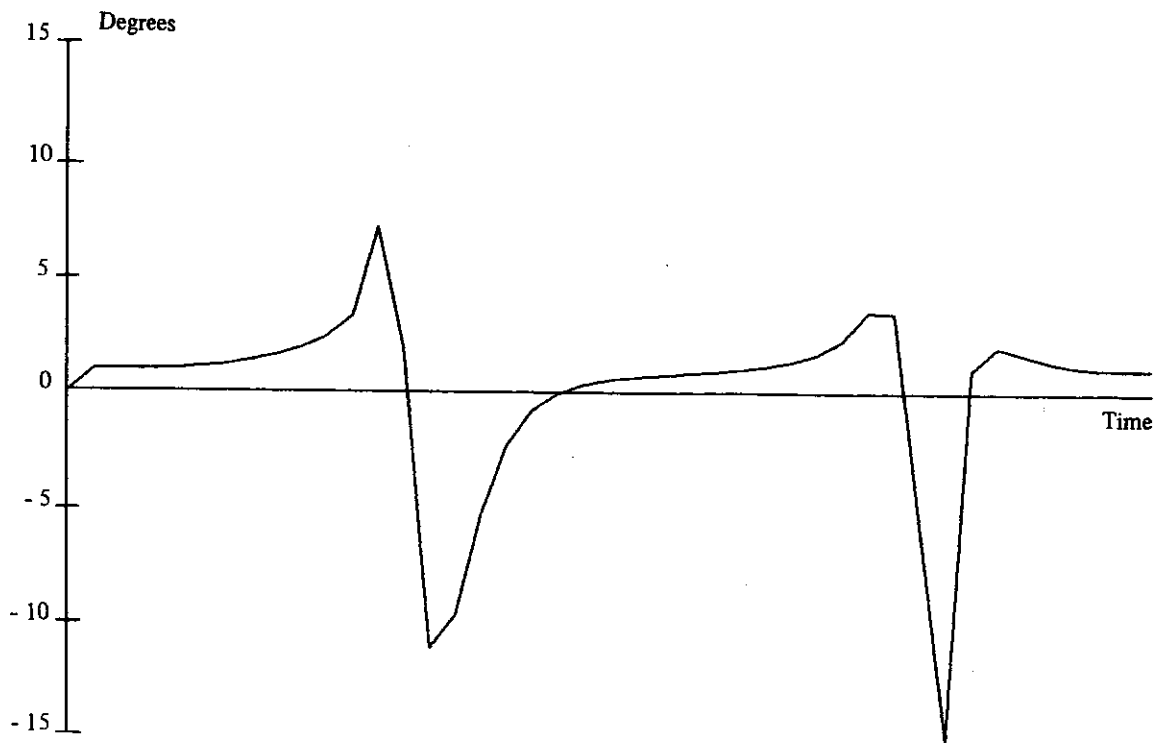


fig. 45.

Evolution with time over one tidal period of the difference between the directions of the mean velocity computed respectively by the uncorrected two-dimensional model and by the non-linear model.

Fig. 48 shows that, as long as the mean velocity is sufficiently large, the horizontal velocity vector keeps the same direction from the bottom to the surface. In that case, the classical bottom friction law applies and it may be assumed that the bottom stress is roughly (except for a small wind effect) parallel to the mean velocity. On the other hand, when the mean velocity becomes small, near tide reversal, there is a noticeable rotation of the velocity vector between its directions in the bottom and the surface layers. During a comparatively short period of time, one may thus expect the classical parameterization of the bottom stress to fail both in magnitude and direction. As described above, this may be corrected at each time step in the critical interval by an iteration procedure.

The iteration on the non-linear terms does not, on the other hand, appear to bring significant improvement in the example considered. The effect may of course be larger at other grid points but, in general, it seems to constitute only a minor correction.

In large-scale practical applications of the three-dimensional model, one would thus be wise to define realistically limiting values of  $\bar{u} + \hat{u}(\xi_0)$  and  $n$  which one is willing to tolerate and

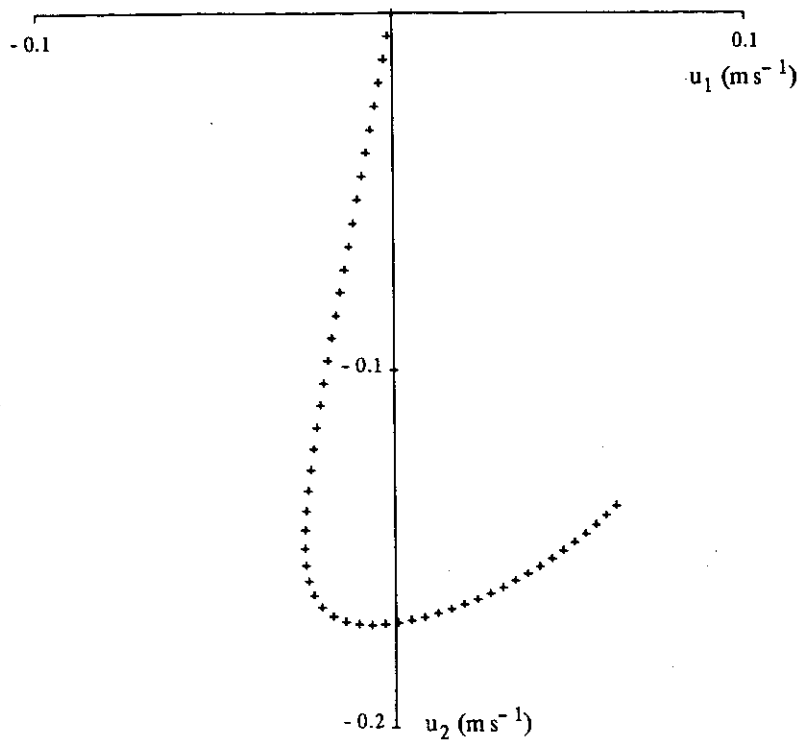


fig. 46.

Vertical veering of the horizontal velocity vector at tide reversal

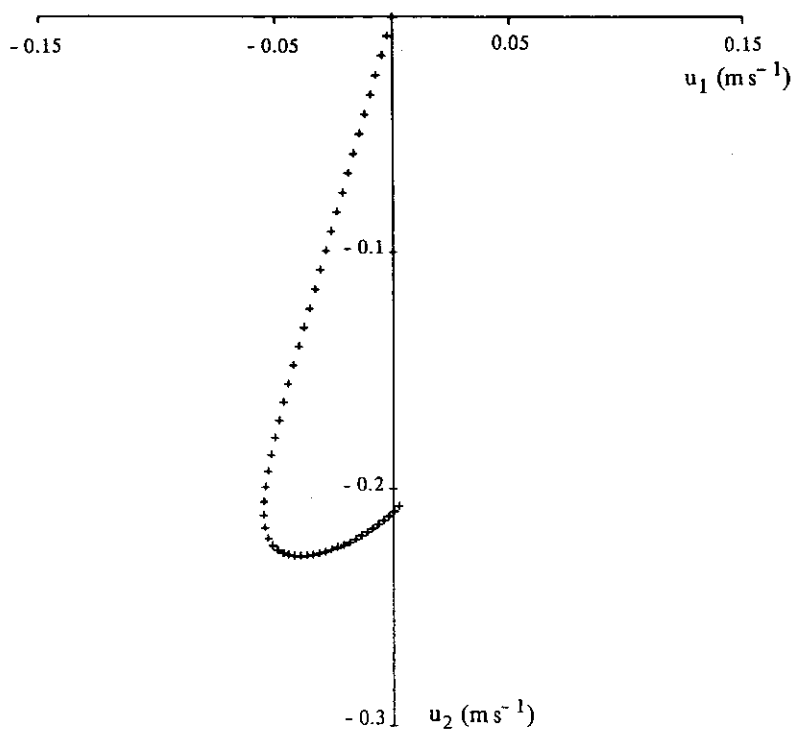


fig. 47.

Vertical veering of the horizontal velocity vector 18° after tide reversal

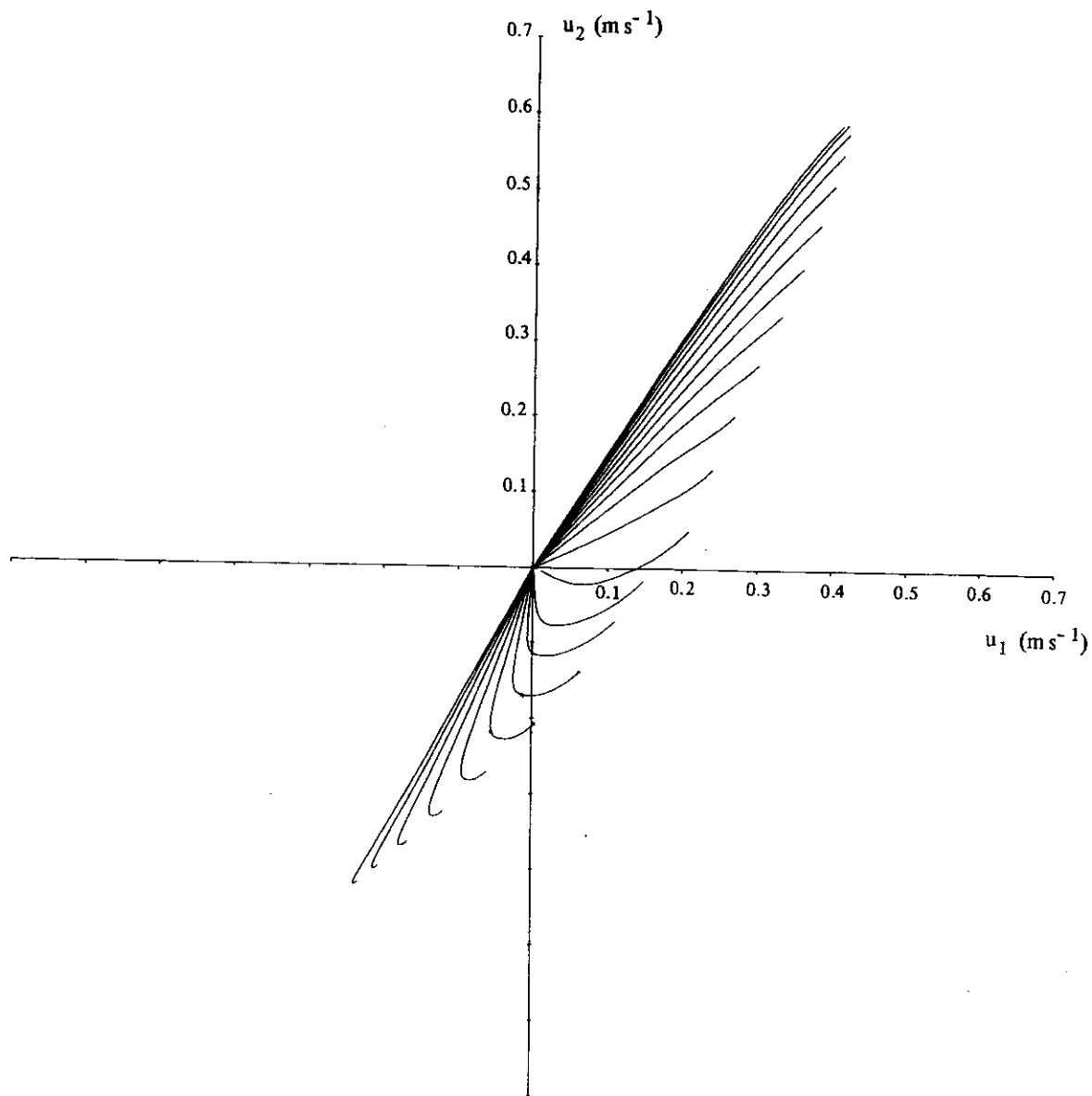


fig. 48.

Evolution with time over the first half tidal period of the Ekman diagram showing the vertical veering of the horizontal velocity vector. The separation between two successive curves is 18'.

instruct the model to proceed without any vainly expensive iteration whenever the calculated values do not exceed the limits of tolerance.

The three-dimensional model presented above has been applied mainly to the prediction of tides and storm surges in well-mixed continental seas like the North Sea. It can, however, be easily extended to other mesoscale processes and to different situations, including, in particular, partially stratified waters.

The model is the superposition of a depth-integrated two-dimensional model and a locally one-dimensional model where the variations of the eddy viscosity with depth is properly taken into account, the bottom friction is parameterized without excessive empiricism and the non-linear effects are taken into consideration.

The inclusion of the non-linear terms and of a variable eddy viscosity is, according to Cheng (Cheng et al., 1976) a significant improvement on former models developed along the same line (e.g. Heaps, 1972, 1976; Foristall, 1974; Cheng, 1976).

#### 11. - Three-dimensional and two-dimensional models of the residual circulation.

Hydrodynamic models of the North Sea are primarily concerned with tides and storm surges and the associated currents which can have velocities as high as several meters per second.

However the period of the dominant tide is only about a half day and the characteristic life time of a synoptic weather pattern is of the order of a few days. The very strong currents which are produced by the tides and the atmospheric forcing are thus relatively transitory and a Marine Biologist will argue that over time scales of biological interest, they change and reverse so many times that they more or less cancel out, leaving only a small residual contribution to the net water circulation (Nihoul, 1981).

The importance of tidal and wind induced currents for the generation of turbulence and the mixing of water properties is of course not denied but many biologists would be content with some rough parameterization of the efficiency of turbulent mixing and, for the rest, some general description of the long term transport of "water masses".

Although the concept of "moving water masses", and its train of pseudo-lagrangian misdoings, appeal to chemists and biologists who would like to find, in the field, near-laboratory conditions, it is impossible to define it in any scientific way and charts of the North Sea's waters like the one shown in fig. 49 and reproduced from Laevastu (1963) are easily misinterpreted and often confuse the situation by superposing a flow pattern on an apparently permanent "geography" of water masses.

The notion of "residual" circulation - which, at least, has an Eulerian foundation - has long remained almost as vague. Some people have defined it as the observed flow minus the computed tidal flow (e.g. Otto, 1970). Such a definition is understandable from a physical point of view but one must realize that the residual flow so-defined contains all wind-induced currents, including small scale fluctuations. It is definitely not a steady or quasi-steady flow and some attempts to visualize it by means of streamlines are questionable. What it represents, in terms of marine chemistry or marine ecology is not at all clear.



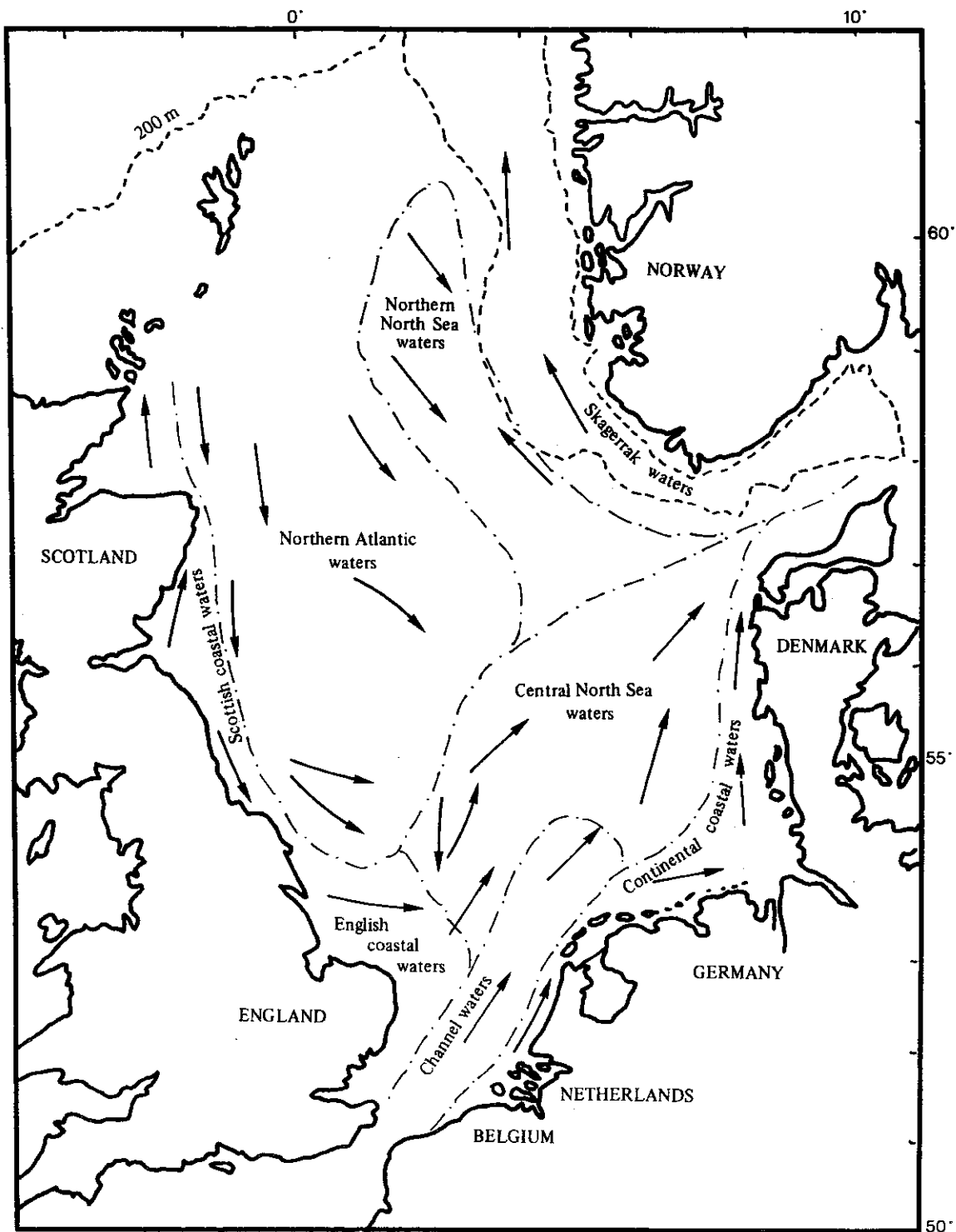


fig. 49.

Water types in the North Sea according to Laevastu (1963). [Adapted from Folio 4 of Serial Atlas of the Marine Environment with the permission of the American Geographical Society.]

Actually, if one wants to take the point of view of the marine ecologist, one should really look at the *mean flow* over some appropriate period of time of biological interest.

It is customary for experimentalists to compute, from long series of observations, daily, weekly and monthly averages. What such averages actually represent is debatable.

No doubt that tidal currents are essentially removed in this process. However with tidal velocities, one or two orders of magnitude higher than residual velocities and the latter of the order of traditional current-meters' errors, one may fear that, as a result of the non-linearities of the equipment, the error remains the same order of magnitude after averaging and leads to a 100 % inaccuracy in the calculated mean residual (e.g. Nihoul, 1980).

Moreover the choice of the periods of time over which the averages are made is not obvious as it seems to rely more on the calendar than on physical processes. One must be quite clear of what one gets from such averages.

With tides reversing four times daily and changes in the synoptic weather pattern taking several days, one may expect daily averages to remove tidal motions while still catching most of the residual currents responding to the evolving meteorological conditions.

Monthly averages, on the other hand, will have a more "climatic" sense and will presumably represent the residual circulation which is induced by macroscale oceanic currents (such as the North-Atlantic current in the case of the North Sea) and the mean effect of non-linear interactions of mesoscale motions (tides, storm surges, ...).

Here, the terms "macroscale", "mesoscale" (and later on "microscale") are used in reference with the time scales of motion. In general time scales and length scales are related but it doesn't have to be so and no such assumption is made here at this stage.

The role of residual currents and residual structures (fronts, ...) in the dynamics of marine populations, the long term transport of sediments or the ultimate disposal of pollutants, for example, is universally recognized but different schools of theoreticians and experimentalists still favour different definitions which, in the case of the North Sea, may have little in common, apart from the fact that the strong tidal oscillations have been removed.

Obviously each definition addresses a particular kind of problem and if, as it is now universally agreed, the residual circulation is defined as the mean motion over a period of time sufficiently large to cancel tidal oscillations and transient wind-induced currents, there is still the problem of choosing the time interval of averaging, taking into account the objectives of the study.

In any case, it is not demonstrated that such a time average may be obtained with sufficient accuracy from experimental records. As pointed out before, the averaging takes away more than 90 % of the signal and the final result is of the same order as the instrumental error.

In the following, one examines how the problem can be approached through mathematical modelling.

**The governing equations.**

As shown in section 2, the three-dimensional hydrodynamic equations applicable to a well-mixed continental sea, like the North Sea, can be written

$$(133) \quad \nabla \cdot \mathbf{v} = 0$$

$$(134) \quad \frac{\partial \mathbf{v}}{\partial t} + \nabla \cdot (\mathbf{v}\mathbf{v}) + 2 \boldsymbol{\Omega} \wedge \mathbf{v} = - \nabla q + \nabla \cdot \mathbf{R}$$

where  $\boldsymbol{\Omega}$  is the Earth's rotation vector,

$$q = \frac{p}{\rho} + gx_3,$$

$p$  is the pressure,  $\rho$  the specific mass of sea water,  $x_3$  the vertical coordinate and  $\mathbf{R}$  the turbulent Reynolds stress tensor (the stress is here per unit mass of sea water) resulting from the non-linear interactions of three-dimensional microscale turbulent fluctuations.

The turbulent Reynolds stress tensor can be parameterized in terms of eddy viscosity coefficients. In microscale three-dimensional turbulence, these coefficients are of the same order of magnitude in the horizontal and vertical directions. Then, horizontal length scales being much larger than the depth, the last term in the right-hand side of eq. (134) can be written simply, with a very good approximation

$$(135) \quad \nabla \cdot \mathbf{R} = \frac{\partial \boldsymbol{\tau}}{\partial x_3} = \frac{\partial}{\partial x_3} (\tilde{\nu} \frac{\partial \mathbf{v}}{\partial x_3})$$

where  $\tilde{\nu}$  is the vertical eddy viscosity and  $\boldsymbol{\tau}$  the turbulent Reynolds stress (vector).

The residual flow is defined as the mean flow over a time  $T$  sufficiently large to cover at least one or two tidal periods. If the subscript  $_0$  denotes such an average, one may write

$$(136) \quad \mathbf{v} = \mathbf{v}_0 + \mathbf{v}_1$$

with

$$(137) \quad (\mathbf{v})_0 = \mathbf{v}_0$$

$$(138) \quad (\mathbf{v}_1)_0 = \mathbf{0}$$

What  $v_0$  and  $v_1$  respectively include depends on the time of integration  $T$ .

If  $T$  is of the order of one day (exactly two or three periods of the dominant  $M_2$  tide),  $T \sim 10^5$ , the averaging eliminates the tidal currents and smoothes out all current fluctuations - generated by variations of the wind field, for instance - which have a characteristic time smaller than  $T$ .

However, as mentioned before, changes in the synoptic weather pattern often have time scales comparable with  $T \sim 10^5$ . Then, unless one considers periods of negligible meteorological forcing,  $T \sim 10^5$  does not correspond to a valley in the energy spectrum of the currents. In that case, one cannot derive an equation for  $v_0$  by averaging eq. (134) and assuming that, as for an ensemble average, the averaging commutes with the time derivative. Furthermore,  $v_0$  defined in this way, depends very much on time and doesn't correspond to the quasi-steady drift-flow the biologists have in mind when they talk about residuals.

One might argue that such a time dependent daily mean is still worth calculating to follow the response of the sea to the evolving weather pattern, especially in storm conditions. This however would be equivalent to modelling a storm surge with a time step of  $10^5$  and the results cannot be very accurate. It is much wiser, in that case, to solve eqs. (133) and (134) without averaging for tides and storm surges simultaneously.

Actually, "daily" residuals (i.e. mean currents over exactly two or three tidal periods) are meaningful only when the atmospheric forcing is negligible or exceptionally persistent.

In the first case, they represent the so-called "tidal residuals" which result from in- and out-flowing macroscale oceanic currents and from the residual effect of non-linear tidal interactions.

Tidal residuals represent a major contribution to the total residual circulation and, with very much less computer work needed, they already give a good idea of the long term residual circulation, such as the climatic circulation described below, where a substantial part of the atmospheric contribution is actually removed by averaging over a variety of different weather conditions.

If one takes, for instance, the averaging time  $T$  between  $10^6$  (~ two weeks) and  $10^7$  (~ four months), one may expect, over such a long time, a diversity of meteorological conditions resulting in an almost random atmospheric forcing on the sea. The current patterns will reflect the atmospheric variability and, on the average, there will be only a small residue.

The mean flow over a time  $T \sim 10^6, 10^7$  may be regarded as the "climatic residual" flow which affects the dynamics of biological populations, the long term transport of sediments and the slow removal of pollutants.

As pointed out before, one may conceive a third kind of residuals obtained by averaging over two or three tidal periods ( $T \geq 10^5$  s) in conditions of exceptionally persistent atmospheric forcing.

The persistence of the meteorological conditions drives off the atmospheric energy input to small frequencies and a time of the order of  $10^5$  is acceptable for averaging as it corresponds again to a valley in the energy spectrum.

This kind of residuals may be called in brief "wind residuals". One must be aware, however, that they give a rather limited view of wind-induced currents in the sea. If a typical weather pattern has a characteristic time of a few days, one must either determine the time dependent wind-induced and tidal flow described by eqs. (133) and (134) or the climatic residual flow which contains only the macroscale residue of changing weather patterns.

Still, with moderate computer work needed, wind residuals may perhaps provide a first idea of various wind effects on the residual flow pattern which would not be apparent in the climatic or tidal residual pattern but which might occasionally be spotted by instruments in the field.

In the following "residual circulation" will refer to the climatic residual circulation ( $T \geq 10^6$  s) or the tidal and wind residual circulations ( $T \geq 10^5$  s) with the restrictions made above.

The equations for the residual flow may be obtained by taking the average of eqs. (133) and (134) over the chosen time  $T$ .

The time derivative in the left-hand side of eq. (134) gives a contribution

$$(139) \quad \frac{v(t+T) - v(t)}{T}$$

One may argue that, since the time  $T$  is always a multiple of the main tidal period, the numerator of (139) is of the same order as the residual velocity  $v_0$ . Then, for  $T \geq 10^5$ ,

$$(140) \quad \frac{v(t+T) - v(t)}{T} \lesssim 0(10^{-5} v_0)$$

The average of the Coriolis acceleration is

$$(141) \quad 2 \Omega \wedge v_0 \sim 0(10^{-4} v_0)$$

One may thus neglect the contribution of the time derivative in the equation for  $v_0$ . The residual circulation is then given by the steady state equations

$$(142) \quad \nabla \cdot v_0 = 0$$

$$(143) \quad \nabla \cdot (\cancel{v_0} v_0) + 2 \Omega \wedge v_0 = - \nabla q_0 + \frac{\partial \tau_0}{\partial x_3} + \nabla \cdot N$$

where

$$(144) \quad N = (-v_1 v_1)_0$$

Since  $v_0$  is one or two orders of magnitude smaller than  $v_1$  which contains in particular the tidal currents, the first term in the left-hand side of eq. (143) is completely negligible. The tensor  $N$  in the right-hand side plays, for mesoscale motions, a role similar to that of the turbulent Reynolds stress tensor  $R$  in eq. (134) and may be called the "mesoscale Reynolds stress tensor". The last term in the right-hand side of eq. (143) represents an additional force acting on the residual flow and resulting from the non-linear interactions of mesoscale motions (tides, storm surges, ...).

The importance of this force was discovered, first, by depth-integrated numerical models of the residual circulation in the North Sea (Nihoul, 1974; Nihoul and Ronday, 1975) and the associated stress was initially referred to as the "tidal stress" to emphasize the omnipresent contribution of tidal motions.

#### *The mesoscale Reynolds stress tensor.*

The tensor  $N$  can be computed explicitly by solving eqs. (133) and (134) for mesoscale motions and taking the average of the dyadic  $v_1 v_1$ .

In fact the solution of eqs. (133) and (134) with appropriate wind forcing and open sea boundary conditions yields

$$v = v_0 + v_1$$

and one may reasonably ask the question why one must go through the process of computing  $N$  and solving eqs. (142) and (143) to obtain the residual velocity  $v_0$  i.e. why one cannot solve (133) and (134) for the total velocity  $v$  and simply derive  $v_0$  from  $v$  *directly*, by averaging the solution of eqs. (133) and (134) (e.g. Alfrink and Vreugdenhil, 1981).

The problem here, again, is that, in the North Sea,  $v_1$  represents 90 % of  $v$ . If one allows for an error  $\delta v$  on  $v$  of, say, 10 %, resulting from the imprecision of open-sea boundary conditions and from the approximations of the numerical method, the error is of the same order of magnitude as the residual flow  $v_0$ .

Because of non-linearities, one may fear that, in the averaging process, this error does not, for the essential, cancel out as  $v_1$  does. Thus averaging the solution  $v$  of eqs. (133) and (134), one gets  $v_0 + (\delta v)_0$  i.e. the residual velocity with an error which may be as large as 100 % (Nihoul and Ronday, 1976).

The procedure is conceivable when modelling a very limited area (near a coast, for instance) where the mesh size of the numerical grid can be reduced and where the open-sea boundary conditions can be determined with greater accuracy by direct measurements. Then  $\delta v$  can be made small enough for the average

$\mathbf{v}_0 + (\delta\mathbf{v})_0$  to provide a satisfactory evaluation of the residual flow  $\mathbf{v}_0$ .

In the case of the North Sea or, even, the Southern Bight or the English Channel, models of such a high accuracy are prohibitively expensive and cannot be considered for routine forecasting.

However the classical models give  $\mathbf{v}_1$  with a fair accuracy and they can be used to compute the mesoscale stress tensor  $\mathbf{N}$ . The latter can be substituted in eq. (143) and the system of eqs. (142) and (143) can be solved very quickly to obtain  $\mathbf{v}_0$ . One can show that, in this way, one can determine  $\mathbf{v}_0$  with good accuracy.

Typical values for the North Sea show that, in general, the two terms  $2 \boldsymbol{\Omega} \wedge \mathbf{v}_0$  and  $\nabla \cdot (-\mathbf{v}_1 \mathbf{v}_1)_0$  are of the same order of magnitude.

If  $\delta\mathbf{v}_1$  is the error on  $\mathbf{v}_1$ , one has

$$\delta[\nabla \cdot (-\mathbf{v}_1 \mathbf{v}_1)_0] \sim [\nabla \cdot (-\mathbf{v}_1 \mathbf{v}_1)_0] \frac{\delta v_1}{v_1}$$

This error induces an error  $\delta\mathbf{v}_0$  on  $\mathbf{v}_0$  given by

$$2 \boldsymbol{\Omega} \wedge \delta\mathbf{v}_0 \sim \delta[\nabla \cdot (-\mathbf{v}_1 \mathbf{v}_1)_0] \sim 0(2 \boldsymbol{\Omega} v_0 \frac{\delta v_1}{v_1})$$

i.e.

$$\frac{\delta v_0}{v_0} \sim \frac{\delta v_1}{v_1}$$

Hence the *relative* error is the same on  $\mathbf{v}_0$  and on  $\mathbf{v}_1$  and not the *absolute* error as before. Thus if  $\mathbf{v}_1$  can be computed with, say, a 90 % precision, the solution of the averaged eqs. (142) and (143) will give the residual circulation with the same 90 % precision.

#### ***The equation for the horizontal transport.***

If one writes

$$(145) \quad \mathbf{v} = \mathbf{u} + v_3 \mathbf{e}_3$$

$$(146) \quad \mathbf{u} = \mathbf{u}_0 + \mathbf{u}_1$$

emphasizing as before the horizontal velocity vector  $\mathbf{u}$ , one defines the residual horizontal transport as

$$(147) \quad U_0 = \int_{-h}^{\zeta_0} \mathbf{u}_0 \, dx_3 = H_0 \bar{\mathbf{u}}_0$$

where  $\bar{\mathbf{u}}_0$  is the depth-averaged velocity,  $H_0 = h + \zeta_0$ ,  $h$  is the depth and  $\zeta_0$  the residual surface elevation ( $H_0 \sim h$  because  $\zeta_0 \ll h$ ).

The derivation of equations for the residual transport by integration of eqs. (143) and (144) over depth is quite straightforward (e.g. Nihoul, 1975a). One finds, after some reordering,

$$(148) \quad \nabla \cdot \mathbf{U}_0 = 0$$

$$(149) \quad f \mathbf{e}_3 \wedge \mathbf{U}_0 = -H_0 \nabla q_0 - K \mathbf{U}_0 + \Theta$$

where

$$(150) \quad K = \frac{D \|\mathbf{u}_1\|_0}{H_0}$$

$\mathbf{u}_1$  denoting the depth-mean of  $\mathbf{u}_1$  and  $\Theta$  standing in brief for  $\tau_0^s + \tau_0^n - \tau_0^f$  where

(i)  $\tau_0^s$  is the residual wind stress;

(ii)  $\tau_0^n$  is the mesoscale Reynolds stress

$$(151) \quad \tau_0^n = \int_{-h}^{\xi_0} \nabla \cdot (-\mathbf{v}_1 \mathbf{u}_1)_0 dx_3 ;$$

(iii)  $\tau_0^f$  is the mesoscale "friction stress"

$$(152) \quad \tau_0^f = (D \|\mathbf{u}_1\| \mathbf{u}_1)_0$$

The friction stress is the part of the residual bottom stress (the first part is  $-K \mathbf{U}_0$ ) which results from the non-linear interactions of mesoscale motions. It is analogous to the Reynolds stress  $\tau_0^n$  and represents an additional forcing on the residual flow.

Since  $\mathbf{U}_0$  is a two-dimensional horizontal vector, eq. (148) suggests the introduction of a stream function  $\Psi(x_1, x_2)$  such that

$$(153) \quad U_{0,1} = - \frac{\partial \Psi}{\partial x_2}$$

$$(154) \quad U_{0,2} = \frac{\partial \Psi}{\partial x_1}$$

Eliminating  $q$  between the two horizontal components of eq. (149), one obtains then a single elliptic equation for  $\Psi$ , viz. [using (150)]

$$(155) \quad \frac{K}{h} \nabla^2 \Psi + \frac{\partial \Psi}{\partial x_1} \left[ \frac{\partial}{\partial x_1} \left( \frac{K}{h} \right) + \frac{\partial}{\partial x_2} \left( \frac{f}{h} \right) \right] + \frac{\partial \Psi}{\partial x_2} \left[ \frac{\partial}{\partial x_2} \left( \frac{K}{h} \right) - \frac{\partial}{\partial x_1} \left( \frac{f}{h} \right) \right] \\ = \frac{\partial}{\partial x_1} \left( \frac{\Theta_2}{h} \right) - \frac{\partial}{\partial x_2} \left( \frac{\Theta_1}{h} \right)$$

This equation must be solved with appropriate boundary conditions. If one can simply take  $\Psi = \text{const.}$  along the coasts, the



conditions on the open-sea boundaries are much more difficult to assess. One has estimates of the total inflows through the Straits of Dover [ $\sim 7400 \text{ km}^3 \cdot \text{y}^{-1}$  (Carruthers, 1935; Van Veen, 1938)], the Northern boundary [ $\sim 23000 \text{ km}^3 \cdot \text{y}^{-1}$  (Kalle, 1949; Laevastu, 1963)], through the Skagerrak [ $\sim 479 \text{ km}^3 \cdot \text{y}^{-1}$  (Svansson, 1968; Tomczak, 1968)] as well as of the contribution of the main rivers [ $\sim 245 \text{ km}^3 \cdot \text{y}^{-1}$  (Mc Cave, 1974)] but the distribution of these flows along the boundaries are poorly known and one must resort to interpolation formulas which may or may not represent adequately the contribution, to the residual circulation of the North Sea, of inflowing or outflowing macroscale currents.

The open-sea boundary conditions used in the present model are derived from the above estimates following Ronday (1976). Ronday (1976) has shown that they represent the available observations reasonably well and that eventual deviations from the interpolated values at the open-sea boundaries do not generate errors which could propagate far into the North Sea. Still, a better determination of the conditions along open-sea boundaries is needed and should be considered with the highest priority in the near future.

Eq. (155) shows the influence on the residual flow of the residual friction coefficient  $K$  and its gradient, of the distribution of depths, of the curl of the residual wind stress and of the mesoscale stresses  $\tau_0^n$  and  $\tau_0^f$ .

In relatively coarse grid models of the whole North Sea (where the variations of  $K$  and  $h$  are partly smoothed out), the effect of the mesoscale stresses appears to be the most spectacular. This is illustrated by figs. 50, 51 and 52, figuring the residual circulation in negligible wind conditions. Fig. 50 shows the residual flow pattern assuming a constant depth of 80 m and neglecting  $\tau_0^n$  and  $\tau_0^f$ . Fig. 51 shows the flow pattern taking the depth distribution into account and neglecting  $\tau_0^n$  and  $\tau_0^f$ . Fig. 52 shows the flow pattern taking the depth distribution into account and including  $\tau_0^n$  and  $\tau_0^f$  computed from the results of a preliminary time dependent model of mesoscale flows.

The differences between figs. 50 and 51 are small. They both reproduce the broad trend of the residual circulation induced by the in- and out-flow of two branches of the North Atlantic current but they fail to uncover residual gyres which constitute essential features of the residual flow pattern and which have been traced in the field by observations (e.g. Zimmerman, 1976; Beckers et al., 1976; Riepmma, 1977; Prandle, 1978).

A comparison between figs. 52 and 49 shows a good agreement between the predictions of the model and the expected circulation of water masses in the North Sea.

However, as mentioned before, a model covering the whole North Sea does not have a sufficiently fine resolution (of bottom topography, for instance) and cannot detect all the existing gyres. For that reason, three models were run simultaneously, one covering the North Sea, another one, the Southern Bight and the third one, the Belgian coastal waters; the large scale models providing

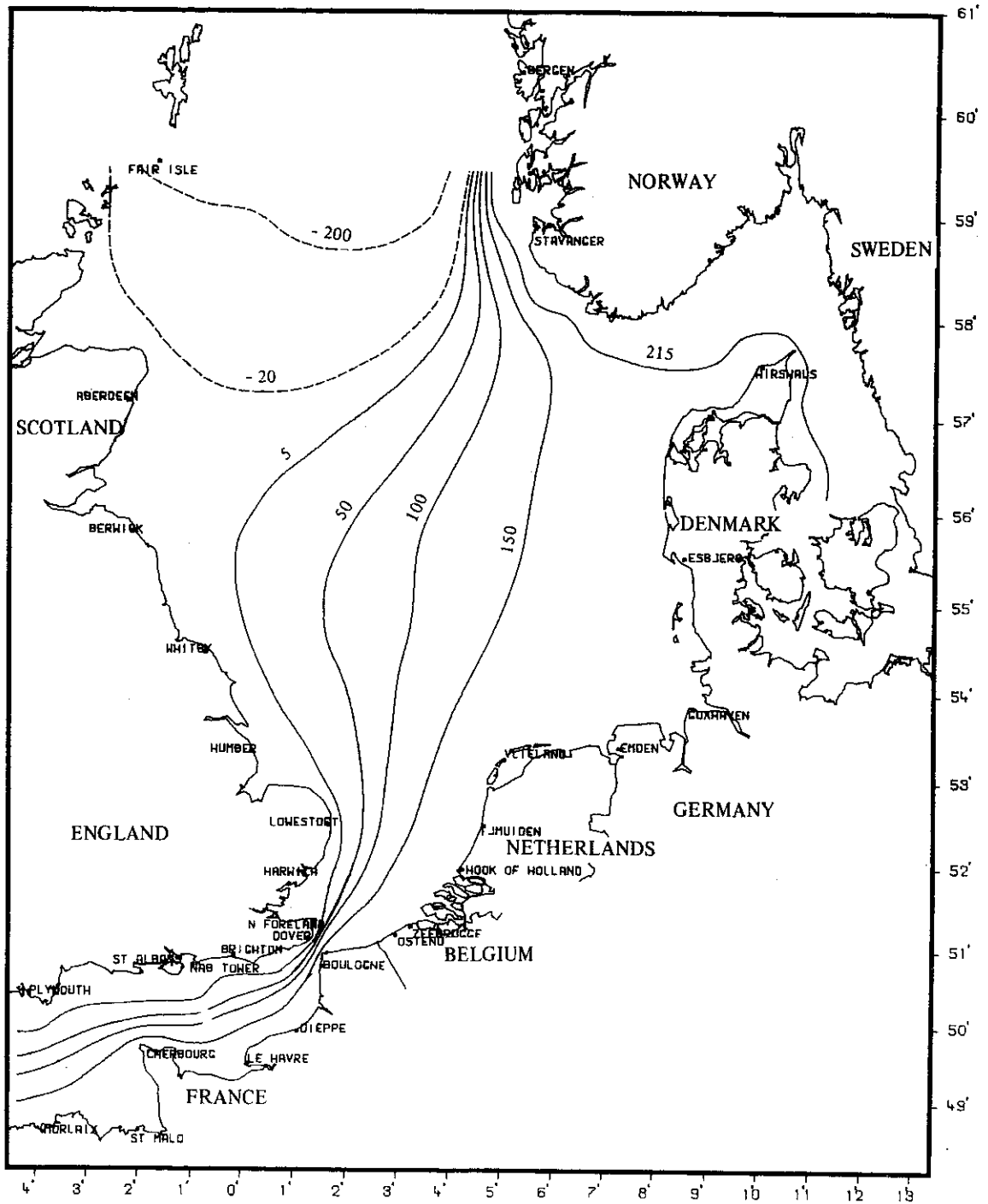


fig. 50.

Residual circulation in the North Sea calculated in negligible wind conditions assuming a constant depth and neglecting the mesoscale stresses. (Streamlines in  $10^3 \text{ m}^3 \text{ s}^{-1}$ .)

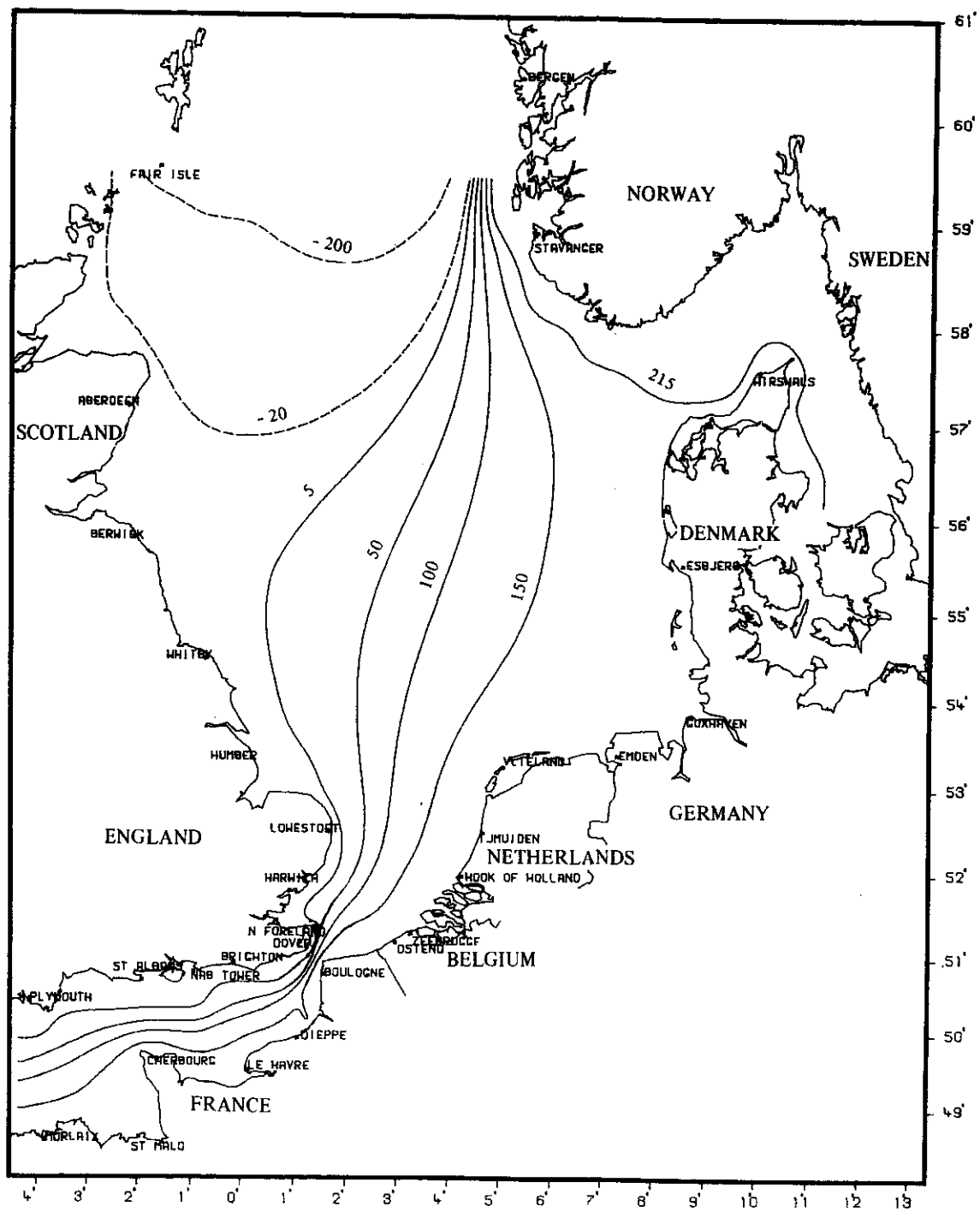


fig. 51.

Residual circulation in the North Sea calculated in negligible wind conditions with the real depth distribution, neglecting the mesoscale stresses. (Streamlines in  $10^3 \text{ m}^3 \cdot \text{s}^{-1}$ .)

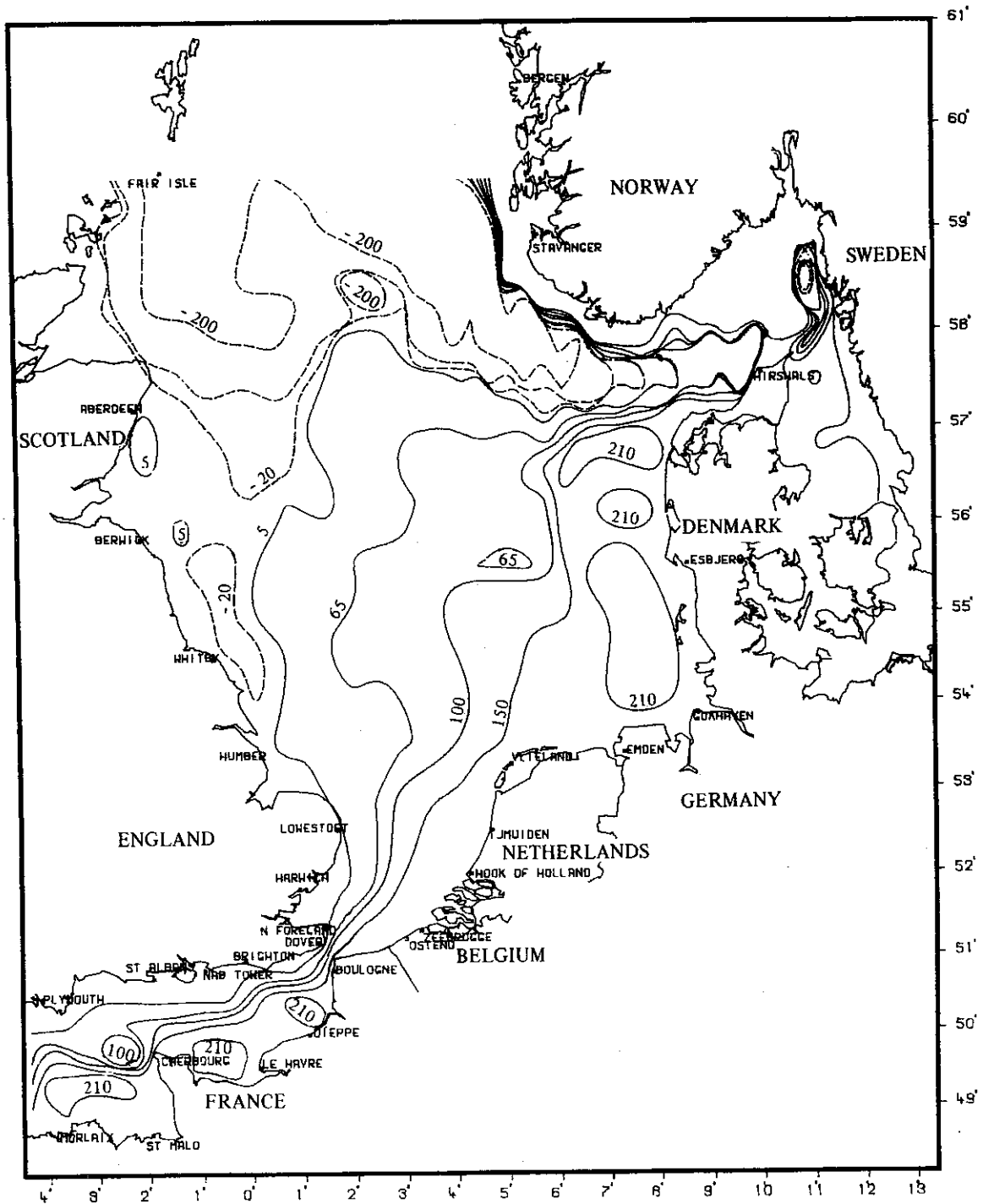


fig. 52.

Residual circulation in the North Sea calculated in negligible wind conditions with the real depth distribution, taking the mesoscale stresses  $\tau_0^n$  and  $\tau_0^f$  into account. (Streamlines in  $10^3 \text{ m}^3 \text{ s}^{-1}$ .)

open-sea boundary conditions for the smaller scale models (Nihoul and Runfola, 1981).

Fig. 53 shows the residual circulation in the Southern Bight. One notices in particular a gyre off the Belgian coast which was not apparent on fig. 52. This gyre is produced by the mesoscale stresses in relation with the spatial variations of the depth and of the residual friction coefficient  $K$  (Nihoul and Ronday, 1976).

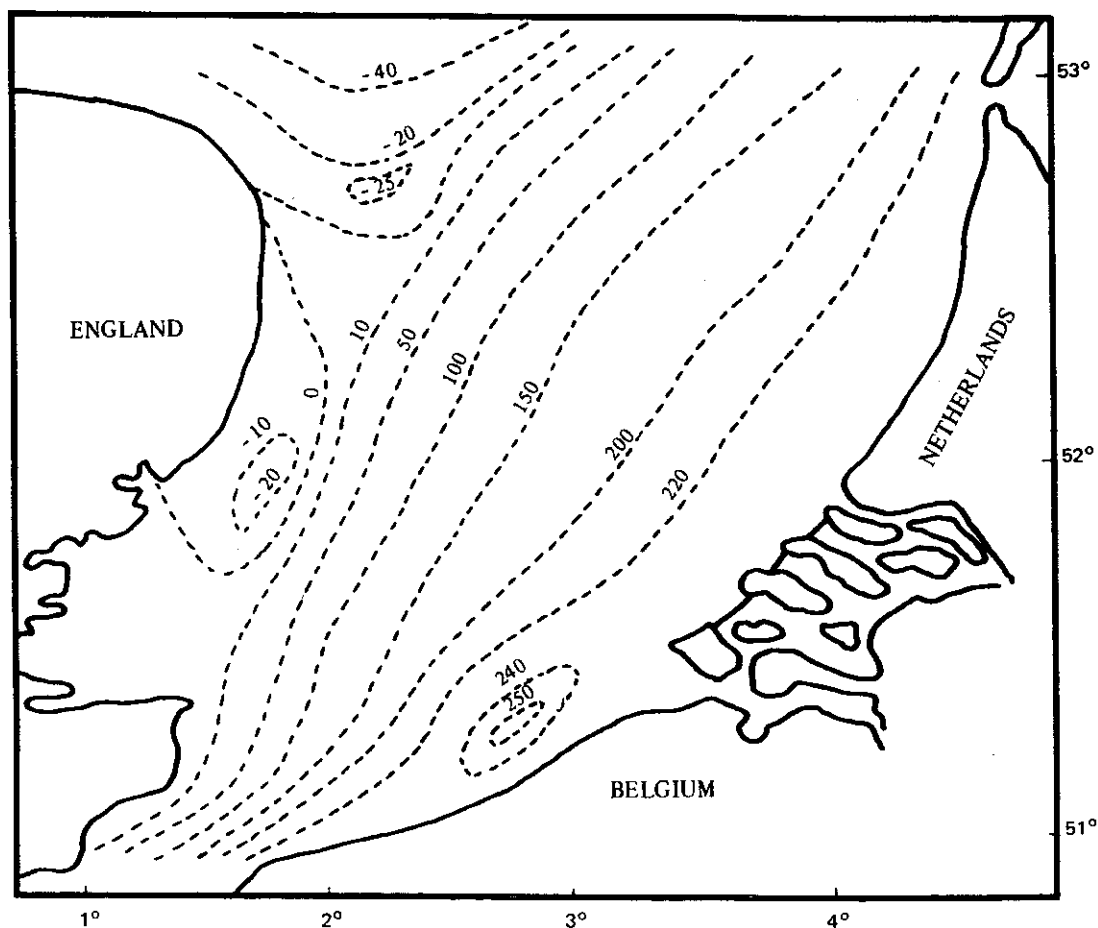


fig. 53.

Residual circulation in the Southern Bight calculated in negligible wind conditions, with the real depth distribution, taking into account the mesoscale stresses  $\tau_0^n$  and  $\tau_0^f$  (Streamlines in  $10^3 \text{ m}^3 \cdot \text{s}^{-1}$ .)

During 1972 and 1973 some 1200 sediment samples were analysed, taken at regular intervals, mostly with a Van Veen sampler, in the Southern Bight of the North Sea. As described by Gullentops (1974) "The Southern Bight is strikingly free of muddy sediments, indicating that currents and here also wave turbulence are high enough to allow only temporary decantation but no final deposition.

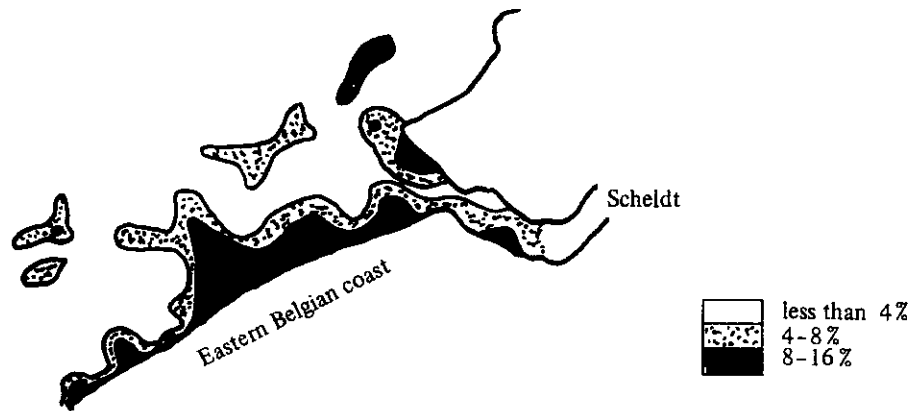


fig. 54.

Bottom sediments off the eastern Belgian coast: weight loss at 550°. (Weight loss at 550° is directly related to the presence of silt.) [Elskens and Wollast, 1974]

Only in front of the Meuse - Rhine mouth, increased fluvial input of suspension material influences the bottom sediments. The big exception is the low energy triangle in front of the eastern Belgian coast in which muddy sedimentation is developing to a considerable extent due to local affluents as the Yser, but mostly to the suspension material dragged out of the Scheldt estuary and trapped in this area.

ERTS-A remote sensing documents proved this fact strikingly, showing a suspension plume in front of the Rhine mouth and a huge turbid area in front of the eastern Belgian coast connected with an extremely turbid Scheldt estuary.

The mud area could in globo be explained by the tendency to form an outer lagoon, behind the prelittoral ridges, in which increased suspended matter arrival tends to be preserved by the current pattern, is flocculated and aggregated by biological activity and preserved from net erosion by weakened wave activity."

Figure 54 (Elskens and Wollast, 1974) shows the eastern Belgian coast to be a privileged zone of mud accumulation in relation to the whole network studied.

The presence of the gyre off the Belgian coast, shown in fig. 53, explains the high turbidity of the water and the accumulation of mud observed in the region off the eastern Belgian coast. The gyre is responsible for partially entraining the highly turbid Scheldt water to the south-west and for increasing the residence time of water masses in the area with only very low escape possibilities of the sediments to the north (Nihoul, 1975b).

12. - Energy transfers between residual flows and mesoscale motions (tides and storm surges, ...).

Using eq. (135), one can write the equations for  $\mathbf{v}$ ,  $\mathbf{v}_0$  and  $\mathbf{v}_1$  in the form

$$(156) \quad \frac{\partial \mathbf{v}}{\partial t} + \nabla \cdot (\mathbf{v}\mathbf{v}) + 2 \boldsymbol{\Omega} \wedge \mathbf{v} = - \nabla q + \frac{\partial \boldsymbol{\tau}}{\partial x_3}$$

$$(157) \quad \nabla \cdot (\mathbf{v}_0 \mathbf{v}_0) + 2 \boldsymbol{\Omega} \wedge \mathbf{v}_0 = - \nabla q_0 + \frac{\partial \boldsymbol{\tau}_0}{\partial x_3} + \nabla \cdot \mathbf{N}$$

$$(158) \quad \frac{\partial \mathbf{v}_1}{\partial t} + \nabla \cdot [\mathbf{v}_1 \mathbf{v}_0 + \mathbf{v}_0 \mathbf{v}_1 + \mathbf{v}_1 \mathbf{v}_1 - (\mathbf{v}_1 \mathbf{v}_1)_0] + 2 \boldsymbol{\Omega} \wedge \mathbf{v}_1 = - \nabla q_1 + \frac{\partial \boldsymbol{\tau}_1}{\partial x_3}$$

with

$$(159)$$

$$(160) \quad \nabla \cdot \mathbf{v} = \nabla \cdot \mathbf{v}_0 = \nabla \cdot \mathbf{v}_1 = 0$$

$$(161)$$

One can see that the equation for  $\mathbf{v}_1$  is essentially the same as the equation for  $\mathbf{v}$ . They only differ by terms which are orders of magnitude smaller. It is the reason why, one can, with the appropriate boundary conditions, determine the mesoscale velocity  $\mathbf{v}_1$ , in a first step, and the residual velocity  $\mathbf{v}_0$ , in a second step, taking the coupling between the two types of motion into account in the calculation of  $\mathbf{v}_0$  only.

Taking the scalar products of eqs. (156), (157) and (158) respectively by  $\mathbf{v}$ ,  $\mathbf{v}_0$  and  $\mathbf{v}_1$ , using eqs. (159), (160) and (161), and averaging over  $T$ , one finds, neglecting again the contributions from the time derivatives under the assumption that  $T$  is sufficiently large:

$$(162) \quad \nabla \cdot (\mathbf{v} \frac{v^2}{2} + \mathbf{v} q)_0 = \frac{\partial}{\partial x_3} (\mathbf{v} \cdot \boldsymbol{\tau})_0 - (\boldsymbol{\tau} \cdot \frac{\partial \mathbf{v}}{\partial x_3})_0$$

$$(163) \quad \nabla \cdot (\mathbf{v}_0 \frac{v_0^2}{2} + \mathbf{v}_0 q_0 - \mathbf{v}_0 \cdot \mathbf{N}) = \frac{\partial}{\partial x_3} (\mathbf{v}_0 \cdot \boldsymbol{\tau}_0) - \boldsymbol{\tau}_0 \cdot \frac{\partial \mathbf{v}_0}{\partial x_3} - \mathbf{N} : \nabla \mathbf{v}_0$$

$$(164) \quad \nabla \cdot (\mathbf{v}_0 \frac{v_1^2}{2} + \mathbf{v}_1 \frac{v_1^2}{2} + \mathbf{v}_1 q_1)_0 = \frac{\partial}{\partial x_3} (\mathbf{v}_1 \cdot \boldsymbol{\tau}_1)_0 - (\boldsymbol{\tau}_1 \cdot \frac{\partial \mathbf{v}_1}{\partial x_3})_0 + \mathbf{N} : \nabla \mathbf{v}_0$$

The terms in the left-hand sides of eqs. (162), (163) and (164) are of the divergence form. They represent fluxes of energy in physical space. The terms in the right-hand sides represent rates of energy production or destruction or energy exchanges between scales of motion.

Integrating over depth, one can see for instance that the first terms represent the average rate of work of the wind stress  $\boldsymbol{\tau}^s$ , i.e.

$$(165) \quad (\mathbf{v}^s \cdot \boldsymbol{\tau}^s) = \mathbf{v}_0^s \cdot \boldsymbol{\tau}_0^s + (\mathbf{v}_1^s \cdot \boldsymbol{\tau}_1^s)_0$$

where  $\mathbf{v}^s$  denotes the surface velocity.

The second term in the right-hand side of eq. (162) is related to the average dissipation of energy. Using eq. (135), one has, indeed

$$(166) \quad -\boldsymbol{\tau} \cdot \frac{\partial \mathbf{v}}{\partial x_3} = -\tilde{\nu} \left\| \frac{\partial \mathbf{v}}{\partial x_3} \right\|^2$$

where  $\tilde{\nu}$  is the eddy viscosity.

The depth-averaged dissipation rate

$$(167) \quad \epsilon = \frac{1}{H_0} \int_{-h}^{\xi_0} (\boldsymbol{\tau} \cdot \frac{\partial \mathbf{v}}{\partial x_3})_0 dx_3$$

can be split in two parts, as seen from eqs. (163) and (164), i.e.

$$(168) \quad \epsilon = \frac{1}{H_0} \int_{-h}^{\xi_0} \boldsymbol{\tau}_0 \cdot \frac{\partial \mathbf{v}_0}{\partial x_3} dx_3 + \frac{1}{H_0} \int_{-h}^{\xi_0} (\boldsymbol{\tau}_1 \cdot \frac{\partial \mathbf{v}_1}{\partial x_3})_0 dx_3$$

***The contribution of the residual stress  $\boldsymbol{\tau}_0$  to the energy budget.***

The second term in the right-hand side of eq. (168) is obviously related to the energy dissipated by the mesoscale motions. It is, by far, the essential contribution to  $\epsilon$  and may serve as a first approximation of it. It is however the first term one is interested in, here, to explain the physical mechanisms which contribute to shape the residual circulation.

In evaluating this term, one can obviously restrict attention to the horizontal components of the vectors  $\boldsymbol{\tau}_0$  and  $\mathbf{v}_0$ , and this is also true for any scalar product of the form

$$\boldsymbol{\tau} \cdot \frac{\partial \mathbf{v}}{\partial x_3}$$

One has indeed, from the continuity equation,

$$\frac{\partial v_3}{\partial x_3} \leq \nabla \cdot \mathbf{u} \sim 0\left(\frac{u}{\ell}\right)$$

where  $\ell$  is the characteristic scale of horizontal variations. On the other hand

$$\frac{\partial u}{\partial x_3} \sim 0\left(\frac{u}{H}\right)$$

Since  $h \ll \ell$ , the contributions from the vertical velocity are completely negligible in the integrals of eq. (168).

The application of the three-dimensional equations (133) and (134) to the North Sea (section 9) shows that



(i) the turbulent stress can be written

$$(169) \quad \tau = \tau^s \xi + \tau^b (1 - \xi) + k \|\tau^b\|^{1/2} \sum_1^{\infty} A_n \lambda(\xi) \frac{df_n}{d\xi}$$

where  $\tau^s$  and  $\tau^b$  are respectively the surface stress and the bottom stress (per unit mass of sea water),  $\xi = H^{-1}(x_3 + h)$ ,  $H = h + \zeta$ ,  $h$  is the depth and  $\zeta$  the surface elevation, the  $A_n$ 's are functions of  $t$ ,  $x_1$  and  $x_2$  involving  $\tau^s$ ,  $\tau^b$  and their time derivatives,  $k$  is the Von Karman constant,

$$(170) \quad \lambda(\xi) = \frac{\tilde{v}}{\kappa \|\tau^b\|^{1/2} H}$$

and the functions  $f_n(\xi)$  are the eigenfunctions of the problem

$$(171) \quad \frac{d}{d\xi} \left( \lambda \frac{df_n}{d\xi} \right) = -\alpha_n f_n$$

$$(172) \quad \lambda \frac{df_n}{d\xi} = 0 \quad \text{at} \quad \xi = 0 \quad \text{and} \quad \xi = 1$$

$\alpha_n$  being the corresponding eigenvalue.

The last term in the right-hand side of eq. (169) plays an important role in the determination of the velocity field  $\mathbf{v}$  but its effect is limited to relatively short periods of weak currents (at tide reversal, for instance) [Nihoul, 1977; Nihoul et al., 1979] and it contributes very little to the residual turbulent Reynolds stress obtained by averaging over a time  $T$  covering several tidal periods.

Hence, setting  $z = x_3 + h$ , one may write, with a good approximation

$$(173) \quad \tau_0 \sim \tau_0^b + \left( \frac{\tau^s - \tau^b}{H} \right)_0 z$$

(ii) the bottom stress  $\tau^b$  is a function of  $\tau^s$ , the depth-averaged velocity  $\bar{\mathbf{u}}$  and the time derivatives of  $\bar{\mathbf{u}}$ .

If one excepts, again, short periods of weak currents,  $\tau^b$  can be approximated by the classical "quadratic bottom friction law"

$$(174) \quad \tau^b = D \|\bar{\mathbf{u}}\| \bar{\mathbf{u}}$$

where  $D$  is the drag coefficient. Averaging over a time  $T$  as before and neglecting small order terms, one obtains then

$$(175) \quad \tau_0^b \sim D \|\bar{\mathbf{u}}_1\|_0 \bar{\mathbf{u}}_0 + (D \|\bar{\mathbf{u}}_1\| \bar{\mathbf{u}}_1)_0$$

i.e., using eqs. (150) and (152),

$$(176) \quad \tau_0^b \sim H_0 K \bar{\mathbf{u}}_0 + \tau_0^f$$

Changing variable to  $z$  and using eq. (173), one can write

$$\begin{aligned}
 \frac{1}{H_0} \int_{-h}^{z_0} \tau_0 \cdot \frac{\partial \mathbf{v}_0}{\partial x_3} dx_3 &\sim \frac{1}{H_0} \int_{z_0}^{H_0} \tau_0 \cdot \frac{\partial \mathbf{u}_0}{\partial z} dz \\
 (177) \qquad \qquad \qquad &\sim \frac{1}{H_0} \int_{z_0}^{H_0} \tau_0^b \cdot \frac{\partial \mathbf{u}_0}{\partial z} dz \\
 &\quad + \frac{1}{H_0} \int_{z_0}^{H_0} \left( \frac{\tau^s - \tau^b}{H} \right)_0 \cdot \frac{\partial \mathbf{u}_0}{\partial z} z dz
 \end{aligned}$$

The horizontal velocity  $\mathbf{u}$ , however it may for the rest vary with depth, always has a logarithmic profile near the bottom. This implies that  $\partial \mathbf{u} / \partial z$  behaves like  $z^{-1}$  near  $z = 0$ . A first consequence of this asymptotic behaviour of the velocity profile is that integrals over depth are, strictly speaking, not taken from  $z = 0$  to the surface but some very small height  $z_0$  (the "roughness length") to the surface. This has been taken into account in eq. (177). A second consequence is that the first integral in the right-hand side of eq. (177) is largely dominant, the singularity at  $z = 0$  being cancelled in the second integral by the factor  $z$ .

Since the second integral is only a small correction, one may make the approximation

$$\left( \frac{\tau^s - \tau^b}{H} \right)_0 \sim \frac{\tau_0^s - \tau_0^b}{H_0}$$

Eq. (177) can thus be rewritten

$$\begin{aligned}
 \frac{1}{H_0} \int_{-h}^{z_0} \tau_0 \cdot \frac{\partial \mathbf{v}_0}{\partial x_3} dx_3 &\sim \frac{\tau_0^b}{H_0} \cdot \int_{z_0}^{H_0} \left( 1 - \frac{z}{H} \right) \frac{\partial \mathbf{u}_0}{\partial z} dz \\
 (178) \qquad \qquad \qquad &\quad + \frac{\tau_0^s}{H_0} \cdot \int_{z_0}^{H_0} \frac{z}{H_0} \frac{\partial \mathbf{u}_0}{\partial z} dz
 \end{aligned}$$

Integrating by parts, one gets

$$\frac{1}{H_0} \int_{-h}^{z_0} \tau_0 \cdot \frac{\partial \mathbf{v}_0}{\partial x_3} dx_3 \sim \frac{\tau_0^b \cdot \bar{\mathbf{u}}_0}{H_0} + \frac{\tau_0^s \cdot (\mathbf{u}_0^s - \bar{\mathbf{u}}_0)}{H_0}$$

(179)

i.e., using eq. (176)

$$\frac{1}{H_0} \int_{-h}^{z_0} \tau_0 \cdot \frac{\partial \mathbf{v}_0}{\partial x_3} dx_3 \sim K \bar{\mathbf{u}}_0^2 + \frac{\tau_0^f \cdot \bar{\mathbf{u}}_0}{H_0} + \frac{\tau_0^s \cdot (\mathbf{u}_0^s - \bar{\mathbf{u}}_0)}{H_0}$$

(180)

The first two terms in the right-hand side of eq. (164) integrated over depth give then

$$(181) \quad \int_{-h}^{\xi_0} \left[ \frac{\partial}{\partial x_3} (\mathbf{v}_0 \cdot \boldsymbol{\tau}_0) - \boldsymbol{\tau}_0 \cdot \frac{\partial \mathbf{v}_0}{\partial x_3} \right] dx_3 = \int_{-h}^{\xi_0} \mathbf{v}_0 \cdot \frac{\partial \boldsymbol{\tau}_0}{\partial x_3} dx_3$$

$$\sim \boldsymbol{\tau}_0^s \cdot \bar{\mathbf{u}}_0 - KH_0 \bar{u}_0^2 - \boldsymbol{\tau}_0^f \cdot \bar{\mathbf{u}}_0$$

i.e., the same result one would have obtained from the depth integrated transport equation for the contribution of the wind stress and the bottom stress, by taking the scalar product of eq. (149) by  $\bar{\mathbf{u}}_0$ .

One notes that, in the right-hand side of eq. (180) only the first term can be associated without ambiguity with the dissipation of energy. The second term represents the rate of work of the mesoscale friction stress. Although its "bottom friction" origin is clear, its sign cannot be set a priori and there is no reason why it could not actually provide energy to the residual flow.

The same can be said for the last term in the right-hand side of eq. (163). This term appears with the opposite sign in eq. (164). It thus represents an exchange of energy between residual and mesoscale flows; this term can be either positive or negative. There is no way of knowing a priori whether the energy is extracted from the mean flow and goes from macroscales to mesoscales or if it is supplied to the mean flow by mesoscale motions.

#### *The exchange of energy between scales of motion.*

The exchange of energy between macroscales and mesoscales can be characterized, at each point of the North Sea, by the depth-averaged rates of energy transfer

$$(182) \quad \epsilon_N = \frac{1}{H_0} \int_{-h}^{\xi_0} (\mathbf{N} : \nabla \mathbf{v}_0) dx_3$$

$$(183) \quad \epsilon_F = \frac{1}{H_0} (\boldsymbol{\tau}_0^f \cdot \bar{\mathbf{u}}_0)$$

These quantities, which may be positive or negative should be compared with the rate of energy dissipation by the residual motion, i.e.

$$(184) \quad \epsilon_D = K \bar{u}_0^2$$

The mesoscale Reynolds stress tensor  $\mathbf{N}$  also contributes to the term  $\nabla \cdot (-\mathbf{N} \cdot \mathbf{v}_0)$  in the left-hand side of eq. (163). This is a completely different effect because it implies a flux of energy in physical space while  $\mathbf{N} : \nabla \mathbf{v}_0$ , appearing in both eqs. (163) and (164), represents a transfer of energy between scales, i.e., a flux of energy in Fourier space.

This effect cannot however be ignored if one wants to understand the mechanisms by which the mesoscale stresses act on the residual flow. One shall write

$$(185) \quad \delta = \frac{1}{H_0} \int_{-h}^{\xi_0} [\nabla \cdot (-N \cdot \mathbf{v}_0)] dx_3$$

It is convenient to normalize the rates of energy transfer using the rate of energy dissipation  $\epsilon_D$  as the normalizing factor. Let

$$(186) \quad \hat{\delta} = \frac{\delta}{\epsilon_D}$$

$$(187) \quad \hat{\epsilon}_N = \frac{\epsilon_N}{\epsilon_D}$$

$$(188) \quad \hat{\epsilon}_F = \frac{\epsilon_F}{\epsilon_D}$$

$$(189) \quad \hat{\epsilon}_T = \hat{\delta} + \hat{\epsilon}_N + \hat{\epsilon}_F + 1$$

In non-dimensional forms,

(i)  $\hat{\delta}$  is the rate of change of kinetic energy due to energy divergence or convergence in physical space;

(ii)  $\hat{\epsilon}_N$  is the rate of energy exchange between macroscale and mesoscale motions resulting from the action of the mesoscale Reynolds stresses;

(iii)  $\hat{\epsilon}_F$  is the rate of energy exchange between macroscales and mesoscales resulting from the action of the mesoscale friction stress;

(iv)  $\hat{\delta} + \hat{\epsilon}_N$  is the rate of work of the mesoscale Reynolds stresses on the residual flow;

(v)  $\hat{\epsilon}_T$  is the net rate at which energy is extracted from the residual flow by the combination of energy fluxes in physical space, energy transfers between scales of motion and energy dissipation by bottom friction.

A positive value of  $\hat{\epsilon}_N$  or  $\hat{\epsilon}_F$  implies a transfer of energy from the mean flow to the mesoscale motions. At the opposite, negative values indicate a transfer of energy from the mesoscales to the mean flow. Using turbulence terminology, these situations will be referred to as cases of positive eddy viscosity and negative eddy viscosity respectively. [The word "eddy" is here used in an extended sense referring to mesoscale non-linear waves and turbulence. A similar definition was proposed by Rhines and Holland (1979).]

### 13. - Application of the residual model to the North Sea.

#### *Tidal residuals.*

A detailed study of the tidal residuals in the North Sea was made by means of two coupled three-dimensional models, one for tides and storm surges (Nihoul, 1977; Nihoul et al., 1979) and one for the residual circulation described by eqs. (141) and (143) [Nihoul and Runfola, 1981].

The data of the three-dimensional models were used to compute the depth-averaged circulation and the spatial distributions of the depth-averaged transfer functions  $\hat{\epsilon}_N$ ,  $\hat{\epsilon}_F$  and  $\hat{\delta}$ . The results are presented in figs. 55 to 61.

Fig. 55 shows the residual streamlines. One can see that there is, in general, a good agreement between the result of the three-dimensional model and those of the depth-integrated model represented in fig. 52. The main differences are observed in regions of very weak residual circulation where the three-dimensional models have a better resolution. The existence of extended regions of very small residual currents (less than  $1 \text{ cm.s}^{-1}$ ) is one important characteristic of the tidal residual flow pattern. It has been found almost impossible to give any comprehensible representation of the flow field using the traditional method which consist in drawing the velocity vector at each grid point. To display the residual flow in some regions, it has been necessary to draw streamlines  $5 \cdot 10^3 \text{ m}^3 \text{ s}^{-1}$  apart while, in other regions, the difference between two consecutive streamlines is  $20 \cdot 10^3 \text{ m}^3 \text{ s}^{-1}$  or more.

Although the small scale gyres are essential to understand the hydrodynamics of the North Sea, especially in coastal zones, they contain little of the total residual energy of the North Sea and the tidal residual circulation appears to be constituted essentially of two main energetic streams corresponding to the penetration in the North Sea of two branches of the North-Atlantic current. These are the analogue of the macroscale gyres of oceanic circulation and, in this sense, the residual circulation which has been qualified as "macroscale" with reference to its time scale (i.e. its quasi steady character) may be classified also among macroscale motions with respect to length scales (with a peak of energy in the small wave number range in a spectral analysis of the North Sea energy).

The maps of the functions  $\hat{\delta}$ ,  $\hat{\epsilon}_N$  and  $\hat{\epsilon}_F$  (figs. 56, 57 and 58) show a marked patchiness with alternating positive and negative values.

Absolute values are one or two orders of magnitude larger for  $\hat{\delta}$  and  $\hat{\epsilon}_N$  than for  $\hat{\epsilon}_F$  and  $\hat{\epsilon}_D$  ( $\hat{\epsilon}_D = 1$ , in non-dimensional form). Thus the mesoscale Reynolds stresses play the main role

---

\* In interpreting these figures, and those which follow in the next section, one must remember that, having to calculate horizontal gradients, the model can only provide results one grid point away from the coast. One cannot say anything from the figures about the coastal fringe.

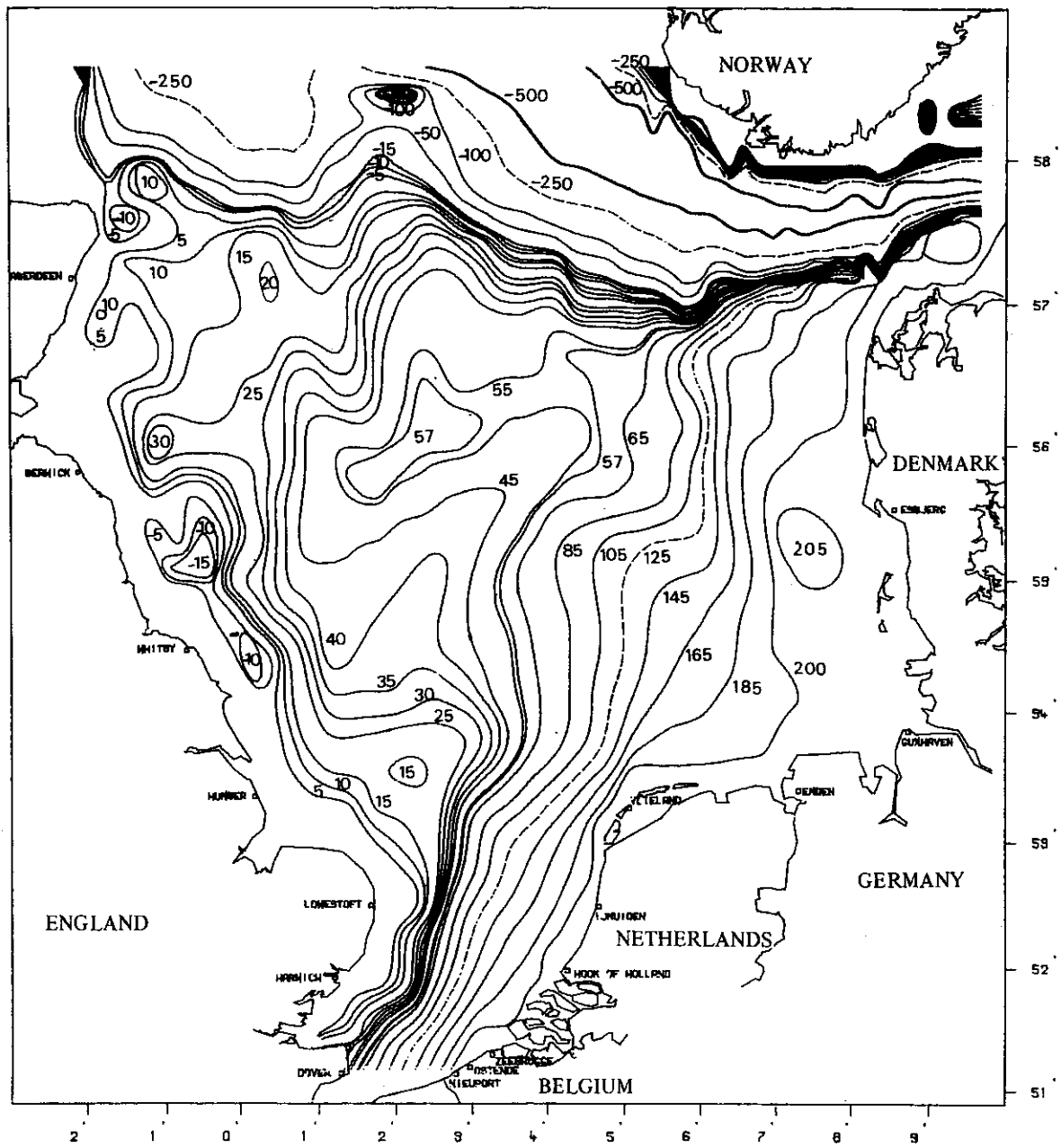


fig. 55.

Tidal residuals in the North Sea. Residual flow pattern.  
 Streamlines  $\psi = \text{const.}$  in  $10^3 \text{ m}^3 \cdot \text{s}^{-1}$ .

in the energetics of the tidal residual flow. They are responsible for a transfer  $\hat{\epsilon}_N$  "in Fourier space", i.e. an exchange of energy between macroscale residual flow and mesoscale motions, and for a flux "in physical space", i.e. a transport of energy from one region of the North Sea to another. These two effects tend to compensate each other and the sum  $\hat{\delta} + \hat{\epsilon}_N$  is about one order of magnitude smaller than each of its terms (fig. 59). Thus, when energy is supplied to the mean flow in some region (negative viscosity effect), it is, to a large extent, exported to other regions where energy is extracted from the mean flow by the mesoscale motions.

The pattern of streamlines (fig. 55) shows that the regions of negative eddy viscosity contain little residual energy (the residual currents are in general very small as indicated by the wide spacing of the streamlines) and most of the residual vorticity (the streamlines are curved and often closed, forming secondary gyres).

This is confirmed by the vorticity pattern (fig. 61) showing vorticity scales as small as 10 km associated with the gyres.

In the regions of negative eddy viscosity where the mesoscale stresses transfer energy from the mesoscale motions to the residual flow, they also generate vorticity in the residual flow.

What is actually happening is that the energy supplied to the residual flow in these regions is immediately exported away to the regions of positive eddy viscosity related to the main streams. This energy supply thus contributes to enhance the large scale currents and, in this sense, the energy is truly going from mesoscales to macroscales, referring now indifferently to time scales or length scales.

The secondary flows which are generated in the regions of negative eddy viscosity contain little energy but most of the vorticity. This vorticity is characterized by length scales smaller in many places than the typical length scale of tidal motions (referred to as the mesoscale motions before) i.e. the energy cascade to larger scales is paralleled by an enstrophy cascade to smaller scales.

It is tempting to see here a case of two-dimensional turbulence and identify the patches of intense energy exchanges between scales of motions as the "synoptic eddies" of the North Sea.

The fact that, in these eddies, the bottom dissipation is comparatively completely negligible is perhaps an argument in favor of such interpretation.

As a final remark, it is interesting to note that  $\hat{\epsilon}_T$ , the net rate at which energy is extracted from the residual flow (or supplied to it) is not positive everywhere. A rather extensive patch of negative values (in the range [-1, -10]) spreads out from the western North Sea, off the coasts of Scotland and northern England, into the central part of the North Sea.

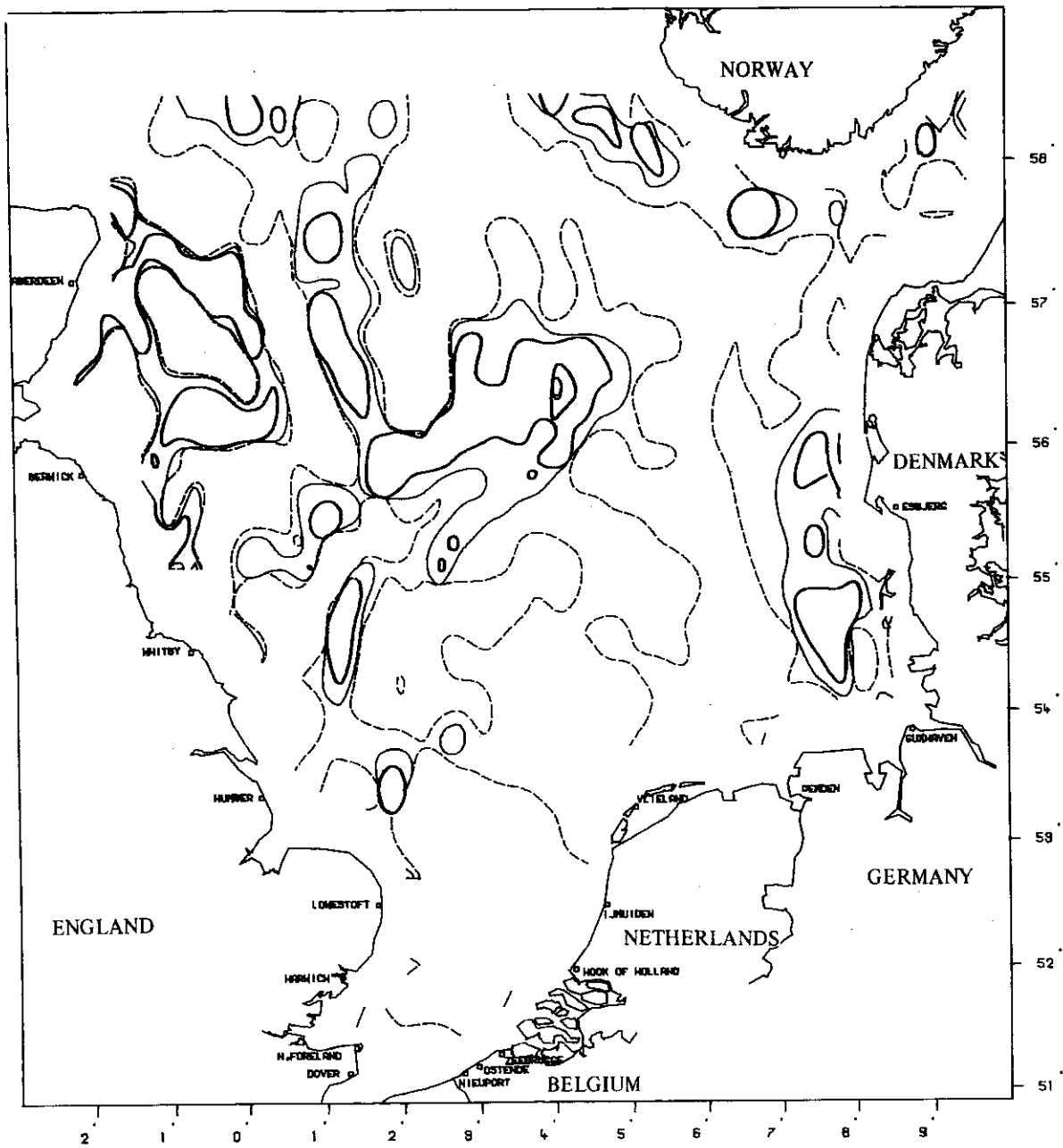


fig. 56a.

Tidal residuals in the North Sea. Map of positive values of the non-dimensional function  $\delta$  representing the rate at which the residual kinetic energy is redistributed in physical space. (Positive values indicate regions of residual energy divergence.)

Heavy line  $\delta = 50$   
 Slender line  $\delta = 10$   
 Broken line  $\delta = 0$



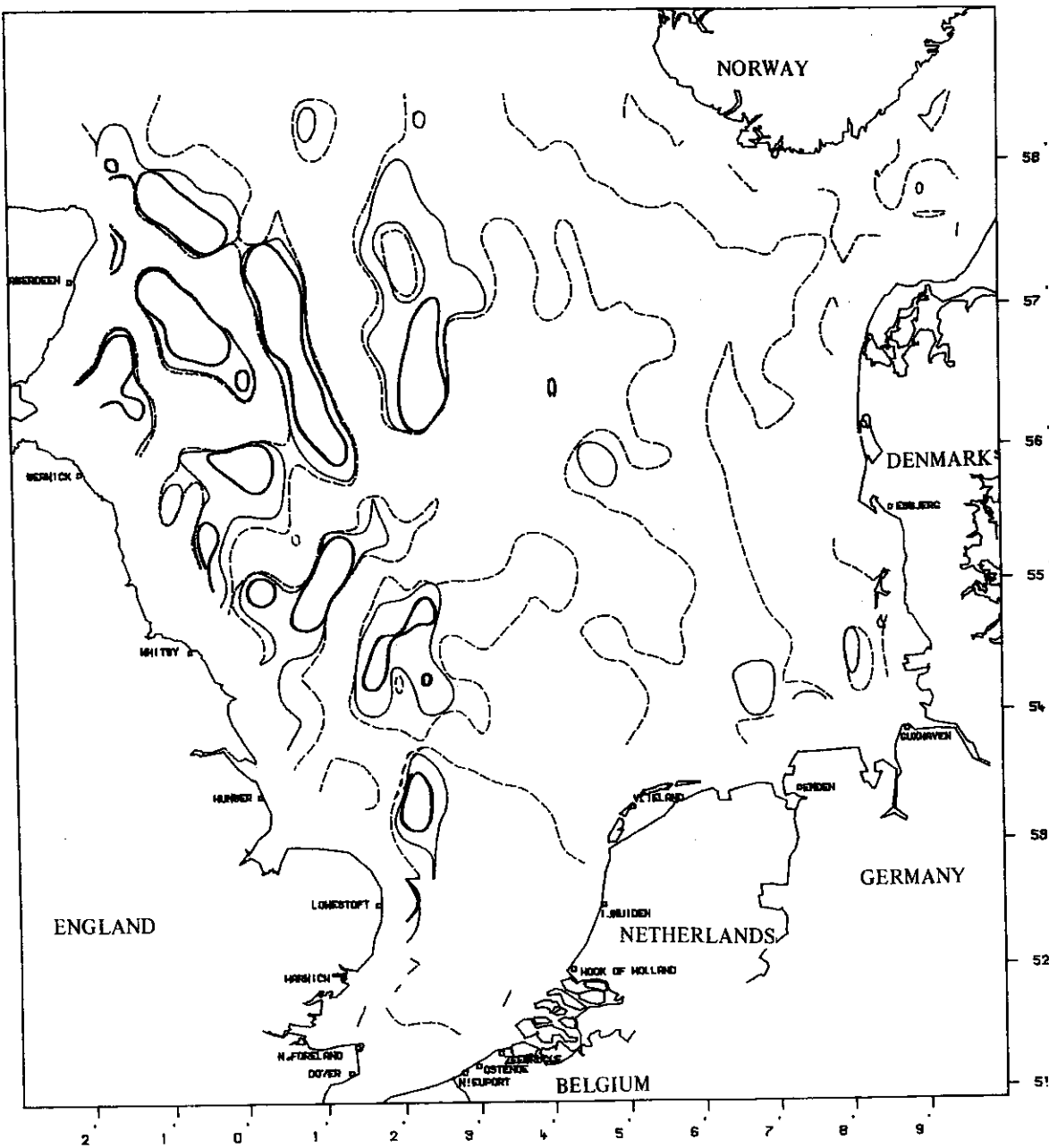


fig. 56b.

Tidal residuals in the North Sea. Map of negative values of the non-dimensional function  $\hat{\delta}$  representing the rate at which the residual kinetic energy is redistributed in physical space. (Negative values indicate regions of residual energy convergence.)

- Heavy line  $\hat{\delta} = -50$
- Slender line  $\hat{\delta} = -10$
- Broken line  $\hat{\delta} = 0$

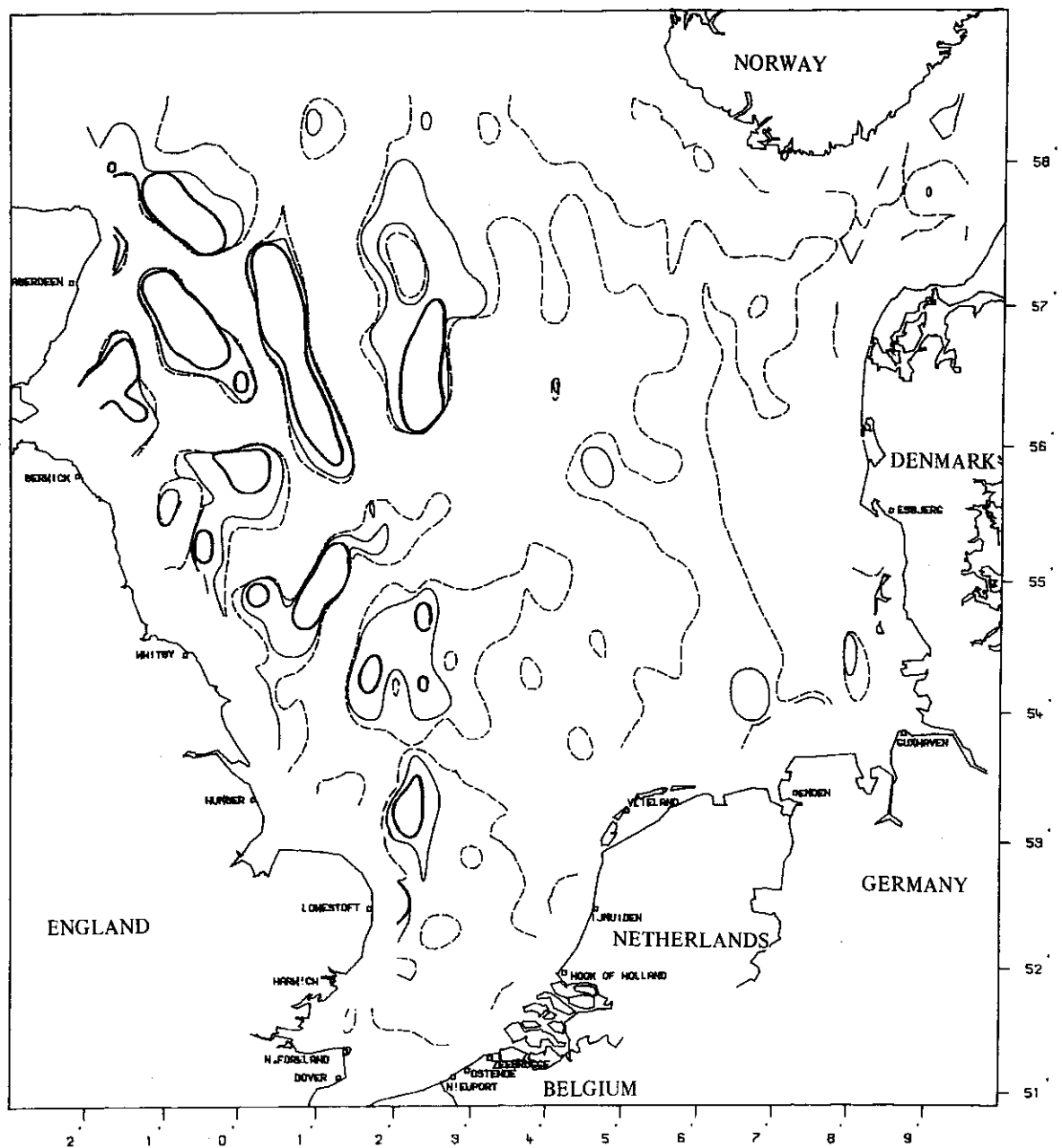


fig. 57a.

Tidal residuals in the North Sea. Map of positive values of the non-dimensional function  $\hat{\epsilon}_N$  representing the rate of energy transfer between residual and meso-scale Reynolds stresses. (Positive values indicate regions of positive eddy viscosity.)

Heavy line —————  $\hat{\epsilon}_N = 50$   
 Slender line —————  $\hat{\epsilon}_N = 10$   
 Broken line - - - - -  $\hat{\epsilon}_N = 0$

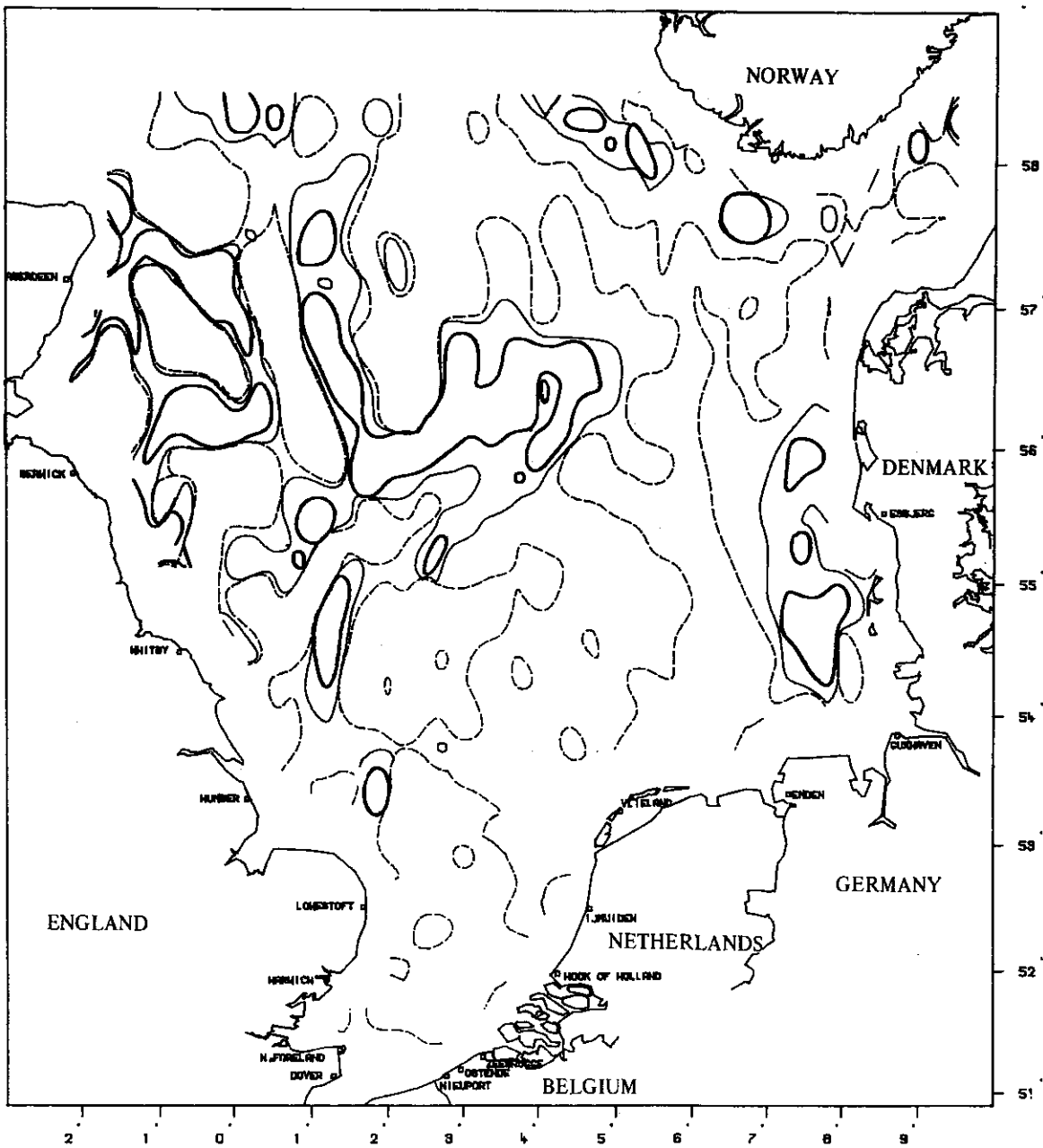


fig. 57b.

Tidal residuals in the North Sea. Map of negative values of the non-dimensional function  $\hat{\epsilon}_N$  representing the rate of energy transfer between residual and meso-scale Reynolds stresses. (Negative values indicate regions of negative eddy viscosity.)

Heavy line  $\hat{\epsilon}_N = -50$   
 Slender line  $\hat{\epsilon}_N = -10$   
 Broken line  $\hat{\epsilon}_N = 0$

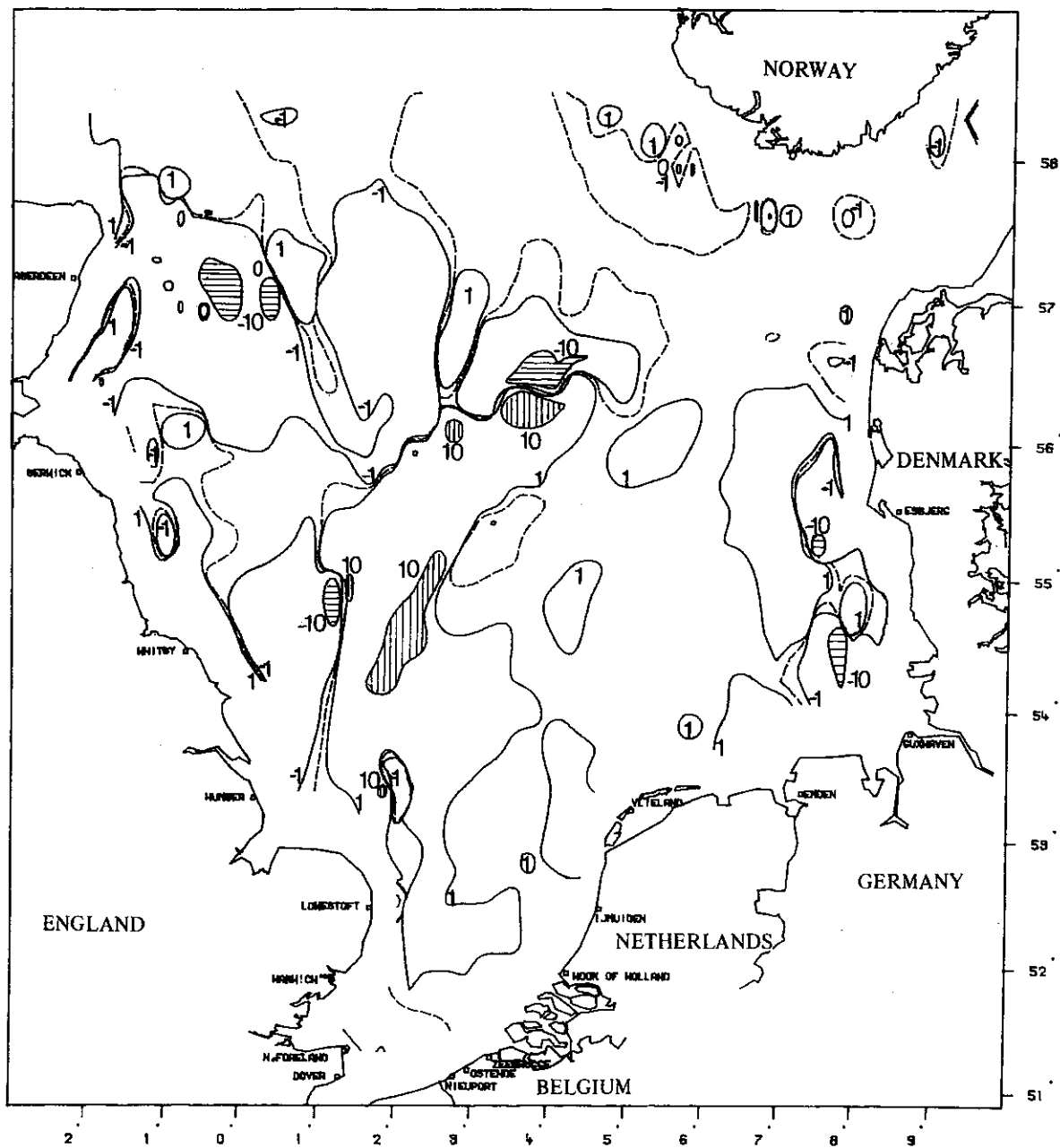


fig. 58.

Tidal residuals in the North Sea. Map of positive and negative values of the non-dimensional function  $\hat{\epsilon}_F$  representing the rate of energy transfer between residual and mesoscale flows by the friction stress.

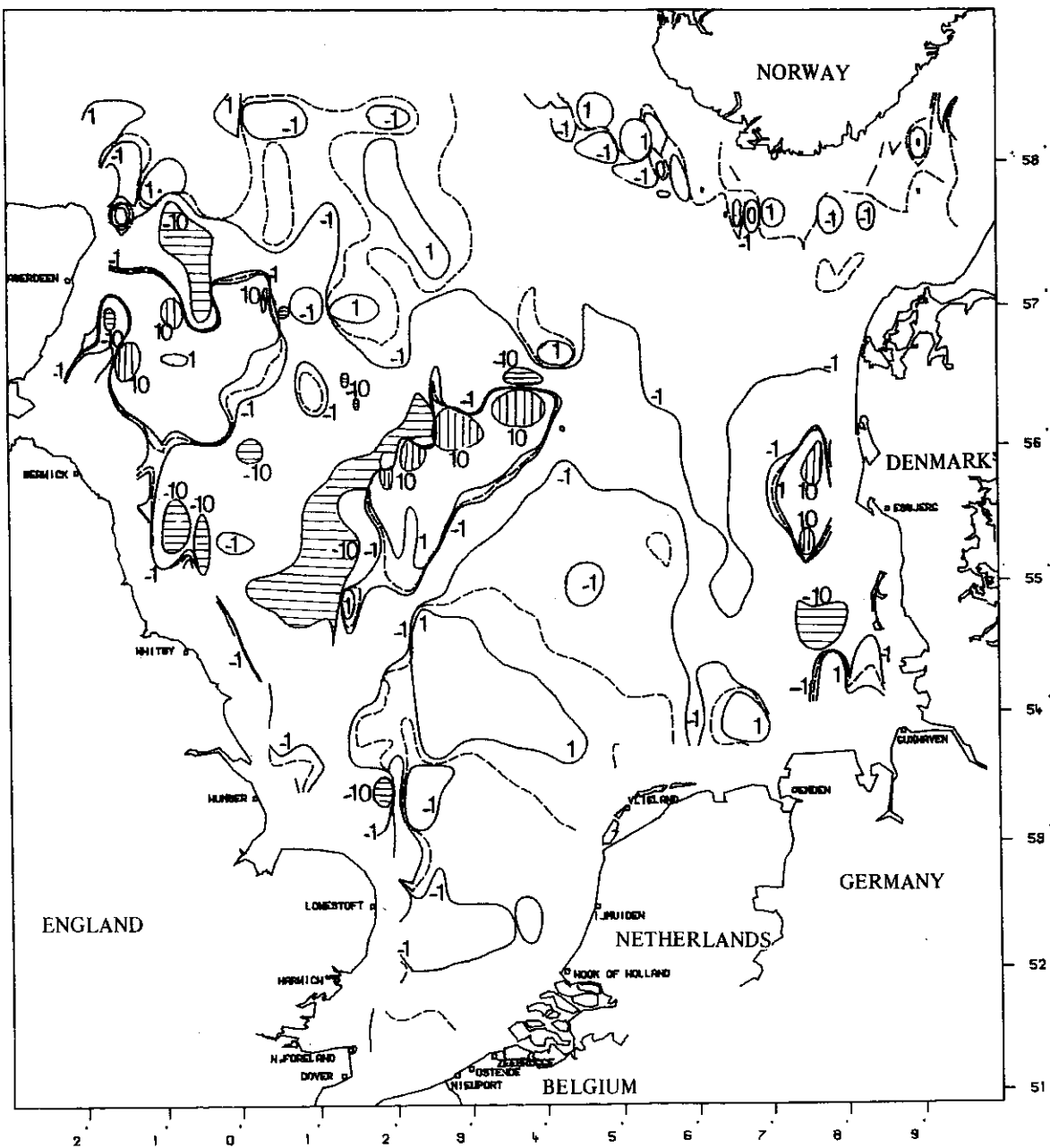


fig. 59.

Tidal residuals in the North Sea. Map of positive and negative values of the non-dimensional function  $\hat{\delta} + \hat{\epsilon}_N$  representing the rate of work of the mesoscale Reynolds stresses on the residual flow.

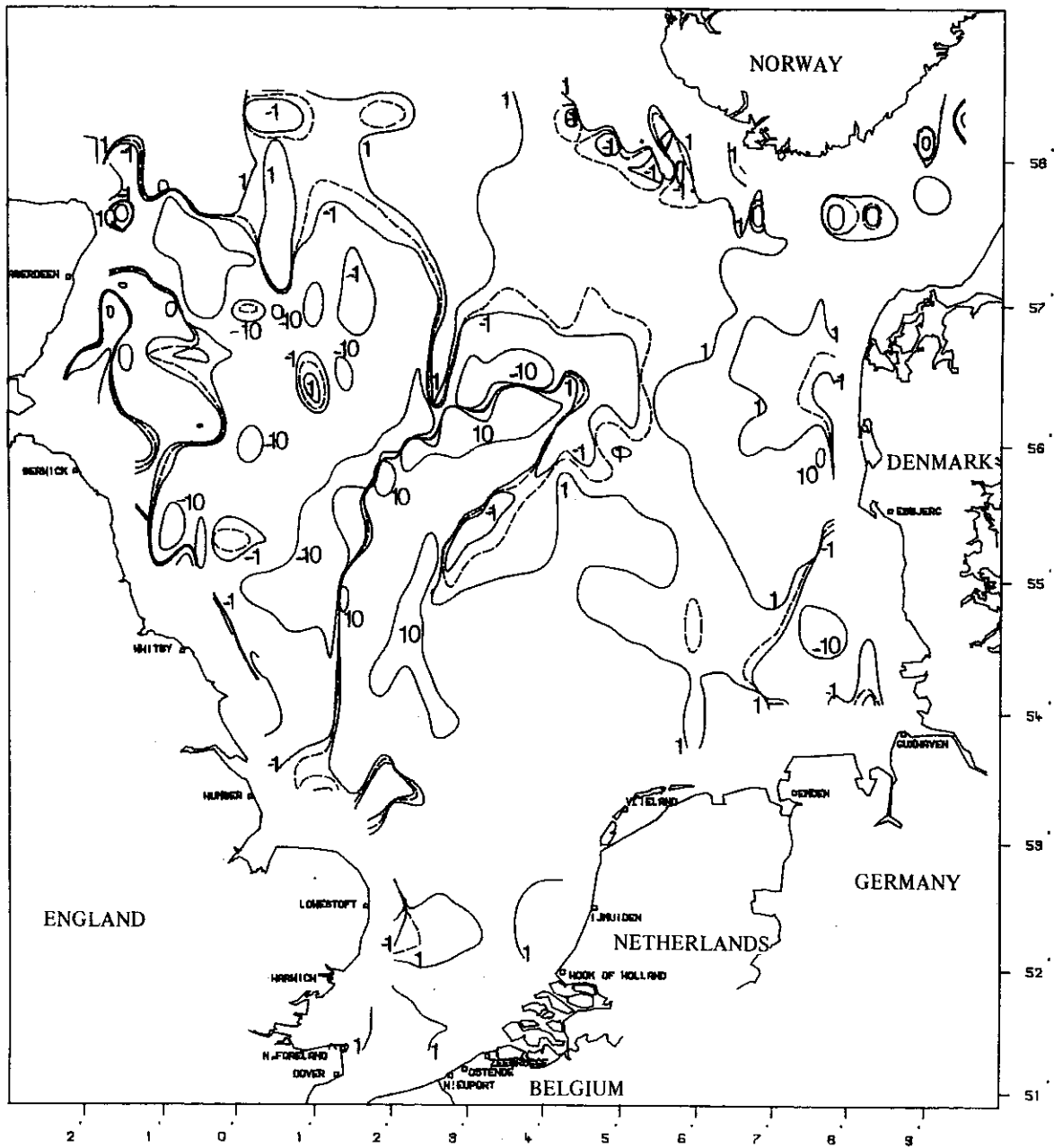


fig. 60.

Tidal residuals in the North Sea. Map of positive and negative values of the non-dimensional function  $\hat{\epsilon}_T = \hat{\delta} + \hat{\epsilon}_N + \hat{\epsilon}_F + 1$  representing the rate at which energy is extracted from the residual flow (positive values) or supplied to the residual flow (negative values).

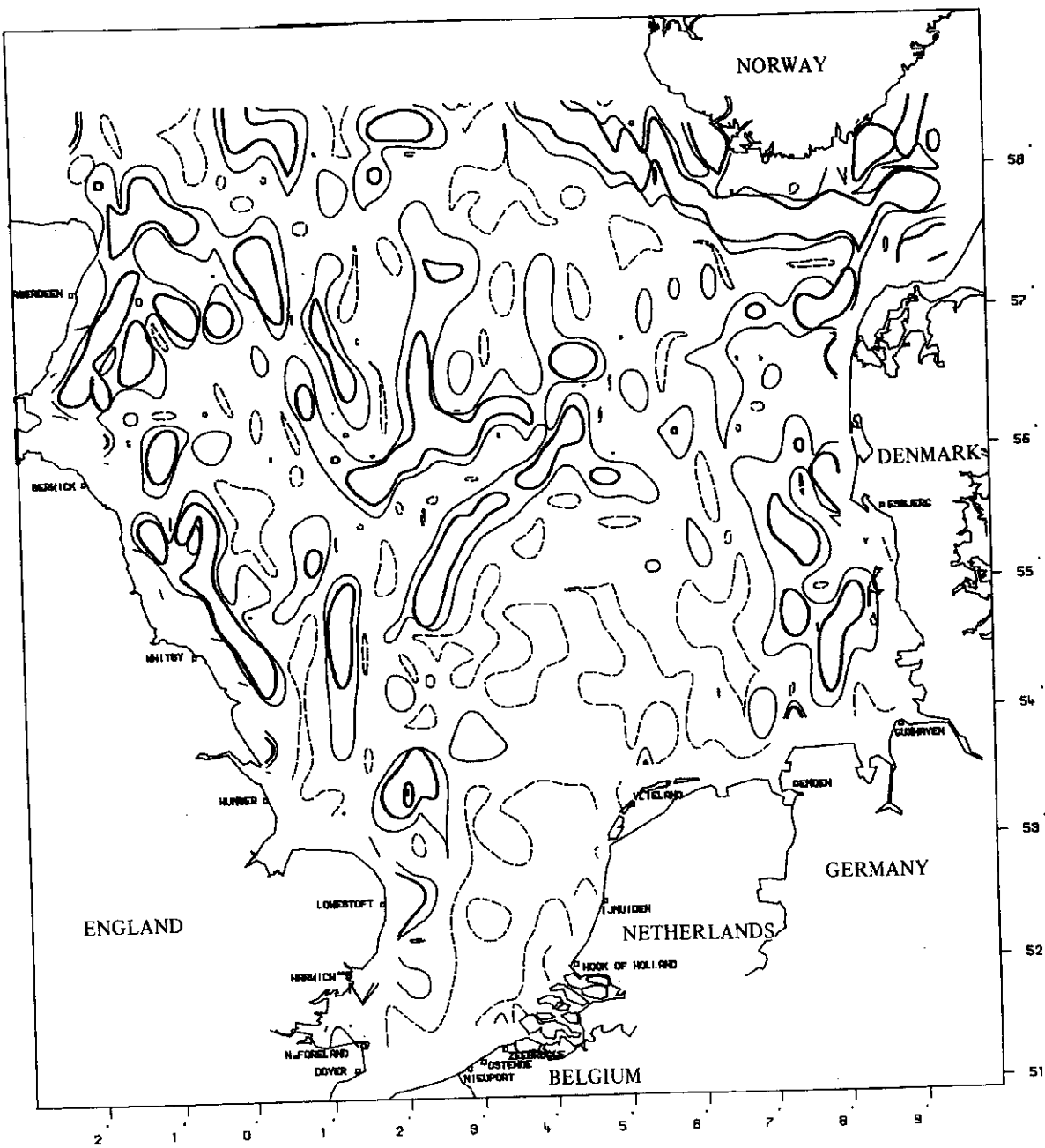


fig. 61.

Tidal residuals in the North Sea. Map of the function  $\hat{\omega} = \frac{\|\nabla \wedge \bar{\mathbf{u}}_0\|}{\|\bar{\mathbf{u}}_0\|}$  indicating the scale of the residual vorticity.

Heavy line	—————	$\hat{\omega} = 10^{-4} \text{ m}^{-1}$
Slender line	—————	$\hat{\omega} = 5 \cdot 10^{-5} \text{ m}^{-1}$
Broken line	- - - - -	$\hat{\omega} = 10^{-5} \text{ m}^{-1}$

Going back to eq. (163) where the term

$$\nabla \cdot \left( \mathbf{v}_0 \frac{v_0^2}{2} \right)$$

is always completely negligible, one sees that, in the absence of wind forcing, negative values of  $\hat{\epsilon}_T$  imply

$$\nabla \cdot (\mathbf{v}_0 q_0) = \mathbf{v}_0 \cdot \nabla q_0 > 0$$

i.e. the mesoscale stresses are actually driving the residual flow "up the residual slope and pressure gradient".

#### **Wind residuals.**

As pointed out in the introduction, the tidal residuals considered in the preceding section can only constitute a first approximation of what a real climatic residual circulation is. The atmospheric forcing has been neglected both in determining the mesoscale motion and in computing the resulting residuals. The advantage was that the time of averaging could be limited to two or three tidal periods. This is not possible if one includes the effect of a wind field which itself evolves with a characteristic time of the same order.

In some cases, one may have to go to averaging over several weeks to ensure that the average is meaningful. This implies that the mesoscale velocity field must be calculated over the same period of time and the cost of operating the model becomes rapidly prohibitively large.

Although an effort of this size is now being considered to model the residual circulation during the period of the JONSDAP '76 experiment, it has not been possible so far to apply the three-dimensional model with real atmospheric conditions.

However, to have some idea of the effect of wind forcing, two cases of constant uniform wind fields have been considered.

The concept of a uniform wind field over the whole North Sea is certainly idealistic.

Moreover, the direct effect of the wind on the residual circulation, which is associated with the curl of the wind stress, is not taken into account.

Going back to eq. (157), one can see that if one takes the curl of this equation to eliminate  $\nabla q_0$ , the second term in the right-hand side will give a contribution

$$(190) \quad \nabla \wedge \frac{\partial \boldsymbol{\tau}_0}{\partial x_3}$$

Eq. (169) shows that the Reynolds stress  $\boldsymbol{\tau}$  contains a term  $\boldsymbol{\tau}^s \boldsymbol{\xi}$  where  $\boldsymbol{\tau}^s$  is the wind stress. Hence, a constant wind stress contributes to eq. (190) a term



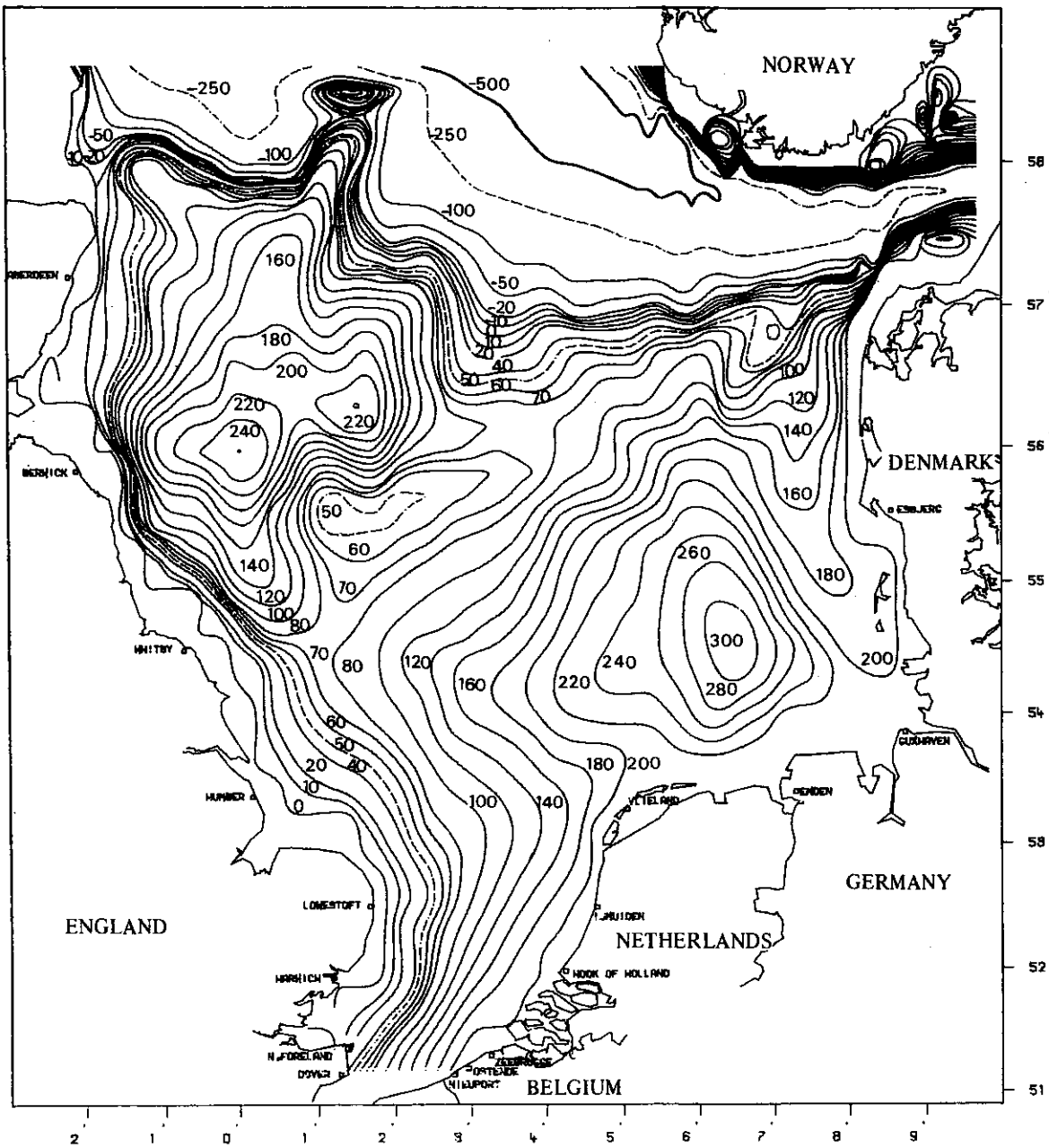


fig. 62.

Wind residuals in the North Sea. (Uniform constant wind of  $15 \text{ m} \cdot \text{s}^{-1}$  from the north-west.) Residual flow pattern. Streamlines  $\psi = \text{const.}$  in  $10^3 \text{ m}^3 \cdot \text{s}^{-1}$ .

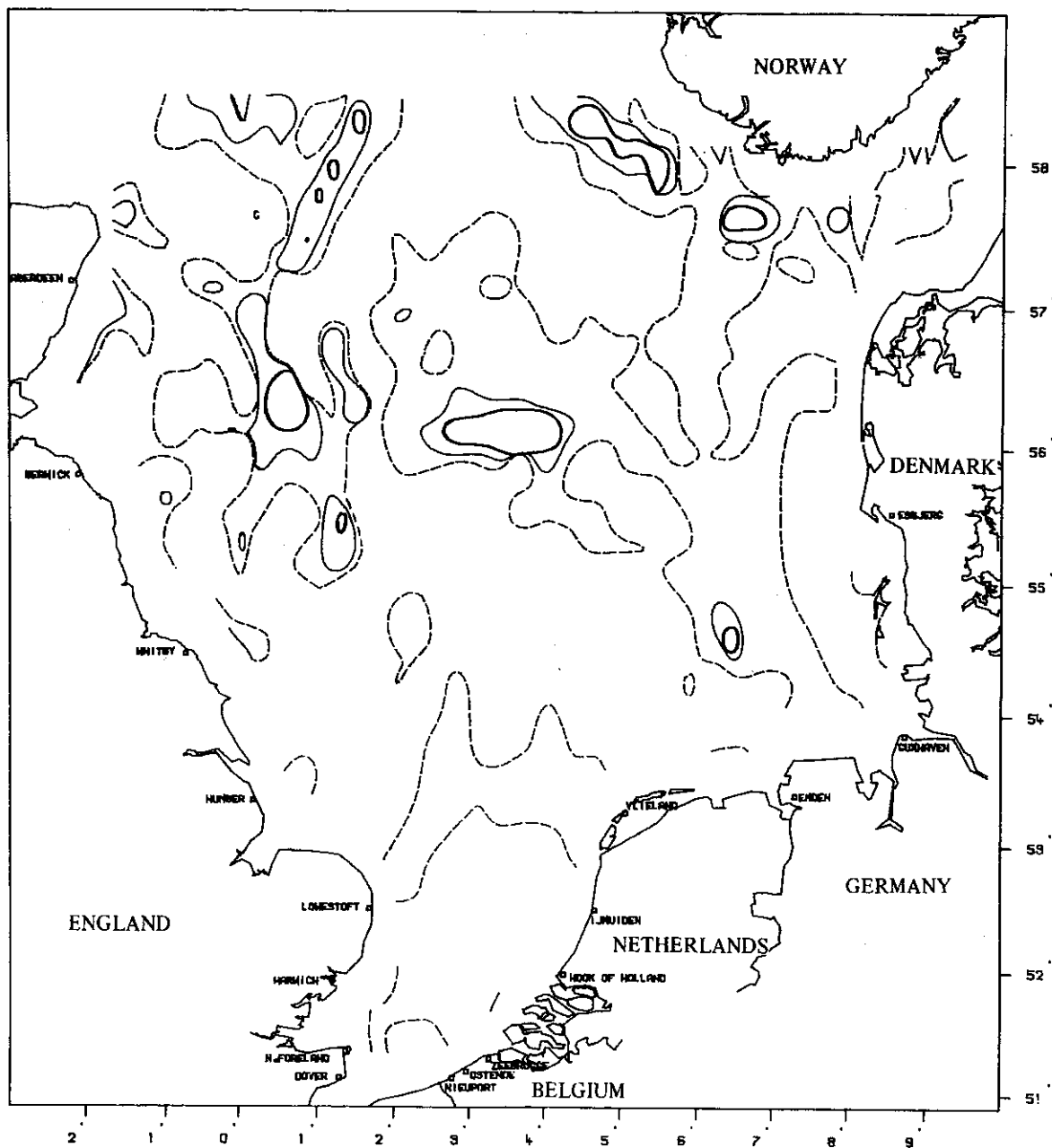


fig. 63a.

Wind residuals in the North Sea. (Uniform constant wind of  $15 \text{ m.s}^{-1}$  from the north-west.) Map of positive values of the non-dimensional function  $\hat{\delta}$  representing the rate at which the residual kinetic energy is redistributed in physical space. (Positive values indicate regions of residual energy divergence.)

Heavy line       $\hat{\delta} = 50$   
 Slender line     $\hat{\delta} = 10$   
 Broken line      $\hat{\delta} = 0$

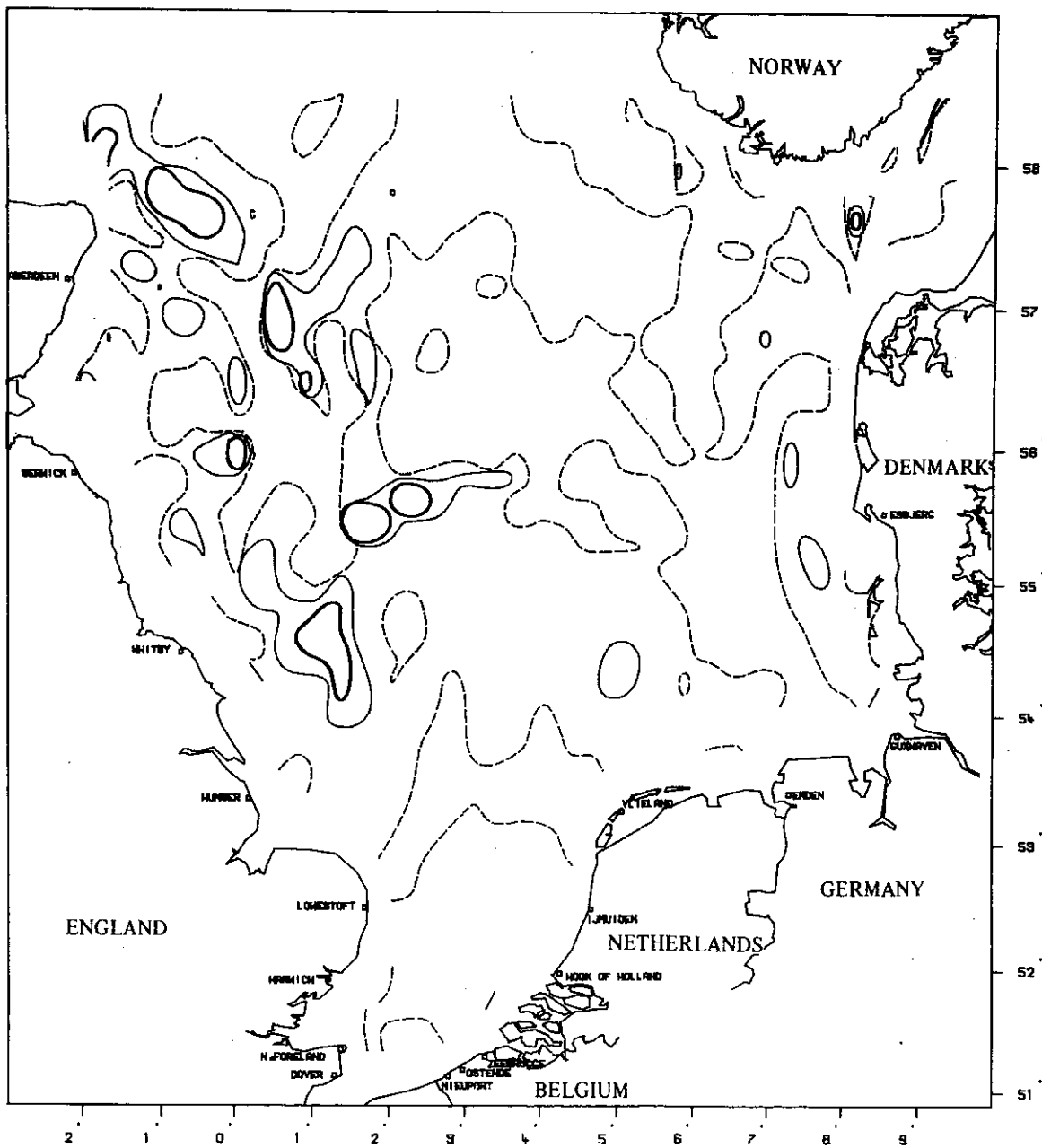


fig. 63b.

Wind residuals in the North Sea. (Uniform constant wind of  $15 \text{ m.s}^{-1}$  from the north-west.) Map of negative values of the non-dimensional function  $\hat{\delta}$  representing the rate at which the residual kinetic energy is redistributed in physical space. (Negative values indicate regions of residual energy convergence.)

Heavy line       $\hat{\delta} = -50$   
 Slender line     $\hat{\delta} = -10$   
 Broken line      $\hat{\delta} = 0$

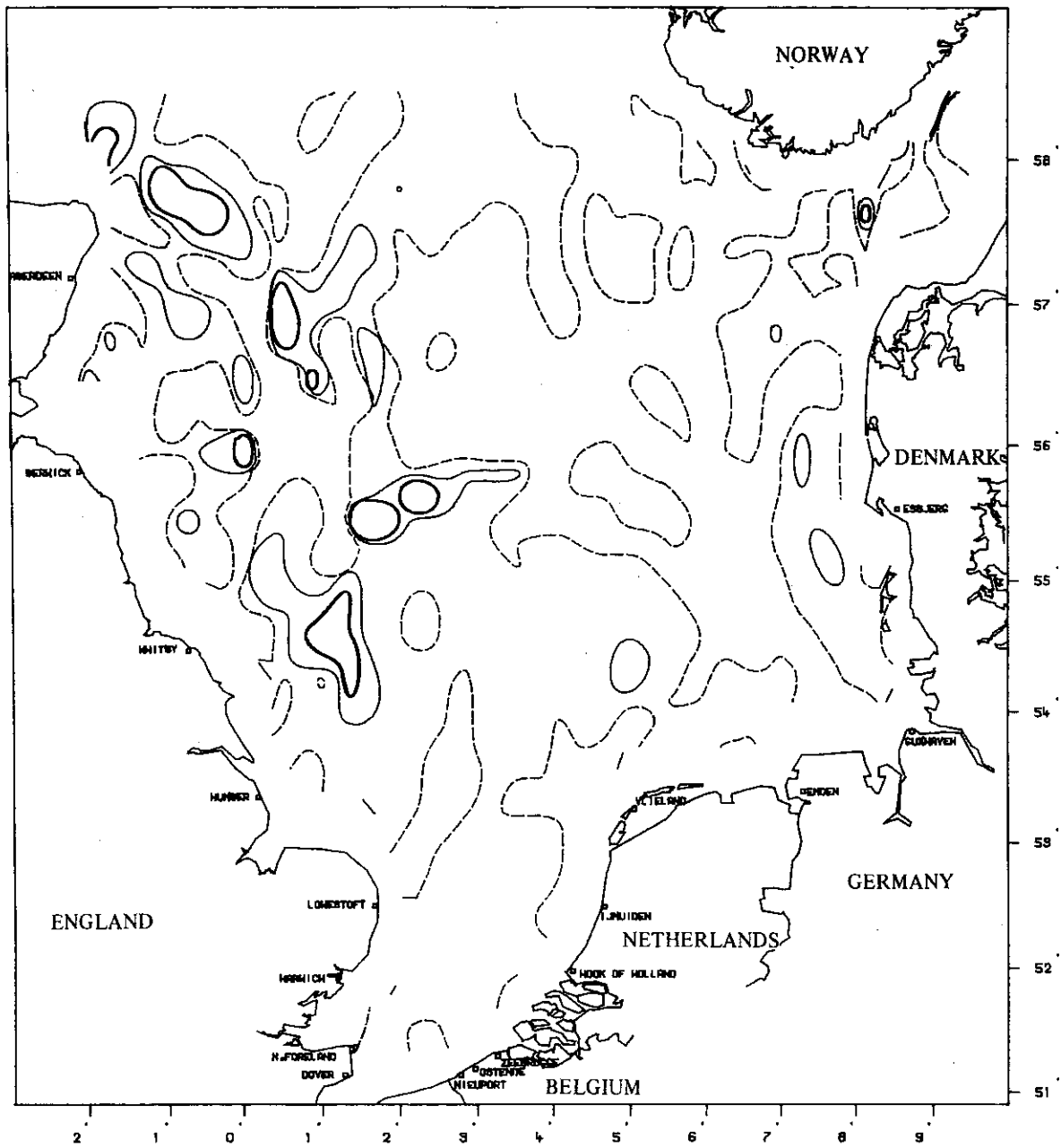


fig. 64 a.

Wind residuals in the North Sea. (Uniform constant wind of  $15 \text{ m.s}^{-1}$  from the north-west.) Map of positive values of the non-dimensional function  $\hat{\epsilon}_N$  representing the rate of energy transfer between residual and mesoscale flows by the mesoscale Reynolds stresses. (Positive values indicate regions of positive eddy viscosity.)

Heavy line       $\hat{\epsilon}_N = 50$   
 Slender line     $\hat{\epsilon}_N = 10$   
 Broken line      $\hat{\epsilon}_N = 0$

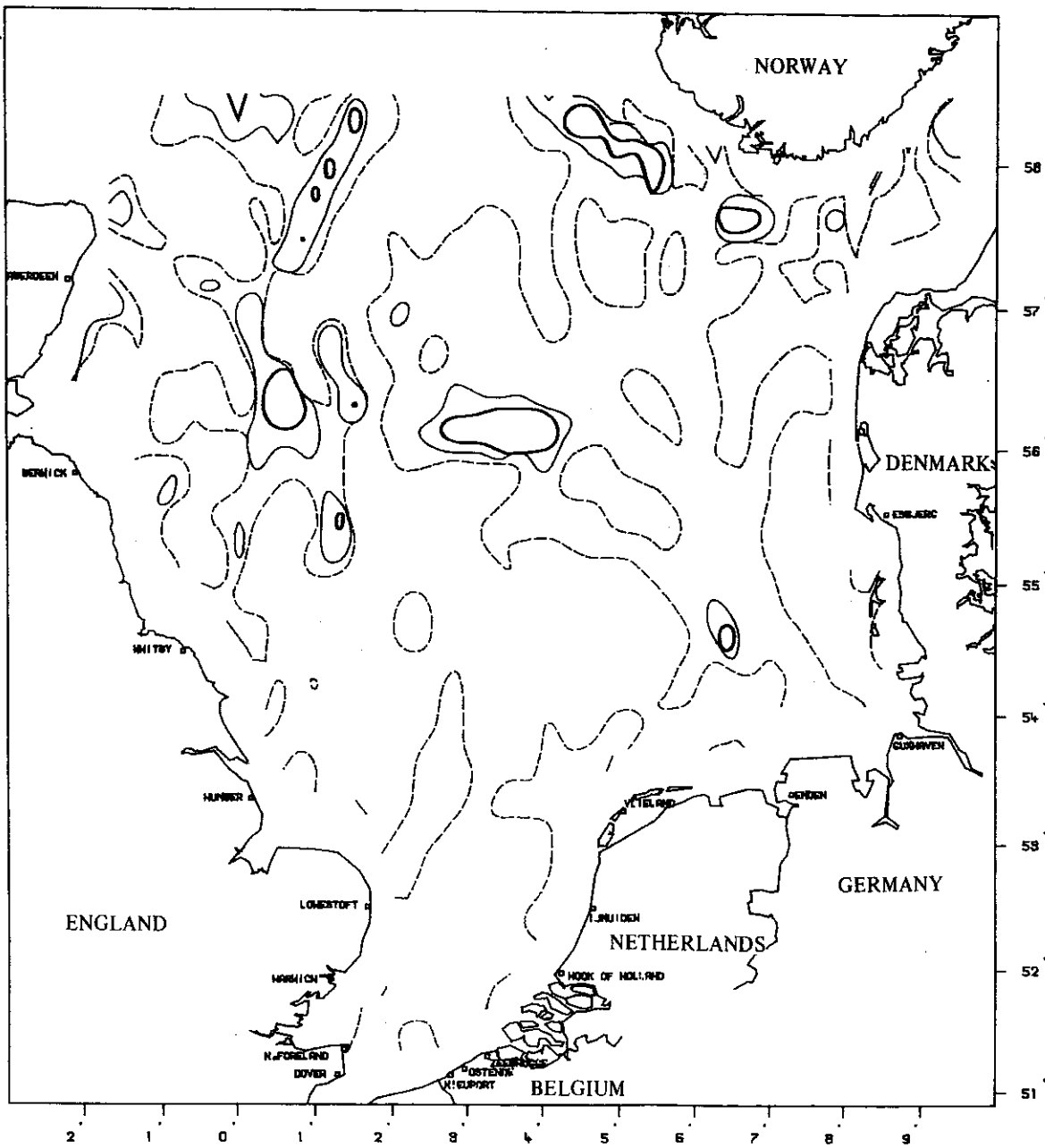


fig. 64b.

Wind residuals in the North Sea. (Uniform constant wind of  $15 \text{ m.s}^{-1}$  from the north-west.) Map of negative values of the non-dimensional function  $\hat{\epsilon}_N$  representing the rate of energy transfer between residual and mesoscale flows by the mesoscale Reynolds stresses. (Negative values indicate regions of negative eddy viscosity.)

Heavy line	—————	$\hat{\epsilon}_N = -50$
Slender line	—————	$\hat{\epsilon}_N = -10$
Broken line	- - - - -	$\hat{\epsilon}_N = 0$

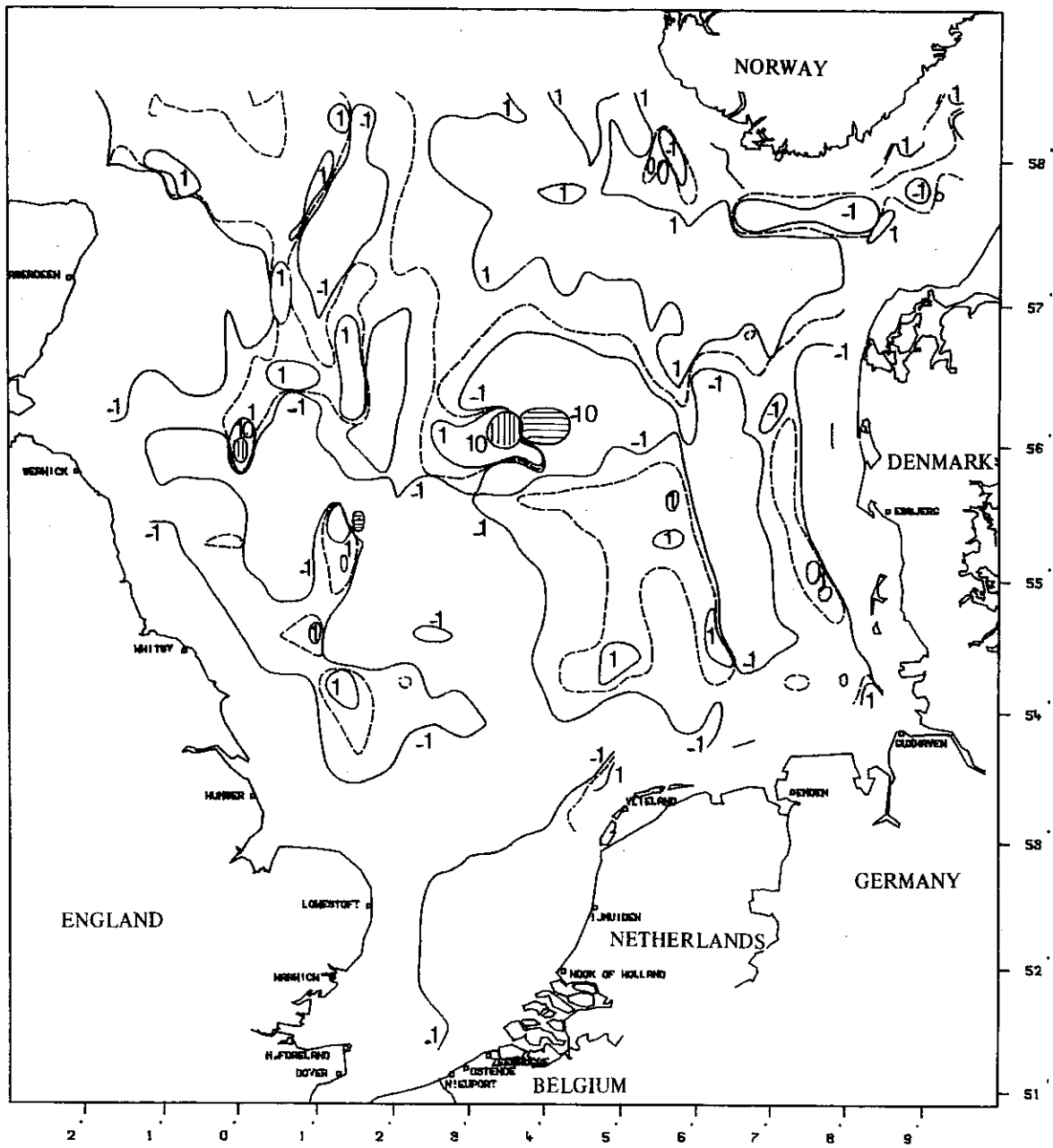


fig. 65.

Wind residuals in the North Sea. (Uniform constant wind of  $15 \text{ m.s}^{-1}$  from the north-west.) Map of positive and negative values of the non-dimensional function  $\hat{\epsilon}_F$  representing the rate of energy transfer between residual and mesoscale flows by the friction stress.

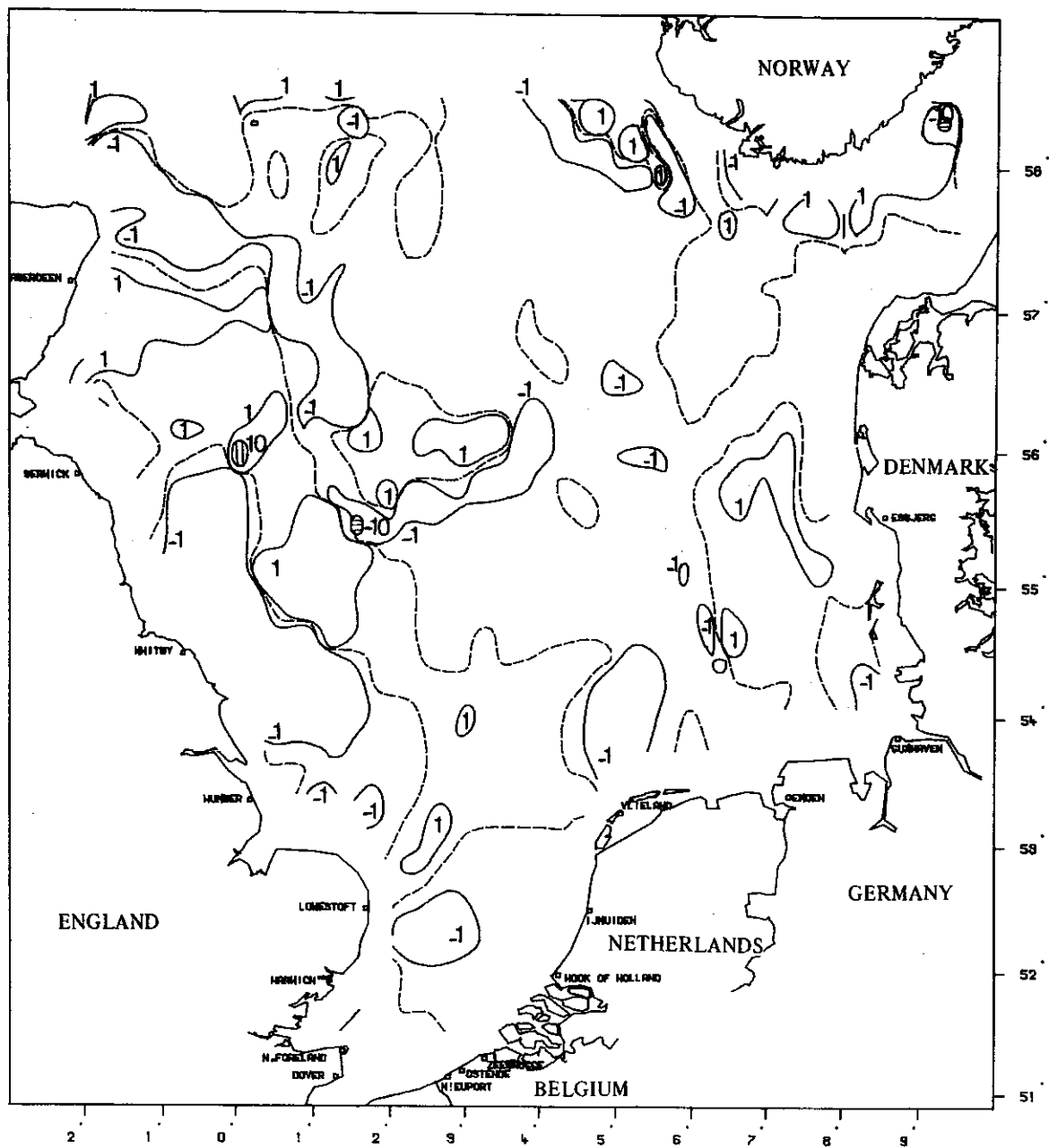


fig. 66.

Wind residuals in the North Sea. (Uniform constant wind of  $15 \text{ m.s}^{-1}$  from the north-west.) Map of positive and negative values of the non-dimensional function  $\delta + \hat{\epsilon}_N$  representing the rate of work of the mesoscale Reynolds stresses on the residual flow.

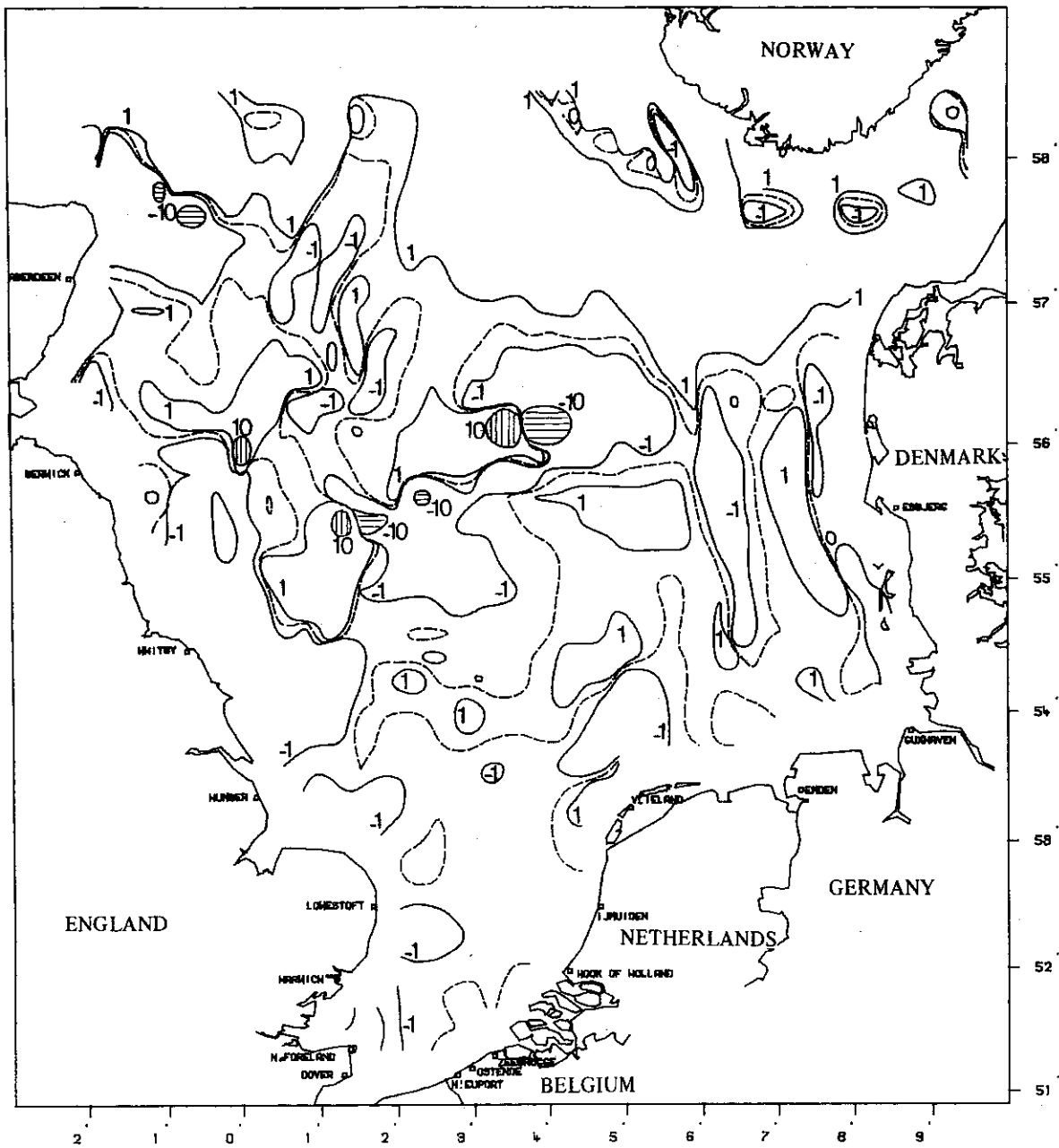


fig. 67.

Wind residuals in the North Sea. (Uniform constant wind of  $15 \text{ m.s}^{-1}$  from the north-west.) Map of positive and negative values of the non-dimensional function  $\hat{\epsilon}_T = \hat{\delta} + \hat{\epsilon}_N + \hat{\epsilon}_F + 1$  representing the rate at which energy is extracted from the residual flow (positive values) or supplied to the residual flow (negative values).



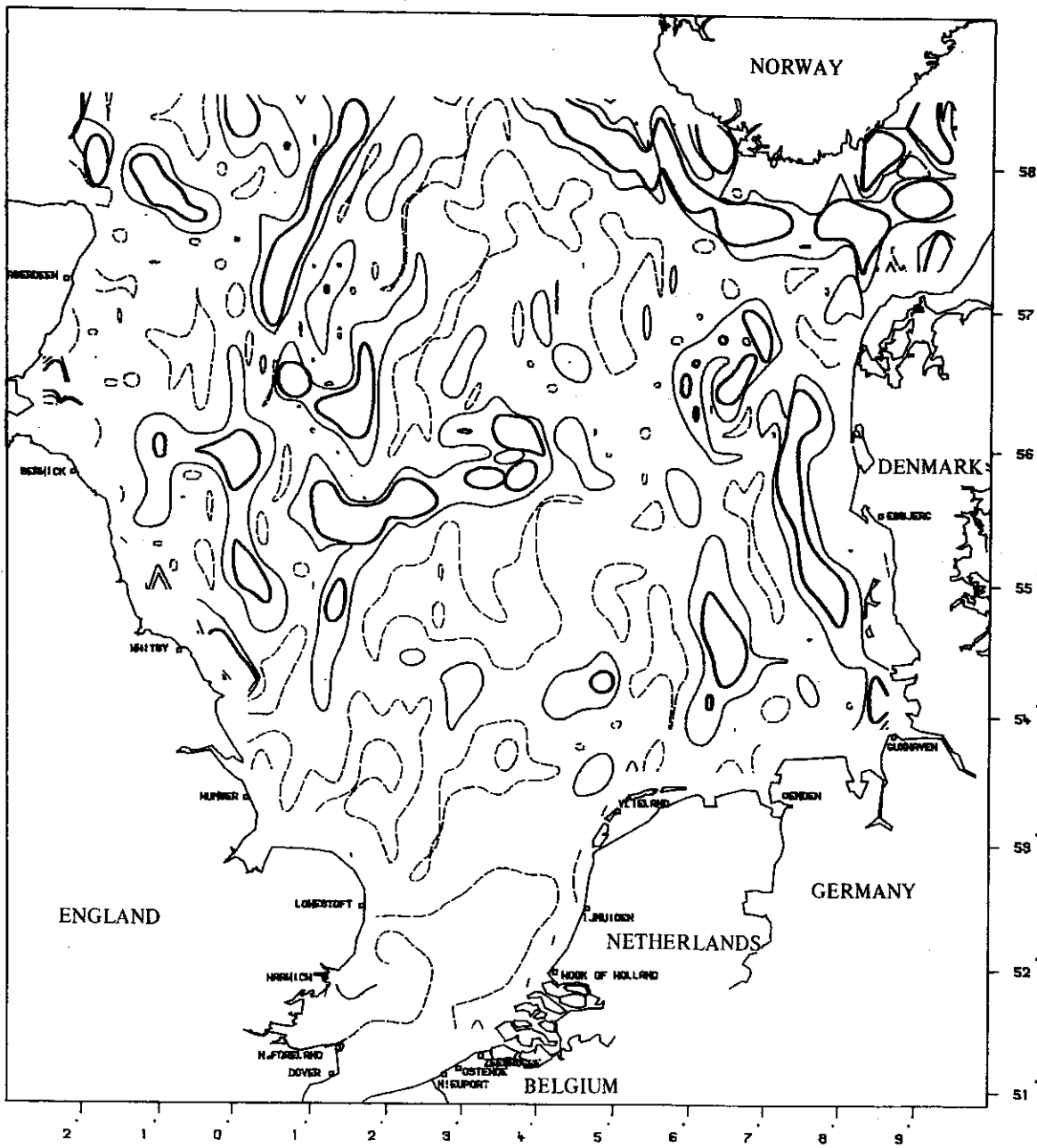


fig. 68.

Wind residuals in the North Sea. (Uniform constant wind of  $15 \text{ m.s}^{-1}$

from the north-west.) Map of the function  $\hat{\omega} = \frac{\|\nabla \wedge \bar{u}_0\|}{\|\bar{u}_0\|}$

indicating the scale of the residual vorticity.

Heavy line  $\hat{\omega} = 10^{-4} \text{ m}^{-1}$

Slender line  $\hat{\omega} = 5 \cdot 10^{-5} \text{ m}^{-1}$

Broken line  $\hat{\omega} = 10^{-5} \text{ m}^{-1}$

$$(191) \quad \nabla \wedge \left( \frac{\tau^s}{H} \right)_0 = \frac{\nabla \wedge \tau_0^s}{H_0} + \frac{\tau_0^s \wedge \nabla H_0}{H_0^2}$$

If the wind field is uniform, the first term of the right-hand side of eq. (191) drops out. The effect of the wind stress on the residual circulation is then due, in part, to the last term in the right-hand side of eq. (191) and, in part, to the modification of the mesoscale stresses resulting from the action of the wind field on the time dependent mesoscale motions.

There is thus no "direct" transfer of vorticity from the wind field to the residual circulation.

In the present case, it is perhaps preferable since the objective of the study is to elucidate the role played by the mesoscale stresses in determining the residual flow pattern and in particular in generating secondary gyres.

The hypothesis that the wind is constant in time (i.e., that it has a very large characteristic time of evolution) is of course limitative. It justifies however the averaging over a few tidal periods as this corresponds again to a valley in the energy spectrum of the currents.

In this process, the tidal currents are also removed but they are evidently taken into account in the time dependent mesoscale flow which determines the mesoscale stresses. One should not be misled by the name "wind residuals". The effect of the wind cannot be dissociated from the effect of the tides. All "wind residuals" are wind and tidal residuals.

Two cases of reasonably strong wind have been considered :

- (i) a constant wind of  $15 \text{ m.s}^{-1}$  from the North-West,
  - (ii) a constant wind of  $15 \text{ m.s}^{-1}$  from the South-West.
- The results are presented in figs. 62 to 68 for the first case and in figs. 69 to 75 for the second case.

In both cases, the streamlines pattern (figs. 62 and 69) show a deflection, under the influence of the wind field, of the main streams originating from the North Atlantic current's inflows. The tracery of the streamlines is more contorted and encloses large (length) scale gyres associated with relatively strong residual currents.

These gyres appear to determine the vorticity distribution and only few small scale secondary gyres are apparent in regions of weak residual currents.

The maps of energy transfer functions reflect the streamlines patterns. The energy dissipation  $\epsilon_D$  is more important (stronger currents) than in the absence of wind and the rates of energy transfer  $\epsilon_N$ ,  $\epsilon_F$ , ... are found generally comparable to  $\epsilon_D$ , the normalized functions  $\hat{\delta}$ ,  $\hat{\epsilon}_N$  and  $\hat{\epsilon}_F$  having only a few located peaks of values significantly larger than 1.

One can still find "eddies" where the exchange of energy between scales of motion sharply dominates the energy dissipation by bottom friction and, induced to look for it by one's understanding

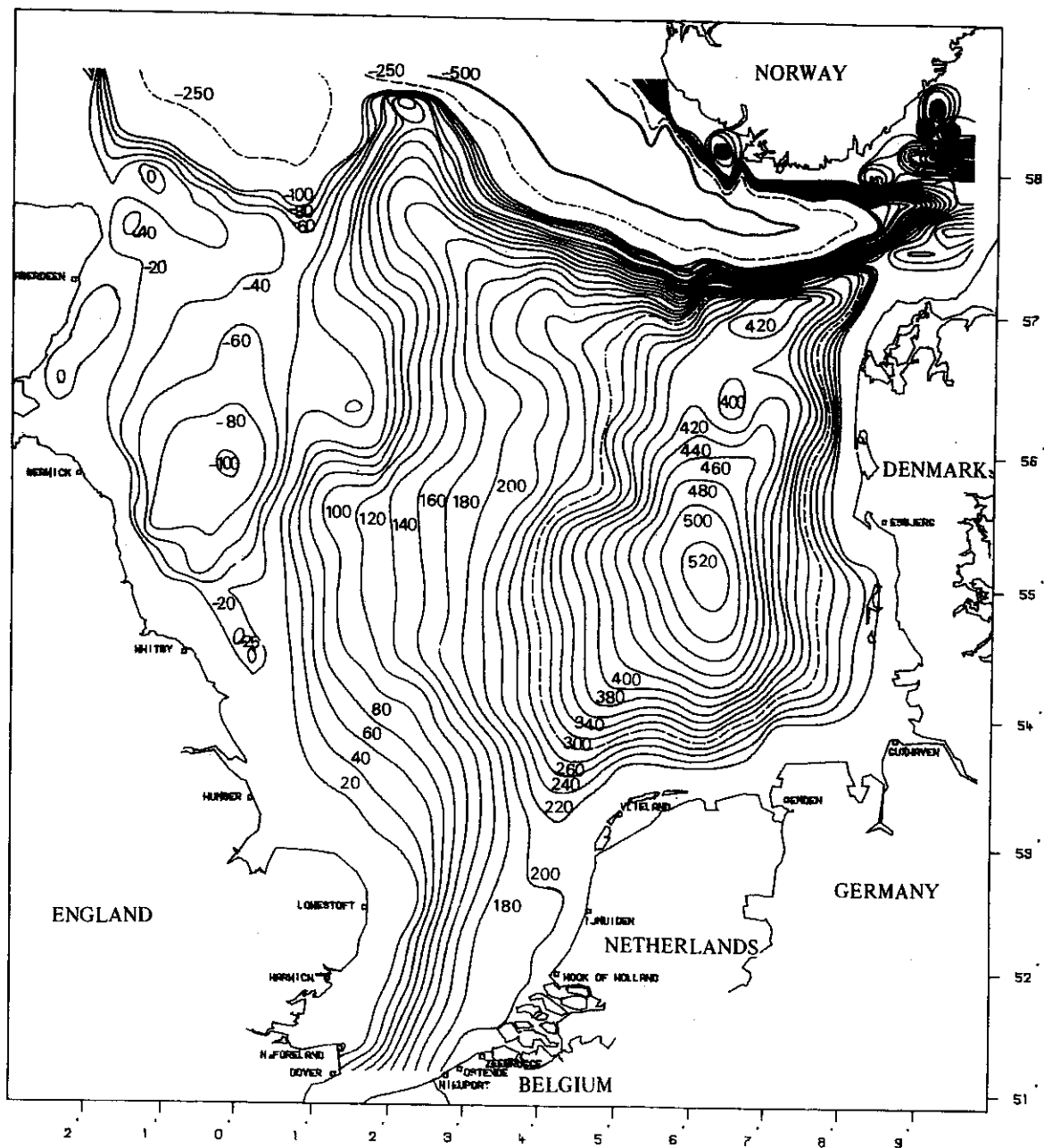


fig. 69.

Wind residuals in the North Sea. (Uniform constant wind of  $15 \text{ m}\cdot\text{s}^{-1}$  from the south-west.) Residual flow pattern. Streamlines  $\psi = \text{const.}$  in  $10^3 \text{ m}^3\cdot\text{s}^{-1}$ .

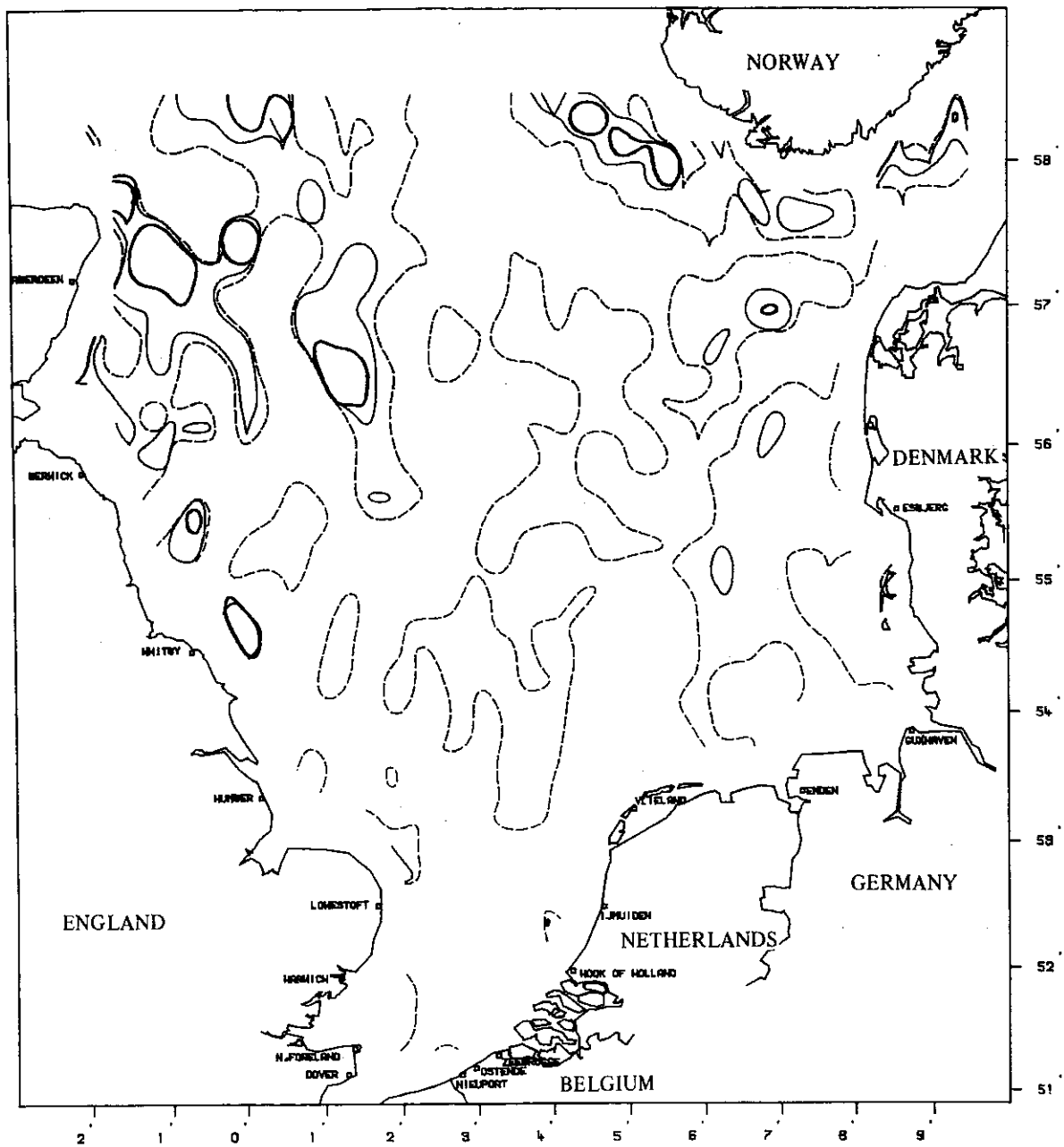


fig. 70a.

Wind residuals in the North Sea. (Uniform constant wind of  $15 \text{ m.s}^{-1}$  from the south-west.) Map of positive values of the non-dimensional function  $\hat{\delta}$  representing the rate at which the residual kinetic energy is redistributed in physical space. (Positive values indicate regions of residual energy divergence.)

Heavy line  $\hat{\delta} = 50$   
 Slender line  $\hat{\delta} = 10$   
 Broken line  $\hat{\delta} = 0$

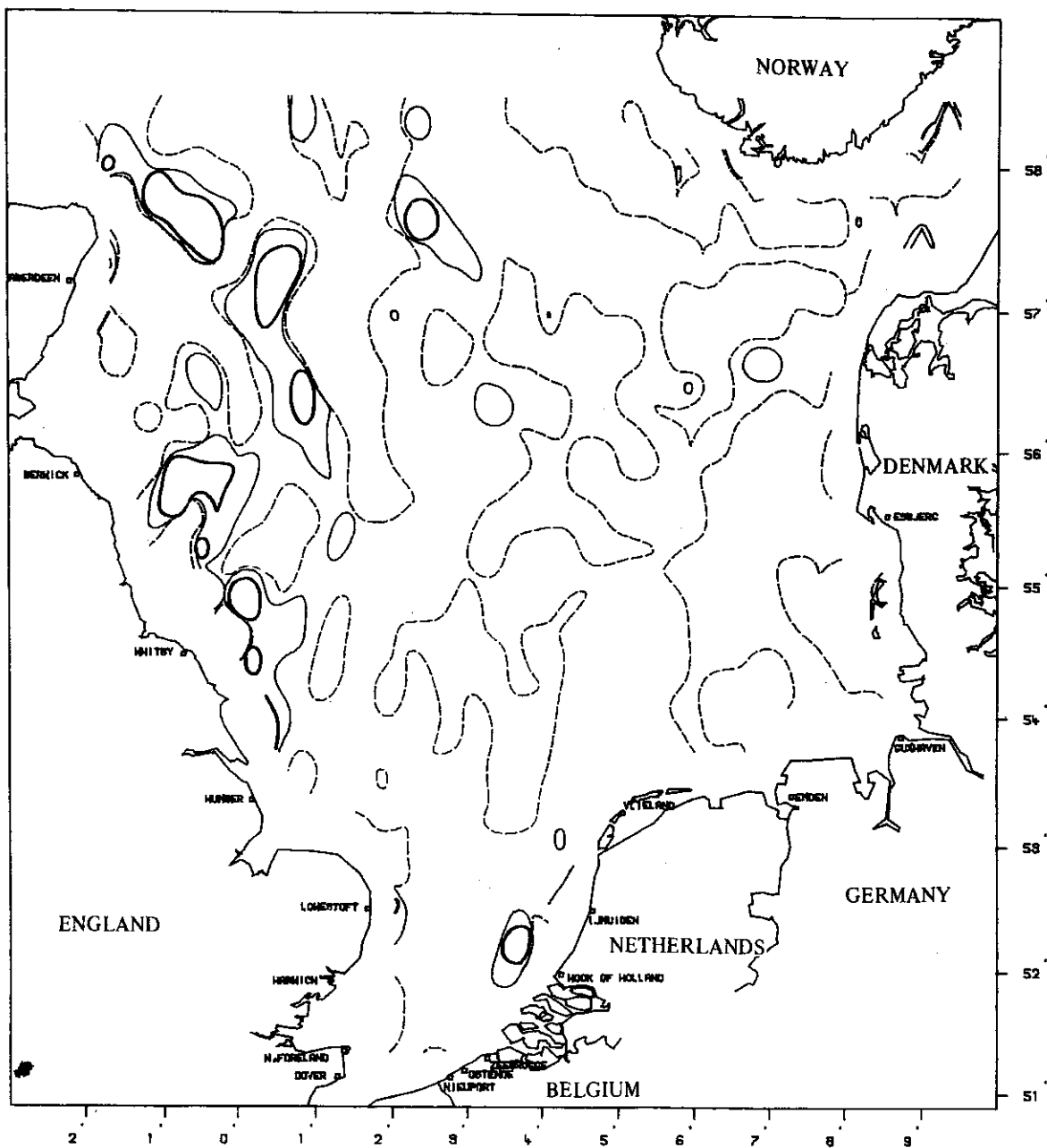


fig. 70b.

Wind residuals in the North Sea. (Uniform constant wind of  $15 \text{ m.s}^{-1}$  from the south-west.) Map of negative values of the non-dimensional function  $\hat{\delta}$  representing the rate at which the residual kinetic energy is redistributed in physical space. (Negative values indicate regions of residual energy convergence.)

Heavy line       $\hat{\delta} = -50$   
 Slender line     $\hat{\delta} = -10$   
 Broken line      $\hat{\delta} = 0$

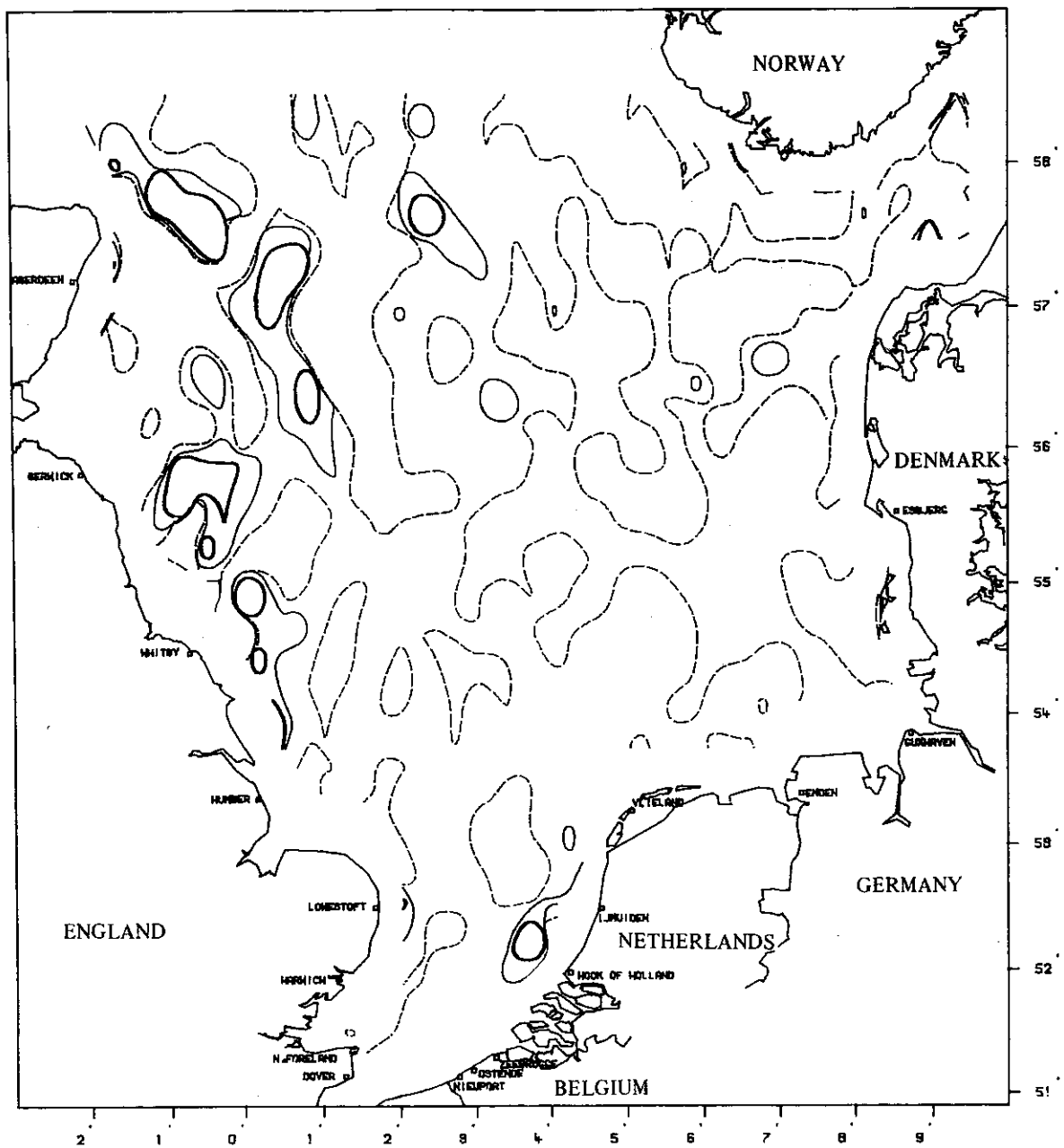


fig. 71a.

Wind residuals in the North Sea. (Uniform constant wind of  $15 \text{ m.s}^{-1}$  from the south-west.) Map of positive values of the non-dimensional function  $\hat{\epsilon}_N$  representing the rate of energy transfer between residual and mesoscale flows by the mesoscale Reynolds stresses. (Positive values indicate regions of positive eddy viscosity.)

Heavy line ———  $\hat{\epsilon}_N = 50$   
 Slender line ———  $\hat{\epsilon}_N = 10$   
 Broken line - - - -  $\hat{\epsilon}_N = 0$

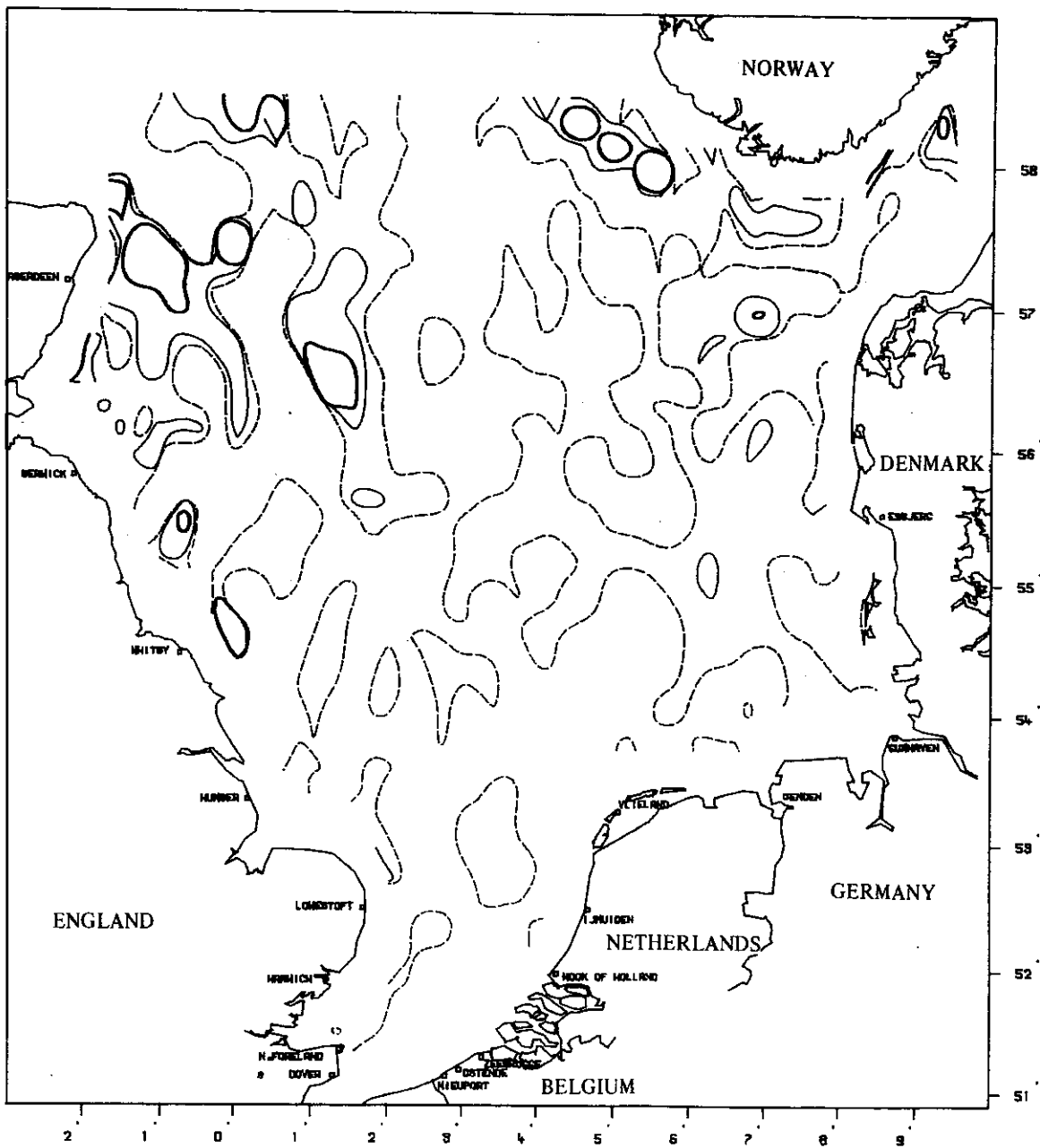


fig. 71 b.

Wind residuals in the North Sea. (Uniform constant wind of  $15 \text{ m.s}^{-1}$  from the south-west.) Map of negative values of the non-dimensional function  $\hat{\epsilon}_N$  representing the rate of energy transfer between residual and mesoscale flows by the mesoscale Reynolds stresses. (Negative values indicate regions of negative eddy viscosity.)

Heavy line  $\hat{\epsilon}_N = -50$   
 Slender line  $\hat{\epsilon}_N = -10$   
 Broken line  $\hat{\epsilon}_N = 0$

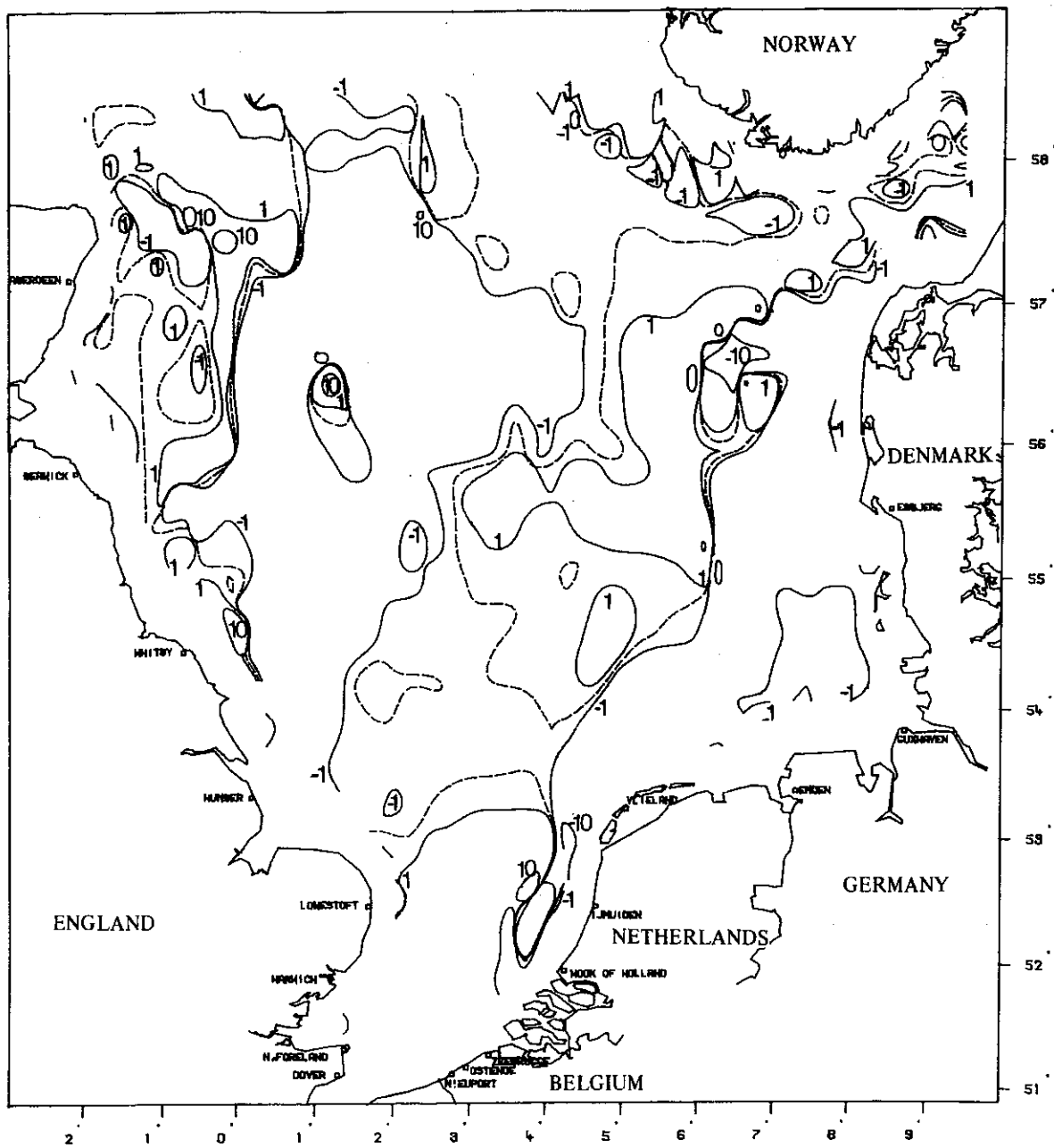


fig. 72.

Wind residuals in the North Sea. (Uniform constant wind of  $15 \text{ m.s}^{-1}$  from the south-west.) Map of positive and negative values of the non-dimensional function  $\hat{\epsilon}_F$  representing the rate of energy transfer between residual and mesoscale flows by the friction stress.



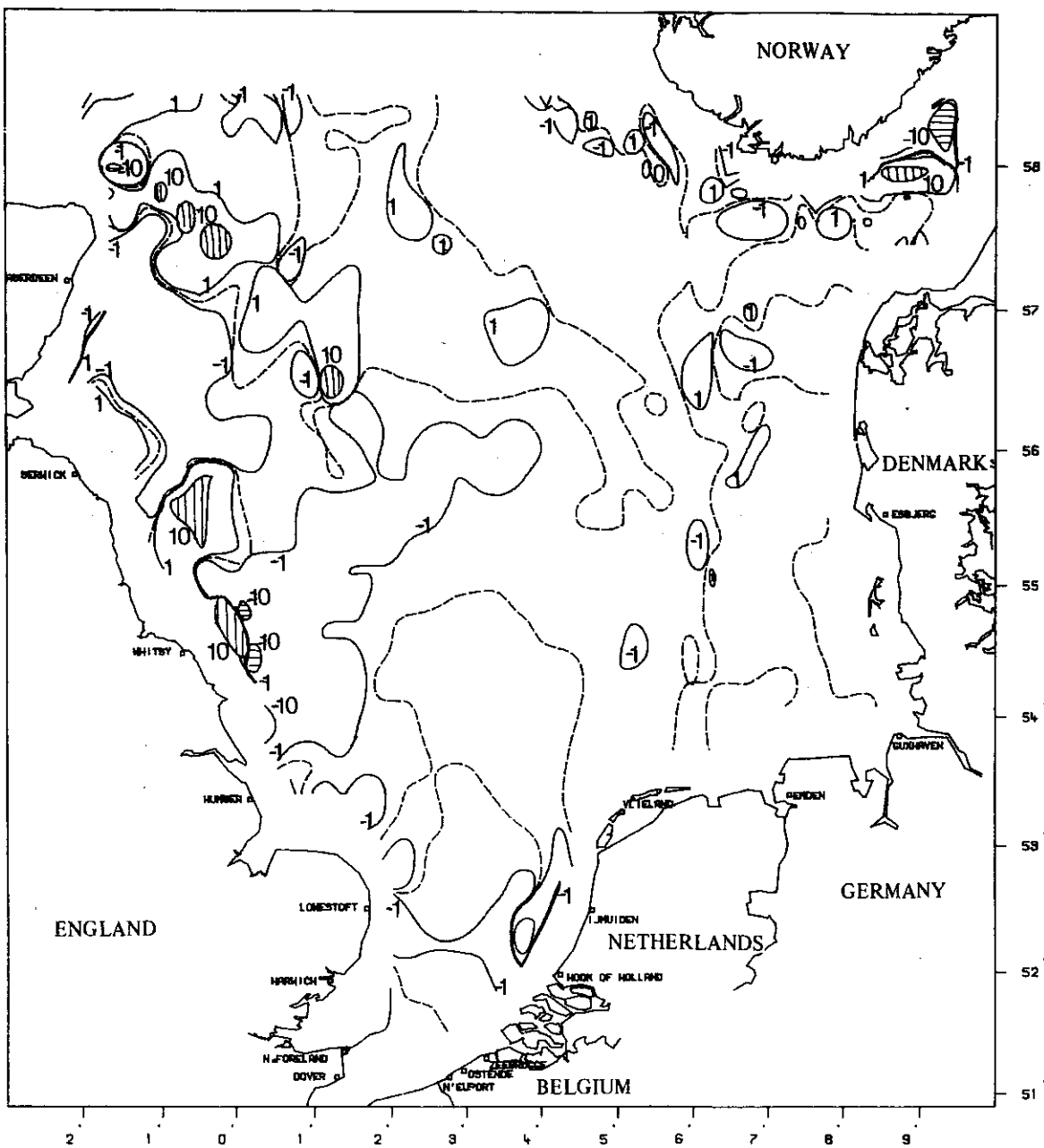


fig. 73.

Wind residuals in the North Sea. (Uniform constant wind of  $15 \text{ m.s}^{-1}$  from the south-west.) Map of positive and negative values of the non-dimensional function  $\hat{\delta} + \hat{\epsilon}_N$  representing the rate of work of the mesoscale Reynolds stresses on the residual flow.

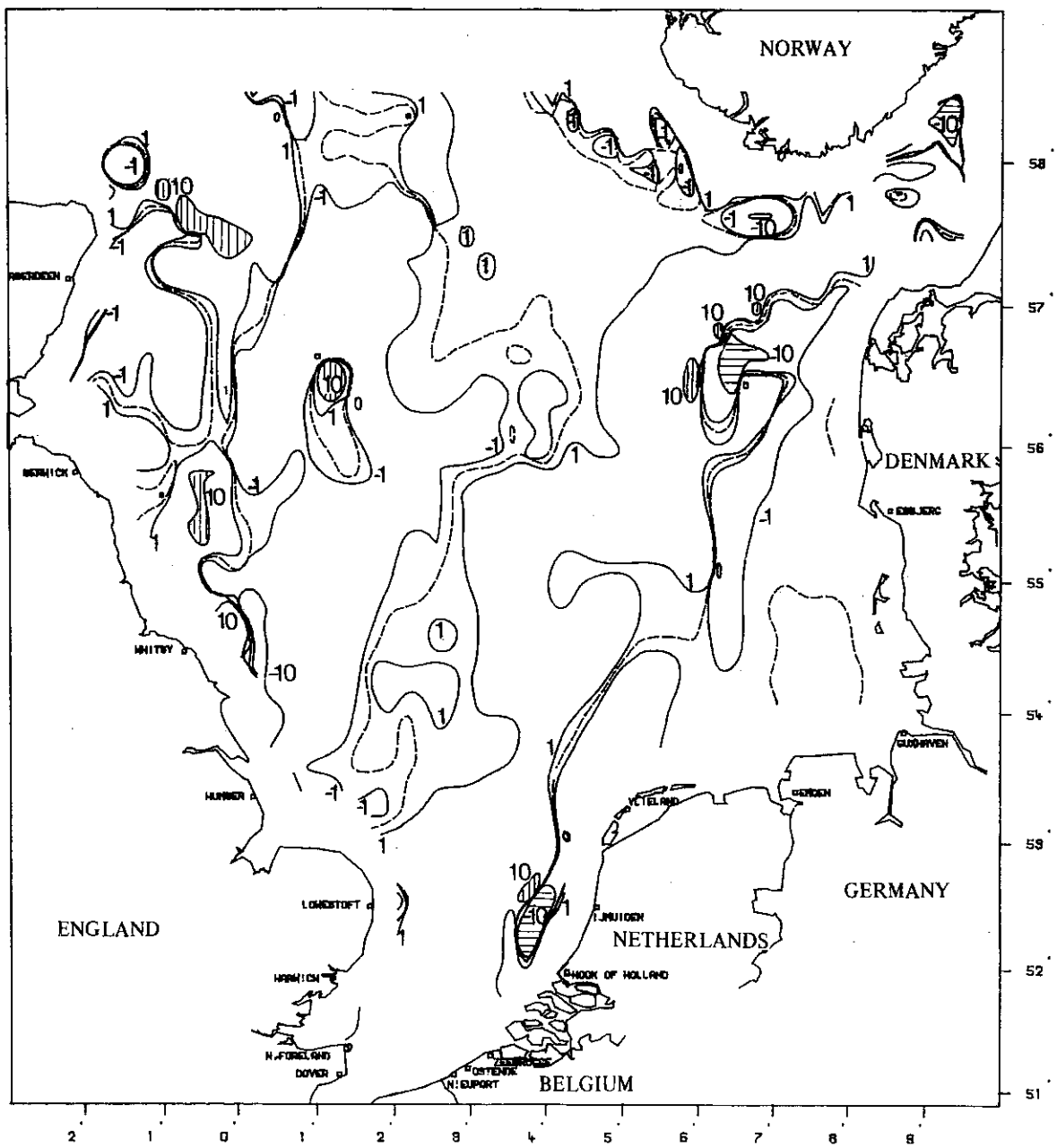


fig. 74.

Wind residuals in the North Sea. (Uniform constant wind of  $15 \text{ m.s}^{-1}$  from the south-west.) Map of positive and negative values of the non-dimensional function  $\hat{\epsilon}_T = \hat{\delta} + \hat{\epsilon}_N + \hat{\epsilon}_F + 1$  representing the rate at which energy is extracted from the residual flow (positive values) or supplied to the residual flow (negative values).

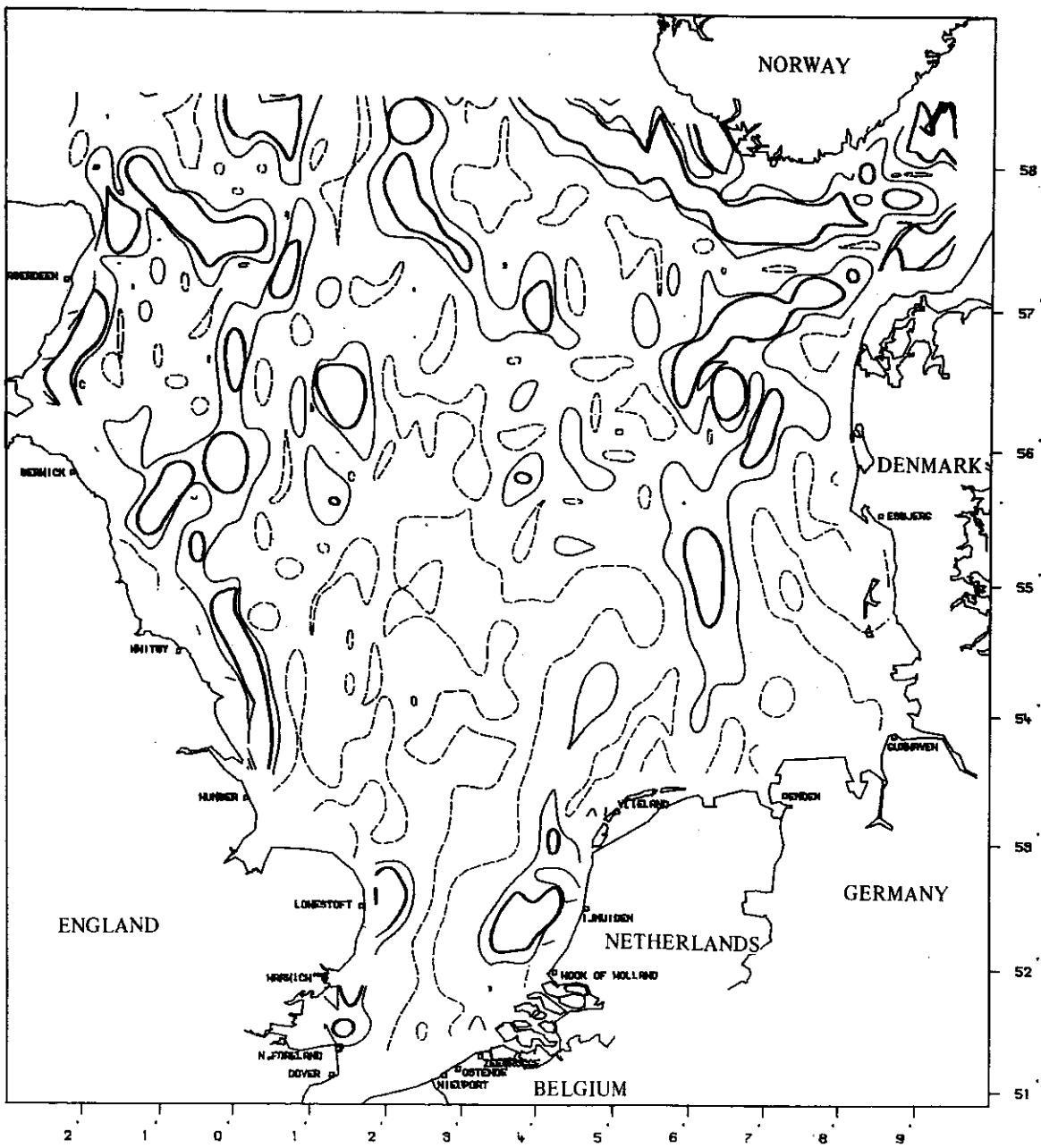


fig. 75.

Wind residuals in the North Sea. (Uniform constant wind of  $15 \text{ m.s}^{-1}$  from the north-west.) Map of the function  $\hat{\omega} = \frac{\|\nabla \wedge \mathbf{u}_0\|}{\|\mathbf{u}_0\|}$

indicating the scale of the residual vorticity.

Heavy line	$\hat{\omega} = 10^{-4} \text{ m}^{-1}$
Slender line	$\hat{\omega} = 5 \cdot 10^{-5} \text{ m}^{-1}$
Broken line	$\hat{\omega} = 10^{-5} \text{ m}^{-1}$

of tidal residuals, one can still see a relationship between negative viscosity eddies and small (length) scale vorticity in secondary gyres but basically, bottom friction has gained control of energy and enstrophy cascades and an interpretation of the residual flow's energetics in terms of two-dimensional turbulence is no longer profitable.

#### 14.- Three-dimensional dispersion models for passive constituents.

The evolution of a passive constituent is described by eq. (15). By restricting attention to a *passive* constituent, one makes the assumption that the constituent is involved in no significant interaction with others and that eq. (15) can be solved, once the velocity field  $v$ , and the diffusion coefficient  $\tilde{\lambda}$  have been determined, independently of similar equations for the concentrations of other constituents.

In the first instance, the rate of production (destruction)  $Q$  is, in this approximation, a function of inputs (outputs) which represent the transfers of matter between the marine system and the outside world (dumpings, ...).

One can also include in  $Q$  "self-destruction" mechanisms like radioactive decay, natural death (for a biological species) or precipitation of suspended sediments, after eventual flocculation.

In the first two cases indeed the corresponding contribution  $Q_d$  to the rate of production  $Q$  depends only on the constituent's concentration and may be written, with often a very good approximation,

$$(192) \quad Q_d = -kc$$

where  $k$  is a suitable constant.

In the third case, the sedimentation (or the ascension of light constituents) may be expressed as the divergence of a flux, i.e.

$$(193) \quad Q_s = -\nabla \cdot (c w) = -\frac{\partial}{\partial x_3} (cw)$$

where  $w = w e_3$  is the sedimentation (ascension) velocity.

If one denotes by  $Q_e$  the contribution of inputs and outputs, one has thus

$$(194) \quad Q = Q_e + Q_d + Q_s$$

A special case of great interest is the instantaneous release at a given time which may be taken as the initial time. In that case,  $Q_e$  may be left out in eqs. (194) and (15) and taken into account in the initial conditions which are used later to determine constants of integration in the solution.

Horizontal diffusion due to microscale three-dimensional turbulence has been neglected in eq. (15). This approximation requires some explanation. The argument is basically that horizontal gradients are much smaller than vertical gradients and that since the horizontal and the vertical eddy diffusivities are of the same order of magnitude in three-dimensional microscale turbulence,

$$(195) \quad \nabla_h \cdot (\tilde{\lambda}_h \nabla_h c) \sim \nabla_h \cdot (\tilde{\lambda} \nabla_h c) \ll \frac{\partial}{\partial x_3} \left( \tilde{\lambda} \frac{\partial c}{\partial x_3} \right)$$

$\tilde{\lambda}_h$  denoting the horizontal eddy diffusivity.

Eq. (195) is almost always verified in shallow continental seas like the North Sea because the depth is much smaller than any horizontal length scale. There are however exceptions and, in particular, immediately after a dumping or in the immediate vicinity of a continuous source, there may be important horizontal gradients of concentration and effective horizontal diffusion by microscale turbulence. Yet, marine turbulence has relatively little to do with it; the mixing of the effluent being, at this stage, still largely dominated by "intrinsic" turbulence resulting from the release operation (high jet velocity or temperature, stirring by the ship's propeller, ...).

This initial phase of the dispersion is not described by the equations of marine hydrodynamics but it is usually very limited in space and (or) in time. In practical applications, one starts the simulation after the initial phase has ended, taking the preliminary mixing into account in new initial conditions.

Thus, discarding the delicate intrinsic phase, one may assume that eq. (195) holds and neglect horizontal microscale turbulent diffusion. This does not imply, however, that there is no horizontal dispersion. Indeed, with only microscale turbulence taken away by averaging, the horizontal velocity field  $\mathbf{u}$  still contains a continuity of components of different time scales and length scales reflecting the natural variability of mesoscale processes in the atmosphere and in the sea (fig. 76).

The variability of sea motions in the mesoscale range cannot be reproduced by the hydrodynamic models of tides and storm surges. For instance, these models operate with "average" meteorological conditions and do not respond to fluctuations in the wind and pressure fields which perturb the flow pattern in the sea. The length-scales of such perturbations are, in any case, smaller than or comparable with the grid-scale and cannot be represented.

One can visualize the situation by considering that the horizontal velocity vector is, actually, the sum of a "representative" velocity  $\mathbf{u}$  and a variable and changing velocity  $\mathbf{u}'$  responsible for a disorganized advection equivalent to dispersion.

The irregular shape of a patch of pollutant in the sea is explained by this erratic advection which never quite recurs and observations made in similar circumstances reveal dispersion patterns which are *globally* similar but differ in the details. However, if one superimposes the results of several experiments conducted

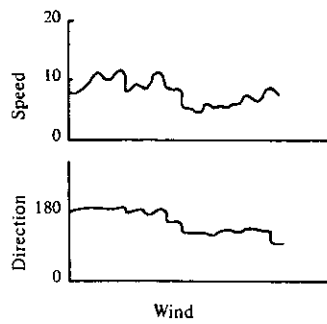
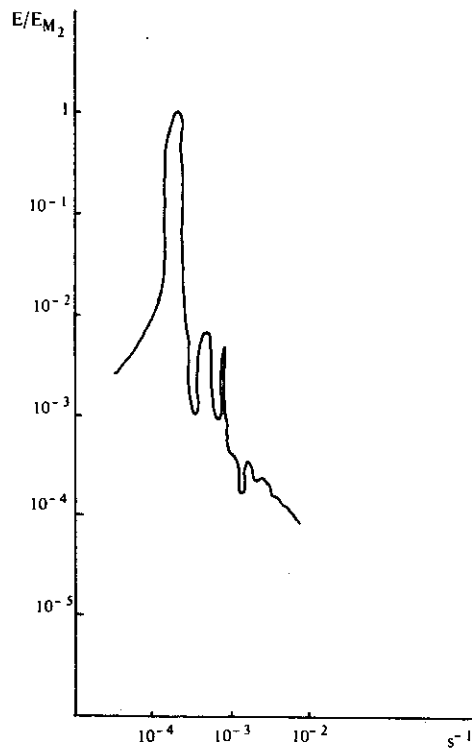


fig. 76.

Above : observed energy density spectrum during a dye release experiment in the North Sea in October 1969. (The spectrum is normalized with the energy density of the  $M_2$  tide.)

Below : wind recording during the experiment.

[Talbot, 1972].

in the same global conditions, a "representative" pattern of dispersion emerges which can be reproduced in a second series of experiments.

It is, obviously, the *representative* dispersion that one wants to model and, for this purpose, eq. (15) must be further averaged over an ensemble of identical situations. The ensemble average eliminates the fluctuations  $u'$  and  $c'$  from the linear terms but

their mean product remains from the non-linear advection term. The additional term has the same form as its microscale turbulent equivalent and more or less the same effect : horizontal diffusion.

This diffusion is called "pseudo-turbulent" to emphasize that it is the product of scales of motions with a highly anisotropic structure (the horizontal length-scales are much larger than the depth) and with some degree of organization, i.e. a pseudo-random phenomenon not quite comparable with the three-dimensional perfect disorder of microscale turbulence.

If  $u$  now denotes the representative velocity, one can write eq. (15) in the following form which takes into account the pseudo-turbulent horizontal diffusion

$$(196) \quad \frac{\partial c}{\partial t} + \nabla \cdot (u c) + \frac{\partial}{\partial x_3} (v_3 c) = Q + \frac{\partial}{\partial x_1} (\tilde{\kappa}_1 \frac{\partial c}{\partial x_1}) + \frac{\partial}{\partial x_2} (\tilde{\kappa}_2 \frac{\partial c}{\partial x_2}) + \frac{\partial}{\partial x_3} (\tilde{\lambda} \frac{\partial c}{\partial x_3})$$

$\tilde{\kappa}_1$  and  $\tilde{\kappa}_2$  are the two coefficients of pseudo-turbulent horizontal diffusion (including *ipso facto* the small contribution from microscale turbulence). In many cases, one may take

$$(197) \quad \tilde{\kappa}_1 = \tilde{\kappa}_2 \equiv \tilde{\kappa}$$

In three-dimensional isotropic turbulence, one can associate, to a given length-scale  $\ell$ ,

(i) a time scale  $\tau$

$$(198) \quad \tau \sim \epsilon^{-1/3} \ell^{2/3}$$

and

(ii) a velocity scale  $v$

$$(199) \quad v \sim \epsilon^{1/3} \ell^{1/3} \sim \epsilon^{1/2} \tau^{1/2}$$

characteristic of motions at the scale  $\ell$ ;  $\epsilon$  (in  $m^2 \cdot s^{-3}$ ) is the rate of energy transfer between scales of motions.

If  $\ell$  is the size of a patch of contaminant, smaller scale motions produce a diffusion of the patch. The associated eddy diffusivity scale is

$$v\ell \sim \epsilon^{1/3} \ell^{4/3} \sim \epsilon \tau^2$$

The differences between pseudo-turbulence and three-dimensional isotropic turbulence have been emphasized. There is however considerable experimental evidence that horizontal diffusion by pseudo-turbulence is, by many aspects, similar to three-dimensional turbulent diffusion and Ozmidov (1961, 1967) has argued that the pseudo-turbulent horizontal diffusivity  $\tilde{\kappa}$  can be written

$$(200) \quad \tilde{\kappa} = \alpha \epsilon^{1/3} \ell^{4/3}$$

where  $\alpha$  is an empirical constant and where a different value of  $\epsilon$  must be used in three distinct ranges of scales to take into account the inputs of energy at intermediate scales.

Although it is generally agreed that, as a result of the wide spectrum of horizontal motions, the horizontal eddy diffusivity must increase with the scale of mixing considered, there has been so far no definite evidence that it behaves exactly as the  $4/3$  power of  $\ell$ .

According to Joseph and Sendner (1958), the pseudo-turbulent horizontal diffusivity  $\tilde{\kappa}$  should be proportional to the length scale of the mixing process. Introducing a *diffusion velocity*  $P$ , they take

$$(201) \quad \tilde{\kappa} \sim P \ell$$

where the diffusion velocity - which is related to the root-mean-square value of the velocity fluctuations - is assumed to be constant ( $P \sim 10^{-2}$  m/s).

Okubo (1971a,b), reviewing data from a large number of experiments, derived the relation

$$(202) \quad \tilde{\kappa} \sim \beta \ell^{1.15}$$

The exponent 1.15 is intermediate between the value 1 given by Joseph and Sendner and the value  $4/3$  advocated by Ozmidov (fig. 77).

Results from a diffusion experiment in the North Sea reported by Joseph et al. (1964) suggest on the contrary that the exponent is less than 1 and actually decreases to 0 with increasing scale, the eddy diffusivity tending to a constant value. A similar behaviour was apparently observed by Talbot (1970).

As pointed out by Okubo, the experimental data cannot definitely prove or rule out any theory. One must remember in particular that coefficients like  $\epsilon$  or  $P$  are functions of time and may vary appreciably during a series of observations. Such variations produce a scattering of the experimental data through which, in most cases, curves like (200), (201) and (202) can be drawn with an equally good fit. The three curves are, however, very close and they all provide good estimates of the horizontal eddy diffusivity when the control parameters ( $\epsilon$ ,  $P$ , etc.) are properly adjusted.

Using formula (200), one finds, for patches of contaminants ranging from a few meters to a few kilometers in size, pseudo-turbulent horizontal diffusivities ranging from  $10^{-1} \text{ m}^2 \cdot \text{s}^{-1}$  to  $10 \text{ m}^2 \cdot \text{s}^{-1}$  (e.g. Nihoul, 1975a) and, for a typical patch size of  $10^2$  to  $10^3$  meters, one can put down, for later estimates a typical value of  $\tilde{\kappa} \sim 1 \text{ m}^2 \cdot \text{s}^{-1}$ .

Examining the different terms of eq. (196), one can see that one can associate, with vertical turbulent diffusion, a characteristic time

$$(203) \quad t_v \sim H^2 \tilde{\lambda}^{-1}$$



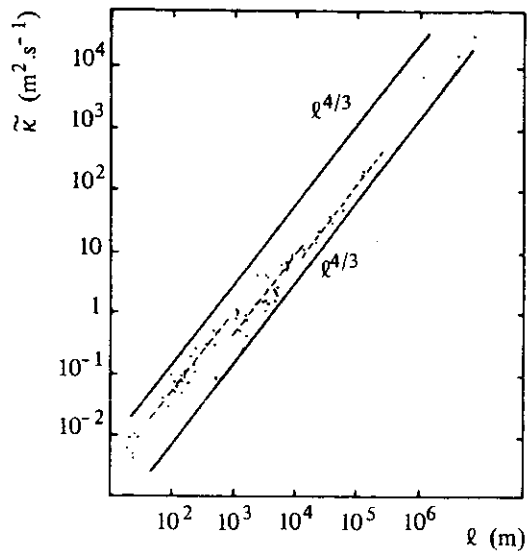
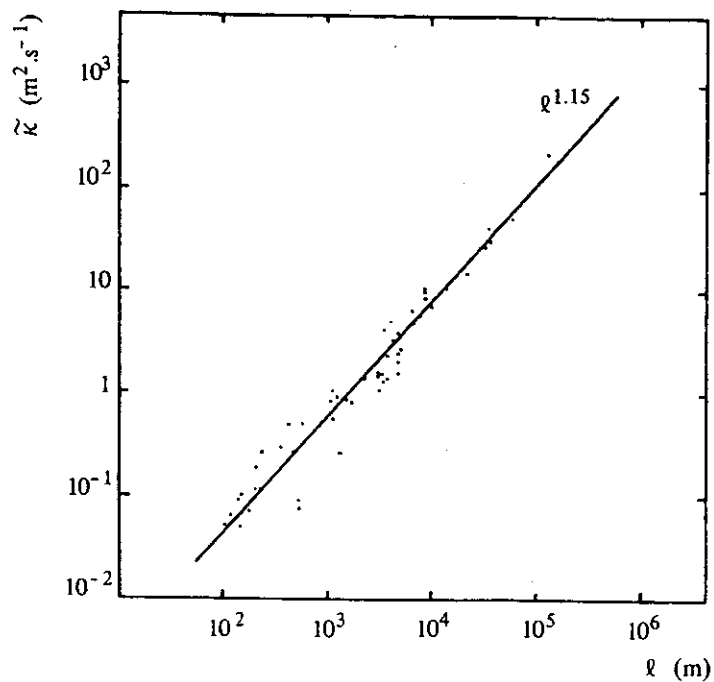


fig. 77.

Pseudo-turbulent horizontal diffusivity  $\tilde{\kappa}$  as a function of scale

In fairly well-mixed shallow seas,  $t_v$  has values ranging from a few hours to a few days. In deeper regions (when  $h$  is larger) or in partially stratified waters (where  $\tilde{\lambda}$  can be considerably decreased),  $t_v$  can be one or two orders of magnitude larger. (The case of a light constituent which tends to concentrate at the sea surface may be regarded as an extreme case of stratification, characterized also by large values of  $t_v$ .)

If one considers a dumping at  $t = 0$ , one may distinguish between successive stages of the dispersion process.

- (i) For  $t \ll t_v$ , vertical diffusion is inoperative and vertical advection being quite negligible with respect to horizontal advection, one can drop the last terms in the left-hand side and right-hand side of eq. (196) and consider the two-dimensional dispersion of a constituent confined to a thin layer at discharge or equilibrium level.
- (ii) For  $t \sim t_v$ , the problem is a three-dimensional one.
- (iii) For  $t \gg t_v$ , the constituent is almost uniformly distributed over the water column and it is reasonable to restrict attention to the horizontal dispersion of the depth-averaged concentration  $\bar{c}$ , introduced in eq. (39).

In eq. (39), the pseudo-turbulent horizontal diffusion is still included in the advection term and could be extracted by ensemble averaging of the equation. The corresponding contribution however turns out to be small compared with the shear effect and one is justified to use eq. (39) as it is, with  $u$  as the *representative* velocity, even if it entails to add a second horizontal diffusion term with an appropriate diffusivity  $\tilde{\kappa}$  synthesizing the effects of mesoscale pseudo-turbulence and microscale turbulence.

The observations by Joseph et al. (1964) and Talbot (1970) of a horizontal diffusivity coefficient tending to become, after some time, independent of the horizontal scale, suggest that their experiments extended beyond the first phase and that shear effect had taken over the mechanism of diffusion.

The self-destruction term  $Q_d$ , if it can be expressed in the single form (192) can always be eliminated by the change of variables

$$(204) \quad c = c^* e^{-kt}$$

Eq. (196) gives, substituting eq. (204) and using eqs. (193), (194) and (197)

$$(205) \quad \frac{\partial c^*}{\partial t} + \nabla_h \cdot (u c^*) + \frac{\partial}{\partial x_3} (c^* v_3) = Q^* - \frac{\partial}{\partial x_3} (c^* w) + \nabla_h \cdot (\tilde{\kappa} \nabla_h c^*) + \frac{\partial}{\partial x_3} (\tilde{\lambda} \frac{\partial c^*}{\partial x_3})$$

where

$$(206) \quad Q^* = Q_e e^{kt}$$

is a given function of  $x$  and  $t$  representing external sources and sinks and where

$$(207) \quad \nabla_h = e_1 \frac{\partial}{\partial x_1} + e_2 \frac{\partial}{\partial x_2}$$

In the following, one shall assume that the transformation (204) has been made and set  $Q_d = 0$ . For simplicity, the asterisks will be dropped.

The roles of the different terms of eq. (205) are easily identified. The variation of the concentration  $c$  with time results from the combined effects of

- horizontal advection :  $\nabla_h \cdot (c \mathbf{u})$
- vertical advection :  $\frac{\partial}{\partial x_3} (c v_3)$
- vertical migration :  $-\frac{\partial}{\partial x_3} (c w)$
- horizontal diffusion :  $\nabla_h \cdot (\tilde{\kappa} \nabla_h c)$
- vertical diffusion :  $\frac{\partial}{\partial x_3} (\tilde{\lambda} \frac{\partial c}{\partial x_3})$
- local production or destruction by external sources and sinks :  $Q$

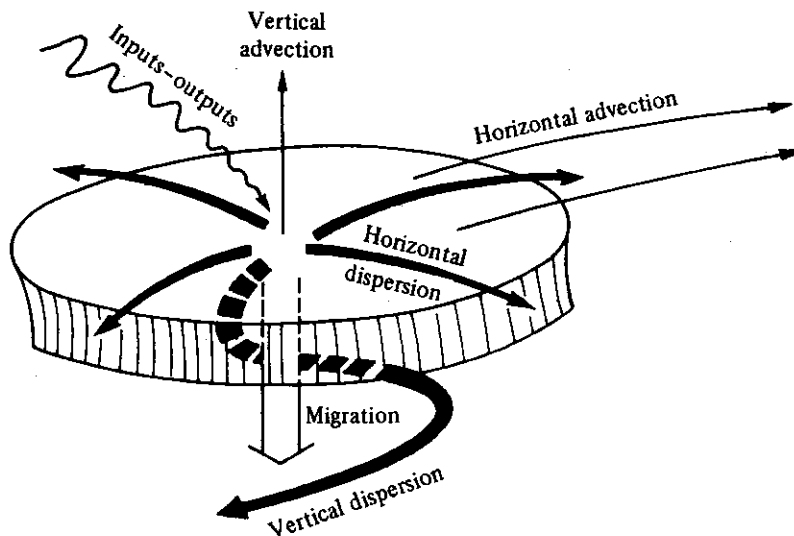


fig. 78.

Schematic diagram of the different effects affecting the evolution of a passive constituent

### 15.- Two-dimensional models of horizontal dispersion.

One of the most important problems of passive dispersion is the diffusion of a contaminant, released at a given point of the marine region and subsequently dispersed by sea motions around the point of release. This problem is associated with the accidental or organized dumping of pollutants, the discharge of sewage and used industrial waters, etc.

In many cases, the diffusion may be considered to be two-dimensional, the contaminant being confined to a thin homogeneous

layer at discharge level and essentially spreading in a horizontal plane. One can then neglect the vertical components of advection, migration and diffusion. If furthermore the horizontal velocity field may be assumed reasonably uniform over the area of dispersion, the horizontal advection reduces to a simple translation.

Thus, if the  $x_1$ -axis is taken in the direction of the translation and if  $u_0$  is the translation velocity, eq. (205) can be written in the simple form:

$$(208) \quad \frac{\partial c}{\partial t} + u_0 \frac{\partial c}{\partial x_1} = Q + \nabla_h \cdot (\tilde{\kappa} \nabla_h c)$$

It is convenient to change to axis moving with the horizontal velocity  $u_0 e_1$ . The new coordinates  $x_1^*, x_2^*$  are given by

$$(209) \quad x_1^* = x_1 - u_0 t$$

$$(210) \quad x_2^* = x_2$$

Hence the time derivative becomes

$$\frac{\partial c}{\partial t} - u_0 \frac{\partial c}{\partial x_1^*}$$

and, substituting in eq. (208), one gets

$$(211) \quad \frac{\partial c}{\partial t} = Q + \nabla_h \cdot (\tilde{\kappa} \nabla_h c)$$

Of particular interest is the case of an instantaneous release at a given time. If the time of release is taken as the initial time, the inputs into the system, from the outside, are zero, except at  $t = 0$ . They thus appear in the initial conditions and, in eq. (211),  $Q = 0$ .

Assuming horizontal isotropy in the axes moving with the center of the patch, in polar coordinates  $(r, \theta)$ , the concentration  $c$  is a function of  $r$  and  $t$  only.

The eddy diffusivity  $\tilde{\kappa}$  is also, in general, a function of  $r$  because it depends on the scale of mixing ( $\ell \sim r$ ). The formulae (200), (201) and (202) are all of the form:

$$(212) \quad \tilde{\kappa} = \mu r^q$$

The particular values

$$(213) \quad \mu = \text{const.}, \quad q = 0$$

correspond to the case of constant diffusivity. In general however,  $\mu$  is a function of time.

The formulae proposed by Ozmidov and Joseph are particular cases of eq. (212) given respectively by

① Ozmidov :

$$(214) \quad \mu = \alpha \epsilon^{1/3}$$

$$(215) \quad q = \frac{4}{3}$$

② Joseph :

$$(216) \quad \mu = P$$

$$(217) \quad q = 1$$

Using eq. (212), eq. (211) reduces to

$$(218) \quad \frac{\partial c}{\partial t} = \frac{1}{r} \frac{\partial}{\partial r} (\mu r^{q+1} \frac{\partial c}{\partial r})$$

The conditions of validity of this equation are obviously related to the three hypotheses made : ① vertical homogeneity in a thin layer where the contaminant is confined, ② horizontal homogeneity over some region embodying the dispersion patch and ③ horizontal isotropy in axes moving with the center of the patch.

Although the first two hypotheses constitute a valuable first approximation to estimate the speed and the extent of the dispersion, a weak vertical or horizontal shear may modify the dispersion pattern in a non-negligible way. This effect will be examined later.

The assumption of horizontal isotropy may not seem very realistic if one examines the shape of the patches observed in dispersion experiments. Indeed, while all solutions of eq. (218) have a radial symmetry, dispersion patches often show irregular elongated shapes which do not seem to be compatible with the assumed symmetry. However the superposition of several patterns of dispersion from many similar experiments, very often produces a much more symmetrical configuration, in good agreement with the predictions of eq. (218).

Eq. (218) must really be regarded as describing a *representative* dispersion process allowing simple estimates of the extent and rapidity of the dispersion.

The solutions of eq. (218) can be used to calculate the effective eddy diffusivity from field observations and experiments with tracers and it is interesting to discuss them briefly here.

In general, solutions of eq. (218) are sought in the form

$$(219) \quad c = \gamma(t) e^{-\tilde{\sigma}(t) r^m}$$

Substitution in eq. (218) gives

$$(220) \quad \frac{d\gamma}{dt} - \gamma \frac{d\tilde{\sigma}}{dt} r^m = m^2 \tilde{\sigma}^2 \mu \gamma r^{2m+q-2} - (q+m) \mu \gamma \tilde{\sigma}^m r^{q+m-2}$$

The existence of a similarity solution of the type (219) depends on the possibility of choosing  $m$  in such a way that the same powers of  $r$  appear in the two members. It is readily seen that the only sensible choice is ( $q \neq 2$ ):

$$(221) \quad q + m - 2 = 0$$

$$(222) \quad 2m + q - 2 = m$$

and

$$(223) \quad \frac{dY}{dt} = -2(2-q)\mu Y \tilde{\sigma}$$

$$(224) \quad \frac{d\tilde{\sigma}}{dt} = -(2-q)^2 \mu \tilde{\sigma}^2$$

Solving eq. (224) for  $\tilde{\sigma}$ , substituting in eq. (223) and integrating, one gets

$$(225) \quad \tilde{\sigma}^{-1} = (2-q)^2 \int_0^t \mu dt$$

$$(226) \quad Y = A \tilde{\sigma}^{\frac{2}{2-q}}$$

where  $A$  is a constant of integration.

Hence

$$(227) \quad c = A \tilde{\sigma}^{\frac{2}{2-q}} e^{-\tilde{\sigma} r^{2-q}}$$

When  $t$  tends to zero,  $\tilde{\sigma}$  tends to infinity and  $c$  tends to zero everywhere except at  $r = 0$ . The similarity solution (227) is thus the appropriate solution for the problem of an instantaneous point release at  $r = 0$ ,  $t = 0$ .

If  $C$  is the total amount released per unit depth — one remembers here that the contaminant is actually uniformly distributed over a thin layer — the constant of integration  $A$  can be determined in terms of  $C$  either by imposing the initial condition or by expressing the conservation of mass:

$$(228) \quad \int_0^{2\pi} d\theta \int_0^\infty cr dr = 2\pi \int_0^\infty cr dr = C$$

Using eq. (227), the left-hand side of eq. (228) can be written

$$(229) \quad 2\pi A \int_0^\infty \tilde{\sigma}^{\frac{2}{2-q}} e^{-\tilde{\sigma} r^{2-q}} r dr = \frac{2\pi A}{2-q} \int_0^\infty e^{-\xi} \xi^{\frac{2}{2-q}-1} d\xi$$

$$= \frac{2\pi A}{2-q} \Gamma\left(\frac{2}{2-q}\right)$$

where  $\Gamma$  is the gamma function.

Hence

$$(230) \quad A = \frac{(2 - q)C}{2\pi \Gamma(\frac{2}{2 - q})}$$

and

$$(231) \quad c = \frac{(2 - q)C}{2\pi \Gamma(\frac{2}{2 - q})} \tilde{\sigma}^{\frac{2}{2 - q}} e^{-\tilde{\sigma} r^{2 - q}}$$

Special forms of eq. (231) have been used by several authors assuming constant  $\mu$  [in eq. (225)] and  $q$  either 0, 1 or  $4/3$ . With these assumptions  $\tilde{\sigma}$  is proportional to  $t^{-1}$  and the following simple formulae are obtained:

①  $\mu = \text{const.}$  ,  $q = 0$  ; constant eddy diffusivity :

$$(232) \quad c = \frac{C}{4\pi\mu t} e^{-\frac{r^2}{4\mu t}}$$

②  $\mu = \text{const.}$  ,  $q = 1$  ; Joseph's formula for the eddy diffusivity :

$$(233) \quad c = \frac{C}{2\pi\mu^2 t^2} e^{-\frac{r}{\mu t}}$$

③  $\mu = \text{const.}$  ,  $q = \frac{4}{3}$  ; Ozmidov's formula for the eddy diffusivity :

$$(234) \quad c = \frac{C}{6\pi t^3} \left(\frac{9}{4\mu}\right)^3 e^{-\frac{9r^{2/3}}{4\mu t}}$$

Eq. (231) shows that the concentration at the center of the patch ( $r = 0$ ) is given by

$$(235) \quad c_0 = \frac{(2 - q)C}{2\pi \Gamma(\frac{2}{2 - q})} \tilde{\sigma}^{\frac{2}{2 - q}}$$

Hence, combining eqs. (231) and (235) and setting

$$(236) \quad \eta = \ln \ln \frac{c_0}{c}$$

$$(237) \quad \xi = \ln \frac{r}{r_1}$$

$$(238) \quad \varphi(t, q) = \ln (\tilde{\sigma} r_1^{2 - q}) = \ln \frac{r_1^{2 - q}}{(2 - q)^2 \int_0^t \alpha dt}$$

where  $r_1$  is a reference value of  $r$  introduced to make the variables non-dimensional, e.g. the smallest  $r$  where concentrations are measured, one obtains

$$(239) \quad \eta = (2 - q)\xi + \phi$$

This formulation is extremely convenient to interpret the observations. Indeed  $\eta$  can easily be calculated as a function of  $\xi$  from the survey of the patch of contaminant at any given time. If the solution (239) is correct, all points must lie on a straight line. The slope of the line determines  $q$ . Figs. 79, 80 and 81 show the diagrams of  $\eta$  plotted from observations of diffusion experiments in the North Sea. The value of  $q$  seems to be intermediate between 0 (constant diffusivity) and 1 (Joseph's law), close to 1 during the early stage of the dispersion and approaching zero as the dispersion progresses.

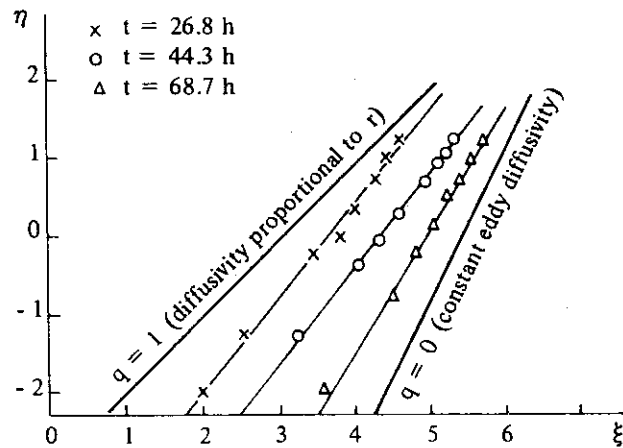


fig. 79.

Diagram of  $\eta$  versus  $\xi$  from observations during a diffusion experiment in the North Sea. (After Joseph et al., 1964.)  $r_1 = 10$  m.

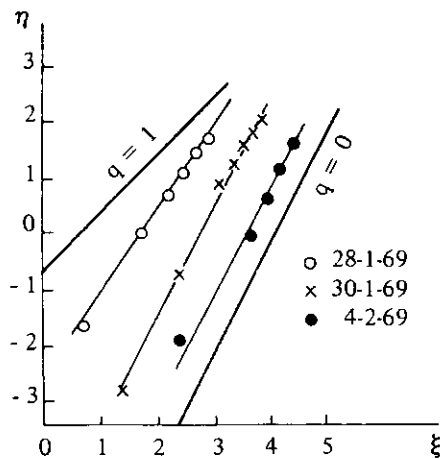


fig. 80.

Diagram of  $\eta$  versus  $\xi$  from observations during a diffusion experiment in the Southern Bight of the North Sea. (After Talbot, 1970.)  $r_1 = 100$  m.



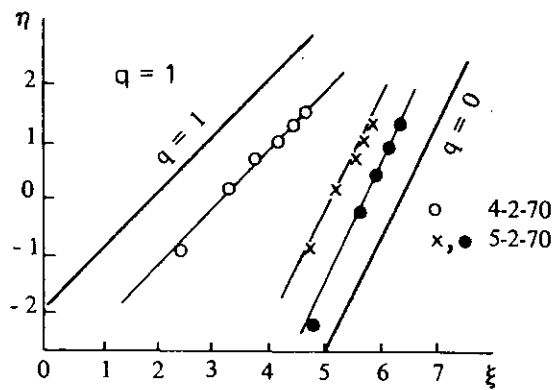


fig. 81.

Diagram of  $\eta$  versus  $\xi$  from observations during a diffusion experiment in the North Sea off the Yorkshire coast. (After Talbot, 1970.)  $r_1 = 10$  m.

The two-dimensional isotropic solution (227) is based on the assumptions of horizontal homogeneity over some region embodying the patch and vertical homogeneity over a thin layer where the contaminant is confined. In that case, the advection velocity is uniform and in axes moving with that velocity, the diffusion may be assumed isotropic.

The effect of weak lateral and vertical shears has been examined by Carter and Okubo (1965). They consider the mixing from an instantaneous source in an unbounded sea. They take constant but different eddy diffusivities in the directions of the three axes and, allowing for weak lateral and vertical inhomogeneities, they assume a horizontal velocity in the  $x_1$ -direction which varies slowly with  $x_2$  and  $x_3$  and may thus be approximated by the first two terms of its Taylor expansion near the origin. They write :

$$(240) \quad u_1 = u(t) + \xi_2 x_2 + \xi_3 x_3 \quad ; \quad u_2 = u_3 = 0$$

and

$$(241) \quad \frac{\partial c}{\partial t} + (u + \xi_2 x_2 + \xi_3 x_3) \frac{\partial c}{\partial x_1} = \kappa_1 \frac{\partial^2 c}{\partial x_1^2} + \kappa_2 \frac{\partial^2 c}{\partial x_2^2} + \kappa_3 \frac{\partial^2 c}{\partial x_3^2}$$

The solution, for an instantaneous point source at  $x_1 = x_2 = x_3 = 0$ , is found to be

$$c = \frac{B}{8\pi^{3/2} (\kappa_1 \kappa_2 \kappa_3)^{1/2} t^{3/2} (1 + \xi^2 t^2)^{1/2}} \times \exp - \left\{ \frac{[x_1 - \int_0^t u dt - \frac{1}{2}(\xi_2 x_2 + \xi_3 x_3)t]^2}{4\kappa_1 t(1 + \xi^2 t^2)} + \frac{x_2^2}{4\kappa_2 t} + \frac{x_3^2}{4\kappa_3 t} \right\}$$

where  $B$  is the total amount released and where  $\xi$  is a kind of weighted average of the shear given by

$$(243) \quad \xi^2 = \frac{1}{12} \left( \xi_2^2 \frac{\kappa_2}{\kappa_1} + \xi_3^2 \frac{\kappa_3}{\kappa_1} \right)$$

$\xi^{-1}$  can be interpreted as the time at which the velocity shears begin to affect the mixing significantly.

The mean characteristics of the dispersion predicted by eq. (242) are the following :

- ① The surfaces of equal concentration are ellipsoids. The principal axes of the ellipsoids are all in the same direction at any time but their orientation varies with time in the coordinate axes.
- ② The maximum concentration decreases as  $t^{-3/2}$  during the initial period  $t \ll \xi^{-1}$  and as  $t^{-5/2}$  for  $t \gg \xi^{-1}$  when the shear dominates.
- ③ In the period of shear diffusion  $t \gg \xi^{-1}$ , the patch is greatly elongated in the  $x_1$ -direction.

Fig. 82 shows the variation with time of the maximum concentration measured by Carter and Okubo (1965) during dye-release experiments in the Cape Kennedy area.

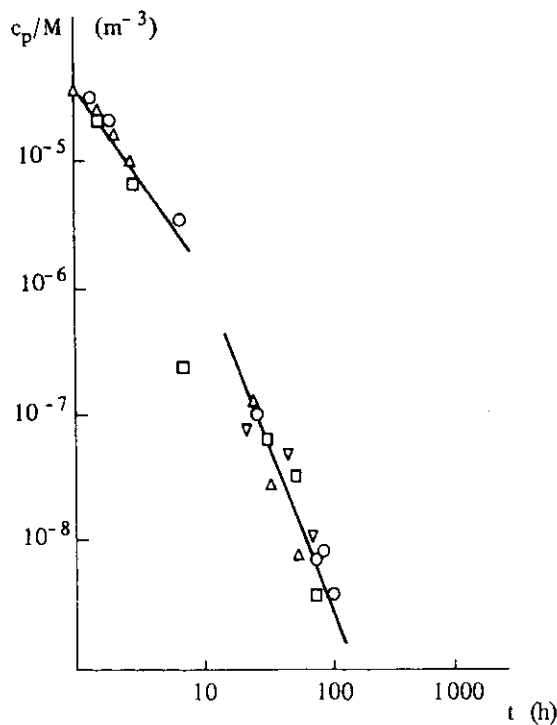


fig. 82.

Variation of peak concentration  $c_p/M$  with time for instantaneous dye-release experiments in the sea off Cape Kennedy. (After Carter and Okubo, 1965.)

The data distinctly reveals two stages of decay : an initial stage negligibly affected by the inhomogeneity, and a final stage dominated by the velocity shear. The corresponding laws of decay are in good agreement with the predictions of the model.

The solutions (231) and (242) correspond to the very specific situation of an instantaneous point release in a simple current field. Other equally important cases are, for instance, the diffusion from a continuous source, the steady (long-time average) dispersion by residual currents, the distribution of contaminants in stratified waters, etc. Idealized models of such situations and some exact solutions can be found in Crank (1956), Okubo (1971a) and Bowden (1972).

Although analytical solutions have proved extremely useful to interpret the observations or to obtain valuable indications to predict the general features of the diffusion of contaminants, one must realize that they are limited to simple idealized situations where one can ascribe simple forms to the advection velocity and to the diffusion coefficients.

More detailed descriptions and refined predictions require however the solution of eq. (206) taking into account the actual (observed or computed) current pattern and, in most cases, this can only be done numerically.

#### 16. - Depth-integrated models of horizontal dispersion.

When the contaminant is confined to a thin homogeneous layer at discharge level and essentially spreads in a horizontal plane, the dispersion process is described by the two-dimensional equation (208). This type of situation may be expected in strongly stratified waters where the vertical eddy diffusivity  $\lambda$  is small.

In shallow continental seas with strong tidal or wind-induced currents, intense mixing is produced by three-dimensional micro-scale turbulence and the kind of two-dimensional vertically confined dispersion described above is ephemeral; vertical turbulent diffusion acting to distribute rapidly the contaminant over the whole water column.

Vertical gradients of concentrations may exist in localized areas where vertical mixing is partly (and temporarily) inhibited by stratification or during short periods of time - a few hours following an off-shore dumping, for instance - before vertical mixing is completed. However such cases are very limited in space and time and, in most problems, it is sufficient to study, in a first approach, the horizontal distribution of depth-averaged concentrations (Nihoul et al., 1980; Warluzel and Benque, 1980).

Let, as in eq. (39),

$$(244) \quad \bar{c} = H^{-1} \int_{-h}^{\xi} c \, dx_3$$

$$(245) \quad \hat{c} = c - \bar{c}$$

Integrating eq. (205) over depth and using eq. (28), one finds

$$(246) \quad \frac{\partial \bar{c}}{\partial t} + \bar{u} \cdot \nabla_h \bar{c} = \Lambda + \Sigma + T$$

where  $\Lambda$  and  $\Sigma$  are defined by eqs. (40) and (41) and where

$$(247) \quad T = H^{-1} \int_{-h}^{\xi} [\nabla_h \cdot (\tilde{\kappa} \nabla_h c)] dx_3$$

Eq. (246) reduces to eq. (39) if the pseudo-turbulent diffusion is neglected with respect to the shear effect.

One emphasizes that the non-linear terms give two contributions, the first of which is the product of the means while the second,  $\Sigma$ , is related to the mean product of the deviations. One can see that  $\Sigma$  is a result of the vertical shear. It would be zero if the velocity was uniform over the depth. (This, however, cannot be the case because the velocity is maximum at the surface and vanishes at the bottom.) Hence, the name "shear effect".

The shear effect described here, in the context of depth-integrated models, should not be confused with the effect of a *lateral* shear of the advecting velocity on the two-dimensional dispersion of a contaminant confined to a thin layer.

In fact, the appellation "shear effect" is widely used to denote similar but not identical phenomena. In this context, it is meant in the following sense: space-average concentrations (e.g. over the depth or over the cross-section) are governed by equations which are derived from the three-dimensional ones by space integration. In this process, the quadratic convection terms give two contributions, the first of which represents the advection by the mean motion while the second contains the mean product of deviations around the means and contributes to the dispersion.

This effect has been described by several authors in pipes, channels and estuaries where, after integration over the cross-section, the flow - steady or oscillating - is essentially in one direction (Taylor, 1953, 1954; Elder, 1959; Bowden, 1965).

In shallow waters, it is generally sufficient to consider the mean concentrations over the depth but, out at sea, no further averaging is possible and the dispersion mechanism is fundamentally two-dimensional. The models valid for estuarine diffusion have been generalized by Nihoul (1972, 1973b) to account for transient wind-changing currents and rotating tidal currents.

#### *Parameterization of the shear effect.*

Subtracting eq. (246) from eq. (15), one obtains

$$(248) \quad \begin{aligned} \frac{\partial \hat{c}}{\partial t} + \bar{u} \cdot \nabla \hat{c} + \hat{u} \cdot \nabla \hat{c} + v_3 \frac{\partial \hat{c}}{\partial x_3} + \Sigma - \nabla_h \cdot (\tilde{\kappa} \nabla_h c) + T + \hat{u} \cdot \nabla \bar{c} \\ = \frac{\partial}{\partial x_3} \left( \tilde{\lambda} \frac{\partial \hat{c}}{\partial x_3} - w \hat{c} \right) + Q - \Lambda \end{aligned}$$

It is reasonable to assume that the deviation  $\hat{c}$  is much smaller than the mean concentration  $\bar{c}$  while the velocity deviation  $\hat{u}$  can be a substantial fraction of  $\bar{u}$  over a large part of the water column as a result of the velocity profile imposed by the boundary conditions.

It is generally accepted that the vertical advection and the turbulent diffusion residue can be neglected as compared to the horizontal advection. For instance, one estimates (introducing the diffusion velocity  $P$  and, as before, a characteristic length  $\ell$  of horizontal variations) :

$$(249) \quad T - \nabla_h \cdot (\tilde{\kappa} \nabla_h c) \sim 0 \left( \frac{P\hat{c}}{\ell} \right) \ll \hat{u} \cdot \nabla \bar{c} \sim 0 \left( \frac{\bar{u}\bar{c}}{\ell} \right)$$

Under these conditions, all terms in the left-hand side of eq. (248) are small compared to the last one, and one may write :

$$(250) \quad \hat{u} \cdot \nabla \bar{c} \sim \frac{\partial}{\partial x_3} \left( \lambda \frac{\partial \hat{c}}{\partial x_3} - w\hat{c} \right) + Q - \Lambda$$

The physical meaning of this equation is clear; weak vertical inhomogeneities are constantly created by the inhomogeneous convective transfer of the admixture and they adapt to this transfer in the sense that the effects of convection, transverse diffusion and unequal migration are balanced for them.

Eq. (250) can be used to calculate  $\hat{c}$  in terms of the gradient of the mean concentration  $\bar{c}$ . Multiplying the result by  $\hat{u}$  and integrating over depth, one obtains thus an estimate of the shear effect.

In general, one may further neglect the migration term as migration velocities, for instance sedimentation velocities, are often comparable with or smaller than the vertical advection velocity. The sedimentation flux may be quite important compared with the turbulent flux in the bottom boundary layer where the eddy diffusivity becomes small but this is a small region compared to the water depth and it affects very little the shear effect which is obtained after several integrations over the water column.

The last term  $Q - \Lambda$  may presumably also be neglected. Indeed, it is of order  $\Lambda$ . The corresponding contribution to the shear effect, calculated by twice integrating over  $x_3$  multiplying by  $\hat{u}$  and taking the horizontal divergence, will be of the order of  $\Delta H^2 \bar{u} \lambda^{-1} \ell^{-1}$ .

In shallow continental seas, one has (e.g. Bowden, 1965; Nihoul, 1975a)  $\lambda \sim 0(\bar{u}H)$ . Thus the contribution of the term  $Q - \Lambda$  in eq. (250) to the shear effect  $\Sigma$  in eq. (246) will be of the order of  $\Delta H \ell^{-1} \ll \Lambda$  since  $H \ll \ell$ . Hence this contribution may be neglected as compared to the term  $\Lambda$  which is already present in the right-hand side of eq. (246).

In these conditions, eq. (250) reduces to

$$(251) \quad \hat{u} \cdot \nabla \bar{c} = \frac{\partial}{\partial x_3} \left( \tilde{\lambda} \frac{\partial \hat{c}}{\partial x_3} \right)$$

In the following, one shall admit for simplicity that eq. (251) is applicable. Furthermore, restricting attention to neutrally buoyant ( $w = 0$ ) or sedimenting ( $w < 0$ ) constituents, one shall assume that the flux at the free surface is zero\*.

In that case, integrating eq. (251), one obtains :

$$(252) \quad H \hat{r} \cdot \nabla \bar{c} = \tilde{\lambda} \frac{\partial \bar{c}}{\partial x_3}$$

where

$$(253) \quad \hat{r} = H^{-1} \int_{\zeta}^{x_3} \hat{u} \, dx_3$$

Integrating by parts and taking into account that  $\hat{r} = 0$  at  $x_3 = \zeta$  and  $x_3 = -h$ , one gets

$$(254) \quad \Sigma = H^{-1} \nabla \cdot (H \mathbf{R} \cdot \nabla \bar{c})$$

where  $\mathbf{R}$  is the shear effect diffusivity tensor, i.e.:

$$(255) \quad \mathbf{R} = H \int_{-h}^{\zeta} \frac{\hat{r} \hat{r}}{\tilde{\lambda}} \, dx_3$$

To determine  $\mathbf{R}$ , one must know the turbulent eddy diffusivity  $\tilde{\lambda}$  and the function  $\hat{r}$ , i.e. the velocity deviation  $\hat{u}$ .

In a well-mixed shallow sea, where the Richardson number is very small and the turbulence fully developed, it is reasonable to take (e.g. Nihoul, 1975a) :

$$(256) \quad \tilde{\lambda} \sim \tilde{v}$$

Eqs. (80) and (117) can be written

$$(257) \quad \tilde{\lambda} = H^2 \sigma(t, x_1, x_2) \lambda(\xi)$$

$$(258) \quad \hat{u} = v_s [s(\xi) - \bar{s}] + v_b [b(\xi) - \bar{b}] - \left( \frac{s_1}{\alpha_1 \sigma} \dot{v}_s + \frac{b_1}{\alpha_1 \sigma} \dot{v}_b \right) f_1(\xi)$$

where  $s(\xi)$  and  $b(\xi)$  are given by eqs. (94) and (95) and where

$$(259) \quad v_s = \frac{\tau_s}{\sigma H} \quad ; \quad v_b = \frac{\tau_b}{\sigma H}$$

$\bar{s}$  and  $\bar{b}$  are the depth-averages of  $s$  and  $b$ ,

$$(261) \quad s_1 = \int_0^1 s f_1 \, d\xi \quad , \quad b_1 = \int_0^1 b f_1 \, d\xi$$

\* The case  $w > 0$  can be treated in the same way with only trivial modifications of the algebra.

$\alpha_1$  and  $f_1$  are respectively the first eigenvalue and the first eigenfunction of the problem (103) and (104). A dot denotes a total derivation with respect to time.

**Application to the North Sea.**

Combining eqs. (119), (120), (121) and (253), one gets

$$(263) \quad \hat{r} = v_s S(\eta) + v_b B(\eta) + \frac{\dot{v}_s + 2 \dot{v}_b}{\sigma} F(\eta)$$

with

$$(264) \quad S(\eta) = 4 \ln 2(\eta - 1) + 2(2 - \eta) \ln (2 - \eta)$$

$$(265) \quad B(\eta) = -2 \ln 2(\eta - 1) + \eta \ln \eta - (2 - \eta) \ln (2 - \eta)$$

$$(266) \quad F(\eta) = \frac{5}{36} (\eta^3 - 3 \eta^2 + 2 \eta)$$

The shear effect diffusivity tensor can then be written

$$(267) \quad \begin{aligned} \mathbf{R} &= \int_{\xi_0}^1 \frac{\hat{r} \hat{r}}{\sigma \lambda} d\xi \\ &= \frac{Y_{ss}}{\sigma} v_s v_s + \frac{Y_{sb}}{\sigma} (v_s v_b + v_b v_s) + \frac{Y_{bb}}{\sigma} v_b v_b \\ &\quad + \frac{Y_{sf}}{\sigma^2} (v_s \dot{v}_s + 2 v_s \dot{v}_b + \dot{v}_s v_s + 2 \dot{v}_b v_s) \\ &\quad + \frac{Y_{bf}}{\sigma^2} (v_b \dot{v}_s + 2 v_b \dot{v}_b + \dot{v}_s v_b + 2 \dot{v}_b v_b) \\ &\quad + \frac{Y_{ff}}{\sigma^2} (\dot{v}_s + 2 \dot{v}_b) (\dot{v}_s + 2 \dot{v}_b) \end{aligned}$$

with

$$Y_{ss} = \int_{\xi_0}^1 \frac{S^2}{\lambda} d\xi \sim 0.048$$

$$Y_{sb} = \int_{\xi_0}^1 \frac{SB}{\lambda} d\xi \sim 0.090$$

$$Y_{bb} = \int_{\xi_0}^1 \frac{B^2}{\lambda} d\xi \sim 0.196$$

$$Y_{sf} = \int_{\xi_0}^1 \frac{SF}{\lambda} d\xi \sim -0.015$$

$$\gamma_{bf} = \int_{\xi_0}^1 \frac{BF}{\lambda} d\xi \sim -0.031$$

$$\gamma_{ff} = \int_{\xi_0}^1 \frac{F^2}{\lambda} d\xi \sim 0.005$$

In shallow seas, the bottom stress  $\tau_b$  maintained by bottom friction of tidal currents, wind induced currents and residual currents is always fairly important. One can estimate that, in general, the characteristic time  $\sigma^{-1}$  is one order of magnitude larger than the characteristic time of variation of  $v_s$  and  $v_b$  (e.g. Nihoul, 1975, 1977b).

The terms of eq. (267) which contain the derivatives  $\dot{v}_s$  and  $\dot{v}_b$  - the coefficients of which are already smaller than the others - may then be neglected.

The shear effect diffusivity tensor reduces then to

$$(268) \quad \mathbf{R} = \frac{H}{\|\mathbf{v}_b\|} [\beta_1 \mathbf{v}_b \mathbf{v}_b + \beta_2 (\mathbf{v}_s \mathbf{v}_b + \mathbf{v}_b \mathbf{v}_s) + \beta_3 \mathbf{v}_s \mathbf{v}_s]$$

with

$$\beta_1 \sim 1.2 \quad ; \quad \beta_2 \sim 0.6 \quad ; \quad \beta_3 \sim 0.3$$

In weak wind conditions ( $v_b \leq 10^{-2} \bar{u}$ ), the first term in the bracket is largely dominant. Similarly, the bottom stress reduces to the simple form (Nihoul, 1977) :

$$(269) \quad \tau_b = \frac{k^2}{b^2} \|\bar{\mathbf{u}}\| \bar{\mathbf{u}}$$

where  $k$  is the Von Karman constant.

One can then write, with a good approximation,

$$(270) \quad \mathbf{R} = \alpha \frac{H}{\bar{u}} \bar{\mathbf{u}} \bar{\mathbf{u}}$$

$$(271) \quad \Sigma = H^{-1} \nabla \cdot \left[ \alpha \frac{H^2}{\bar{u}} \bar{\mathbf{u}} (\bar{\mathbf{u}} \cdot \nabla \bar{C}) \right]$$

with

$$(272) \quad \alpha \sim 0.14$$

From eqs. (270) and (271), one can see that the shear effect produces a diffusion in the direction of the instantaneous velocity with an apparent diffusivity of the order of  $\alpha \bar{u} H$ . In regions of strong tidal currents, the eddy diffusivity  $\tilde{\kappa}$  can be two orders of magnitude smaller than  $\alpha \bar{u} H$ . After one or two tidal periods, there results an enhanced dispersion in the direction of the maximum tidal velocity. Rapid variations of depth and strong winds can of course modify the situation but the tendency



remains and the patches of pollutants have very often an elongated shape with a maximum dispersion roughly in the direction of the maximum current (fig. 83).

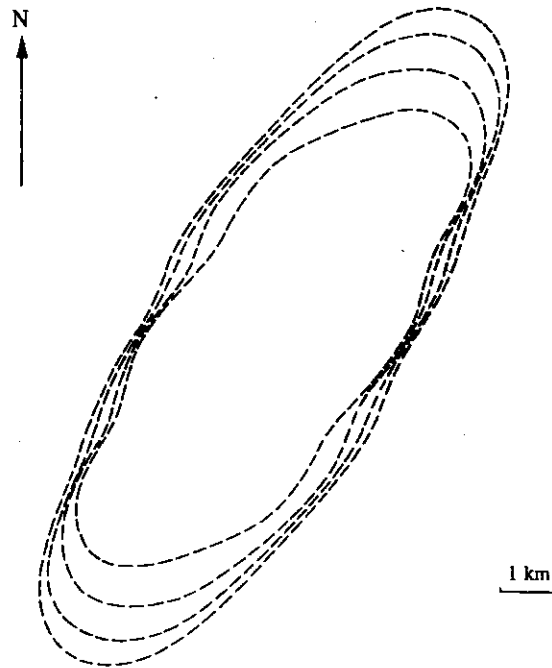


fig. 83.

Simulation of a dye-release experiment in the North Sea (after Adam and Runfola, 1972). Position: 51° 20' N 1° 34' E. Curves: 1/50 of initial concentration 48 h, 72 h, 96 h, 108 h after release.

In weak wind conditions, however, one may question the validity of eq. (257). If the wind is too weak to maintain turbulence in the sub-surface layer, one may expect, in some cases, a turbulent diffusivity which, instead of growing continuously from the bottom to the surface, passes through a maximum at some intermediate depth to decrease afterwards to a smaller surface value. This type of behaviour is described by the family of curves

$$(273) \quad \lambda = \xi(1 - \delta\xi)$$

Eq. (257) corresponds to the case  $\delta = 0.5$ . Values of  $\delta$  from 0.5 to 1 correspond to lower intensity turbulence in the surface layer and the limiting value  $\delta = 1$  would correspond to the case of an ice cover and the existence, below the surface, of a logarithmic boundary layer analogous to the bottom boundary layer.

In the North Sea, it is reasonable to assume that  $\delta$  does not differ significantly from 0.5 and, in any case, never reaches extreme values close to 1. Nevertheless, to estimate the

maximum error one can make on  $\alpha$ , it is interesting to compute the coefficients  $\beta_1$ ,  $\beta_2$  and  $\beta_3$  for some very different values of  $\delta$ . One finds

$\delta$	0.5	0.7	0.9
$\beta_1$	1.2	1.5	2
$\beta_2$	0.6	0.8	1.3
$\beta_3$	0.3	0.5	1
$\alpha$	0.14	0.17	0.23

The increase of the coefficients  $\beta_1$ ,  $\beta_2$ ,  $\beta_3$  and  $\alpha$  with  $\delta$  is obviously associated with more important variations of  $u$  over depth, i.e. with larger values of  $\hat{u}$ .

One should note also that the existence of a vertical stratification even a weak one, reduces the turbulent diffusivity

$$(\tilde{\lambda} = \tilde{\lambda}_0 \phi \quad \text{with} \quad \phi < 1)$$

and contributes similarly to increase the value of  $\alpha$  (e.g. Bowden, 1965).

In the Southern Bight of the North Sea, eventual modifications of the magnitude ( $\phi < 1$ ) or of the form ( $\delta > 0.5$ ) of the turbulent diffusivity are not likely to be very important and eq. (270) can presumably be used with  $\alpha = 0.14$  or some slightly higher value obtained by calibration of the model with the observations.

#### *Vertical concentration profile.*

When  $\bar{c}$  has been calculated, it is possible to compute the deviation  $\hat{c}$  by eq. (251). Changing variable to  $\xi$ , one gets

$$(274) \quad \frac{\partial \hat{c}}{\partial \xi} = \frac{\hat{r}}{\lambda} \cdot \frac{\nabla \bar{c}}{\sigma}$$

with

$$(275) \quad \int_0^1 \hat{c} \, d\xi = 0$$

Restricting attention to the dominant terms, one finds

$$(276) \quad \hat{c}(\xi) = [H(\xi) v_s + G(\xi) v_b] \cdot \frac{\nabla \bar{c}}{\sigma}$$

where

$$(277) \quad H(\xi) = 4[P(\xi) + \ln(2-\xi) \ln \frac{\xi}{4} + \ln 2 (4 \ln 2 - 1 - \ln \xi) - 2]$$

$$(278) \quad G(\xi) = -2 \left[ 2 L_2\left(\frac{1}{2}\right) + \ln \frac{2-\xi}{2} \ln \frac{\xi}{2} + \ln 2 \ln 2 + 2 \right]$$

and

$$(279) \quad P(\xi) = L_2\left(\frac{\xi}{2}\right) + 2 L_2\left(\frac{1}{2}\right) - \bar{L}_2$$

$$(280) \quad L_2(\xi) = \text{Dilo}(1-\xi) = \sum_{\nu=1}^{\infty} (-1)^{\nu} \frac{(\xi-1)^{\nu}}{\nu^2}$$

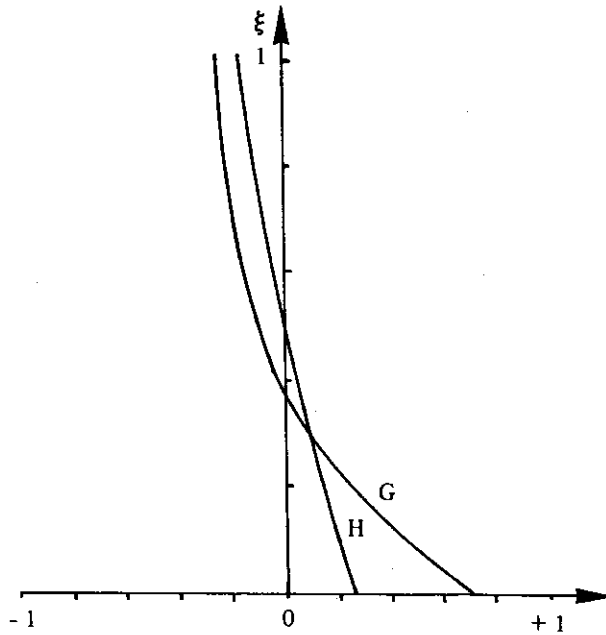


fig. 84.

Fig. 84 shows the functions  $H$  and  $G$ . They are both negative near the surface and positive near the bottom. This is what one should expect from a physical point of view. Higher velocities near the surface carry water masses farther. If this transport is directed towards increasing mean concentrations the corresponding inflow of lower concentration fluid decreases the local concentration below the mean value  $\bar{c}$ . If the transport in the upper layer is directed towards decreasing mean concentrations, the corresponding inflow of high concentration fluid increases the local concentration above the mean value  $\bar{c}$ . The opposite situation occurs near the bottom. This is illustrated in fig. 85 showing the concentration profiles at two points situated downstream and downwind and respectively upstream and upwind on the same isoconcentration curve following a dumping.

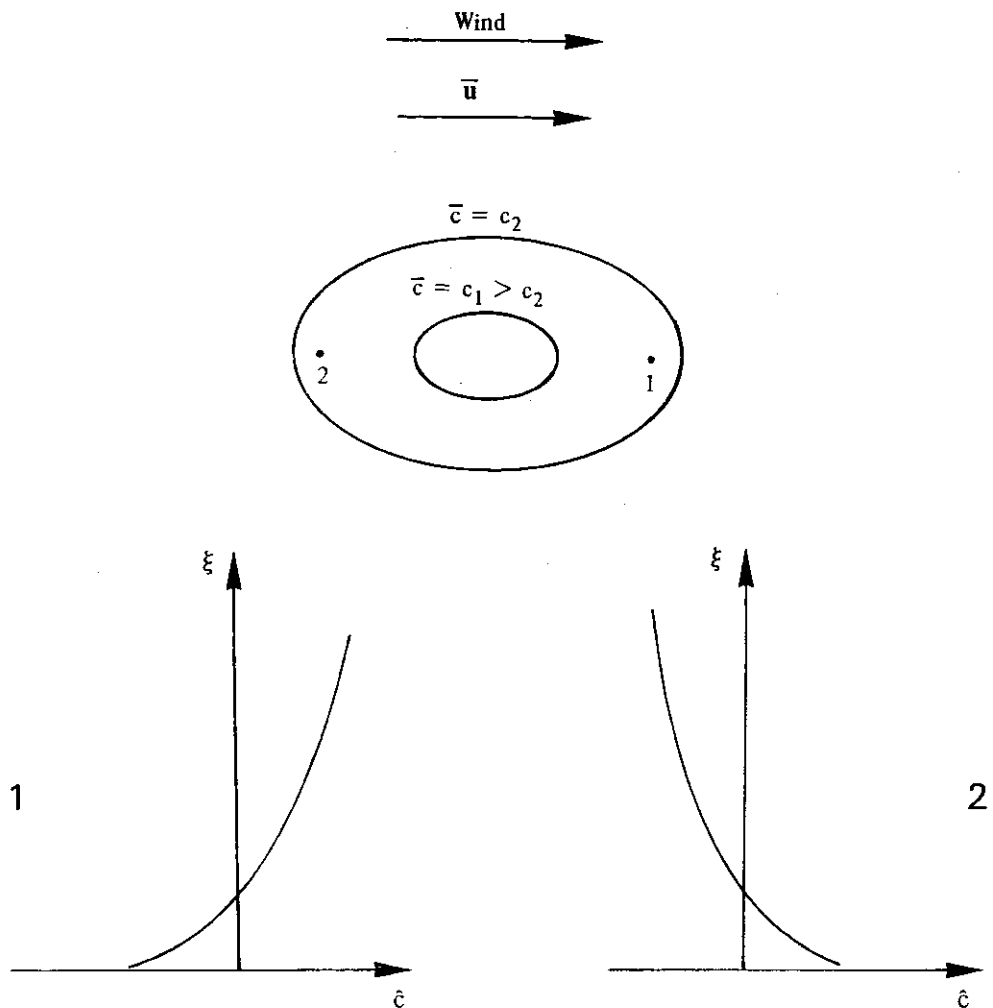


fig. 85.

***Influence of the wind on the shear effect diffusivity tensor.***

The shear effect diffusivity is generally at least one order of magnitude larger than the eddy diffusivity. One can then neglect the last term in the right-hand side of eq. (246) or implicitly include it in  $\Sigma$ .

Locally, one can choose the system of reference in such a way that the shear effect diffusivity tensor is diagonal, i.e.

$$(281) \quad \mathbf{R} = \kappa_1 \mathbf{e}_1 \mathbf{e}_1 + \kappa_2 \mathbf{e}_2 \mathbf{e}_2$$

$$(282) \quad \Sigma = \kappa_1 \frac{\partial^2 \bar{c}}{\partial x_1^2} + \kappa_2 \frac{\partial^2 \bar{c}}{\partial x_2^2} + \text{terms containing derivatives of } \bar{c} \text{ of smaller order}$$

One shall define

$$(283) \quad \kappa_i = \sqrt{\kappa_1 \kappa_2}$$

$\kappa_i$  is the equivalent isotropic diffusion coefficient. It is directly related to the increase in time of the surface of the patch of contaminant (e.g. Nihoul, 1975a).  $\kappa_i$  will be used to evaluate the effect of wind on shear effect diffusion.

The direct effect of wind is represented by the terms containing  $v_s$  in the shear effect diffusivity tensor  $R$ . The relative importance of this effect can be evaluated by the non-dimensional function

$$(284) \quad \tilde{\mu} = \frac{\kappa_i(v_s, v_b) - \kappa_i(0, v_b)}{\kappa_i(v_s, v_b)} \times 100$$

The functions  $\kappa_i$  and  $\tilde{\mu}$  have been computed in the North Sea for four typical situations :

- (i) no wind;
- (ii) mean wind from the west ( $5.5 \text{ m.s}^{-1}$ );
- (iii) strong wind from the south-west ( $15 \text{ m.s}^{-1}$ );
- (iv) strong wind from the north-west ( $15 \text{ m.s}^{-1}$ ).

The results are shown on figs. 86-92.

The wind affects the shear effect diffusivity tensor in two ways. First, the currents are modified and thus  $u$  and  $v_b$  are modified. Secondly, extra terms (proportional to  $v_s$ ) appear in the diffusivity coefficients. These terms represent the direct effect of the wind. One can see on figs. 86-92 that this effect; localized in the northern part of the North Sea, in the case of a weak mean wind, can be quite important everywhere for stronger winds.

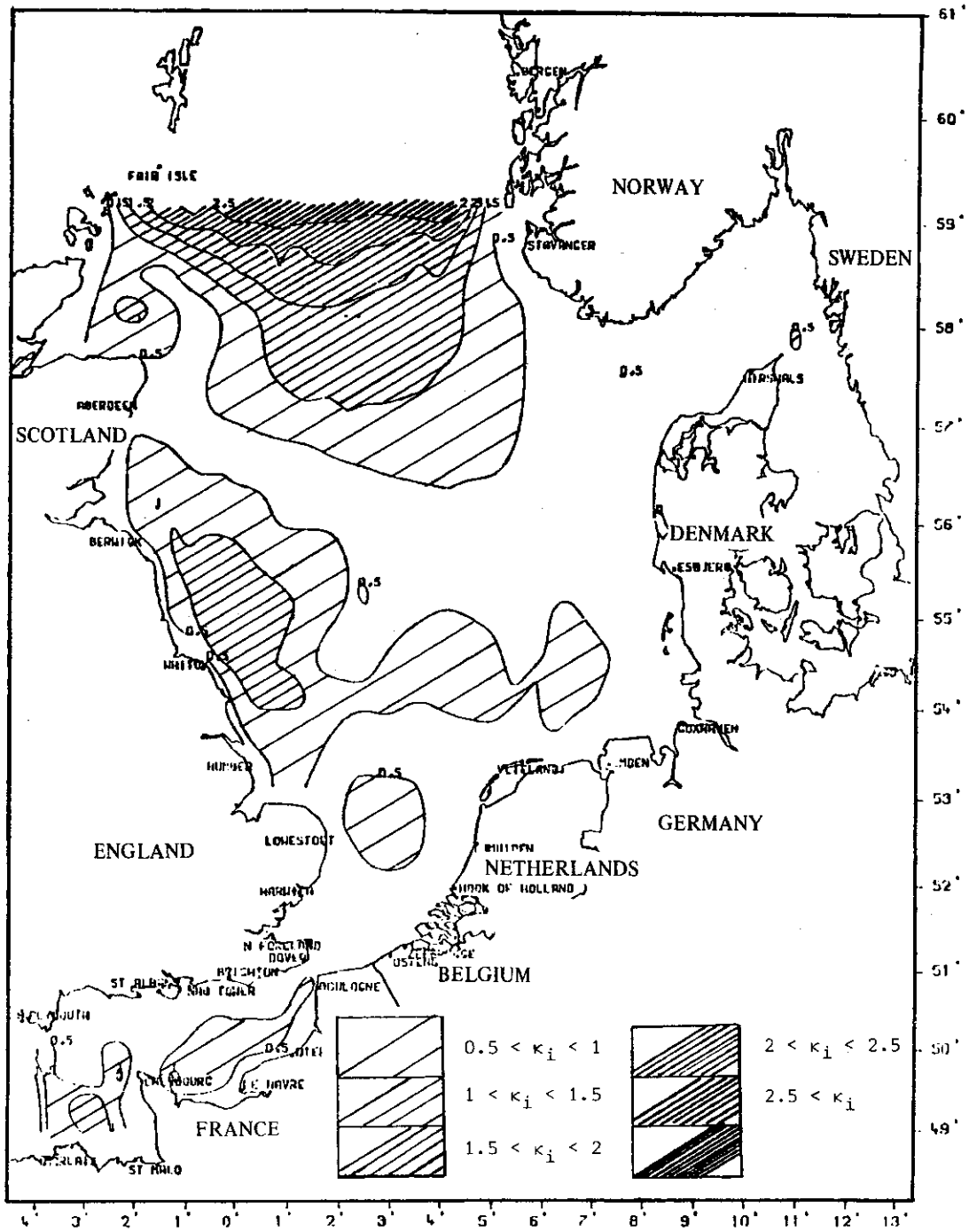


fig. 86.

Shear effect diffusivity in the North Sea. Equivalent isotropic diffusion coefficient  $\kappa_i$  ( $\text{m}^2 \cdot \text{s}^{-1}$ ) in absence of wind.

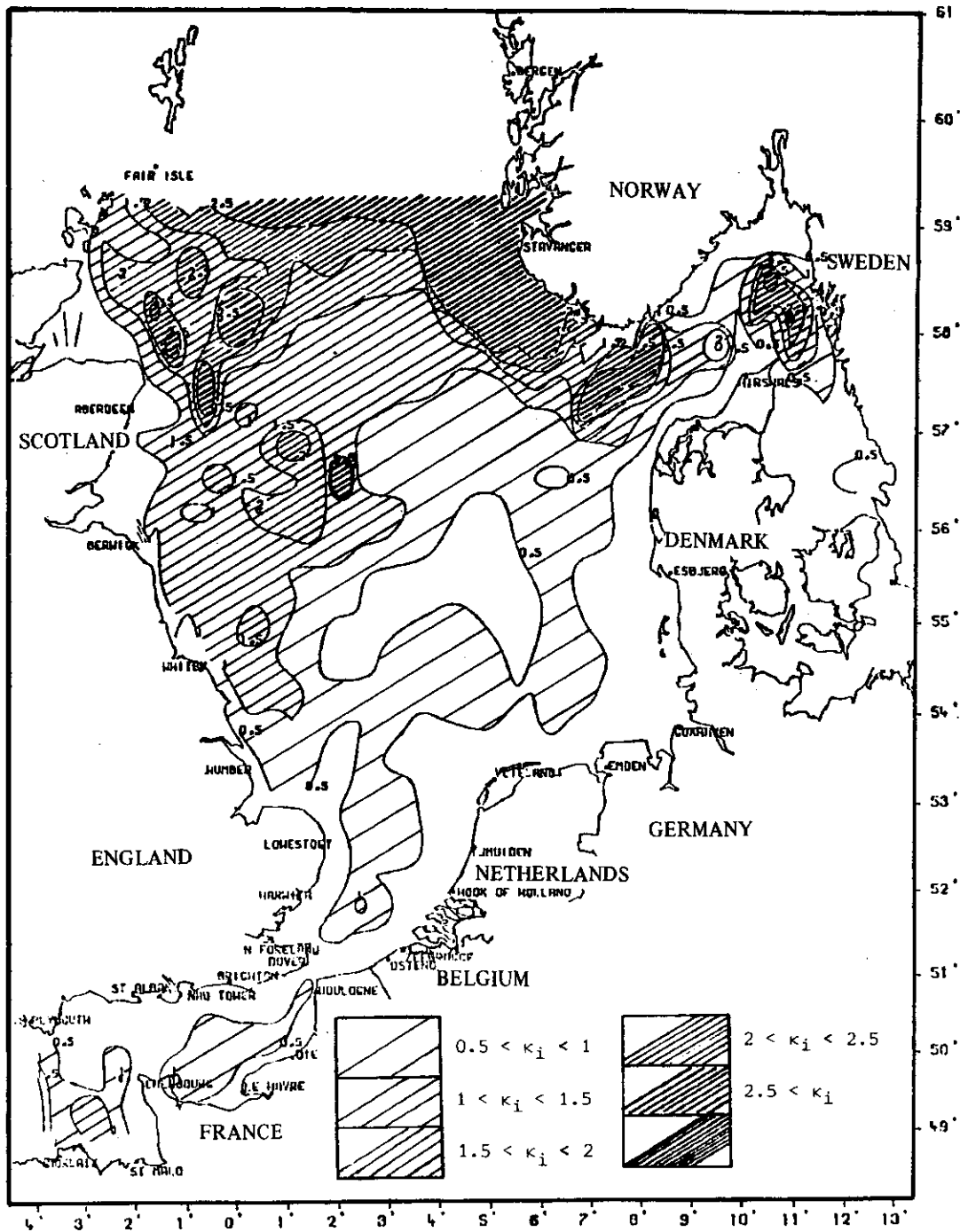


fig. 87.

Shear effect diffusivity in the North Sea. Equivalent isotropic diffusion coefficient  $\kappa_i$  ( $\text{m}^2 \cdot \text{s}^{-1}$ ), mean wind from the west ( $5.5 \text{ m} \cdot \text{s}^{-1}$ ).

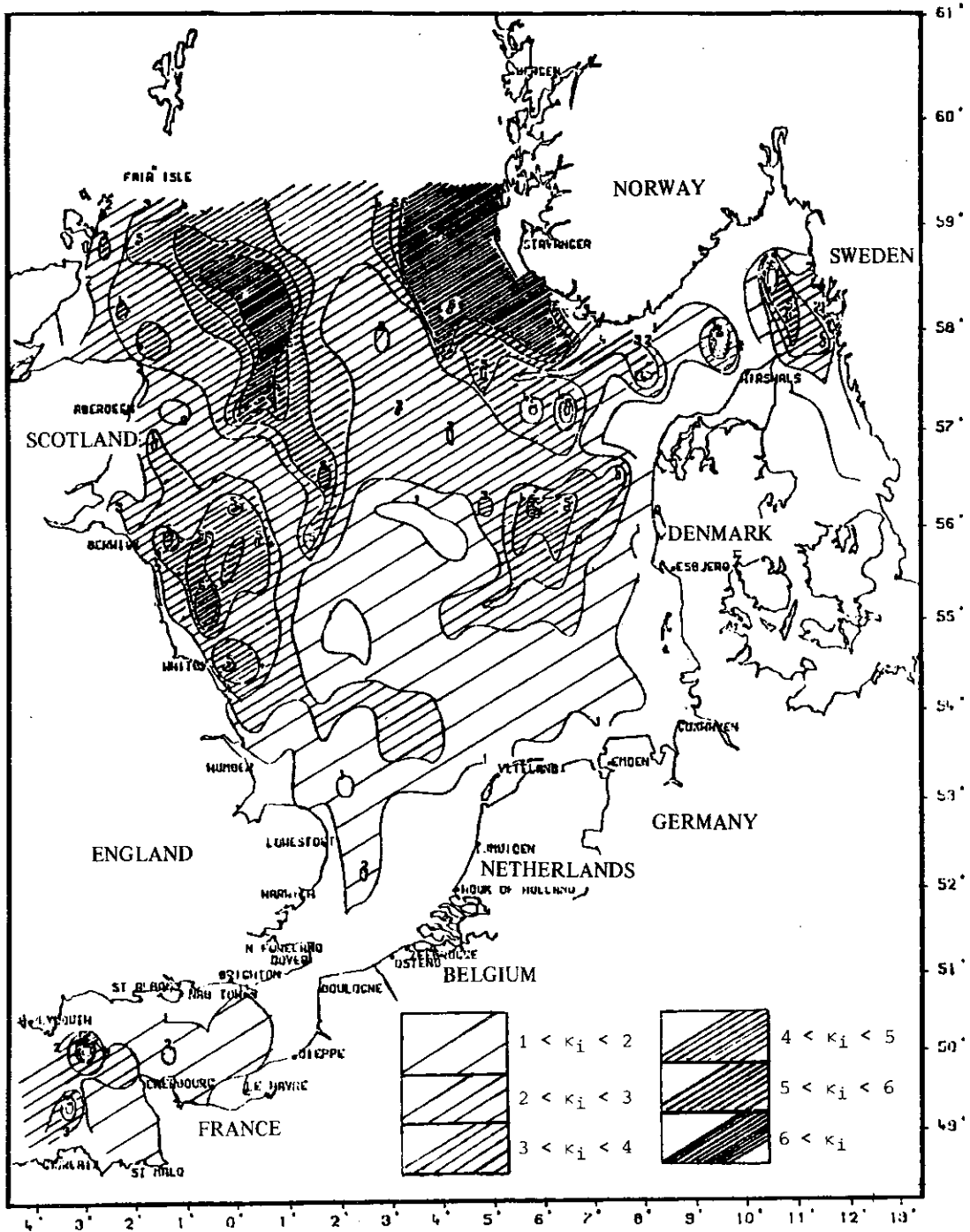


fig. 88.

Shear effect diffusivity in the North Sea. Equivalent isotropic diffusion coefficient  $\kappa_i$  ( $\text{m}^2 \cdot \text{s}^{-1}$ ), strong wind from the south-west (15  $\text{m} \cdot \text{s}^{-1}$ ).



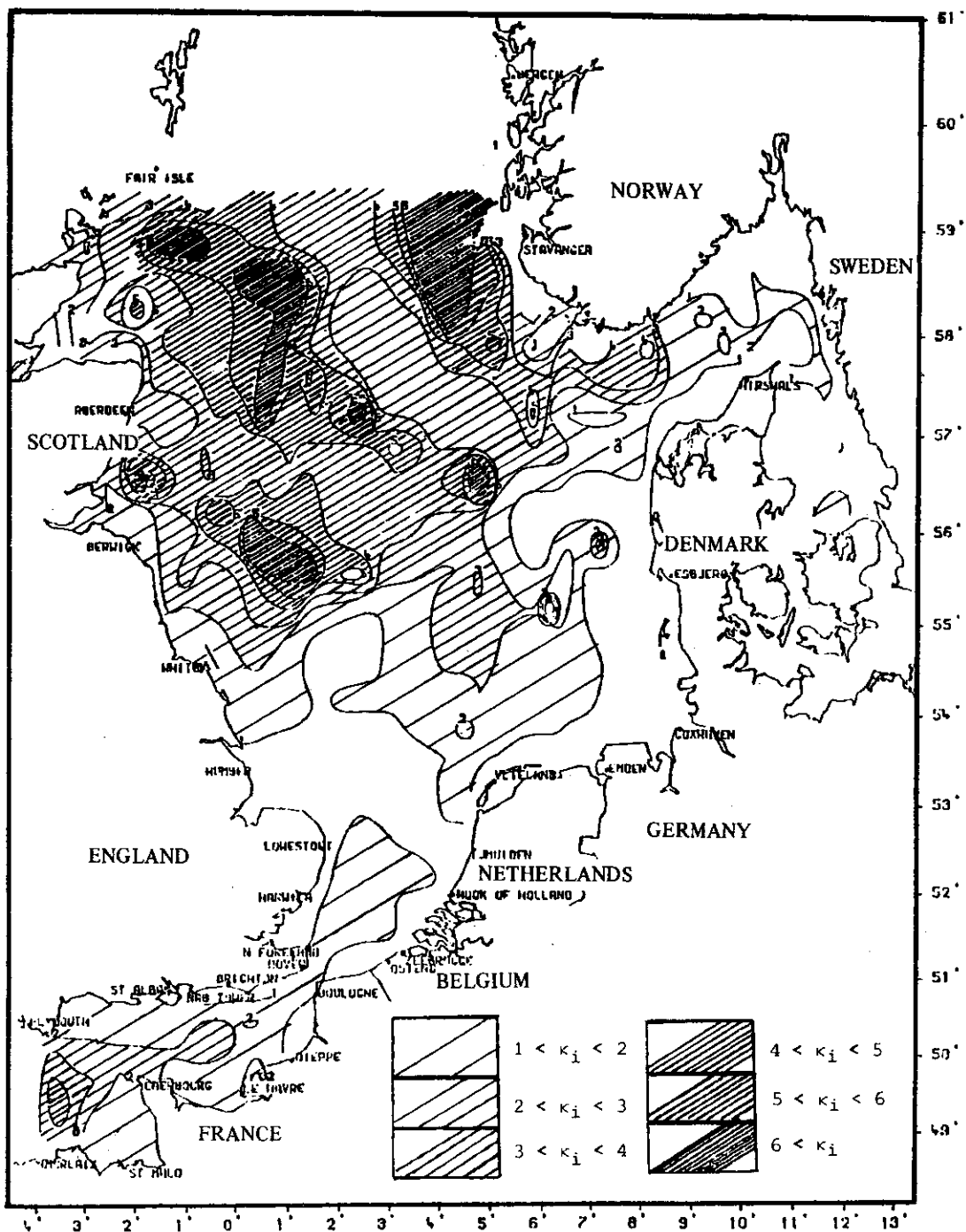


fig. 89.

Shear effect diffusivity in the North Sea. Equivalent isotropic diffusion coefficient  $\kappa_i$  ( $\text{m}^2 \cdot \text{s}^{-1}$ ), strong wind from the north-west ( $15 \text{ m} \cdot \text{s}^{-1}$ ).

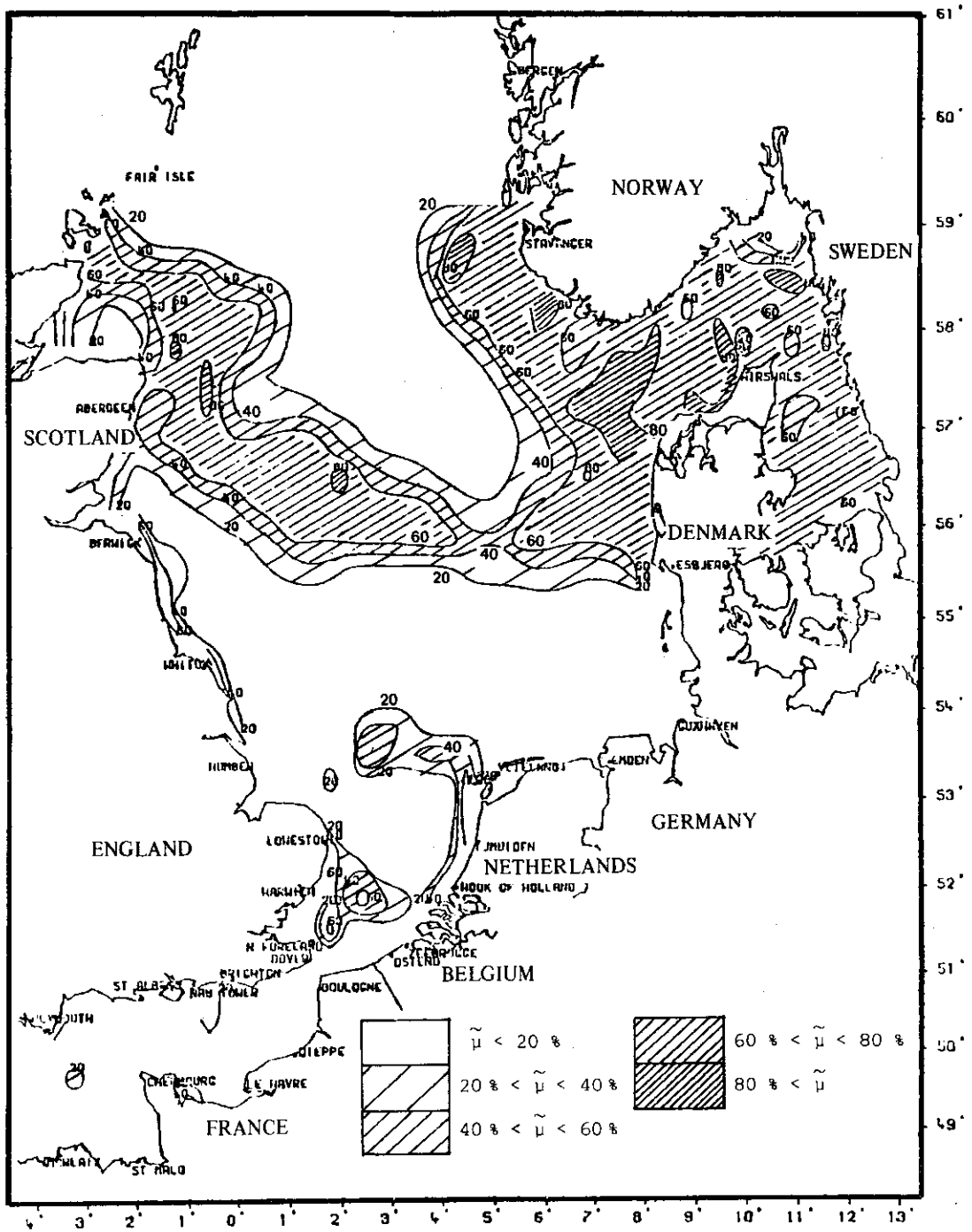


fig. 90.

Effect of wind on shear effect diffusion in the North Sea. Curves of equal values of  $\tilde{\mu}$  (%) for a mean wind from the west ( $5.5 \text{ m.s}^{-1}$ ).

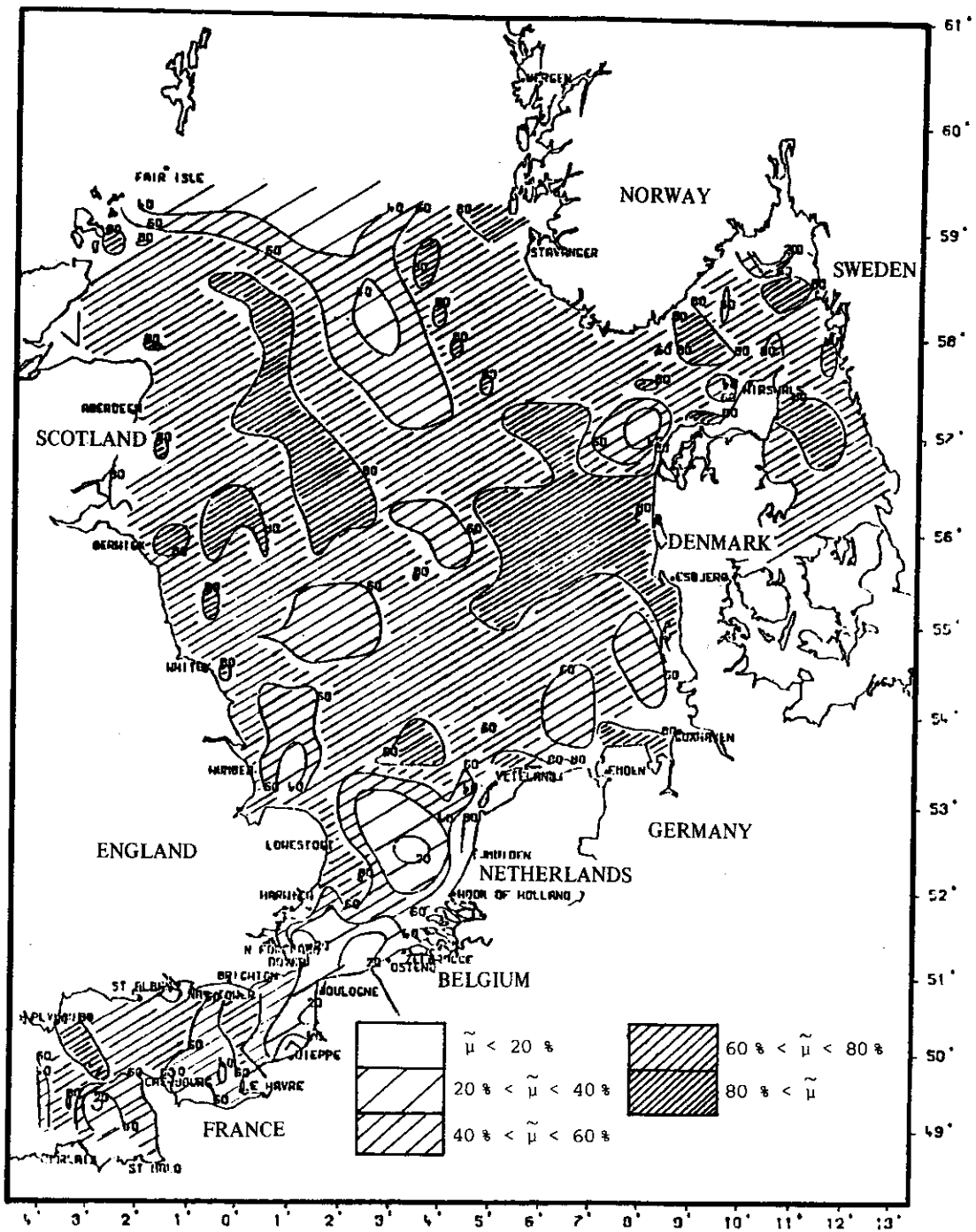


fig. 91.

Effect of wind on shear effect diffusion in the North Sea. Curves of equal values of  $\tilde{\mu}$  (%) for a strong wind from the south-west ( $15 \text{ m.s}^{-1}$ ).

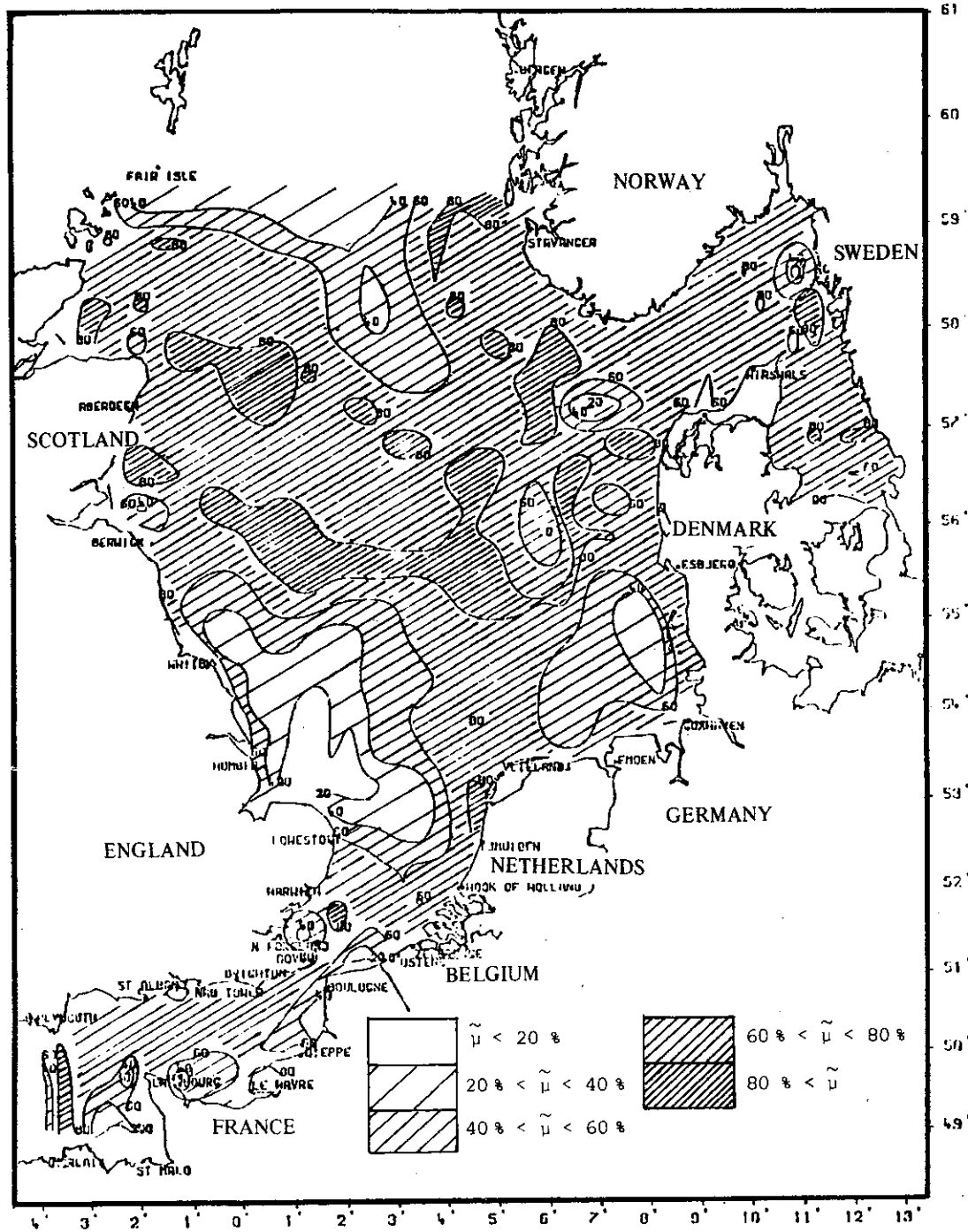


fig. 92.

Effect of wind on shear effect diffusion in the North Sea. Curves of equal values of  $\tilde{\mu}$  (%) for a strong wind from the north-west ( $15 \text{ m}\cdot\text{s}^{-1}$ ).

***A case study : dispersion and sedimentation around a waste disposal point in the Southern Bight of the North Sea.***

Even when wastes are not toxic their disposal into the sea gives rise to considerable pollution problems associated with local increases in turbidity and with the deposit of sediments on the sea bed. Turbidity, which is a function of the concentration of the solid particles in suspension, reduces the depth of penetration of sunlight and hence the chlorophyll synthesis intensity. Sludge deposits on the sea bed are liable to be harmful to benthos colonies and to destroy larvae in shallow, spawning areas.

In shallow seas ( $H$  around 20 m) where tidal currents may be as much as 1 m/s, turbulent mixing in the vertical direction is very pronounced. In the absence of such turbulent mixing, the vertical distribution of suspended matter concentration would be very far from uniform, increasing from almost nothing at the free surface to quite large values near the bottom. The situation is markedly different in the presence of turbulence. There is a thin boundary layer in which the turbulence level is very slight owing to the closeness of the bed and through which settling occurs in quasi-laminar fashion with high concentration gradients. Throughout the entire water layer lying above the boundary layer, mixing is considerable and the concentration almost uniform. With the strongest currents it may occasionally happen that turbulence near the bed is sufficient to modify the boundary layer and to put back into suspension particles of sediment which were about to settle.

One considers here the turbidity and sediment deposits resulting from an initial dumping into a sea where the bed Reynolds stresses, though they may occasionally upset the boundary layer, are nevertheless too weak to cause erosion of the actual sea bed (most of which is made up of sediment of quite different characteristics from those of the waste). A distinction is therefore made between sediment *in suspension* in the turbulent water column on the one hand and the *bed sediment* which accumulates in the boundary layer on the other (and which may later consolidate on the sea bottom). Accordingly, the vertical integration performed in the preceding section proceeds from the free surface to the upper limit of the boundary layer and the sediment "deposited" is defined in such a model as being the total mass of sediment contained in the boundary layer. In this case, the term  $\Lambda$  in eq. (246) reduces to the flux of suspended material at the bottom.

As already noted there exists a quasi-laminar boundary layer on the bottom provided the bed shear stress is not too high. In such cases, the flux of suspended material is equal to the settling flux. However, when the shear stress on the bottom exceeds some critical value, the boundary layer is disturbed and material is put back into suspension by turbulence.

With moderate Reynolds stresses which only exceed the critical boundary-layer stability stress during a small fraction of the tidal cycle and which, moreover, are always less than the value required to erode consolidated sediment on the sea bottom, it may be assumed as a first approximation that the flux  $HA$  is propor-

tional to the difference between the effective stress and the critical stability stress (e.g. Owen and Odd, 1970; Nihoul, 1975a).

The bed stress may be expressed in terms of the velocity at some specified distance from the bottom (e.g. 1m) by introducing a resistance coefficient. If the vertical velocity profile in the waste disposal area is known, the bed stress may be deduced in terms of the mean velocity and a mean critical velocity may be defined corresponding to the critical stress. In such circumstances,  $\Lambda$  may be written as\* (e.g. Nihoul, 1975a):

$$(285) \quad \Lambda = -\frac{w}{H} \bar{c} \left(1 - \frac{\bar{u}^2}{u_c^2}\right)$$

The factor within the brackets constitutes an estimate of the proportion of sediment which is not absorbed by the boundary layer and makes allowance for the fact that instabilities in the boundary layer (the frequency of occurrence of which increases with  $\bar{u}$ ) enable turbulence to put sediment back into suspension – and even when  $\bar{u} > u_c$ , to reverse the process and feed the water column with sediment which has previously settled on the bottom.

If  $C$  is the density of the deposit (i.e. total mass in the boundary layer per unit surface of bed), the following deposit time-variation equation may be associated with eq. (246)

$$(286) \quad \frac{\partial C}{\partial t} = -\Lambda H$$

Wastes are dumped periodically off the Belgian coast in the neighbourhood of position  $51^\circ 30' N$   $3^\circ E$  and such waste disposal operations have been simulated on an *IBM 370-58* computer to investigate the dispersion and deposition phenomena. In the example now to be described, the predominant currents are those of tides. The critical velocity  $u_c$  for bed erosion is estimated to be approximately 0.8 m/s, this value being exceeded during a portion of the tidal cycle. For the waste disposal operation considered, the settling velocity  $w$  is estimated to be approximately  $10^{-3}$  m/s.

Fig. 93 shows how the concentration contours of the suspension and deposited sediment vary with time throughout one tidal period. The dumping point lies at the southern end of the area enclosed by curve 6 in figs 93 (a) and (b).

Fig. 94 shows how the total quantity of material in suspension varies with time expressed as number of tidal cycles. As dumping does not take place instantaneously, the curve starts not at zero time but rather at the end of the dumping.

---

\* In fact, the concentration entering into eq. (285) should be the concentration  $c$  immediately above the boundary layer. However, it was shown that throughout the water column (from the free surface to the boundary layer) the following is true:  $c \sim \bar{c}$  and  $\hat{c} \ll \bar{c}$ .

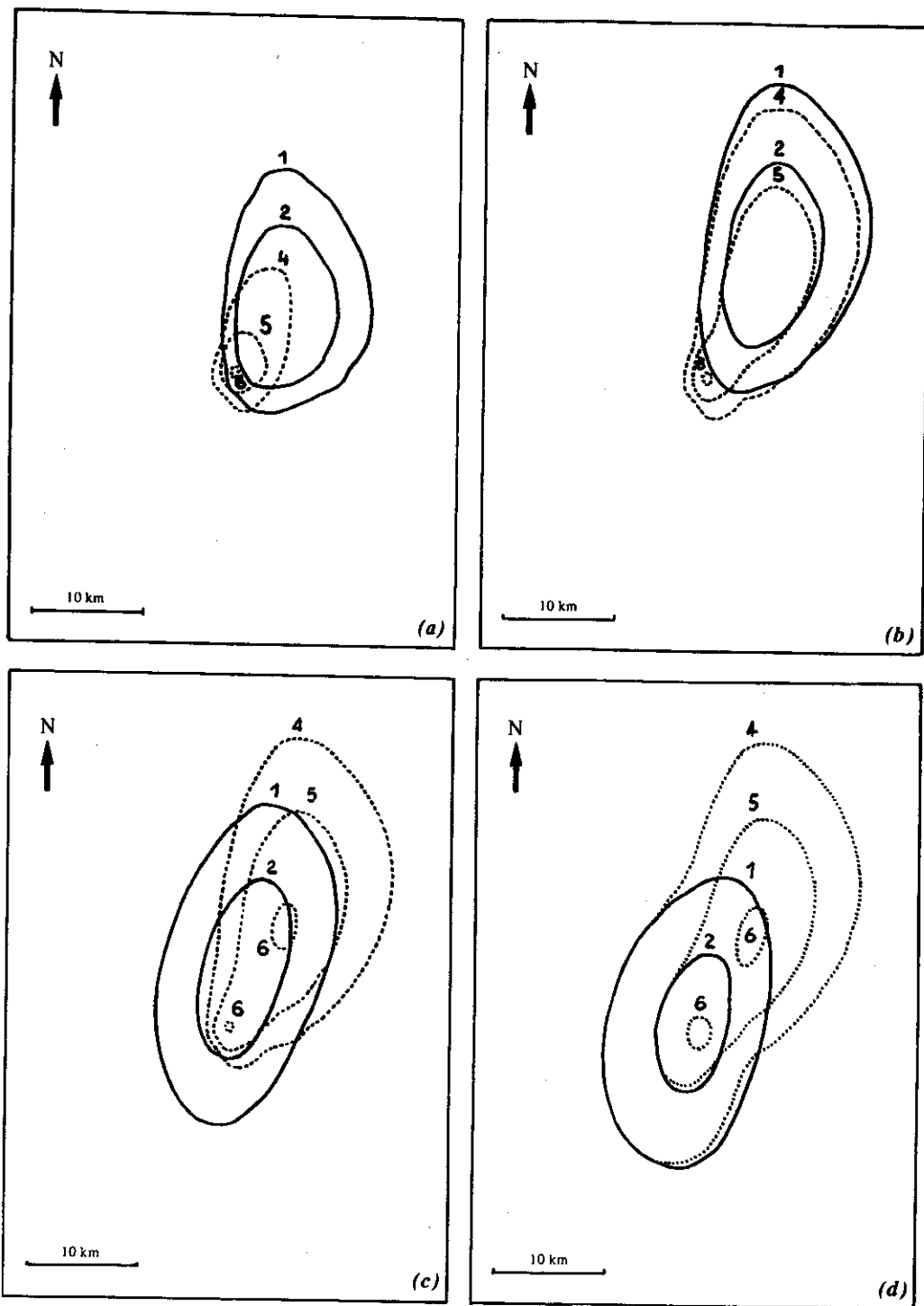


fig. 93.

Concentration contours of suspended and settled material after  $1/4$  (a),  $1/2$  (b),  $3/4$  (c), and one tidal period (d) following a dumping. Full-line curves 1 and 2 relate to water column concentrations  $c$  of 1 and  $10 \text{ mg/m}^3$  respectively. Concentrations of  $100 \text{ mg/m}^3$  were labelled as number 3; however, although such concentrations appear around the dumping, they are no longer found after a quarter tidal period. Curves 4, 5 and 6 relate to sediment surface densities on the bed C of 10, 100 and  $500 \text{ mg/m}^2$  respectively.

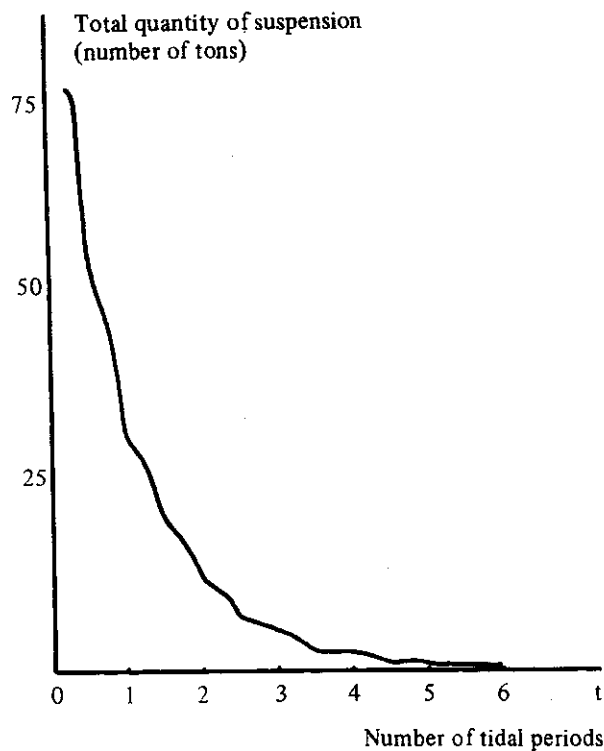


fig. 94.

Decay of total suspended material after a dumping

The results of theory are in agreement with observations made (a) during the *Belgian National Programme on the Biological and Physical Environment* and (b) by the *Ostend Fisheries Research Station* in the course of dumping supervision operations (e.g. Math. Modelsea, 1974; De Clerck et al., 1972). Conclusions may be drawn as follows:

- (i) The total quantity of suspended material decreases rapidly in spite of the fact that a certain amount is put periodically back into suspension when the strongest tidal currents occur. The bumps which appear at regular intervals along the decay curve in fig. 94 are due to solids being returned to the suspended state.
- (ii) As it has been previously observed (Math. Modelsea, 1974), dispersion is anisotropic with a marked lengthening of the concentration contours in the direction of the major tidal axis.
- (iii) The concentration contours relating to suspensions in the water column tend to be quasi-elliptical in shape with their centre-point situated in the general neighbourhood of the dumping point. A configuration of this type, which agrees with *in situ* measurements (Nihoul, 1975a; Math. Modelsea, 1974), may be derived theoretically using a simplified model in which the equations are first integrated over one tidal period (e.g. Nihoul, 1975a).



## References.

- ADAM, Y., (1977). Highly accurate compact implicit methods and boundary conditions, *J. Comput. Phys.*, 24, 10-22.
- ADAM, Y., (1979). *Belgian Real-Time System for the forecasting of currents and elevation in the North Sea*, in *Marine Forecasting*, J.C.J. Nihoul (Ed.), Elsevier Publ. Co, Amsterdam, 411-425.
- ADAM, Y. and RUNFOLA, Y., (1972). Programme national sur l'environnement physique et biologique, Projet Mer, N 14, Department for Science Policy, Brussels, 26 pp.
- ALFRINK, B.J. and VREUGDENHIL, C.B., (1981). Residual currents. Analysis of Mechanisms and model types, Delft Hydraulics Laboratory, TOW R 1469-11, 42 pp.
- BACKAUS, J., (1979). *First results of a three-dimensional model on the dynamics in the German Bight*, in *Marine Forecasting*, J.C.J. Nihoul (Ed.), Elsevier Publ. Co, Amsterdam, 333-349.
- BANKS, J.E., (1974). A mathematical model of a river-shallow sea used to investigate tide, surge and their interactions in the Thames - Southern North Sea region, *Phil. Trans. Roy. Soc. London*, A 275, 567-609.
- BECKERS, O., NIHOUL, J.C.J. and WOLLAST, R., (1976). *La circulation résiduelle et la caractérisation des masses d'eau dans la zone côtière belge*, in *Modélisation des systèmes marins. Projet Mer. Rapport final*, J.C.J. Nihoul (Ed.), Services du Premier Ministre, Programmation de la Politique Scientifique, Bruxelles, 1976, vol. 1, 95-130.
- BENQUÉ, J.P., HAUGUEL, A. and VIOLLET, P.L., (1981). Quelques Modélisations numériques en Mécanique des Fluides dans l'Environnement, Laboratoire d'Hydraulique EDF, Paris, 191 pp.
- BENWELL, G.R.R., GADD, A.J., KEERS, J.F., TIMPSON, M.S. and WHITE, P.W., (1971). The Bushby-Timpson 10 level model on a fine mesh, Meteorological Office London Scientific Papers, 32, 23 pp.
- BOWDEN, K.F., (1965). Horizontal mixing in the sea due to a shearing current, *J. Fluid Mech.*, 21, 83-95.
- BOWDEN, K.F., (1972). Turbulent diffusion, *Mém. Soc. Roy. Sc. Lg.*, 2, 67-97.
- BRETTSCHEIDER, G., (1967). Anwendung des hydrodynamisch-numerischen Verfahrens zur Ermittlung der  $M_2$  Mitschwingungszeit der Nordsee, Mittl. Inst. Meereskunde Univ. Hamburg, 7, 65 pp.
- CARRUTHERS, J.N., (1935). The flow of water through the Straits of Dover, Fishery Invest., London, 2, 14, 1-67.
- CARTER, H.H. and OKUBO, A., (1965). A study of the physical processes, movement and dispersion in the Cape Kennedy area, Chesapeake Bay Institute Johns Hopkins Univ., NYO-2973-1, 164 pp.
- CHENG, R.T., (1976). ASCE Nat. Water Res. Convent., San Diego, Preprint Paper n° 2692.
- CHENG, R.T., POWELL, T.M. and DILLON, T.M., (1976). Numerical models of wind-driven circulation in lakes, *Appl. Math. Modelling*, 1, 141-159.
- CLÉMENT, F., RUNFOLA, Y., RONDAY, F.C. and NIHOUL, J.C.J., (1981). Modèle mathématique de la baie sud de la mer du Nord, Unité de Gestion de la mer du Nord et de l'estuaire de l'Escaut, CDN 120978, 422 pp.

- CORMAULT, P., (1971). Détermination expérimentale du débit solide d'érosion de sédiments fins cohésifs, Proc. 14th Congress IAHR, Paris, vol. 4, 9-16.
- CRANK, J., (1956). *The Mathematics of Diffusion*, Oxford University Press, Oxford, 356 pp.
- DAVIES, A.M., (1976a). A Numerical Model of the North Sea and its Use in Choosing Locations for the Deployment of Off-Shore Tide Gauges in the JONSDAP '76 Oceanographic Experiment, *Deutsche Hydrographische Zeitschrift*, 29, 11-24.
- DAVIES, A.M., (1976b). Application of a fine mesh numerical model of the North Sea to the calculation of storm surge elevations and currents, Institute of Oceanographic Sciences, Bidston Observatory, 28, 70 pp.
- DAVIES, A.M., (1977). *The numerical solution of the three-dimensional hydrodynamic equations, using a B-spline representation of the vertical current profile*, in *Bottom Turbulence*, J.C.J. Nihoul (Ed.), Elsevier Publ. Co, Amsterdam, 1-48.
- DE CLERCK, R., VAN DE VELDE, J. et VYNCKE, W., (1972). Fisheries Res. Station Ostend, Rep. Biol. 01.
- DEFANT, A., (1961). *Physical Oceanography*, Pergamon Press, New York, 598 pp.
- DE LEONIBUS, P.S., (1971). Momentum flux and wave spectra observations from an ocean tower, *J. Geoph. Res.*, 76, 6506-6527.
- DUUN-CHRISTENSEN, J., (1971). Investigation on the practical use of a hydrodynamic numeric model for calculation of sea level variations in the North Sea, the Skaggerak and the Kattegat, *Deutsche Hydrographische Zeitschrift*, 24, 210-240.
- DUUN-CHRISTENSEN, J., (1974). The analysis of surface pressure field for application in a H-N model for the North Sea, I.C.E.S. Special Meeting on Models of water circulation in the Baltic, 15, 11 pp.
- DUUN-CHRISTENSEN, J., (1975). The representation of the surface pressure field in a two-dimensional hydrodynamic numeric model for the North Sea, the Skaggerak and the Kattegat, *Deutsche Hydrographische Zeitschrift*, 28, 97-116.
- DURANCE, J.A., (1976). A three-dimensional numerical model of tidal motion in a shallow sea, *Mém. Soc. Roy. Sc. Lg.*, 10, 125-132.
- ELDER, J.W., (1959). The dispersion of marked fluid in turbulent shear flow, *J. Fluid Mech.*, 5, 544-560.
- ELSKENS, I. and WOLLAST, R., (1974). Some aspects of the dynamic behaviour of metallic and other pollutants in the water column and the associated sectors, Math. Modelsea, I.C.E.S. Hydrography Committee, C.M. 1974-C 1, 439-450.
- FISHER, G., (1959). Ein numerisches Verfahrens zur Errechnung von Windstau und Gezeiten in Randmeeren, *Tellus*, 9, 60-76.
- FLATHER, R.A., (1976a). A tidal model of the north-west European continental shelf, *Mém. Soc. Roy. Sc. Lg.*, 10, 141-164.
- FLATHER, R.A., (1976b). Results from a storm surge prediction model of the north-west European continental shelf for april, november and december 1973, Institute of Oceanographic Sciences, Bidston Observatory, 24, 33 pp.

- FLATHER, R.A., (1979). *Recent results from a storm surge prediction scheme for the North Sea*, in *Marine Forecasting*, J.C.J. Nihoul (Ed.), Elsevier Publ. Co, Amsterdam, 385-409.
- FLATHER, R.A. and DAVIES, A.M., (1975). The application of numerical models to storm surge prediction, Institute of Oceanographic Sciences Bidston, 16, 23 pp.
- FLATHER, R.A. and DAVIES, A.M., (1976). Note on a preliminary scheme for storm surge prediction using numerical models, *Quartely J. Roy. Met. Soc.*, 102, 123-132.
- FORRISTALL, G.Z., (1974). Three-dimensional structure of storm generated currents, *J. Geophys. Res.*, 79, 2721-2729.
- FREEMAN, N.G., HALE, A.M. and DANARD, M.B., (1972). A modified sigma equations' approach to the numerical modelling of great lakes hydrodynamics, *J. Geophys. Res.*, 7, 1050-1060.
- GARRETT, W.D., (1967). Damping of capillary waves at the air-sea interface by oceanic surface-active material, *J. Mar. Res.*, 25, 297-301.
- GARRETT, W.D., (1972). In *The changing chemistry of the oceans*, D. Dyrssen and D. Jaeger (Eds.), Wiley, New York, 75-91.
- GEDNEY, R.T. and LICK, W., (1972). Wind-driven currents in Lake Erie, *J. Geophys. Res.*, 77, 2715-2723.
- GROEN, P. and GROVES, G.W., (1966). *Surges*, in *The Sea*, N. Hill (Ed.), Wiley, Interscience, New York, 611-646.
- GROTKOP, G., (1973). Finite element analysis of long-period water waves, *Comp. Methods Appl. Mech. and Eng.*, 2, 147-157.
- GULLENTOPS, F., (1974). Detrital sedimentology in the Southern Bight of the North Sea, Math. Modelsea, I.C.E.S. Hydrography Committee, C.M. 1974-C1, 55-80.
- HANSEN, W., (1956). Theorie zur Errechnung des Wasserstandes und der Strömungen in Randmeeren nebst Anwendungen, *Tellus*, 8, 287-300.
- HANSEN, W., (1966). The reproduction of the motion in the sea by means of hydrodynamical-numerical methods, NATO Subcommittee on Oceanographic Research, 25, 57 pp.
- HEAPS, N.S., (1967). *Storm surges*, in *Oceanogr. Mar. Biol. Annu. Rev.*, H. Barnes (Ed.), Allen and Unwin, London, 11-47.
- HEAPS, N.S., (1969). A two-dimensional numerical sea model, *Philos. Trans. Roy. Soc. London*, A 265, 93-137.
- HEAPS, N.S., (1972). On the numerical solution of the three-dimensional hydrodynamical equations for tides and storm surges, *Mém. Soc. Roy. Sc. Lg.*, 6, 143-180.
- HEAPS, N.S., (1976). *On formulating a non-linear numerical model in three dimensions for tides and storm surges*, in *Computing Methods in Applied Sciences*, R. Glowinski and J.L. Lions (Eds.), Springer, Heidelberg, 368-387.
- HEAPS, N.S. and JONES, J.E., (1975). Storm surge computations for the Irish Sea using a three-dimensional numerical model, *Mém. Soc. Roy. Sc. Lg.*, 7, 289-333.

- HIDAKA, K., (1933). Non-stationary ocean currents, Part I, *Mém. Imp. Mar. Obs. Kobe*, 5, 141-266.
- HIDY, G.M., (1972). A view of recent air-sea interaction research, *Bull. Am. Met. Soc.*, 53, 1083-1102.
- HILL, H.W., (1973). *Currents and water masses*, in *North Sea Science*, E.D. Goldberg (Ed.), MIT University Press, Cambridge Mass. U.S.A., 17-42.
- JELESNIANSKI, C.P., (1970). Bottom stress time-history in linearized equations of motion for storm surges, *Mon. Weather Rev.*, 98, 462-478.
- JENSEN, H.E. and WEYWADT, S., (1966). Forecasting of storm surges in the North Sea, NATO Subcommittee on Oceanographic Research, 28, 62 pp.
- JOSEPH, J. and SENDNER, H., (1958). Über die horizontale Diffusion im Meere, *Deutsche Hydrographische Zeitschrift*, 11, 49-77.
- JOSEPH, J. and SENDNER, H., (1962). On the spectrum of the mean diffusion velocities in the ocean, *J. Geophys. Res.*, 67, 3201-3205.
- JOSEPH, J., SENDNER, H. and WEIDEMANN, H., (1964). Untersuchungen über die horizontale Diffusion in der Nordsee, *Deutsche Hydrographische Zeitschrift*, 17, 57-75.
- KALLE, K., (1949). *Die natürlichen Eigenschaften der Gewässer*, in *Handbuch der Seefischerei Nordeuropas*, Schweizerbart (Ed.), Stuttgart, 1, part 2.
- KITAIGORODSKII, S.A., (1979). *Review of the theories of wind-mixed layer deepening*, in *Marine Forecasting*, J.C.J. Nihoul (Ed.), Elsevier Publ. Co, Amsterdam, 1-33.
- KRAUSS, E.B., (1967). Wind stress along the sea surface, *Advances in Geophysics*, 12, 213-255.
- KRAUSS, E.B., (1972). *Atmosphere-Ocean Interaction*, Clarendon Press, Oxford, 255 pp.
- LAEVASTU, T., (1963). *Water types in the North Sea and their characteristics*, in *Serial Atlas of Marine Environment*, Amer. Geogr. Soc. (Ed.), Folio 4.
- LAUWERIER, H.A., (1960). The North Sea Problem, *Proc. Kon. Ned. Akad. Wet.*, A 63, 266-290.
- LEENDERTSE, J.J., (1967). *Aspects of computational model for long-period water-wave propagation*, Ph. D. Dissertation Technische Hogeschool Delft, Rand Corporation, R.M. 5294-PR, 165 pp.
- LEMNIN, U., SCOTT, J.T. and CZAPSKI, U.K., (1974). The development from two-dimensional to three-dimensional turbulence generated by breaking waves, *J. Geoph. Res.*, 79, 3442-3448.
- MARCHUK, G.I., GORDEEV, R.G. and RIVKING, V.Y., (1973). A numerical method for the solution of tidal dynamics equations and the results of its application, *J. of Computation*, 13, 15-34.
- MC CAVE, I.N., (1970). Deposition of fine grained suspended sediment from tidal currents, *J. Geophys. Res.*, 75, 4151-4159.
- MC CAVE, I.N., (1974). *Mud in the North Sea*, in *North Sea Science*, E.D. Goldberg (Ed.), MIT University Press, Cambridge Mass. U.S.A., 74-100.
- MC INTYRE, F., (1971). Geochemical fractionation during mass transfer from sea to air by breaking bubbles, *Tellus*, 22, 451-462.

- NIILER, P.P., (1977). *One-dimensional models of the seasonal thermocline*, in *The Sea*, 6, E.D. Goldberg, I.N. Mc Cave, J.J. O'Brien and J.M. Steele (Eds.), Wiley Interscience Publ., New York, 97-115.
- NIILER, P.P. and KRAUSS, E.B., (1977). *One-dimensional models of the upper ocean*, in *Modelling and Prediction of the Upper Layers of the Ocean*, E.B. Krauss (Ed.), Pergamon, Oxford, 143-172.
- NIHOUL, J.C.J., (1972). Shear effect diffusion in shallow open seas, *Bull. Soc. Roy. Sc. Lg.*, 9-10, 521-526.
- NIHOUL, J.C.J., (1973a). *Mathematical models*, in *North Sea Science*, E.D. Goldberg (Ed.), MIT University Press, Cambridge Mass. U.S.A., 43-57.
- NIHOUL, J.C.J., (1973b). Diffusion of turbidity by shear effect and turbulence in the Southern Bight of the North Sea, Proc. 2d IUTAM - IUGG Symposium on Turbulent Diffusion in Environmental Pollution, Charlottesville, *Advances in Geophysics*, 18 A, 331-337.
- NIHOUL, J.C.J., (1974). Mesoscale secondary flows and the dynamics of ecosystems in the Southern Bight of the North Sea, *Mém. Soc. Roy. Sc. Lg.*, 7, 83-91.
- NIHOUL, J.C.J., (1975a). *Modelling of marine systems*, Elsevier, Amsterdam, 272 pp.
- NIHOUL, J.C.J., (1975b). Effect of the tidal stress on residual circulation and mud deposition in the Southern Bight of the North Sea, *Pure and Appl. Geophys.*, 113, 577-581.
- NIHOUL, J.C.J., (1976). *Mathematical hydrodynamic models for the study of marine circulation and dispersion of pollutants in a shallow sea*, in *Computing Methods in Applied Sciences*, R. Glowinski and J.L. Lions (Eds.), Springer, Heidelberg, 447-472.
- NIHOUL, J.C.J., (1977a). *Modèles mathématiques et Dynamique de l'environnement*, Ele, Liège, 198 pp.
- NIHOUL, J.C.J., (1977b). Three-dimensional model of tides and storm surges in a shallow well-mixed continental sea, *Dynamics of Atmospheres and Oceans*, 2, 29-47.
- NIHOUL, J.C.J., (1980). Residual circulation, long waves and mesoscale eddies in the North Sea, *Oceanologica Acta*, 3, 309-316.
- NIHOUL, J.C.J., (1981). *Marine Hydrodynamics at ecological scale*, in *Ecohydrodynamics*, J.C.J. Nihoul (Ed.), Elsevier Publ. Co, Amsterdam, 1-12.
- NIHOUL, J.C.J. and RONDAY, F.C., (1975). The influence of the tidal stress on the residual circulation, *Tellus*, 29, 484-490.
- NIHOUL, J.C.J. and RONDAY, F.C., (1976). Hydrodynamic models of the North Sea, *Mém. Soc. Roy. Sc. Lg.*, 10, 61-96.
- NIHOUL, J.C.J. and RUNFOLA, Y., (1981). *The residual circulation in the North Sea*, in *Ecohydrodynamics*, J.C.J. Nihoul (Ed.), Elsevier Publ. Co, Amsterdam, 219-271.
- NIHOUL, J.C.J., RUNFOLA, Y. and ROISIN, B., (1979). *Non-linear three-dimensional modelling of mesoscale circulation in seas and lakes*, in *Marine Forecasting*, J.C.J. Nihoul (Ed.), Elsevier Publ. Co, Amsterdam, 235-259.

- NIHOUL, J.C.J., RUNFOLA, Y. and ROISIN, B., (1980). *Shear effect dispersion in shallow tidal seas*, in *Marine Turbulence*, J.C.J. Nihoul (Ed.), Elsevier Publ. Co, Amsterdam, 345-362.
- OKUBO, A., (1971a). *Horizontal and vertical mixing in the sea*, in *Impingement of Man on the Oceans*, D.W. Wood (Ed.), Interscience, New York, 89-168.
- OKUBO, A., (1971b). Oceanic diffusion diagrams, *Deep Sea Research*, 18, 789-802.
- OTTO, L., (1970). The mean residual transport pattern in the southern North Sea, I.C.E.S. Hydrography Committee, C.M. 1970 - C 21, 15 pp.
- OWEN, M.W. and ODD, N.V.M., (1970). A mathematical model of the effect of a tidal barrier on siltation in an estuary, Proc. Internat. Conf. on the Utilization of Tidal Power, Halifax N.S. Dept of Energy, Mines and Resources, Ottawa, 1-36.
- OZMIDOV, R.V., (1965). Energy distribution between oceanic motions of different scales, *Izv. Atmos. Ocean. Phys. Series*, 1, 439-484.
- OZMIDOV, R.V., (1967). The dependence of the horizontal turbulent exchange coefficient in the ocean on the scale of the phenomenon, *Izv. Atmos. Ocean. Phys. Series*, 4, 1224-1225.
- PHILLIPS, O.M., (1977). *Entrainment*, in *Modelling and Prediction of the Upper Layer of the Ocean*, E.B. Kraus (Ed.), Pergamon, Oxford, 92-101.
- PINGREE, R.D. and GRIFFITHS, D.K., (1978). Tidal fronts on the shelf seas around the British Isles, *J. Geoph. Res.*, 83, 4615-4622.
- PINGREE, R.D. and GRIFFITHS, D.K., (1981a). S<sub>2</sub> tidal simulation on the north-west European shelf, *J. Mar. Biol. Ass. U.K.*, 61, 609-616.
- PINGREE, R.D. and GRIFFITHS, D.K., (1981b). The N<sub>2</sub> tide and semidiurnal amphidromes around the British Isles, *J. Mar. Biol. Ass. U.K.*, 61, 617-625.
- POND, S., PHELPS, G., PAQUIN, J.E., MC BEAN, G. and STEWART, R.W., (1971). Measurements of the turbulent fluxes of momentum, moisture and sensible heat over the ocean, *J. Atmospheric Sciences*, 28, 901-917.
- PRANDLE, D., (1975). Storm surges in the southern North Sea and River Thames, *Proc. Roy. Soc. London*, A 344, 509-539.
- PRANDLE, D., (1978). Residual flows and elevations in the southern North Sea, *Proc. Roy. Soc. London*, A 359, 189-228.
- PRANDLE, D. and WOLF, J., (1978). *Surge-Tide interaction in the southern North Sea*, in *Hydrodynamics of Estuaries and Fjords*, J.C.J. Nihoul (Ed.), Elsevier Publ. Co, Amsterdam, 161-185.
- PROUDMAN, J., (1955). The propagation of tide and surge in an estuary, *Proc. Roy. Soc. London*, A 231, 8-24.
- PROUDMAN, J. and DOODSON, A.J., (1924). The principal constituents of the tides of the North Sea, *Phil. Trans. Roy. Soc. London*, A224, 185-219.
- RAMMING, H.G., (1976). A nested North-Sea model with fine resolution in shallow coastal areas, *Mém. Soc. Roy. Sc. Ig.*, 10, 9-26.
- RAMMING, H.G., (1978). *Numerical investigations of the influence of coastal structures upon the dynamic off-shore process by application of a nested tidal model*, in *Hydrodynamics of Estuaries and Fjords*, J.C.J. Nihoul (Ed.), Elsevier Publ. Co, Amsterdam, 315-348.

- RHINES, P.B. and HOLLAND, W.R., (1979). A theoretical discussion of eddy-driven mean flows, *Dynamics of Atmospheres and Oceans*, 3, 289-325.
- RIEPMA, H., (1977). Spatial variability of residual currents in an area of the southern North Sea, I.C.E.S. Hydrography Committee, C.M. 1977 - C 43, 7 pp.
- ROISIN, B., (1977). Modèles tri-dimensionnels des courants marins, Actions concertées en Océanographie, ACN 3, Department for Science Policy, Brussels, 124 pp.
- ROLL, H.U., (1965). *Physics of the Marine Atmosphere*, Academic Press, New York, 426 pp.
- RONDAY, F.C., (1973). Modèle mathématique pour l'étude de la circulation due à la marée en mer du Nord, Marine Sciences Directorate Canada, 29, 42 pp.
- RONDAY, F.C., (1976). *Modèles hydrodynamiques*, in *Modélisation des systèmes marins. Projet Mer. Rapport final*, J.C.J. Nihoul (Ed.), Services du Premier Ministre, Programmation de la Politique Scientifique, Bruxelles, 1976, vol. 3, 270 pp.
- RONDAY, F.C., (1979). *Tidal and residual circulation in the English Channel*, in *Marine Forecasting*, J.C.J. Nihoul (Ed.), Elsevier Publ. Co, Amsterdam, 351-384.
- RONDAY, F.C. and NIHOUL, J.C.J., (1978). Mathematisch model van de zeevaartse uitbouw van de haven van Zeebrugge, Deelkontrakt 3, Department for Public Works, Brussels, Mod. 382 1, 262 pp.
- RONDAY, F.C. and NIHOUL, J.C.J., (1979). Mathematisch model van de zeevaartse uitbouw van de haven van Zeebrugge, Deelkontrakt 3, Department for Public Works, Brussels, Mod. 382 2, 397 pp.; Mod. 382 3, 147 pp.
- SHEPPARD, P.A., (1958). Transfer across the earth's surface and through the air above, *Quarterly J. Roy. Meteor. Soc.*, 84, 205-224.
- STEWART, R.W., (1967). Mechanics of the Air-Sea interface, *Phys. Fluids*, 10, Review papers, 547-555.
- SVANSSON, A., (1968). Hydrography of the Kattegat and the Skagerrak area, Swedish observations, Meddn. Havsfiskelaboratoriet, Lysckil, 48, 2.
- TALBOT, J.W., (1970). The influence of tides, waves and other factors on diffusion rates in marine and coastal situations, FAO Technical Conference on marine pollution and its effects on living resources and fishing, FIR MP/70/E, 43 pp.
- TALBOT, J.W., (1972). Diffusion in shallow seas, Symposium on the physical processes responsible for the dispersal of pollutants in the sea with special reference to the nearshore zone, 36-37, I.C.E.S., Copenhagen.
- TAYLOR, G.I., (1920). Tidal oscillations in gulfs and rectangular basins, *Proc. London Math. Soc.* 2, 20, 148-180.
- TAYLOR, G.I., (1953). Dispersion of soluble matter in solvent flowing slowly through a tube, *Proc. Roy. Soc. London*, A 219, 186-203.
- TAYLOR, G.I., (1954). The dispersion of matter in turbulent flow through a pipe, *Proc. Roy. Soc. London*, A 223, 446-467.
- THACKER, W.C., (1979). *Irregular-grid finite-difference techniques for storm surge calculations for curving coastlines*, in *Marine Forecasting*, J.C.J. Nihoul (Ed.), Elsevier Publ. Co, Amsterdam, 261-283.

- TOMCZAK, G., (1968). Die Wassermassenverteilung und Strömungsverhältnisse am Westausgang des Skagerraks, während der Internationalen Skagerrak-Expedition in Sommer 1966.
- VAN VEEN, J., (1938). Water movements in the Straits of Dover, *J. Cons. ICES*, 13, 7-38.
- WARLUZEL, A. and BENQUÉ, J.P., (1980). *Dispersion in a tidal sea*, in *Marine Turbulence*, J.C.J. Nihoul (Ed.), Elsevier Publ. Co, Amsterdam, 363-373.
- WEATHERLY, G.L., (1977). *Bottom boundary layer observations in the Florida current*, in *Bottom Turbulence*, J.C.J. Nihoul (Ed.), Elsevier Publ. Co, Amsterdam, 237-254.
- WELANDER, P., (1957). Wind action on a shallow sea : some generalization of Ekman's theory, *Tellus*, 9, 45-52.
- WITTEN, A.J. and THOMAS, J.H., (1976). Steady wind-driven currents in a large lake with depth-dependent eddy viscosity, *J. Phys. Oceanogr.*, 6, 85-92.
- ZIMMERMAN, J.T.F., (1976). Mixing and flushing of tidal embayments in the Western Dutch Wadden Sea, II, *Neth. J. Sea Res.*, 10, 397-439.

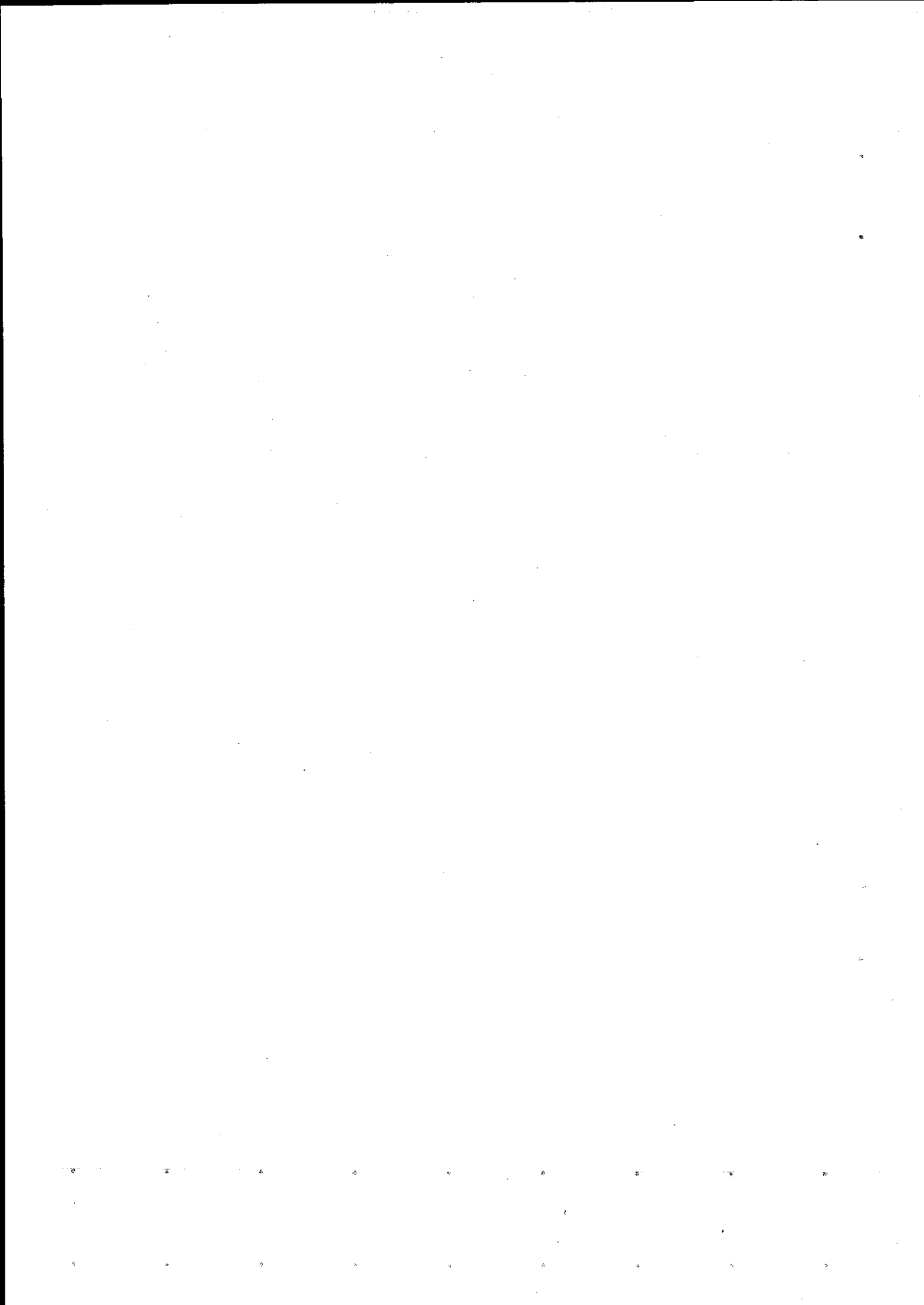


**BEHAVIOUR OF ORGANIC CARBON, NITROGEN  
AND PHOSPHOROUS IN THE SCHELDT ESTUARY  
AND THE ADJACENT COASTAL ZONE**

Roland WOLLAST

---

Université de Bruxelles.



## 1.- Introduction.

A major part of the Belgian research activities in the Southern part of the North Sea Bight have been devoted these last years to a better understanding of the various and complex aspects of the carbon cycle in this environment. This zone is strongly influenced by the terrestrial input of organic carbon, nitrogen and phosphorus either due to the river input via the Scheldt estuary or to numerous more diffuse coastal sources such as sewers and canals. It is obvious that in such a highly populated zone with intensive agricultural and industrial activities, the natural fluxes of many elements have been largely disturbed. It is especially the case for the dissolved inorganic species of nitrogen and phosphorous which are of great importance in the organic carbon cycle. However, the evaluation of the river fluxes to the adjacent coastal zone is complicated by the fact that they are strongly influenced by physical, chemical and biological processes occurring in the estuarine zone and furthermore that they are submitted to large seasonal fluctuations.

In the first part of this chapter, we have tried to evaluate the present day fluxes of organic carbon, nitrogen and phosphorous carried by fresh water in the Scheldt river system and to compare them to other well studied river systems in order to estimate the influence of man's activities on the disturbances of the natural cycle.

In the second part, we have analyzed qualitatively and tried to estimate quantitatively the influence of various physical, chemical and biological processes on the transfer of these materials through the estuarine zone.

In the last part, we have discussed the relative importance and the influence of these terrestrial fluxes on the cycle of organic carbon and nitrogen in the Belgian coastal zone.

It should be pointed out here that many attempts made in order to evaluate the river input to the marine systems are only based on a limited amount of hydrodynamical and chemical data and that important events for material transport like flood events are generally poorly sampled and accordingly not correctly taken into account in the calculations. All the data presented here for the Scheldt are based on monthly longitudinal profiles of the species considered at approximately 50 stations over a period of ten years. These longitudinal profiles of the hydrodynamical and chemical parameters were recorded over several tidal periods, covering various seasonal conditions.

Furthermore, a special attention was devoted to distinguish between the fresh water input and the marine input and thus to understand quantitatively the estuarine processes able to modify the transfer of the chemical species through the estuarine zone.

## 2.- The fresh water input of organic carbon and nutrients in the estuarine zone of the Scheldt.

The relative importance of the potential impact of man activities on a river system may be estimated by considering the number of inhabitants in the drainage basin and to the development of their agricultural and industrial activities which may be estimated by the annual per capita income, both expressed per unit of flow of fresh water discharge. We have compared in table 1 these values for the river Scheldt to the values computed by Stumm and Morgan (1981) for other major rivers of Europe and to the mean values for the U.S. rivers. It is obvious from this comparison that the Scheldt has to support an unusually high stress due to man's activities. This is reflected in the high concentration values found for organic matter and nutrients in the river.

Table 1

Rivers	Population density	Inhabitants per runoff	Gross National product per unit flow
	inh. per km	inh. per m <sup>3</sup> /s	dollars per m
Scheldt	270	73 000	16.3
Rhine	140	15 000	3.4
Danube	83	10 000	1.1
Rhone	63	3 700	0.55
All European rivers	66	6 500	-
All U.S. rivers	28	4 200	1.0

The mean concentration of dissolved organic matter (DOC) in the fresh water entering the estuarine zone is 7 mg C/ℓ whereas the concentration of particulate organic matter (POC) reaches 15 mg C/ℓ. This gives a total organic content (TOC) of 22 mg C/ℓ. For comparison, Meybeck (1982) estimated that the mean values of DOC and POC for unpolluted temperate rivers are respectively around 3 mg DOC/ℓ and 2 mg POC/ℓ which gives a total of 5 mg C/ℓ. If we accept these values as an estimation of the natural contribution in the river Scheldt, it appears that man's activities have increased the organic carbon flux in this system by a factor of 3 to 4.

An important consequence of this high organic load is the existence of an anoxic zone in the estuary over a distance which may exceed 70 km during the summer. The existence of these anaerobic waters plays an important role in the transfer of elements through the estuary and will be discussed later in details.

The influence of man's activities is still more pronounced when we consider the concentrations and fluxes of dissolved nitrogen and phosphorous species.

In order to evaluate the natural and present day nutrient fluxes on a global basis, we have first selected a few well studied rivers which also cover a large range of population density in the corresponding drainage basin. The data selected are presented in table 2 (Wollast, in press).

Except for dissolved silicon, the concentration of the nutrients observed in the fresh waters are extremely variable ranging from 0.4 to 60  $\mu\text{moles}/\ell$  for orthophosphate and from 3 to 800  $\mu\text{moles}/\ell$  for total dissolved inorganic nitrogen. These extreme compositional differences reflect mainly the influence of man's activities. This conclusion is documented in figure 1 where we have plotted the logarithm of the concentration of total

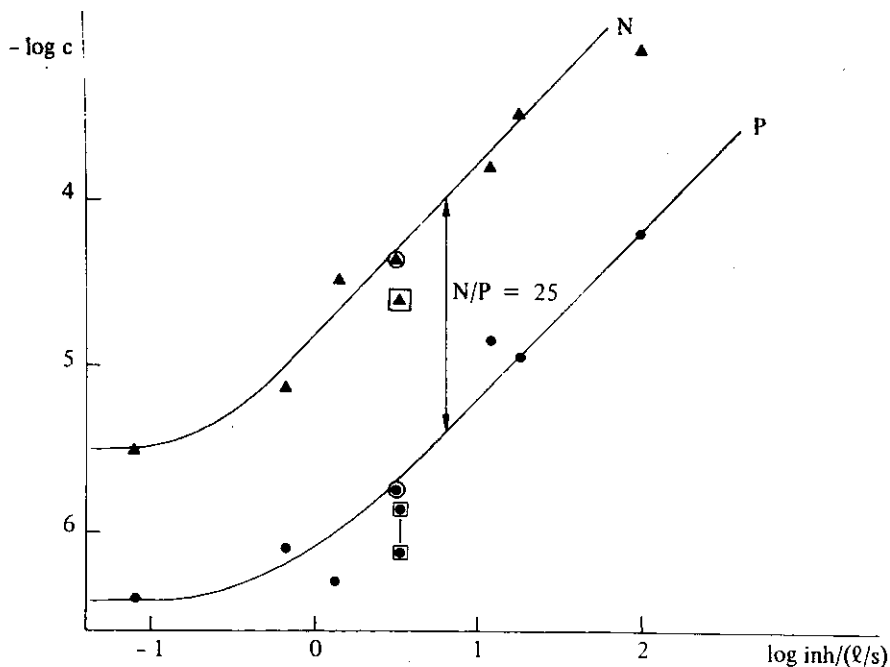


fig. 1.

Evolution of total dissolved N and P concentration (moles/ℓ) in rivers as a function of the number of inhabitants in the hydrographic basin per unit of fresh water discharge. Global mean after Van Bennekom and Salomons (○) and Meybeck (□).

Table 2  
Nutrient concentrations in some typical rivers (in  $\mu\text{moles/l}$ )

	PO <sub>4</sub>	NO <sub>3</sub> + NO <sub>2</sub>	NH <sub>4</sub>	N <sub>T</sub> (d)	H <sub>4</sub> SiO <sub>4</sub>	N/P	Réf.
Amazon	0.4	3.7	-	3.7	187	7.5	(1)
Zaire	0.8	6.7	0.4	7.1	165	8.4	(2)
Niger	0.4	7.6	1.0	8.6	250	21.5	(2)
Mississippi	2.8	156	< 4	160	83	57	(3)
Hudson (a)	3.0 (14)	50 (53)	20 (110)	70 (163)	70 (75)	23 (11.6)	(4)
Rhine (b) upper	0.5	30	2.5	32.5	61	65	(5)
lower	11.4	230	90	320	90	28	(5)
Scheldt	60(c)	150	650	800	230	13.3	(6)
Global mean	2.0	-	-	46	167	23	(7)
	0.6	19	1	20	-	30	(8)

(a) mean maximum concentration levels observed in the Hudson estuary. The values in brackets have been calculated by dividing the mean annual input of each nutrient by the mean fresh water discharge.

(b) upper Alpine Rhine at Schmitter and lower Rhine at Lobith.

(c) including polyphosphate.

(d) total dissolved inorganic nitrogen

References:

(1) Gibbs (1972); (2) Van Bennekom et al., (1978); (3) Ho and Barret (1977); (4) Deck (1981); (5) Zobrist and Stumm (1979); (6) Wollast (1976); (7) Van Bennekom and Salomons (1979); (8) Meybeck (1982).

dissolved phosphorus and nitrogen as a function of the logarithm of the number of inhabitants per unit of river discharge (ℓ/s).

Figure 1 shows for both  $N_T$  and  $P_T$ , a regular increase of the concentration as a function of the population density normalized to the water discharge. The slope of this increase, equal to 1, suggests that the concentration of nutrients in a river system can be approximately evaluated from

$$C = C_0 + ax$$

where  $C_0$  is the concentration of nutrient in pristine water,  $a$  the rate of production of nutrient per inhabitant and  $x$  the number of inhabitants per unit of water discharge of river.

The value for  $C_0$  and  $a$  obtained from this graph are reported in table 3. However, most of the polluted rivers considered here correspond to the more industrialized regions and the rate of N and P input per inhabitant is probably over-estimated on a global basis.

Table 3  
Evaluation of the mean concentrations and global fluxes of nutrients based on the data of fig. 1 (from Wollast, in press)

	P	N
Pristine concentration	0.4 μmoles/ℓ	5 μmoles/ℓ
Pristine flux	15 10 <sup>9</sup> moles/year	180 10 <sup>9</sup> moles/year
Man's perturbation	20 moles/inh.year 640 g P/year	500 moles/inh.year 7 kg N/year
Present day concentration	2 μmoles/ℓ	52 μmoles/ℓ
Present day flux	70 10 <sup>9</sup> moles/year	1600 10 <sup>9</sup> moles/year
$\frac{\text{Present day flux}}{\text{Pristine flux}}$	5	10

We have nevertheless calculated the global river input of nutrients assuming a mean global river discharge equal to 32 000 km<sup>3</sup> per year and using the values computed in table 3.

The calculated values are in fairly good agreement with recent evaluations of the mean global river fluxes of dissolved inorganic nitrogen and phosphorous (Van Bennekom and Salomons, 1979; Meybeck, 1982).

It is obvious that human activities have drastically modified the transport of nutrients from land to ocean.

The increase of the flux of dissolved nitrogen in rivers represents 30 % of the nitrogen fixed annually by man mainly during combustion processes and fertilizer production ( $6 \cdot 10^{12}$  moles/y) according to Simpson et al., 1977). In the case of phosphorus, the increase is only 15 % of the total phosphorus mined annually.

As one may expect from the intensive human activities in the Scheldt drainage basin (table 1), this river exhibits once again unusually high concentrations of dissolved nitrogen and phosphorus. As a consequence, the fresh water system is highly eutrophied and impressive phytoplankton blooms occur in the upper part of the estuary. Figure 2 shows a longitudinal distribution of chlorophyll in the Scheldt after the plankton bloom of May. In the

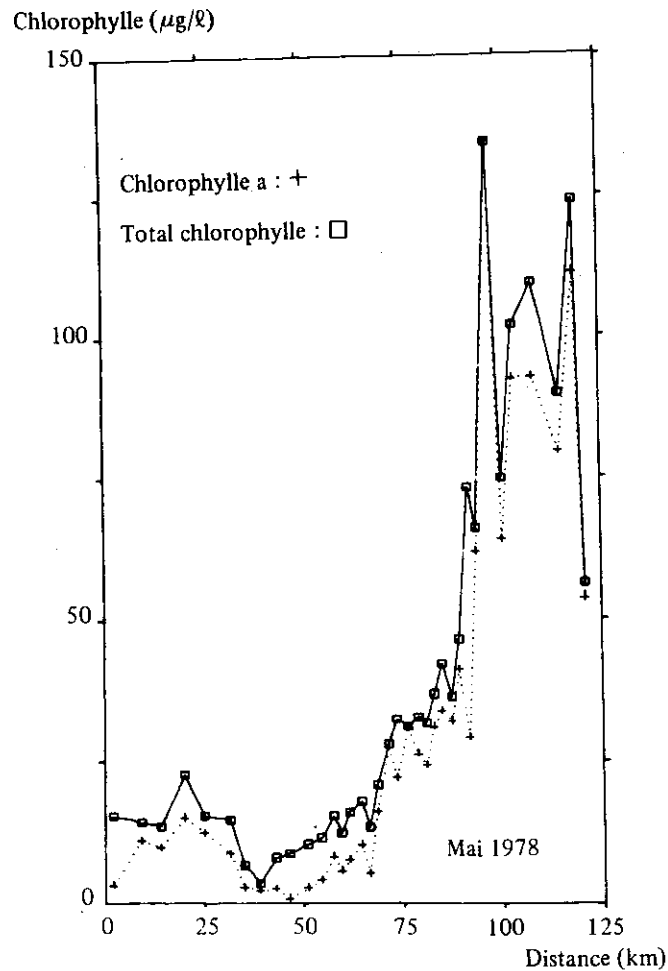


fig. 2.

Concentration profile of a-chlorophyll and total chlorophyll as a function of the distance to the mouth in the Scheldt estuary. (Lancelot, unpublished data, May 1978).



upper part of the estuary the concentration of  $\alpha$ -chlorophyll reaches a value corresponding to the highest values recorded in natural systems. It decreases then rapidly in the anaerobic zone situated between km 90 and 40. It increases again slightly near the mouth of the river when oxygen is restored and turbidity decreases. However this second peak of phytoplankton activity is less pronounced due to the lowering of the concentration of nutrients related to the dilution of the fresh water masses by sea-water poor in nutrients.

As one may expect from figure 2, the primary productivity plays an important role in the fluxes of organic matter and nutrients in the estuarine zone.

### 3.- Transfer of organic matter and nutrients through the estuarine zone.

The estuarine systems is characterized by profound changes in the chemical properties of the water masses and usually by high biological activities which affect to a significant degree the speciation of the elements and transfer to the adjacent coastal zones. This is particularly true in the case of the nutrients and organic matter.

The residence time of fresh water masses in the estuarine zone increases quickly with increasing vertical mixing owing to its dilution in a large body of sea-water. This allows profound changes in the water chemistry under the influence of relatively slow processes.

Furthermore, most of the particles, organic and inorganic, transported by rivers are negatively charged. The increase of ionic strength during mixing of fresh and sea-water neutralizes the surface charges by adsorption of cations and as a result of this and other processes the particles, usually colloidal, flocculate and are more able to settle and accumulate in somewhat restricted zones of an estuary. Again the latter process depends strongly on the type of estuary but generally estuaries are areas of intensive sedimentation. In well mixed or partially stratified estuaries like the Scheldt estuary, the circulation pattern of the water masses induces the occurrence of a turbidity maximum which usually corresponds to the zone of accumulation of bottom sediments and thus withdrawal of particulate matter from the water column.

Biological processes may also drastically affect the transfer of organic matter within the estuarine zone. On one hand, respiration of detrital organic matter may reduce the fluxes of this material through the estuarine zone and, on the other hand, large amounts of fresh organic carbon may be produced in the systems, usually characterized by a high primary productivity.

Mineralization of organic matter affects nutrient budgets owing to the release of dissolved  $\text{NH}_4^+$  and  $\text{PO}_4^{3-}$ . More important for the nutrient behaviour is the possible occurrence of an anoxic zone where the bacterial activity or chemical processes modify drastically the speciation of some nutrients. These processes will be discussed later in more details.

Finally, the high nutrient content of estuarine waters promotes the development of high productivity zones as soon as the turbidity caused by the terrigenous suspended matter drops as a result of flocculation and sedimentation.

### **3.1.— Production, transport and degradation of organic matter in the Scheldt estuary.**

It is now generally accepted that the particulate organic matter of terrestrial origin carried by fresh water into estuaries is at least partly removed in the estuarine zone and does not reach the coastal zone.

However, the extent to which the particulate material deposited in the estuarine zone is definitively trapped is actually a question of debate. During high flood events this material may be resuspended and carried to the sea. We estimate that during low river discharge periods two thirds of the suspended load carried by fresh water may be deposited in a restricted zone 30 km long (km 85 to km 55) corresponding to the 1 to 10 % range of salinity.

In this zone also characterized by long residence times of the water masses, the non refractory organic matter is almost completely mineralized by the heterotrophic bacteria either in the water column or in the few first cm of the freshly deposited sediments.

Mass balance calculation and measurements of the organotrophic activity by  $\text{H}^{14}\text{CO}_3$  incorporation or by biological oxygen demand give very similar results and show that the amount of organic carbon degraded in this zone reaches 100 and 150  $10^3$  t C/year (Somville and Wollast, 1981).

As a consequence one may estimate that no more than 10 % of the terrestrial organic carbon input in the Scheldt estuary is transferred to the coastal zone.

Furthermore the high bacterial activity induces anaerobic conditions especially during the summer when respiration is at his maximum.

As in many other estuaries, the decrease of turbidity with increasing salinity and the large supply of nutrients by the fresh waters produce in the Scheldt, phytoplankton blooms during spring, summer and early autumn. During those periods, the organic matter produced by photosynthesis in the lower part of the estuary equals almost the amount of terrestrial organic carbon

removed by respiration and sedimentation in the upper part (Wol- last and Peters, 1978). Most of this fresh organic matter is trans- ferred to the coastal zone where it is often difficult to distin- guish it from the coastal primary production.

### 3.2.— Behaviour of nitrogen species.

The three main processes which modify the speciation of ni- trogen in aquatic systems (nitrification, denitrification and bio- logical uptake), are commonly very active in estuarine systems and may significantly affect the transfer of forms of nitrogen to the adjacent coastal waters and to the atmosphere in case of denitri- fication. It is interesting to note that the source of nitrate is essentially related to leaching of soil and surface runoff. The use of inorganic fertilizers has considerably increased the con- centration of nitrate carried by rivers. On the other hand, the presence of anthropogenic  $\text{NH}_4^+$  is more directly related to domestic waste water discharge. As the estuarine zone itself is often hea- vily populated, high concentration of ammonia are encountered in many estuaries.

When occurring, denitrification has a pronounced effect on the transfer of nitrogen because nitrate is released as  $\text{N}_2$  or  $\text{N}_2\text{O}$  to the atmosphere. However, denitrification occurs only in sections of estuaries that exhibit oxygen depletion and where nitrate is used by heterotrophic bacteria as an oxidant. It is the case of heavily polluted rivers, with long residence times, or stratified estuaries where organic matter, even of natural origin, accumu- lates. In the Scheldt for instance, denitrification is observed even during the winter when the bacterial activity is lowest. Fi- gure 3 shows the situation in this river under these circumstances; it can be seen that most of the nitrification is consumed in the upper part of the estuary where partially anaerobic conditions prevail. If we extend these observations over one complete year, we estimate that approximately 30 % of the total dissolved ni- trogen input for the river Scheldt is lost to the atmosphere by denitrification in the estuarine zone.

Nitrification is less important for the nitrogen budget except perhaps for the release of  $\text{N}_2\text{O}$  to the atmosphere. Because of the preferential uptake by the phytoplankton of ammonia with respect to nitrate, this process however is of interest for the biologists.

In well oxygenated waters,  $\text{NH}_4^+$  slowly oxidizes to  $\text{NO}_2^-$  and  $\text{NO}_3^-$ ; if the residence time of water masses in the estuary is long enough,  $\text{NH}_4^+$  is almost completely consumed by nitrifying bacteria.

This is the case of the Scheldt, as shown in figure 4, when aerobic conditions are restored in the estuary. It should also be noted that large concentration of  $\text{N}_2\text{O}$  are observed in the ni- trification zone. The net production rates of  $\text{N}_2\text{O}$  computed from this profile by Deck (1981) and having maximum values of  $1.1 \mu\text{g}/(\text{m}^3 \cdot \text{s})$ , are very similar to those computed by McElroy et

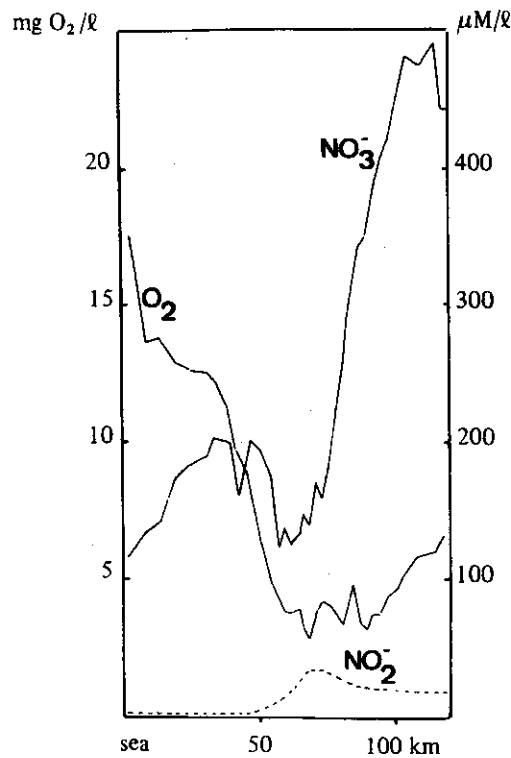


fig. 3.

Longitudinal profile of nitrate, nitrite and oxygen in the Scheldt estuary during February, showing a drastic decrease of nitrate concentration due to denitrification in the oxygen depleted zone (after Somville, 1980).

al. (1978) for the Potomac. These values seem, however, to be small with respect to the global land or ocean production rates.

The high productivity of the estuarine zone must be accompanied by a transfer of dissolved nutrients to the particulate phase. For nitrogen, McCarthy et al. (1975) have shown in the case of Chesapeake Bay, that  $\text{NH}_4^+$  is consumed preferentially to  $\text{NO}_3^-$  as long as the concentration of ammonia is greater than  $0.1 \mu\text{moles/l}$ . Thus we may expect that in most polluted estuaries, the phytoplankton growth will affect mainly the concentration of  $\text{NH}_4^+$ . It is however not easy to distinguish this uptake from the nitrification process which is often dominant in a region where extensive dilution by sea water low in nutrients occurs. Furthermore, McCarthy et al. (1975) have also shown that the turnover time of  $\text{NH}_4^+$  in the euphotic zone range from only 3 to 20 hours and averages 8 hours in Chesapeake Bay. The net removal of this nutrient compared with primary productivity may thus be expected to remain low and hard to quantify from concentration profiles.

We have tried to evaluate the nitrogen uptake by phytoplankton in the Scheldt from the monthly seasonal changes of dissolved and particulate nitrogen at the mouth of the river (Wollast, 1976).

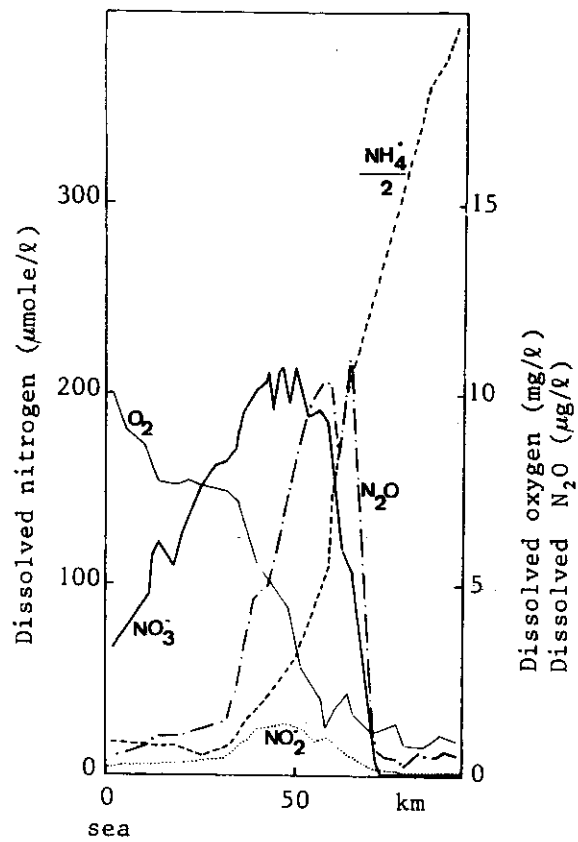


fig. 4.

Longitudinal profiles of dissolved nitrogen species and oxygen in the Scheldt estuary during October (Somville, 1980).

Table 4

Annual mass balance (in 10<sup>3</sup> t N/year) for the nitrogen species in the Scheldt including fresh water input, denitrification, nitrification, primary productivity, sedimentation of particulate nitrogen and output to the North Sea.

	Input	Denitrif.	Nitrif.	Prod.	Sed.	Output
NH <sub>4</sub> <sup>+</sup>	23	-	- 12	- 6	-	5
NO <sub>3</sub> + NO <sub>2</sub>	9	- 11	+ 12	-	-	10
N <sub>part</sub>	2	-	-	+ 6	- 3	5
N <sub>tot</sub>	34	- 11	-	-	- 3	20

A tentative annual budget for nitrogen in the Scheldt is summarized in table 4; these values should be considered only as first approximations. Also it should be recalled that the Scheldt represents an extreme case of a highly polluted estuary. Besides the importance of denitrification processes in such a system, it is also interesting to note that only a small fraction of the available nitrogen is consumed by phytoplankton.

### 3.3.— Behaviour of phosphate.

The speciation of inorganic phosphate is much simpler as it occurs mainly as orthophosphate. In polluted estuaries receiving untreated domestic waste water discharges, polyphosphates may represent a significant portion of the inorganic dissolved phosphate, as shown in the case of the Scheldt estuary (fig. 5). This polyphosphate is then slowly hydrolyzed to orthophosphate in the river itself.

Processes affecting the behaviour of phosphate in estuaries are, however, very complex and probably not entirely identified and certainly not sufficiently understood. First, orthophosphate

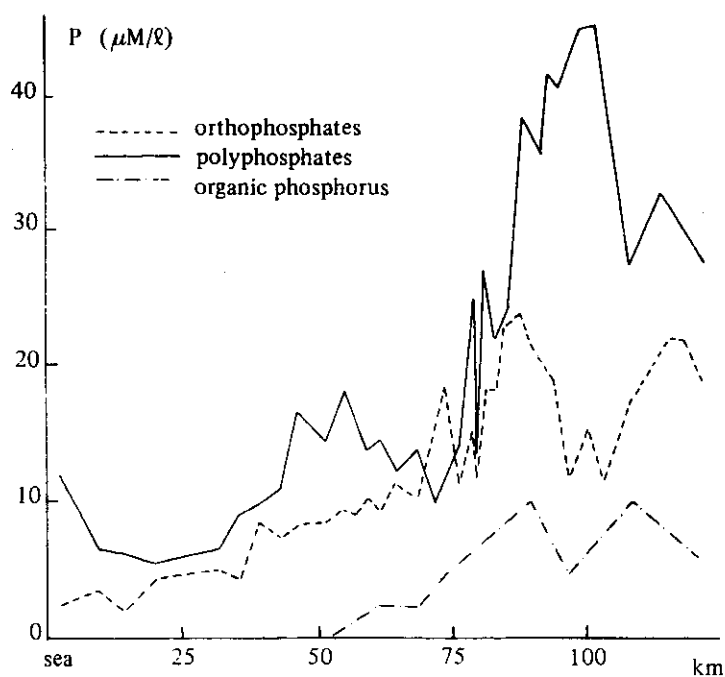


fig. 5.

Longitudinal profile of dissolved phosphorus species in the Scheldt estuary during May

is a chemically active compound which may be involved in various reactions of dissolution-precipitation or adsorption-desorption. The solid phases resulting from these reactions are so complex that basic properties like their solubility or exchange equilibria are poorly known. It seems however that these chemical reactions are reversible and rather fast. They act as a buffering mechanism which tends to maintain dissolved phosphate in a narrow range of concentration (around 1  $\mu\text{mole}/\ell$ ) during the mixing of river and sea-water (Liss, 1976).

Furthermore, the biological processes involving phosphorous are neither simple nor fully understood. The "luxury" uptake of phosphorous by phytoplankton is a well known phenomenon in rich nutrient zones but the data are so scarce that it is not possible to estimate departures from the C/N/P Redfield ratios in estuaries. Also, the direct or indirect role of bacteria in the estuarine phosphorous cycle has been completely neglected.

The behaviour of phosphorous in the Scheldt estuary is furthermore complicated because of the existence of an extended anaerobic zone, long residence time of the water masses, and intensive shoaling occurring in the upper part of the estuary. In the anaerobic zone, low redox potential conditions lead to the reduction of the most reactive iron hydroxides which are dissolved as  $\text{Fe}^{++}$  (Wollast, 1976). The phosphates eventually adsorbed by this particulate phase are then released to the dissolved phase. When the dissolved oxygen is restored by reaeration and by mixing with sea-water,  $\text{Fe}^{++}$  is re-oxidized and precipitates again as iron hydroxide sequestering by coprecipitation and adsorption, large amounts of dissolved phosphate. This particulate material accumulates mainly by sedimentation and is not transported to the lower part of the estuary. In the aerobic zone, phytoplankton growth is responsible for a supplementary uptake of dissolved phosphate. We have no direct measurements of the rate of consumption of  $\text{PO}_4^{---}$  by plankton but if we assume values of twice the Redfield ratio in order to take into account the "luxury" uptake of P, it represents a maximum value of 750 t P/year (0.75 moles/s), compared to a total input of 7 100 t P/year (particulate + dissolved) (7 moles/s).

Table 5

Tentative mass balance for phosphorus in the Scheldt estuary (in  $10^3$  t P/year)

	Input	Chemical precipitation	Plankton uptake	Sediment.	Output
Dissolved P	5.6	- 3.3	- 0.75	0	1.5
Particulate P	1.5	+ 3.3	+ 0.75	- 4.9	0.7
Total P	7.1	-	-	4.9	2.2

Other processes are theoretically possible for removing dissolved phosphorous at the high concentrations encountered in the Scheldt such as precipitation of apatite (Ca phosphate), vivianite (ferrous phosphate) and even magnesium-ammonium phosphate but none of these reactions have been identified *in situ* or in laboratory experiments simulating estuarine conditions. As with nitrogen, we have attempted to compute an annual budget for phosphorous in the Scheldt from the monthly longitudinal concentration profiles of dissolved and particulate phosphorous. The results of these calculations are presented in table 5. These calculations show that a significant fraction of the phosphate input to the estuary never reaches the sea and is entrapped in estuarine sediments.

#### 4.- Interactions of C and N in the coastal zone.

We will now discuss the budget and the circulation of organic carbon and nitrogen in the Belgian coastal zone which is shown in figure 6. This zone defined from the mean residual circulation

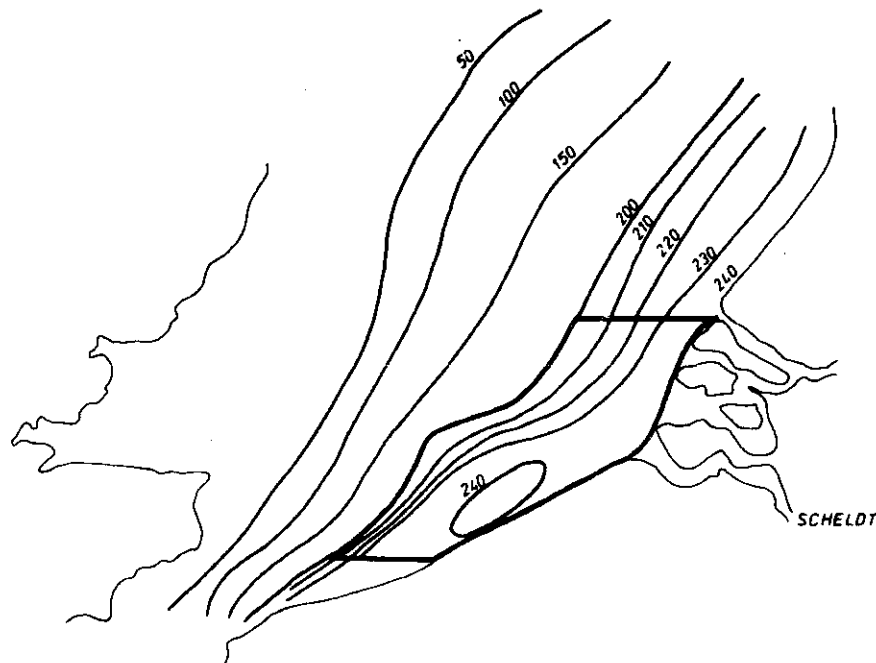


fig. 6.

The Belgian coastal zone defined from the residual circulation pattern of the water masses in the Southern Bight of the North Sea (residual fluxes in  $10^3 \text{ m}^3/\text{s}$ ), surface area :  $5370 \text{ km}^2$ , mean depth : 15 m (adapted from Nihoul, 1976).



pattern (Nihoul, 1976) extends over 5 370 km with a mean depth of 15 m. The carbon and nitrogen cycles have been studied in great detail in this zone and are summarized in figures 7 and 8.

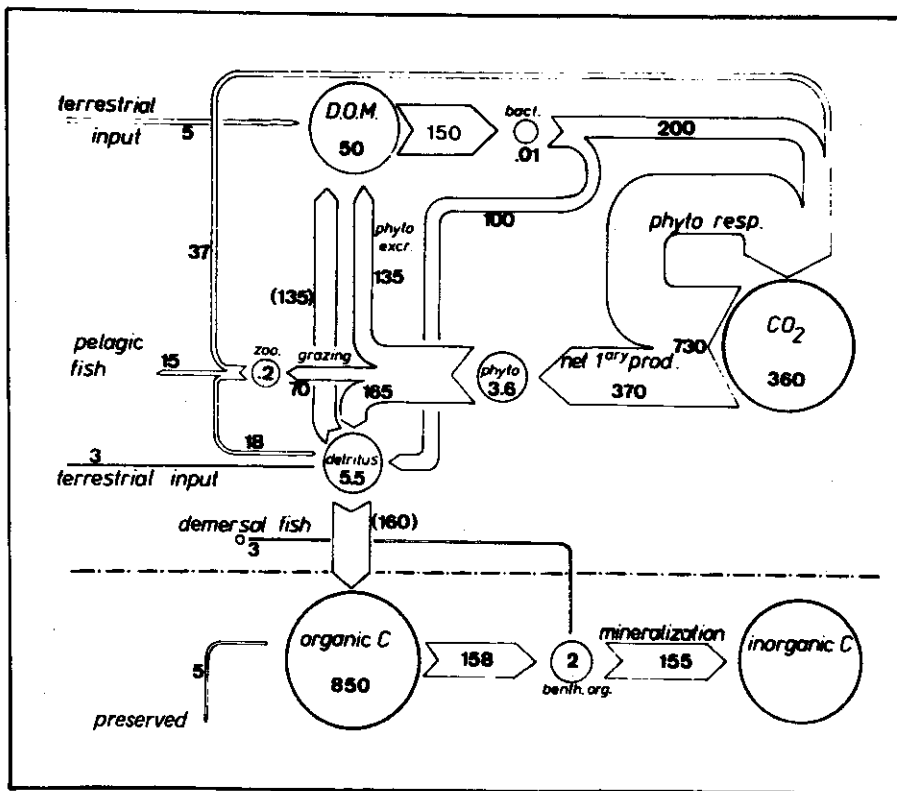


fig. 7.

Cycle of organic C in the Belgian coastal zone  
(Reservoirs in g C/m<sup>2</sup> and fluxes in g C/m<sup>2</sup>/year)

The value of the fluxes and of the sizes of the reservoirs presented in figure 7 have been estimated on the basis of independent measurements performed over several years, and described more extensively in Joiris *et al.* (1979), Wollast and Billen (1981) and Joiris *et al.* (1981). The mass balance obtained for the various species are generally fulfilled within  $\pm 20\%$  or better, which may be considered as very satisfactory. In the case of the nitrogen cycle of figure 8, the various pool sizes have been directly measured. The nitrogen fluxes within and out of the sediments were estimated by Billen (1976). The fluxes in the water column have been computed from the carbon fluxes of figure 7 assuming a C/N ratio equal to 6.4. The annual input of the nitrogen species are given in table 6.

Table 6

Annual input of nitrogen in the Belgian zone (in  $10^3$  t N/year)

	NO <sub>3</sub>	NH <sub>4</sub>	N <sub>org.</sub> diss.	N <sub>prg.</sub> part.	N <sub>tot.</sub>
Scheldt (a)	10	5	2.5	5	22.5
Yser	0.7 (b)	0.8 (b)	1.0 (c)	0.75 (d)	3.25
Lys channel	-	6.6 (c)	1.4 (c)	2.4 (d)	10.4
Total	10.7	12.4	4.9	8.15	36.2
Coastal cities					1 (b)

(a) This work.

(b) Bultynck, 1981.

(c) Mommaerts (personal communication).

(d) Estimated to be 30 % of the total dissolved nitrogen.

The net primary production of the Southern Bight of the North Sea ( $370 \text{ g C/m}^2 \cdot \text{year}$ ) is relatively high if compared to the mean value for the whole oceanic system (about  $100 \text{ g C/m}^2 \cdot \text{year}$ ) but this is generally the case for coastal environments (average : about  $270 \text{ g C/m}^2 \cdot \text{year}$ ; Wollast and Billen, 1981). The input of terrestrial organic matter in the coastal zone is only  $3 \text{ g C/m}^2 \cdot \text{year}$  as particulate C and  $5 \text{ g C/m}^2 \cdot \text{year}$  as dissolved C. Terrigenous organic matter appears thus to play a minor role in the coastal system and constitutes a small flux compared to the flux of organic matter produced by primary production.

About 30 % of the total net primary production is excreted by phytoplankton as dissolved organic matter and only 20 % is grazed by zooplankton. The importance of direct grazing with respect to primary production commonly has been considered to be a characteristic feature of marine ecosystems in contrast with terrestrial ecosystems (Odum, 1962; Crips, 1964; Wiegert and Owen, 1971). However, it recently has become evident that, at least in coastal environments, zooplankton grazing does not account for all the phytoplankton mortality and important pathways of organic matter recycling through detritus and bacteria exist in parallel with the pathways through herbivorous zooplankton (Banse, 1974; Pomeroy and Johannes, 1966, 1968; Joiris *et al.*, 1979, 1981; Walsh *et al.*, 1981). The high rate of recycling is also confirmed by the turnover time of the phytoplankton in the coastal zone which is only 4 days whereas for oceanic systems the turnover time is usually between 7 and 14 days (Cauvet, 1977). The high rate of turnover reflects in turn the species composition of the phytoplankton largely dominated by the colony forming microflagellate *Phaeocystis poucheti*.

The unusually high productivity of dissolved organic matter in this zone is probably related to the excretion of polysaccharides by these organisms, which are however rapidly recycled by the bacteria.

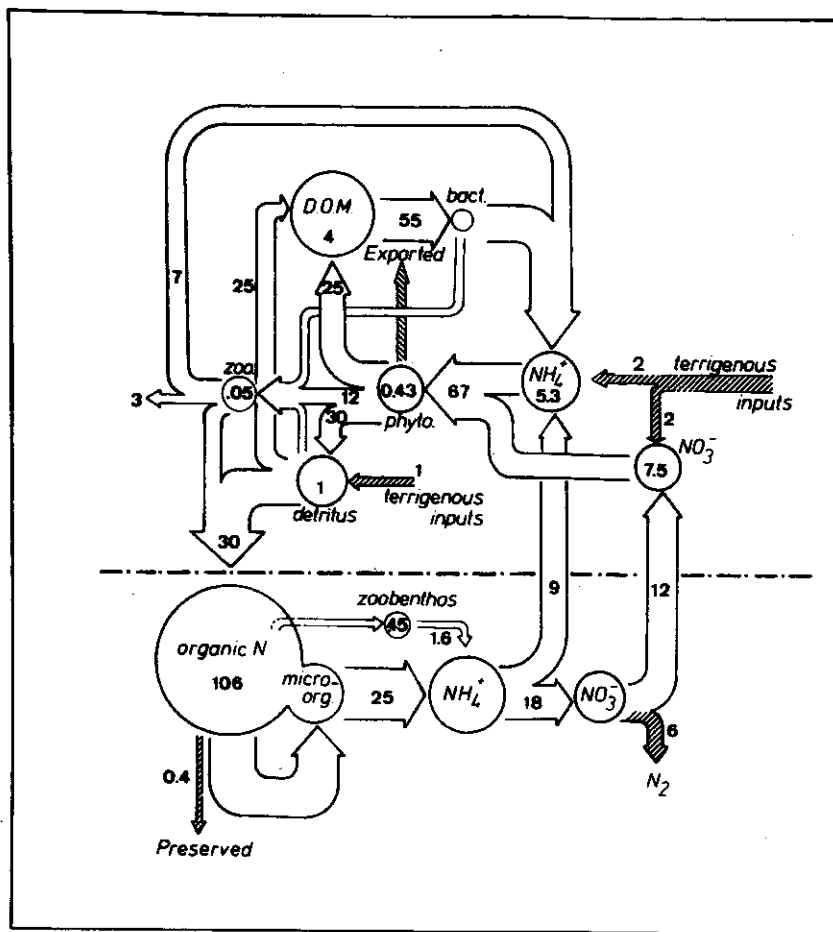


fig. 8.

Cycle of nitrogen in the Belgian coastal zone  
(Reservoirs in  $\text{g N/m}^2$  and fluxes in  $\text{g N/m}^2/\text{year}$ )

It should be pointed out that very similar patterns have been described for various other coastal environments such as the Louisiana-Texas and West Florida shelves of the Gulf of Mexico, and the central shelf of the Bering Sea (Walsh *et al.*, 1981).

The primary productivity requires a flux of nitrogen of  $67 \text{ g N/m}^2 \cdot \text{year}$  (figure 8). In fact, the river input of nitrogen ( $4 \text{ g N/m}^2 \cdot \text{year}$ ) is small compared to the requirements of the phytoplankton. This conclusion can be generalized on a global basis by considering the mean world river input of nutrients presented in table 3 divided by the surface area of the coastal zone ( $30 \cdot 10^6 \text{ km}^2$ ). The global river input of nutrients are respectively equal to  $0.9 \text{ g N/m}^2 \cdot \text{year}$  and  $0.07 \text{ g P/m}^2 \cdot \text{year}$ . The amounts of nutrients required for a mean net primary productivity of  $270 \text{ g C/m}^2 \cdot \text{year}$  are on the order of  $50 \text{ g N/m}^2 \cdot \text{year}$  and  $7 \text{ g P/m}^2 \cdot \text{year}$ . Thus, the input by rivers represents generally only 1 to 2% of the nutrient uptake by phytoplankton.

It is interesting to compare these values to the relative importance of upwelling and vertical diffusion of nutrients for the whole oceanic system. From our previous estimations (Wollast, 1981), the mean inputs of nitrogen and phosphorus to the euphotic zone by vertical diffusion, which is rather uniformly distributed over the pelagic zone of the ocean, are approximately equal to  $0.5 \text{ g N/m}^2 \cdot \text{year}$  and  $0.1 \text{ g P/m}^2 \cdot \text{year}$ . These values are very similar to the actual river inputs, but the oceanic zones where the fluxes of nutrients are due to vertical diffusion alone are less productive areas (less than  $50 \text{ g C/m}^2 \cdot \text{year}$ ) than the coastal zone. In the regions of upwelling, the vertical flux of nutrients is much greater and we estimate that  $5 \text{ g N/m}^2 \cdot \text{year}$  and  $1 \text{ g P/m}^2 \cdot \text{year}$  are reasonable mean values. It should be noted that upwelling is often responsible for the high productivity of the coastal zone.

In all aquatic systems the external input of nutrients is only a small fraction of nutrient uptake because of the rapid turnover of the plankton. However, we will show, by using a simple model, that this external input plays an important role in the control of the productivity of the coastal zone. We will therefore assume that the coastal zone is a stationary system where the external input of nitrogen is compensated by an equal amount exported either to the adjacent oceanic zone or to the deeper parts of the sediments. In fact, the exportation occurs mainly as particulate organic nitrogen by sedimentation or by advection of the water masses. The low concentration and the rather uniform distribution of dissolved inorganic nutrients between the coastal zone and the adjacent marine zones indicate that the export of these species must be small compared to the exportation of the biomass which is much more concentrated in the coastal zone. Thus, the biomass produced from the dissolved nutrients is partly recycled and partly exported. The mass balances of inorganic dissolved nitrogen (N) and of organic nitrogen in the biomass (B) may then be written as

$$\frac{dN}{dt} = I + k_r B - f(N) B = 0$$

$$\frac{dB}{dt} = f(N) B - k_r B - k_c B = 0$$

where  $I$  is the annual input of dissolved nitrogen divided by the volume of water of the coastal zone;  $k_r$  is the rate of recycling of the biomass;  $k_c$  is the rate of exportation of the biomass; and  $f(N)$  is the appropriate function relating the productivity  $P$  of the system to the concentration of nutrients :  $P = f(N) B$ .

The combination of these two equations leads to

$$(1) \quad B = \frac{I}{k_c}$$

$$(2) \quad f(N) = (k_c + k_r)$$

$$(3) \quad P = f(N) B = I \left(1 + \frac{k_r}{k_c}\right)$$

Thus, both the biomass concentration and the productivity are direct functions of the nutrient input. However, the productivity is increased by an amplification factor

$$\left(1 + \frac{k_r}{k_c}\right)$$

which is strongly dependent on the relative rate of remineralisation  $k_r$  with respect to the exportation rate  $k_c$ .

The exportation of biomass to the adjacent marine zone is determined by the residual circulation of the water masses in the coastal zone. The residence time of water masses in that zone may be estimated from figure 6 and is of the order of one month (12 renewals per year).

On the other hand, preservation of organic nitrogen in the sediments constitutes only a minor exportation of N out of the system. From figure 8, one can see that it corresponds to a rate constant of  $1 \text{ y}^{-1}$ . Thus the total exportation rate is

$$k_c = 12 + 1 = 13 \text{ y}^{-1}.$$

One can see from figures 7 and 8 that the effective regeneration time of the phytoplankton obtained by dividing the biomass by the primary productivity is approximately 4 days which implies from relation (2) that

$$k_c + k_r = 91 \text{ y}^{-1}.$$

From the value of  $k_c$  estimated here above, it becomes that

$$k_r = 78 \text{ y}^{-1}.$$

Thus the amplification factor by which the input of nutrients has to be multiplied in order to describe the primary productivity is close to 7. It should be pointed out that this represents a mean annual value and that this amplification factor is higher during the summer due to the increase of the metabolic rates, especially those of the heterotrophic bacteria and of the phytoplankton.

Although oversimplified, the model allows to predict fairly well the biomass and the productivity of the coastal zone. The input of total dissolved nitrogen, taken from table 6, divided by the surface area of the coastal zone gives  $I = 5.2 \text{ g N/m}^2 \cdot \text{year}$ . Then from relation (1) :  $B = 0.43 \text{ g N/m}^2 \cdot \text{year}$  and from relation (3) :  $P = 35 \text{ g N/m}^2 \cdot \text{year}$ . The mean observed value of the biomass  $B$  is exactly the same and the mean value of the particulate productivity is estimated at  $42 \text{ g N/m}^2 \cdot \text{year}$  from figure 8.

## 5.- Conclusions.

We have shown that the input of terrestrial organic carbon in the Belgian coastal zone is very small compared to the natural fluxes of C in the marine cycle. Most of the organic carbon due to man's activities is consumed or trapped in the river system and the estuarine zone and does not reach the sea.

However, the fluxes of nutrients have been considerably increased due to the human activities and are responsible for a significant increase in the primary production. The stimulation of this productivity is accompanied by a modification of the structure of the food chain in the coastal ecosystem which favours a short recycling chain by microorganisms, instead of the classical long trophic chain by zooplankton and by fish. This situation seems to be a general case of the coastal zones submitted to a high input of nutrients.

The human activities have however considerably increased these input and have thus a tendency to emphasize the characteristics unfavourable for the improvement of the sea products.

## References.

- BANSE, K., (1974). On the role of bacterioplankton in the tropical ocean, *Mar. Biol.*, 24, 1-5.
- BILLEN, G., (1976). *Etude écologique des transformations de l'azote dans les sédiments marins*, Thèse de doctorat, Université Libre de Bruxelles.
- BULTYNCK, (1981). De lozing van afvalwater in de kustwater. Studiedag Kustwater en Estuariumverontreiniging, Brugge, 7 oktober 1981.
- CAUWET, G., (1977). Organic chemistry of sea water particulates concepts and developments, *Oceanologica Acta*, 1, 99-105.
- CRISP, D.J., (1964). *Grazing in terrestrial and marine environments*, in *Br. Ecol. Soc. Symp. n° 4*, D.J. Crisp (Ed.), Blackwell Scientific Publ., Oxford, pp. 9-16.
- DECK, B.L., (1981). *Nutrient-element distributions in the Hudson estuary*, Ph. D. Thesis, Columbia University.
- GIBBS, R.J., (1972). Water chemistry of the Amazon river, *Geochim. Cosmochim. Acta*, 36, 1061-1066.
- HO, C.L. and BARRET, B.B., (1977). Distribution of nutrients in Louisiana's coastal waters influenced by the Mississippi river, *Est. coast. Mar. Sc.*, 5, 173-195.
- JOIRIS, Cl., BILLEN, G., LANCELOT, Ch., MOMMAERTS, J.P., DARO, M.H., BOSSICART, M., GILLAIN, G., BERTELS, A., HECQ, J.H. and WIJNANT, J., (1979). *Dynamics of organic matter in three planktonic ecosystems of the southern North Sea*, International Council for the exploration of the Sea, Copenhagen, pp. 165-184.

- JOIRIS, Cl., BILLEN, G., LANCELOT, C., DARO, M.H., MOMMAERTS, J.P., HECQ, J.H., BERTELS, A., BOSSICART, M., NIJS, J., (1982). A budget of carbon cycling in the Belgian Coastal Zone: relative roles of zooplankton, bacterioplankton and benthos in the utilization of primary production. *Neth. J. Sea Res.* (in press).
- LISS, P.S., (1976). *Conservative and non conservative behaviour of dissolved constituents during estuarine mixing*, in *Estuarine Chemistry*, J.D. Burton and P.S. Liss (Eds), Academic Press, London, pp. 93-100.
- MCCARTHY, J.J., TAYLOR, W.R. and TAFT, J.L., (1975). *The dynamics of nitrogen and phosphorus cycling in the open waters of the Chesapeake Bay*, in *Marine Chemistry in the Coastal Environment*, T.M. Church (Ed.), ACS Symposium series, 18, 664-681.
- McELROY, M.B., ELKINS, J.W., WOFISKY, S.C., KOLB, C.E., DURAN, A.P. and KAPLAN, W.A., (1978). Production and release of N<sub>2</sub>O from the Potomac Estuary, *Limnol. Oceanogr.*, 23, 1168-1182.
- MEYBECK, M., (1982). Carbon, Nitrogen and Phosphorus transport by rivers, *Am. Journal of Science*, 282, 401-450.
- NIHOUL, J.C.J., (1976). *Paramétrisation, calibrage et ajustement du modèle. Application à la mer du Nord et au Southern Bight*, in *Modélisation des systèmes marins*, J.C.J. Nihoul (Ed.), Projet Mer, rapport final, vol. 1, Programmation de la Politique Scientifique, Bruxelles.
- ODUM, E.P., (1962). Relationship between structure and function in the ecosystem, *Jap. J. Ecol.*, 12, 108-118.
- POMEROY, L.R. and JOHANNES, R.E., (1966). Total plankton respiration, *Deep Sea Res.*, 13, 971-973.
- POMEROY, L.R. and JOHANNES, R.E., (1968). Respiration of ultra plankton in the upper 500 m of the ocean, *Deep Sea Res.*, 15, 381-391.
- SIMPSON, H.J. et al., (1977). *Man and the global nitrogen cycle*, in *Global Chemical Cycles and their alterations by man*, W. Stumm (Ed.), Dahlem Konferenzen, Berlin.
- SOMVILLE, M., (1980). *Etude écophysiological des métabolismes bactériens dans l'estuaire de l'Escaut*, Thèse de doctorat, Université Libre de Bruxelles.
- SOMVILLE, M. and WOLLAST, R., (1981). Modélisation de la qualité des eaux de l'estuaire de l'Escaut. Studiedag Kustwater en Estuariumverontreiniging, Brugge, Koninklijke Vlaamse Ingenieursvereniging.
- STUMM, W. and MORGAN, J.J., (1981). *Aquatic chemistry. An introduction emphasizing chemical equilibria in natural water*, 2nd ed., J. Wiley, New York.
- VAN BENNEKOM, A.J., BERGER, G.W., HELDER, W. and DE VRIES, R.T.P., (1978). Nutrient distribution in the Zaïre estuary and river plume. *Neth. J. Sea Res.*, 12, 296-323.
- VAN BENNEKOM, A.J. and SALOMONS, W., (1981). *Pathways of nutrients and organic matter from land to ocean through rivers*, in *River input to Ocean Systems*, United Nations (Ed.), New York, pp. 33-41.
- WALSH, J.J., ROWE, G.T., IVERSON, R.L. and McROY, P., (1981). Biological export of shelf carbon is a sink of the global CO<sub>2</sub> cycle, *Nature*, 29, 196-201.

- WIEGERT, R.G. and OWEN, D.F., (1971). Trophic structure, available resources and population density in terrestrial versus aquatic ecosystems, *J. Theor. Biol.*, 30, 69-81.
- WOLLAST, R., (1976). *Transport et accumulation de polluants dans l'estuaire de l'Escaut*, chapitre IV, pp. 190-218, in *L'estuaire de l'Escaut*, J.C.J. Nihoul et R. Wollast (Eds), Projet Mer, rapport final, vol. 10, Programmation de la Politique Scientifique, Bruxelles.
- WOLLAST, R. and PETERS, J.J., (1978). *Biogeochemical properties of an estuarine system: the river Scheldt*, in *Biogeochemistry of estuarine sediments*, E.D. Goldberg (Ed.), UNESCO, Paris, pp. 279-293.
- WOLLAST, R., (1981). *Interactions between major biogeochemical cycle: marine cycles*, in *Some perspectives of the major biogeochemical cycles*, G.E. Likens (Ed.), Wiley, New York, pp. 125-141.
- WOLLAST, R. and BILLEN, G., (1981). *The fate of terrestrial organic carbon, in The flux of carbon from the rivers to the oceans*, U.S. Dept. of Energy, CONF-8009/40/UC/Washington.
- WOLLAST, R., (in press). *Interactions in estuaries and coastal waters*, in *Interactions of biogeochemical cycles*. Scope, B. Bolin (Ed.), Wiley, New York.
- ZOBRIST, J. and STUMM, W., (1981). *Chemical dynamics of the Rhine catchment area in Switzerland; extrapolation to the "Pristine" Rhine river input into the ocean*, in *SCOR Proceeding of the Workshop on River Inputs to Ocean Systems (RIOS)*, United Nations, New York, pp. 52-64.



# BOUNDARY CONDITIONS FOR HEAVY METALS AT THE AIR-SEA INTERFACE

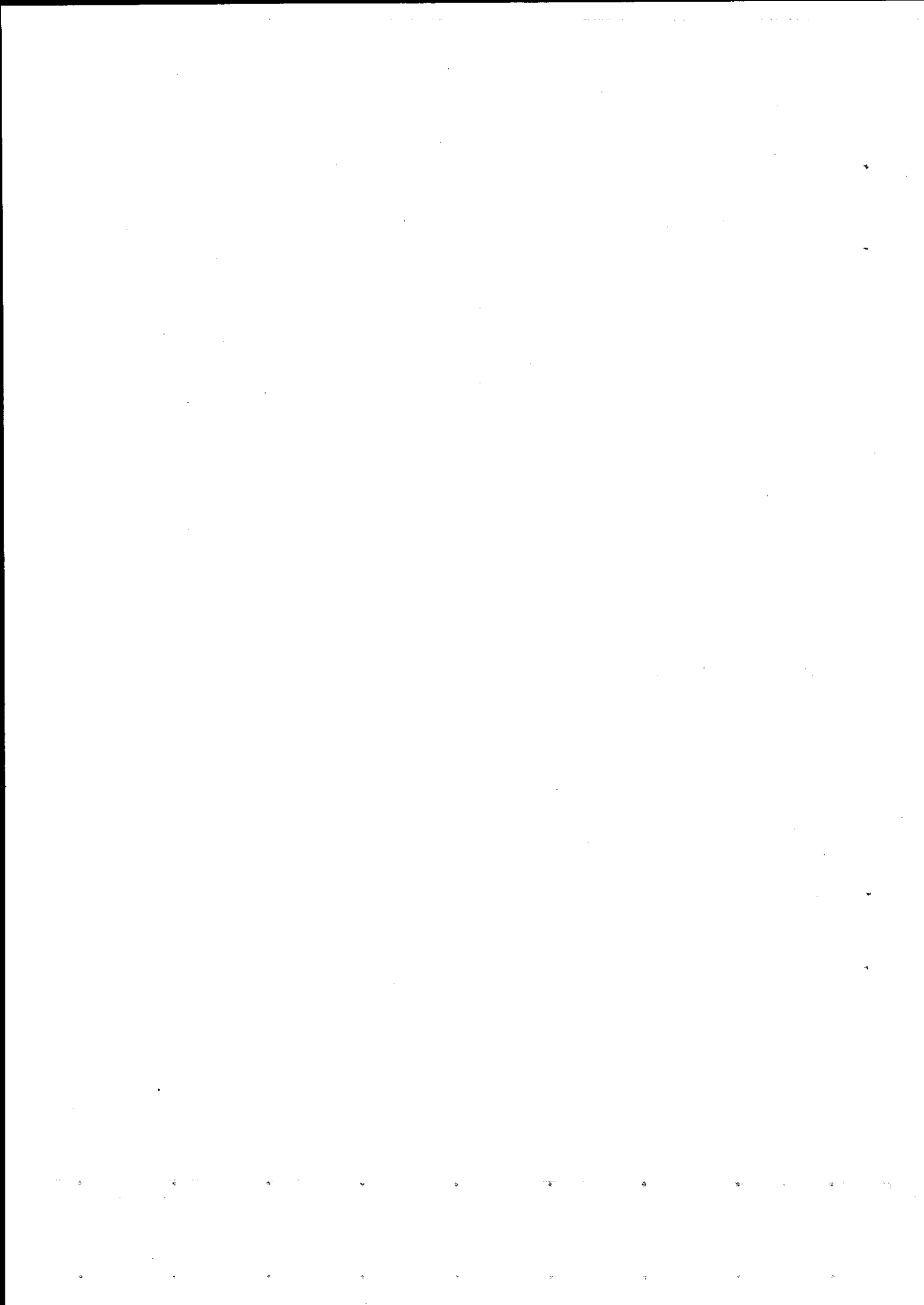
F. DEHAIRS<sup>1</sup>\*, H. DEDEURWAERDER<sup>1</sup>, M. DEJONGHE<sup>1</sup>, G. DECADT<sup>1</sup>,  
G. GILLAIN<sup>2</sup>, W. BAEYENS<sup>1</sup> and I. ELSKENS<sup>1</sup>

---

1. Laboratorium voor Analytische Scheikunde, Vrije Universiteit Brussel, B-1050 BRUSSELS, Belgium.

2. Institut de Chimie, Laboratoire d'Océanologie, Université de Liège, SART-TILMAN, B-4000 LIEGE, Belgium.

\* Senior Research Assistant at the National Fund for Scientific Research, Belgium.



### **Abstract.**

During 1980 and 1981 the aerosol burden as well as the wet and dry atmospheric fall-out of Cu, Cd, Pb, Zn, Fe and Mn to the sea have been studied in the Belgian coastal area. Atmospheric Cu, Zn and Cd are observed to be introduced into the sea mainly by wet fall-out, while Fe, Mn and also Pb have a dry and wet fall-out of similar magnitude. Of these elements, Cu, Zn and Cd have the highest washout factors. Furthermore, for all elements, excepted Mn, discrepancies exist between washout factors above land and sea, with values up to 5 times larger above the sea.

On the scale of the North Sea, atmospheric fall-out of Cu, Zn, Pb and Cd exceeds by one order of magnitude the combined input of the rivers Scheldt, Rhine and Meuse, while fall-out of Fe and Mn is of similar magnitude as river input. As concerns the Belgian coastal area, fall-out of Cu, Zn, Pb and Cd is still larger than, but remains within one order of magnitude of the input by the river Scheldt. Here Fe-inputs are of similar magnitude, while fall-out of Mn is 10 times smaller than river input. In this coastal region, characterized by a large residual flow of water coming from the Channel, the total annual input of Cu, Zn, Pb and Cd from the atmosphere and the river Scheldt represents only from 0.8 (Pb) to 3.4 % (Zn) of the annual flow-through of these heavy metals. Furthermore, it is observed that measured enrichments of the sea-surface microlayer, as sampled with the screen method, can support out-fluxes of heavy metals to the atmosphere which are only < 0.1 % of the atmospheric fall-out to the sea.

### **1.- Introduction.**

During the past decade, the atmospheric aerosol burden and the atmospheric fall-out have been studied in the North Sea area from a series of shore based, coastal sampling platforms and a single maritime platform (Peirson et al., 1974; Cambray et al., 1975 and 1979; Kretzschmar and Cosemans, 1979). The importance of the atmosphere as a main transport route of heavy metals to the sea has been stressed by Cambray et al. (1975 and 1979). The predominant source of these heavy metals in the North Sea area is shown to be the industrial activity on the mainland (Kretzschmar and Cosemans, 1979).

In open ocean areas, evidence exists that winddriven material output from the enriched sea surface microlayer to the atmosphere can to some extent determine the composition of the marine aerosol (see for instance Duce et al., 1976; Lantzy and Mackenzie, 1979). However, also as concerns the North Sea, Peirson et al. (1975) consider the winddriven formation of a heavy metal enriched sea spray, as the most plausible process responsible for the increased Na and heavy metal contents in rainwater above the sea, as compared to rainwater above the mainland. Analysis of screen-sampled microlayer and of sea spray artificially produced *in situ* in the North Sea, point towards important enrichments of some heavy metals relative to Na, at the air sea interface (Hunter, 1977; Pattenden et al., 1980).

For the southernmost part of the North Sea and specifically for the Belgian coastal area, no data exist concerning (i) the composition of the marine aerosols, as sampled above the sea and (ii) air-sea exchanges in general.

From January 1980 on we occupied two sampling platforms on an intermittent basis in the Southern Bight and in the Straits of Dover (Dedeurwaerder et al., 1981). Both marine aerosols and atmospheric fall-out were sampled in order to assess: (i) the impact of the industrial activities in the surrounding countries (Belgium, France, Great-Britain) on the Cu, Cd, Pb, Zn, Fe and Mn content of the aerosols above the southernmost part of the North Sea and (ii) the importance of the atmosphere as a transport route of heavy metals to the sea.

Furthermore, the sea-surface microlayer was sampled in the close vicinity of the atmospheric sampling platforms in order to study enrichments of Cu, Pb, Cd and Zn relative to the bulk sea water and to allow an estimation of the sea to air flux for these heavy metals.

## 2.- The sampling and analysis.

### 2.1.- Sampling location.

The positions of both aerosol sampling platforms and microlayer collection sites are given in figure 1. Most samples of marine aerosols and all samples of atmospheric fall-out were taken aboard the lightvessel *West-Hinder*, anchored in the Southern Bight (position:  $51^{\circ} 23' 30''$  N -  $2^{\circ} 21' 30''$  E). On a few occasions marine aerosols were sampled from the research vessel *Mechelen* anchored in the close vicinity of the lightvessel *West-Hinder* and also in the Straits of Dover (Bassurelle light-buoy, position:  $50^{\circ} 33' 24''$  N -  $0^{\circ} 54'$  E) [fig. 1].

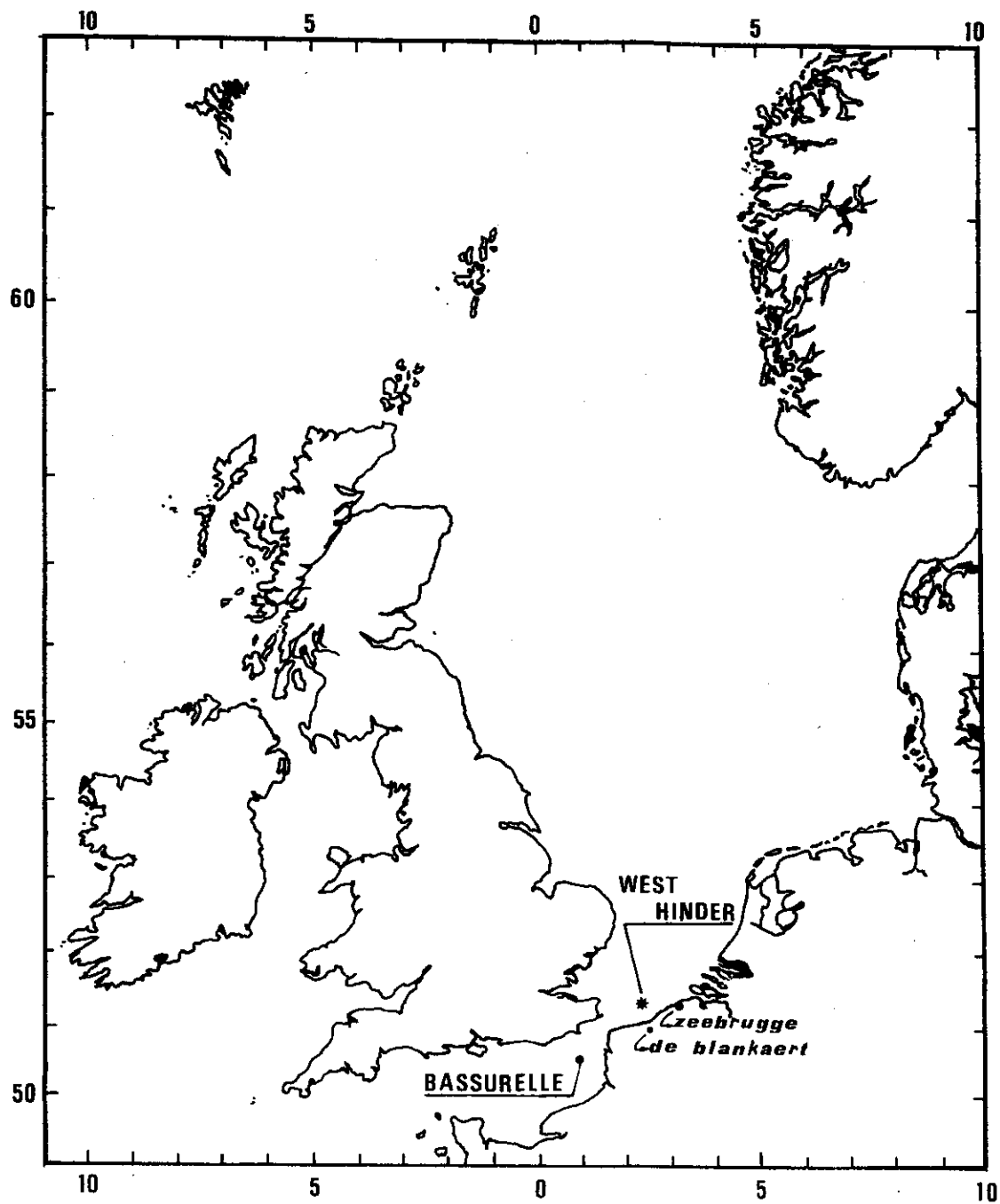


fig. 1.

Positions of both maritime sampling platforms  
West-Hinder ( $51^{\circ} 23' 30''$  N -  $2^{\circ} 21' 30''$  E)  
and Bassurelle ( $50^{\circ} 33' 24''$  N -  $0^{\circ} 54'$  E).

## 2.2.- Aerosol sampling devices and analysis.

Total aerosol burden is sampled with hi-vol samplers ( $\sim 20 \text{ m}^3 \cdot \text{h}^{-1}$ ; velocity of air through the filter :  $58 \text{ cm} \cdot \text{s}^{-1}$ ) by pumping up to  $200 \text{ m}^3$  of air through Whatman 41 cellulose filters. Size fractionated aerosol samples are taken with six stage hi-vol cascade impactors (model Sierra-235). Aerosol collection occurs on five slotted Whatman 41 cellulose substrates and one Whatman 41 cellulose back-up filter. Up to  $1000 \text{ m}^3$  of air are sampled for this purpose. According to the manufacturer, for an air flow of 40 CEM, these impactors separate the particles in the following equivalent aerodynamic diameter classes :  $> 7.2$  ;  $7.2 - 3.0$  ;  $3.0 - 1.5$  ;  $1.5 - 0.95$  ;  $0.95 - 0.49$  ;  $< 0.49 \mu\text{m}$ . The Whatman 41 cellulose substrates are subsequently acid mineralized and the heavy metal contents determined by flame- and electrothermal-AAS.

Up to now, 10 sampling campaigns of two full weeks each were conducted aboard the lightvessel *West-Hinder*, providing us with a total of 78 samples.

## 2.3.- Fall-out sampling and analysis.

The atmospheric dry fall-out is collected on vertically suspended vaselinated plexiglass surfaces of  $400 \text{ cm}^2$  for periods of 12 days. In the laboratory, the vaseline is transferred to a Whatman 41 cellulose filter and is extracted with petroleum ether in a soxhlet apparatus. The Whatman filter with the collected atmospheric dust is then acid mineralized and analysed by flame- and electrothermal-AAS.

Wet atmospheric fall-out is manually collected in acid cleaned polyethylene funnels ( $\phi 18 \text{ cm}$ ) and containers. No attempt was undertaken to filter the rain water as evidence exists that the dissolved phase is the predominant one for all heavy metals of interest (Nguyen *et al.*, 1979). Heavy metal content is measured directly on the untreated rain water samples by flame- or electrothermal-AAS.

Up to now, 8 dry fall-out samples and 15 rainwater samples were taken aboard the *West-Hinder*.

## 2.4.- Microlayer sampling and analysis.

The microlayer is sampled using the Garrett screen technique (Garrett, 1967). The screen consists of an all plexiglass frame stretching a nylon net with a mesh aperture of  $400 \mu\text{m}$  and a fabric thickness of  $440 \mu\text{m}$ .

The sampling is done from a rubber boat at about 1 km upstream from the research-vessel. The operator wears polyethylene gloves and touches the sea surface with the screen in horizontal position.

The collected fractions (about 50 ml each) are then drained into acid cleaned polyethylene containers. For each sampling, about 2 liters of microlayer are collected in this way. At each microlayer sampling site the watercolumn is sampled by immersion of polyethylene containers at - 30 cm.

Once aboard, the samples are immediately deep-frozen.

For the analysis mode of the dissolved and particulate microlayer and bulk sea-water phases, see G. Gillain *et al.* (1982) and Dedeurwaerder *et al.* (1981).

### 3.- Results.

#### 3.1.- Wet and dry fall-out.

The mean values (geometric means) of heavy metal concentrations in marine aerosols (total aerosol and cascade impactor samples for 1980 and 1981 combined) and in rainwater collected at sea are given in table 1, columns 1 and 2.

The annual wet fall-out is given by the product of the mean concentration in rainwater with the annual precipitation above the sea. It is this latter variable which induces most of the uncertainty in the values of heavy metals wet fall-out. Indeed, since no systematic record of precipitation at sea exists for the Southern Bight and since our samplings were only done intermittently, no complete and satisfactory information exists on this matter.

To our knowledge, the only continuous, one-year lasting record of rainfall over the North Sea was done by Cambray *et al.* (1975). These authors observed that rainfall at sea was only about 55 % of the amount collected at land-based stations located at similar latitude. The Royal Meteorological Service of Belgium recorded for 1980 at the Coastal stations Zeebrugge and Kokzijde, respectively, a precipitation of 731 mm and 659 mm. Taking 55 % (see Cambray *et al.*, 1976) of these values, gives an annual precipitation at sea of 362 to 402 mm, with a mean value of 382 mm. Using this mean value and our mean data for heavy metal concentrations in rainwater, we calculated the wet fall-out for the different heavy metals (table 1, column 4).

The measured dry fall-out is given in table 1, column 3. From table 1, it appears that Pb, Fe and Mn have wet and dry fall-out rates, which are similar (Pb, Fe) agree within one order of magnitude (Mn). For Cu, Zn and Cd, wet fall-out

Table 1  
Heavy metal content in air and rainwater  
and heavy metal wet- and dry fall-out above the Southern Bight

Element	(1) Concentration in air		(2) Concentration in rain		(3) Dry fall-out		(4) Wet fall-out
	ng/m <sup>3</sup>	N	μg/l	N	ng/cm <sup>2</sup> .yr	N	ng/cm <sup>2</sup> .yr
Cu	6.5	77	39.5	15	74	8	1509
Zn	86.6	72	193.6	12	411	8	7396
Pb	82.6	75	13.0	10	507	8	497
Cd	2.7	53	3.0	11	4.5	7	114
Fe	250	78	158.9	15	6883	7	6070
Mn	14.6	71	9.5	11	135	8	363

N : number of samples.

is one order of magnitude larger than dry fall-out. This situation is also reflected in the wash-out factors, being the ratios of rainwater over air concentrations of the different heavy metals. For Pb, Fe and Mn, wash-out factors are  $< 1 \times 10^6$ , while for Cu, Zn and Cd they are  $\geq 1 \times 10^6$  (table 2, column 4).

It is furthermore observed that those elements with the largest wash-out factors (Cu, Zn, Cd) have smaller Mass Median Diameter (MMD) values, as deduced from our cumulated aerosol mass distributions (table 2, columns 3 and 4).

Table 2  
Calculated dry and total (wet plus dry) deposition velocities,  
wash-out factors and observed mean mass median diameters (MMD)  
for the considered heavy metals

Element	(1) Dry deposition velocities cm/s	(2) Total (wet + dry) deposition velocities cm/s	(3) Mean M.M.D. μm	(4) Wash-out factor ( $\times 10^6$ )
Cu	0.36	7.75	0.59	6.11
Zn	0.15	2.85	0.28	2.24
Pb	0.19	0.39	0.71	0.16
Cd	0.05	1.40	0.53	1.12
Fe	0.87	1.60	1.58	0.64
Mn	0.29	1.08	0.72	0.65



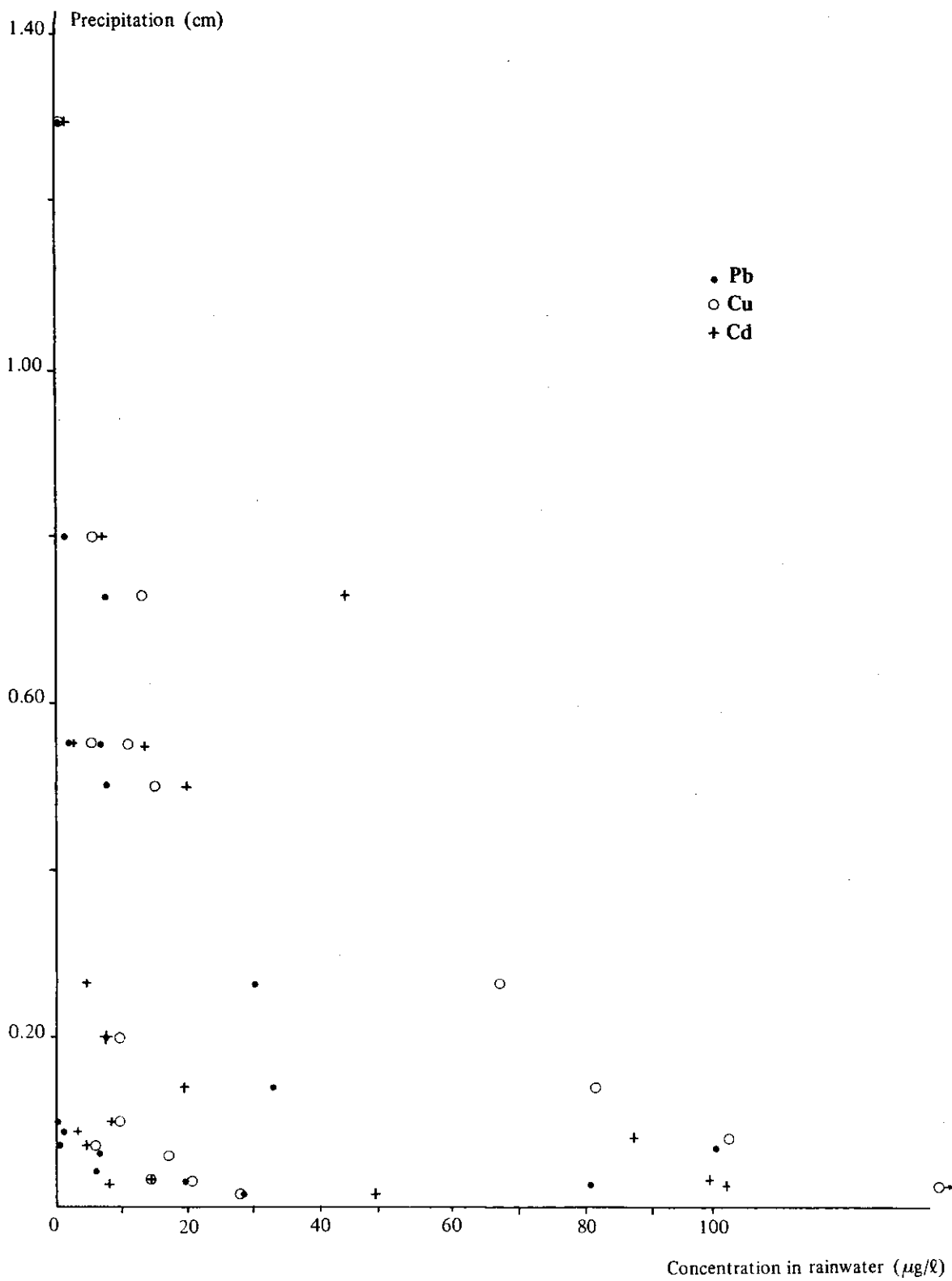


fig. 2.  
Concentrations of dissolved Pb, Cu and Cd (in  $\mu\text{g}/\ell$ )  
in rainwater against collected precipitation

Although it appears that differences exist between elements as concerns the efficiency of their rain-out, the clean-up of the atmosphere is done mostly by the very first fraction of rainfall. Indeed, an exponential-like decrease of heavy metal concentration with increase of precipitation was observed (figure 2). This also indicates a continuous dilution of the concentrated primary rainfall, such as observed by others (see for instance Nguyen *et al.*, 1979).

Dry deposition velocities and total (wet + dry) deposition velocities given by the ratio of dry and total fall-out over the content in air, are given in columns 1 and 2 of table 2. Dry deposition velocities range from 0.15 (Zn) to 0.87 (Fe)  $\text{cm.s}^{-1}$  and total deposition velocities from 0.39 (Pb) to 7.75 (Cu)  $\text{cm.s}^{-1}$ .

From their studies on the  $^7\text{Be}$  distributions in the surface waters of the world oceans and the lower troposphere, Young and Silker (1980) emphasized the important role of the aerosols as the carriers of  $^7\text{Be}$  to the ocean surface. By assuming the validity of the steady state assumption that radioactive desintegration of  $^7\text{Be}$  in the watercolumn is compensated for by wet and dry fall-out to the oceans of  $^7\text{Be}$  associated with the smaller aerosols ( $< 1 \mu\text{m}$ ), Young and Silker deduced a mean aerosol deposition velocity of 0.85  $\text{cm.s}^{-1}$ .

From table 2, it appears that only Pb, Cd, Fe and Mn have total deposition velocities close to the  $^7\text{Be}$  value (deviations are not larger than a factor 2). On the contrary, Zn and Cu have total deposition velocities which are respectively 3.4 and 9.1 times larger than the  $^7\text{Be}$  value. These two elements also have the largest wash-out factors.

However, from table 2 (column 4), it is apparent that all elements, with the exception of Fe, have MMD values  $< 1 \mu\text{m}$  as required the  $^7\text{Be}$  model.

It therefore appears that essentially two factors determine the "fitting" of an element to the  $^7\text{Be}$ -model: (1) the MMD value and (2) the solubility of the element in rainwater. Those elements which fit best to the  $^7\text{Be}$ -model not only have a MMD  $< 1 \mu\text{m}$ , but are also relatively poorly soluble in rainwater; this is the case for Pb and Mn.

### 3.2.- Rain above land and sea: differences in heavy metal content.

During June and September 1981, the sampling campaigns aboard the *West-Hinder* were paralleled by sampling campaigns on land (station "De Blankaert", figure 1), at 25 km from the coastline.

Although concentrations of Cu, Zn, Cd, Pb, Fe and Mn in air above sea are similar or lower than above land, it is observed that such as for Na, the rainwater content of these elements is higher above sea than above land, with the exception of Mn which shows similar concentrations (table 3).

Table 3  
Comparison between heavy metal content (geometric mean values)  
in rainwater and wash-out factors above land and sea

	Cu	Zn	Pb	Cd	Mn	Fe	Na
Concentration in rainwater ( $\mu\text{g}/\ell$ )							
Sea : West-Hinder (N = 15)	39.5	194	13	3	9.5	159	17154
Land : De Blankaert (N = 8)	5.9	91.5	3	1.5	8.9	44.6	446
Wash-out factors ( $\times 10^6$ )							
Sea : West-Hinder	6.10	2.24	0.16	1.11	0.65	0.64	9.38
Land : De Blankaert	1.02	1.20	0.05	0.63	0.46	0.12	-

A similar discrepancy between land- and sea-based sampling platforms was observed in the North Sea by Peirson *et al.* (1974) and Cambray *et al.* (1975). These authors considered that the reduced rainfall at sea alone could not account for the magnitude of the observed enrichments. Therefore, they attributed the enhanced heavy metal content in rainwater above the sea to a contribution from sea spray as indicated by the much enhanced Na content. They concluded that this sea spray should be derived from a strongly enriched sea-surface microlayer. However, as discussed below under point 3.4, the heavy metal output from the sea-surface to the atmosphere, as based on our microlayer enrichment data is negligible compared to the atmospheric input. Therefore, other processes must be considered in order to explain the higher rainwater contents above sea.

When comparing the wash-out factors we obtained for the sea-based station with those obtained for the land-based station (table 3), it appears that these factors are larger at sea for all considered elements, excepted again Mn. This suggests a greater solubility of the aerosols above sea. Therefore, considering the fact that the largest fraction of the marine aerosols are in fact land-derived, it might well be that the chemical transformation

Table 4  
 Heavy metal input in the North Sea (surface :  $5.3 \cdot 10^5$  km<sup>2</sup> ; Cambray et al., 1975)  
 Comparison between atmospheric contribution and river contribution  
 Values of atmospheric fall-out are based on the data of table 1

Element	Wet + dry atmospheric fall-out in t/yr		River input in t/yr					Input by rivers t/yr	
	This work	Cambray et al. (1975)	Scheldt A		Rhine B	Rhine + Meuse C	(4)	min.	max.
			(1)	(2)					
Cu	8390	4850 *	12	62	730	389	401	792	
Zn	41234	47435	28 *	320 (200 *)	7060	3015	3335	7380	
Pb	5321	14045	12	31	2000	444	456	2031	
Cd	628	228 **: :	2.1	1.6 *	77	53	55	79	
Fe	68651	134100	1458	2122	46080	-	47538	48202	
Mn	2639	4876	103 **	700 (400 **)	6000 (5)	-	6700	-	

- No data

(1) Baeyens et al. (1982); dissolved + suspended load.

(2) Wollast (1976) and Duinker et al. (1979); dissolved + suspended load.

(3) Based on data of Duinker and Nolting (1976 and 1979); dissolved + suspended load.

(4) Based on data of Salomons and Eysink (1979); dissolved + suspended load.

(5) Weichart (1973).

\* Dissolved load only.

\*\* Suspended load only.

::: Maximum value.

::: Minimum value.

the aerosols undergo during their aging process, as well as differences in physico-chemical characteristics of rainwater above land and sea, are responsible for this enhanced solubility.

The way to handle this problematic would be to compare the chemical composition of the discrete aerosols particles and the rainwater characteristics above land and sea.

### 3.3.— The atmospheric heavy metal input into the Belgian coastal zone, as compared to river input.

In table 4, the atmospheric fall-out (wet + dry) to the entire North Sea (surface :  $5.3 \times 10^5 \text{ km}^2$  ; Cambray *et al.*, 1975) is compared with inputs through the rivers Rhine, Scheldt and Meuse, as given in the literature. Our fall-out data are compared with those obtained by Cambray *et al.* (1975) for the North Sea area. Both sets of data agree within a factor 3, justifying the extrapolation of our fall-out data to the entire North Sea.

From table 4, it appears that atmospheric fall-out for Cu, Zn, Pb and Cd is up to one order of magnitude larger than the input by the main rivers entering the North Sea. On the contrary, fall-out of Fe and Mn is of the same order of magnitude as river input.

Table 5  
Impact of the atmospheric heavy metal fall-out and the heavy metal input through the river Scheldt on the watermass in the Belgian coastal area

Element	A Average dissolved + particulate conc. in the watercolumn (1)	B Flow through zones A + B (figure 3) (2)	C Atmospheric input (3)		D River Scheldt. input (dissolved + particulate) (4)	
	$\mu\text{g/l} = \text{t}/\text{km}^3$	t/yr	t/yr	C/B in %	t/yr	D/B in %
Cu	2.23	10454	175	1.7	62	0.6
Zn	7.330	34363	859	2.5	320	0.9
Pb	3.921	18382	111	0.6	31	0.2
Cd	0.121	567	13	2.3	2.1	0.4
Fe	-	-	1431	-	2122	-
Mn	-	-	55	-	700	-

(1) Data from Decadt *et al.* (1982).

(2) The water flow is  $4\,688 \text{ km}^3$  (see text; Podamo, 1973).

(3) This study, the considered surface is  $11\,050 \text{ km}^2$  (see figure 3).

(4) Data from Wollast (1976) and Baeyens *et al.* (1982); see table 4.

- No data.

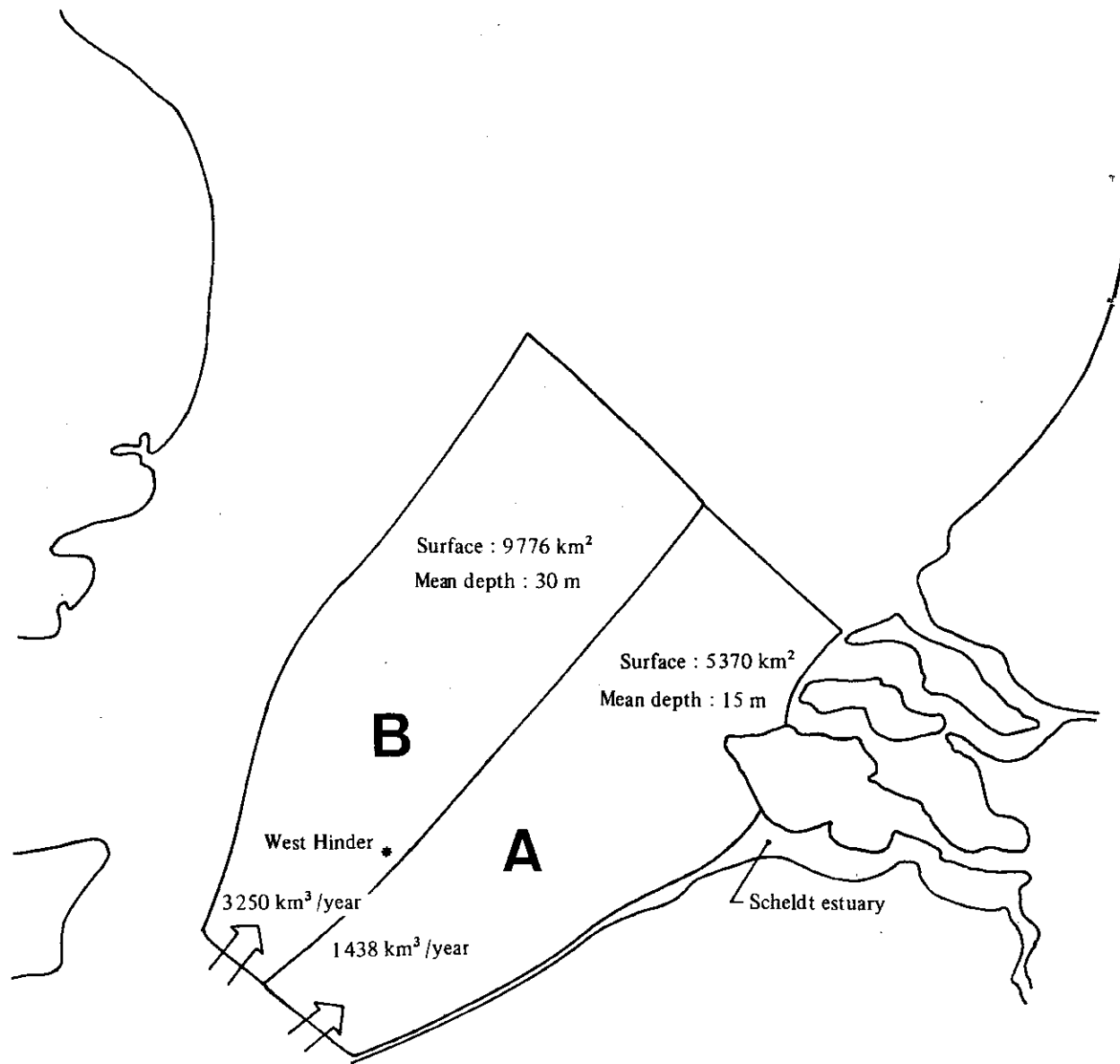


fig. 3.

Characteristics (residual flow, mean depth and surface) of the coastal environment in the Southern Bight for which the impact of atmospheric fall-out and river input is compared to the magnitude of the heavy metal flow through due to the residual flow.

We have also compared the relative inputs by the atmosphere and river run-off in the Belgian coastal environment. The considered area consists of zone 1S and half of zone 2 of the sampling network of the former "National R.D. program *Sea*" (figure 3; Podamo, 1973). The area covers 11 050 km<sup>2</sup> and includes the Scheldt

estuary. The residual flow for zone A (mean depth 15 m) is  $1\,438\text{ km}^3.\text{yr}^{-1}$  and for zone B (mean depth 30 m)  $3\,250\text{ km}^3.\text{yr}^{-1}$  (see figure 3; Podamo, 1973).

The product of this residual flow with the mean particulate plus dissolved heavy metal load in the Belgian coastal environment (table 5, column A) gives the heavy metal transport through the considered zone (table 5, column B). The values of the combined dissolved and suspended loads of Cu, Zn, Pb and Cd used here are the geometric means of the values found for zones II and IV in Decadt *et al.*, (1982). Since no sufficient data exist for the watercolumn load of Mn and Fe in the Belgian coastal area, the transport of these elements resulting from the residual flow was not considered. From table 5, columns C and D, it is seen that the atmospheric impact is much less apparent in this reduced environment affected by the run-off of the river Scheldt. Nevertheless, it is clear that even in this environment the atmospheric fall-out of Cu, Zn, Pb and Cd is still up to 5 times larger (case of Cd) than river input. On the contrary, for Fe and Mn, atmospheric fall-out is similar (Fe) or one order of magnitude lower (Mn) than the river input.

### **3.4.— The heavy metal output from the sea-surface microlayer to the atmosphere.**

#### **3.4.1.— The heavy metal enrichment in the sea-surface microlayer.**

Particulate output from the sea to the atmosphere occurs by sea spray formation. As this process affects the sea-surface microlayer, it is important to know the extent of the element enrichment in this layer. During 1980 and 1981, the microlayer was sampled in the vicinity of the *West-Hinder* and the *Bassurelle* sampling platforms.

The enrichment of the microlayer relative to the bulk seawater is discussed elsewhere (Dehairs *et al.*, 1982). In table 6, the observed average heavy metal concentrations (dissolved + particulate) are given relative to a constant Na content.

#### **3.4.2.— The heavy metal output from the sea-surface microlayer to the atmosphere.**

The heavy metal flux from the sea-surface to the atmosphere can be deduced from the known metal concentrations in the microlayer and from the Na amount emitted from the sea-surface. To estimate the emitted Na amount from the sea-surface, we can assume as a first approximation that the largest fraction of the emitted amount reenters the sea by dry and wet fall-out (Chessellet and Buat-Menard, 1972).

Table 6  
Estimated flux of heavy metals from the sea-surface to the atmosphere

Element (Number of samples)	Ratio of dissolved + particulate conc. over Na conc. in the microlayer $\times 10^{-8}$ (1)	Enrichment (ML/BSW) of total concentrations (1)	Sea-surface to atm. output $(= \frac{\text{element}}{\text{Na}} \times \text{Na output})$ ng/cm <sup>2</sup> ·yr	Ratio of sea-surface output over total atm. input (see table 1) $\times 10^{-4}$
Cu (17)	39	7.9	0.39	2.5
Zn (2)	260	5.3	2.6	3.3
Pb (diss. 2, part. 17)	32	5.1	0.32	3.2
Cd (17)	3.9	3.9	0.039	3.3
Hg (12)	0.49	1.7	0.0049	-

(1) As given in Dehairs et al. (1982).

Na content = 109/liter,  
Na output taken as 1 mg/cm<sup>2</sup>·yr (see text).

ML = microlayer.

BSW = bulk sea-water.



Similarly, for the area of interest we have observed that for the land-based station "De Blankaert", Na in rainwater is in average only 2 % of the Na content collected in rainwater at sea in the same period. Our data on the Na content in rainwater and on the dry deposition of Na collected at sea, allow to compute a Na fall-out  $> 0.65$  and  $\leq 1.03$   $\text{mg.cm}^{-2}.\text{yr}^{-1}$ . This flux is similar to the average value found by Cambray *et al.* (1979) for total Na fall-out in the North Sea area ( $1.1 \text{ mg.cm}^{-2}.\text{yr}^{-1}$ ) and to the value of Na-emission from the sea-surface ( $1 \text{ mg.cm}^{-2}.\text{yr}^{-1}$ ) given by Erikson (1959). Therefore, we will consider here a Na emission of  $1 \text{ mg/cm}^{-2}.\text{yr}^{-1}$ . The heavy metal outflux is thus calculated as :

$$\left( \frac{[\text{Element}]}{[\text{Na}]} \right)_{\text{ML}} \times \text{Na-outflux} .$$

It is assumed here that no fractionation between heavy metals and Na occurs during sea spray formation. The outflux values are given in table 6. They are about 4 orders of magnitude smaller than our atmospheric fall-out values. However, it is probable that our observed enrichments in the microlayer are underestimated, due to possible dilution of the samples with bulk seawater during the sampling and which is inherent to the Garrett-screen sampling technique. Indeed, other microlayer sampling methods, using bubble-burst techniques suggest for Pb and to a lesser extent for Zn in the North Sea microlayer, enrichments relative to Na which are respectively 100 and 5 times greater than our values (Pattenden *et al.*, 1981).

#### 4.- Conclusions.

This study has shown that the atmospheric input of the heavy metals Cu , Zn , Pb and Cd to the North Sea exceeds the river input, even in a restricted, coastal environment fed by river run-off. For Fe , the inputs from rivers and atmosphere are of similar strength, while atmospheric input of Mn is observed to be less important than river input in the coastal environment.

For Cu , Zn and Cd , the atmospheric input to the sea is essentially carried by wet fall-out, while for Pb , Fe and Mn , wet and dry fall-out are of similar strength.

The fact that Cu , Zn and Cd leave the atmosphere mainly by wet fall-out is due to their greater solubility in rainwater as indicated by their larger wash-out factors. Some evidence exists that this greater solubility may in part be favored by the association of Cu , Zn and Cd are with the smaller aerosols (MMD's are  $\leq 0.59 \mu\text{m}$ ), as compared to Pb , Fe and Mn (MMD's are  $\geq 0.71 \mu\text{m}$ ). Besides differences in rainwater solubility between elements, there also exist land to sea differences

in wash-out factors for the individual elements, with the exception of Mn. Although this can partly be explained by the fact that rainfall is less at sea, and should therefore be more concentrated in heavy elements than rainfall above land, other factors, such as a varying chemical composition of the aerosol and varying physico-chemical characteristics of rainwater itself, should be considered.

The enhanced heavy metal content of rainwater above the North Sea is not likely to result mainly from the incorporation in rainwater of a heavy metal enriched sea-spray, derived from the enriched sea-surface microlayer, as proposed by others. Evidence for this is given by the relatively small enrichments we observed in the microlayer in this part of the North Sea and the resulting small heavy metal outflux to the atmosphere compared to the atmospheric input (output < 0.1 % of input). However, the question concerning the real microlayer enrichments is still unresolved, as evidence exist from other studies in the North Sea that microlayer enrichments based on the screen sampling method used here might be underestimated.

#### References.

- BAEYENS, W., DEHAIRS, F., DECADT, G., WARTEL, S., BOGAERT, M., GILLAIN, G., DEDEURWAERDER, H., (1982). *Distribution, transport and fate of Bi, Cu, Cd, Hg, Pb, Sb and Zn in the Belgian coastal marine environment, Part 4, The river Scheldt as a transport route of heavy metals to the sea*, in A. Distèche and I. Elskens (Eds.), *Programmatie van het Wetenschapsbeleid*, Brussel (Belgium), in press.
- CAMBRAY, R.S., JEFFERIES, D.F. and TOPPING, G., (1975). An estimate of the input of atmospheric trace elements into the North Sea and Clyde Sea 1972-73, *AERE report R 7733*, 30 pp.
- CHESSELET, R., MORELLI, J. and BUAT-MENARD, P., (1972). *Some aspects of the geochemistry of marine aerosols*, in *The changing chemistry of the oceans, Nobel Symposium 20*, D. Dyrssen and J. Jagner (Eds.), J. Wiley Inc. N.Y., pp 93 - 114.
- DECADT, G., GILLAIN, G., DEHAIRS, F., DEDEURWAERDER, H., GOEYENS, L. and BAEYENS, W., (1982). *Distribution, transport and fate of Bi, Cu, Cd, Hg, Pb, Sb and Zn in the Belgian coastal marine environment, Part 2, Spatial, temporal and compartmental distribution in the watercolumn*, in A. Distèche and I. Elskens (Eds.), *Programmatie van het Wetenschapbeleid*, Brussel (Belgium), in press.
- DEDEURWAERDER, H., DEJONGHE, M., DEHAIRS, F. and DECADT, G., (1981). *Studie van de immisiewaarden en het transport van zware metalen boven de Noordzee*, Nationaal R. D. programma Leefmilieu - Lucht, Eindrapport, Tak Transferten, 135 pp.

- DEHAIRS, F., DEDEURWAERDER, H., DECADT, G., DEJONGHE, M., GILLAIN, G., BAEYENS, W., (1982). *Distribution, transport and fate of Bi, Cu, Cd, Hg, Pb, Sb and Zn in the Belgian coastal marine environment, Part 3, The marine atmosphere as a transport route of heavy metals to the sea*, in A. Distèche and I. Elskens (Eds.), *Programmatie van het Wetenschapsbeleid*, Brussel (Belgium), in press.
- DUCE, R.A., HOFFMAN, G.L., RAY, B.J., FLETCHER, I.S., WALLACE, G.T., FASCHING, I.L., PIOTROWICZ, S.R., WALSH, P.R., HOFFMAN, E.J., MILLER, J.R. and HEFTER, J.L., (1976). *Trace metals in the marine atmosphere: sources and fluxes*, in *Marine pollutant transfer*, H.L. Windom and R.A. Duce (Eds.), Lexington books, D.C. Heath and Co., Lexington, Toronto, pp. 77-119.
- DUINKER, J.C. and NOLTING, R.F., (1976). Distribution model for particulate trace metals in the Rhine estuary, Southern Bight and Wadden Sea, *Neth. J. Sea Res.*, 10, 71-102.
- DUINKER, J.C. and NOLTING, R.F., (1977). Dissolved and particulate trace metals in the Rhine estuary and the Southern Bight, *Mar. Pollut. Bull.*, 4, 65-71.
- DUINKER, J.C., WOLLAST, R. and BILLEN, G., (1979). Behaviour of manganese in the Rhine and Scheldt estuaries, Part II, Geochemical cycling, *Est. Coast. mar. Sci.*, 9, 727-738.
- ERIKSON, E., (1959). The yearly circulation of chloride and sulfur in nature, meteorological, geochemical and pedological implications. Part I, *Tellus*, 11, 375.
- GARRETT, W.D., (1967). The organic chemical composition of the ocean surface, *Deep-Sea Res.*, 14, 221.
- GILLAIN, G., DECADT, G., DEHAIRS, F., DEDEURWAERDER, H., GOEYENS, L. and BAEYENS, W., (1982). *Distribution, transport and fate of Bi, Cd, Cu, Hg, Pb, Sb and Zn in the Belgian coastal marine environment, Part 1, Sampling techniques and analysis methods*, in A. Distèche and I. Elskens (Eds.), *Programmatie van het Wetenschapsbeleid*, Brussel (Belgium), in press.
- HUNTER, K.A., (1977). *Chemistry of the sea surface microlayer*, Ph. D. Thesis, University of East Anglia, 363 pp.
- KRETZSCHMAR, J.G. and COSEMANS, G., (1979). A five year survey of some heavy metal levels in air at the Belgian North Sea coast, *Atmospheric environment*, 13, 267 - 277.
- LANTZY, R.J. and MACKENZIE, F.T., (1979). Atmospheric trace metals: global cycles and assesement of man's impact, *Geochim. Cosmochim. Acta*, 43, 511 - 525.
- NGUYEN, V.D., VALENTA, P. and NURNBERG, H.W. (1979). Voltammetry in the analysis of atmospheric pollutants, *Sci. Total Environ.*, 12, 151-167.
- PATTENDEN, N.J., CAMBRAY, R.S. and PLAYFORD, K., (1981). Trace and major elements in the sea-surface microlayer, *Geochim. Cosmochim. Acta*, 45, 93-100.
- PEIRSON, D.G., CAWSE, P.A. and CAMBRAY, R.S., (1974). Chemical uniformity of airborne particulate material, and a maritime effect, *Nature*, 251, 675-679.

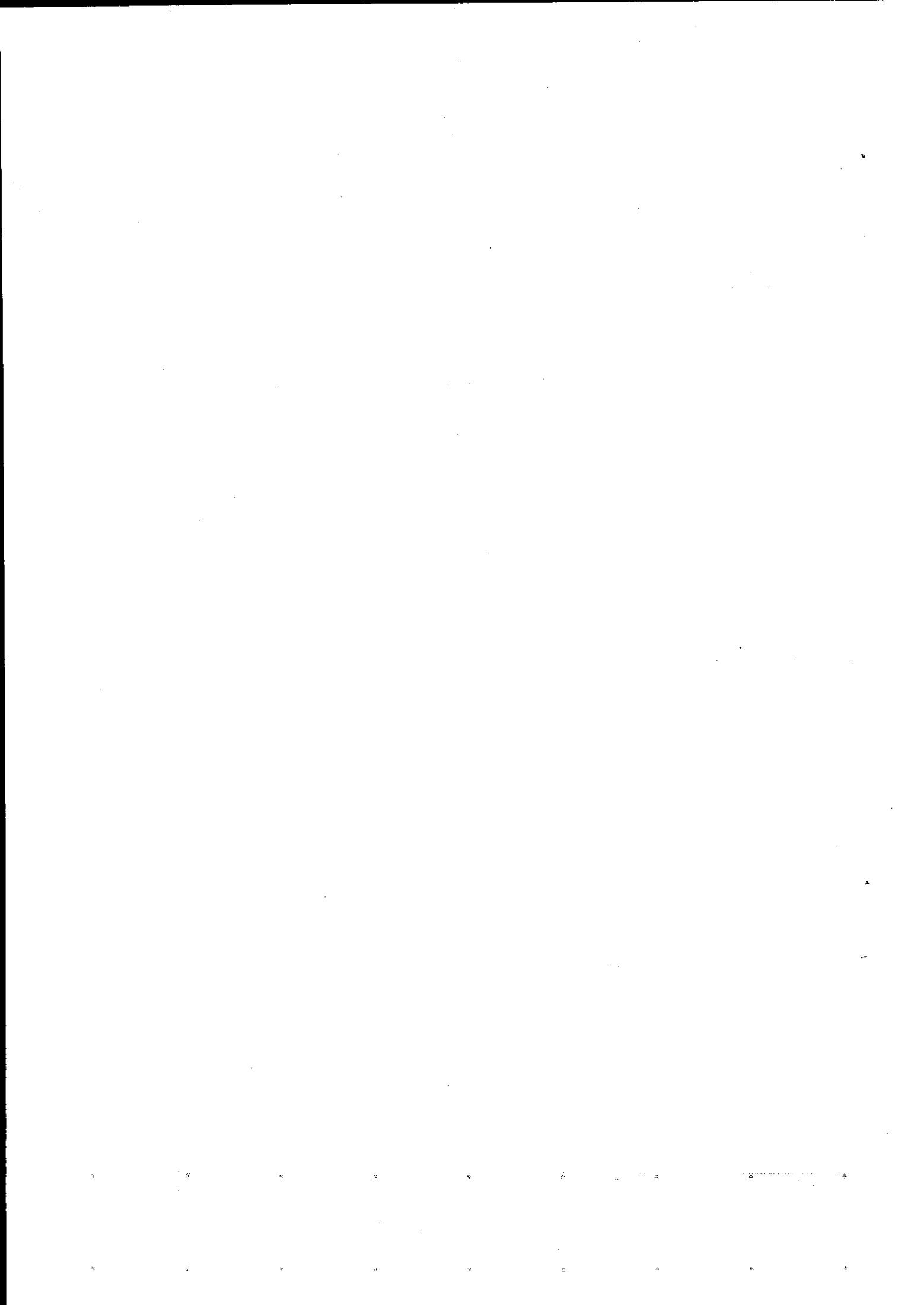
- PODAMO, J., (1973). *Aspects of dynamic biology in the Southern Bight of the North Sea and the Sluice dock at Ostend*, in *Mathematical Model, Annual Report*, National R.D. Program on the environment water, pp. 187-257.
- SALOMONS, W. and EYSINK, W.D., (1979). Pathways of mud and particulate trace metals from rivers to the southern North Sea, Int. Meeting on Holocene Marine Sedimentation in the North Sea Basin, Texel, The Netherlands, (Report, 36 pp.).
- WEICHART, G., (1973). Pollution of the North Sea, *Ambio*, 2, 99-106.
- WOLLAST, R., (1976). *Transport et accumulation de polluants dans l'estuaire de l'Escaut*, chapitre IV, pp. 191-218, in *L'estuaire de l'Escaut*, J.C.J. Nihoul et R. Wollast (Eds.), *Projet Mer, rapport final*, vol. 10, *Programmation de la politique scientifique*, Bruxelles.
- YOUNG, J.A. and SILKER, W.B., (1980). Aerosol deposition velocities on the Pacific and Atlantic Oceans calculated from Be-7 measurements, *Earth Planet. Sci. Letters*, 50, 92-104.

# **MATHEMATICAL MODELLING FOR EVALUATING WATER QUALITY OF AQUATIC ENVIRONMENTS**

**Martine SOMVILLE**

---

Université Libre de Bruxelles, Laboratoire d'Océanologie, avenue F.-D. Roosevelt, 50, B-1050 BRUXELLES (Belgium).



## 1.- Introduction.

International treaties regulating water quality at Belgian borders are on the point to be laid down. Concerning the Scheldt at the Belgian-Dutch border, the norms asked at low tide will at first be 4 mg/l dissolved oxygen and 4 mg N/l ammoniacal nitrogen. In 1987, they will respectively be raised to 5 mg/l O<sub>2</sub> and 2.3 mg N -NH<sub>4</sub><sup>+</sup>/l .

The mean actual oxygen concentration of the Scheldt at the Belgian-Dutch border can be described by figure 1.

This figure shows on an average the distance from the mouth where samples characterized by 4 mg/l O<sub>2</sub> are observed. The arrows represent the interval estimates at 90 % confidence. Figure 1 shows that 4 mg/l O<sub>2</sub> , *i.e.* the first norm to be respected has hardly never been attained between 1973 and 1978. The place of occurrence of 4 mg/l O<sub>2</sub> is located about 10 km downstreams the Belgian-Dutch border.

This situation is the result of the organotrophic activity which consumes dissolved oxygen to oxidize the organic load carried by the stream and the regeneration of oxygen by natural re-aeration and mixing with seawater.

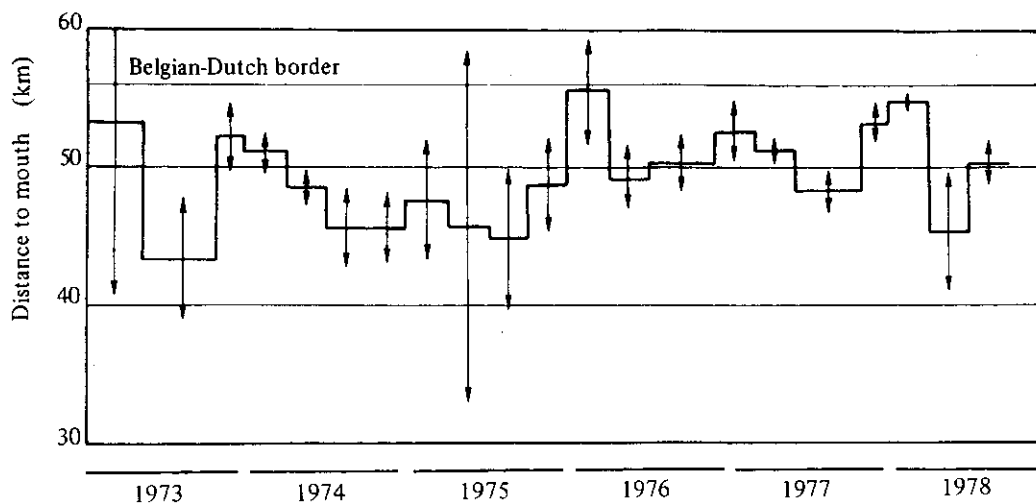


fig. 1.

Evolution with time of the mean oxygen concentration at the Belgian-Dutch border.  
The arrows represent the interval estimates at 90 per cent confidence.

On the other hand, the distribution of ammonium in the Scheldt estuary in the surroundings of the Belgian-Dutch border is governed partly by the dilution of upstreams water, loaded in ammonium, into poor seawater but also by the microbiological process of nitrification which oxidizes ammonium into nitrate (Billen, 1975; Somville, 1978).

The importance of various processes : hydrodynamical, microbiological on the water quality of the Scheldt is then evident. However, the primordial factor affecting water quality is the organic matter concentration, concentration which can be reduced greatly by epuration of domestic and industrial sewages.

A question is then immediately asked : to satisfy the norms fixed by the international treaties, which epuration must be realized ?

Is it sufficient to realize a classical (primary + secondary) treatment or is it necessary to eliminate the nutrients from the effluent, operation which rises considerably the cost of the treatment plan.

The appropriate answer to such problem can be readily obtained by the use of deterministic mathematical models. From initial conditions like organic load, oxygen, nitrogen concentrations, these models can predict water quality of a stream and the influence of environmental parameters on it. They constitute the only approach which summarize the natural processes and therefore are a valuable management tool.

The objectives of this paper is first to describe a physiological model of heterotrophic activity in an ideal river submitted to a punctual organic load.

This model ignoring dispersion processes will however describe a situation comparable with the Scheldt where a high organic load is observed and whose degradation, once the available oxygen exhausted, requires the reduction of other oxidants present in the river :  $\text{MnO}_2$ ,  $\text{NO}_3^-$ ,  $\text{Fe}(\text{OH})_3$  and  $\text{SO}_4^{--}$ .

As shown by the study of Somville and De Pauw (in press) on the evolution of water quality of the Scheldt water on a ten-year period, the hydrodynamics of the estuary influences greatly the water quality. In particular the river discharge is one of parameters determinating the oxygen profile in the Scheldt.

A second mathematical model will thence be presented for the nitrification process.

This simulation will describe the biological process in the self-purification reach of the Scheldt estuary as well as the complex hydrodynamics of the stream.



## 2.- Description of the water quality in the Scheldt estuary.

A typical situation in the Scheldt estuary is described in figure 2. This figure shows, for May 1976, the longitudinal profiles at low tide of mineral species susceptible to be reduced or oxidized by microbiological activity. Following the flow of the river, one can successively observe the oxygen consumption, the production of  $Mn^{++}$  (reduced form of manganese) which never exceed  $0.304 \text{ mg } Mn^{++}/\ell$  which is the solubility of  $MnCO_3$  in fresh water calculated with the free energies tabulated by Garrels and Christ (1965) and Berner (1971) for  $pH = 7.4$  and  $25^\circ C$ . Afterwards, nitrate disappears, reduced iron is produced and a small consumption of sulfate is observed. All these observations correspond to the consumption of oxidants or the production of reducers. Downstreams, the opposite processes occur in the reverse order: rising of sulfate, disappearance of reduced iron, production of nitrate, consumption of reduced manganese and finally reappearance of oxygen due to reaeration of the river.

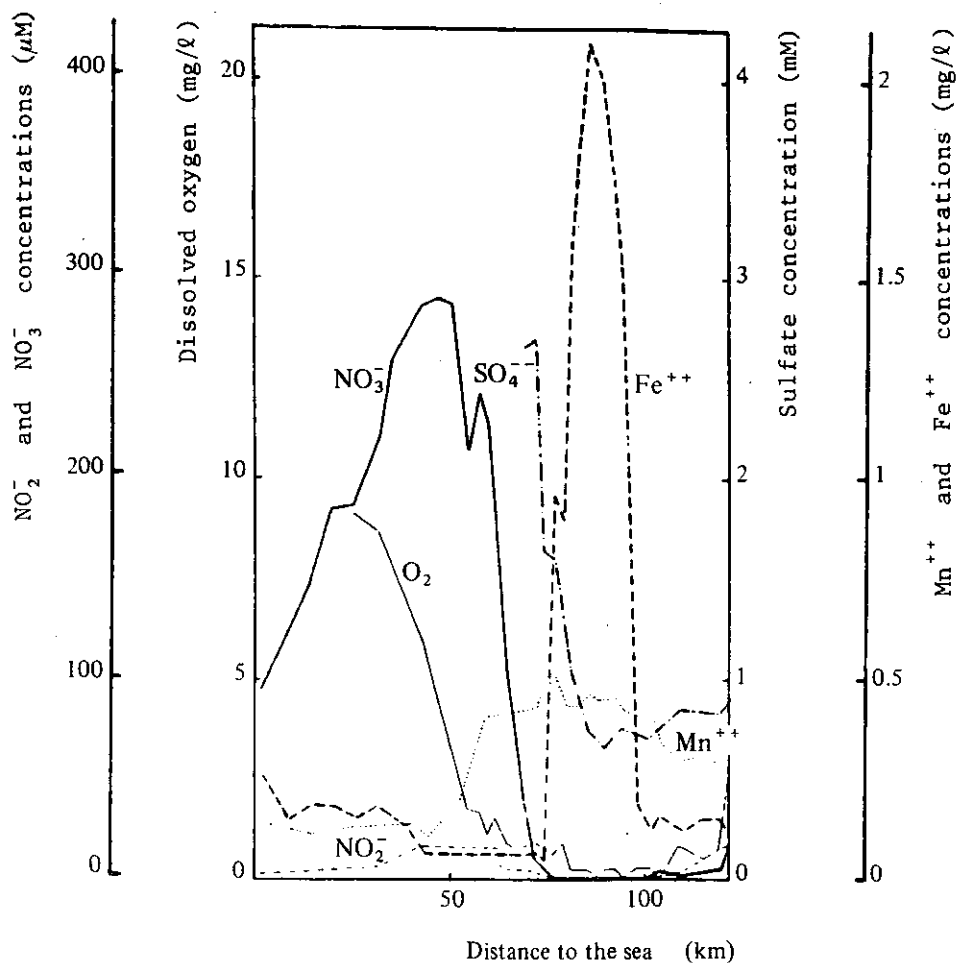


fig. 2.

Longitudinal profiles of  $O_2$ ,  $Mn^{++}$ ,  $NO_2^-$ ,  $NO_3^-$ ,  $Fe^{++}$  and  $SO_4^-$  concentrations at low tide in the Scheldt as a function of the distance to the sea for May 1976

These profiles show that :

- a) the oxygen is rapidly exhausted by aerobic activity and is absent on 30 km ;
- b) when oxygen is absent, heterotrophic activity uses the other oxidants in a definite order :  $\text{MnO}_2$  by mangano-reduction,  $\text{NO}_3^-$  by denitrification,  $\text{Fe}(\text{OH})_3$  by ferro-reduction and  $\text{SO}_4^{--}$  by sulfato-reduction;
- c) downstreams, self-purification processes restore oxidized species in the river : in the order sulfo-oxidation, ferro-oxidation, nitrification and mangano-oxidation.

### 3.- Simulation of organotrophic activity.

The simulation of organotrophic activity in a heavily polluted stream presented below modelates the various microbiological processes pointed out in the Scheldt estuary. The basic principle of the model is that each metabolism occurs in definite conditions of oxygen concentration.

The microbiological activity has been related to the organic load  $C$  carried by the river by the following relation :

$$\text{OA} = B \times a \times f_1(C) \times f_2(t^\circ) \times f_3(\text{Cl}^-) \times f_4(\text{O}_2)$$

where  $\text{OA}$  is the organotrophic activity,  $B$  the corresponding biomass,  $a$  the optimal specific activity, and  $f_1, f_2, f_3, f_4$  are, respectively, functions of organic load ( $C$ ), temperature, chlorinity and oxygen concentration.

The  $f_1$  to  $f_4$  functions have been chosen according to experimental results (Somville, 1980). The principles of the model are graphically represented on figure 3.

Organic carbon  $C$ , present in the stream at km 0, consumed by the organotrophic activity  $\text{OA}$ , is partially oxidized in  $\text{CO}_2$  by the respiratory metabolism  $i$  and partially metabolized by the heterotrophic biomass  $B_i$ . The organic matter oxidation in  $\text{CO}_2$  (OMO) has been expressed by

$$\sum Q_i$$

$Q_i$  corresponding to the oxidation of  $C$  by the metabolism  $i$  according to its particular kinetics.

Organotrophic activity  $\text{OA}$  has been evaluated from the flux of organic matter oxidized in  $\text{CO}_2$  in considering for each metabolism  $i$  the existence of a constant ratio between the biomass synthesis  $C_i$  and the oxidation of the load in  $\text{CO}_2$ . Organic carbon is regenerated by mortality  $M$ .

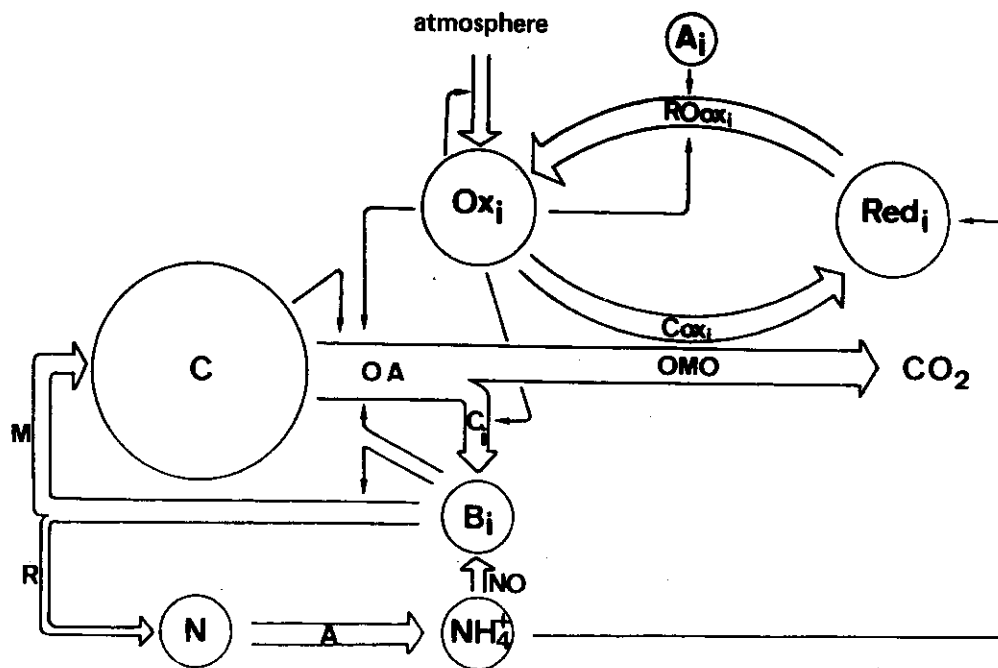


fig. 3.

Principles of the model of organotrophic activity

Organic nitrogen fluxes have been considered proportional to the carbon fluxes : the ammonification A proportional to the organotrophic activity OA , assimilation NO proportional to carbon assimilation C<sub>i</sub> and regeneration R proportional to mortality M by means of the C/N ratio.

The distribution of the oxidants results of their consumption by heterotrophic metabolisms Cox<sub>i</sub> and their regeneration ROox<sub>i</sub> by self-purification and reaeration.

An example of theoretical profiles of organic carbon and oxidants computed by the model are represented on figure 4. This figure shows that the computed profiles reproduce the general trend of experimental profiles measured in the Scheldt estuary : oxidants are consumed in a definite order when the load is high and regenerated in the reverse order during self-purification.

Such a model is particularly interesting for studying the effect of organic carbon concentration on water quality. By example, the effect of the initial load on two parameters often used to assess water quality of a stream has been studied :

- 1) the distance necessary to reobserve 90 % of oxygen saturation;
- 2) the maximum deficit of oxidants in the stream.

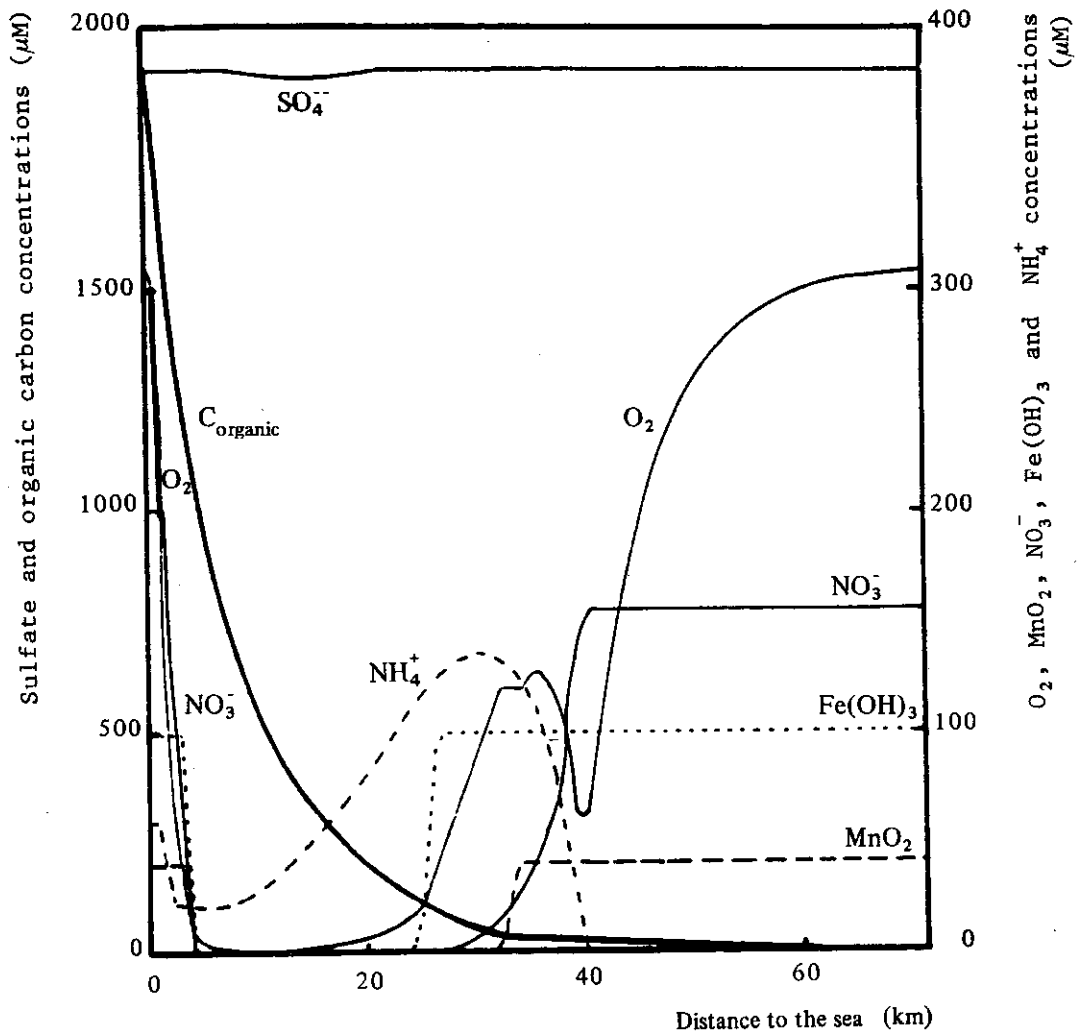


fig. 4.

Calculated profiles of organic carbon, dissolved oxygen,  $\text{MnO}_2$ ,  $\text{NO}_3^-$ ,  $\text{Fe(OH)}_3$ ,  $\text{SO}_4^{2-}$  and  $\text{NH}_4^+$  as a function of the distance from the organic matter discharge

Figure 5 represents both of these parameters as a function of the initial organic load. In this figure, the concentration of the different oxidants ( $\text{O}_2$ ,  $\text{MnO}_2$ ,  $\text{NO}_3^-$ ,  $\text{Fe(OH)}_3$ ,  $\text{SO}_4^{2-}$ ) have been expressed in  $\text{eq e}^-/\ell$  susceptible to be exchanged and summed.

Figure 5 shows that the bigger the organic load the further 90 % oxygen saturation is observed. On the other hand, for small loads, oxygen is sufficient to oxidize the organic matter. For higher loads, the other the oxidants are successively reduced.

Moreover, these results can be extrapolated to the Scheldt estuary. One can evaluate that the biodegradable load in the upstream part of the estuary is actually about  $2000 \mu\text{atg organic C}/\ell$ . For this load, the model predicts (figure 4) the using

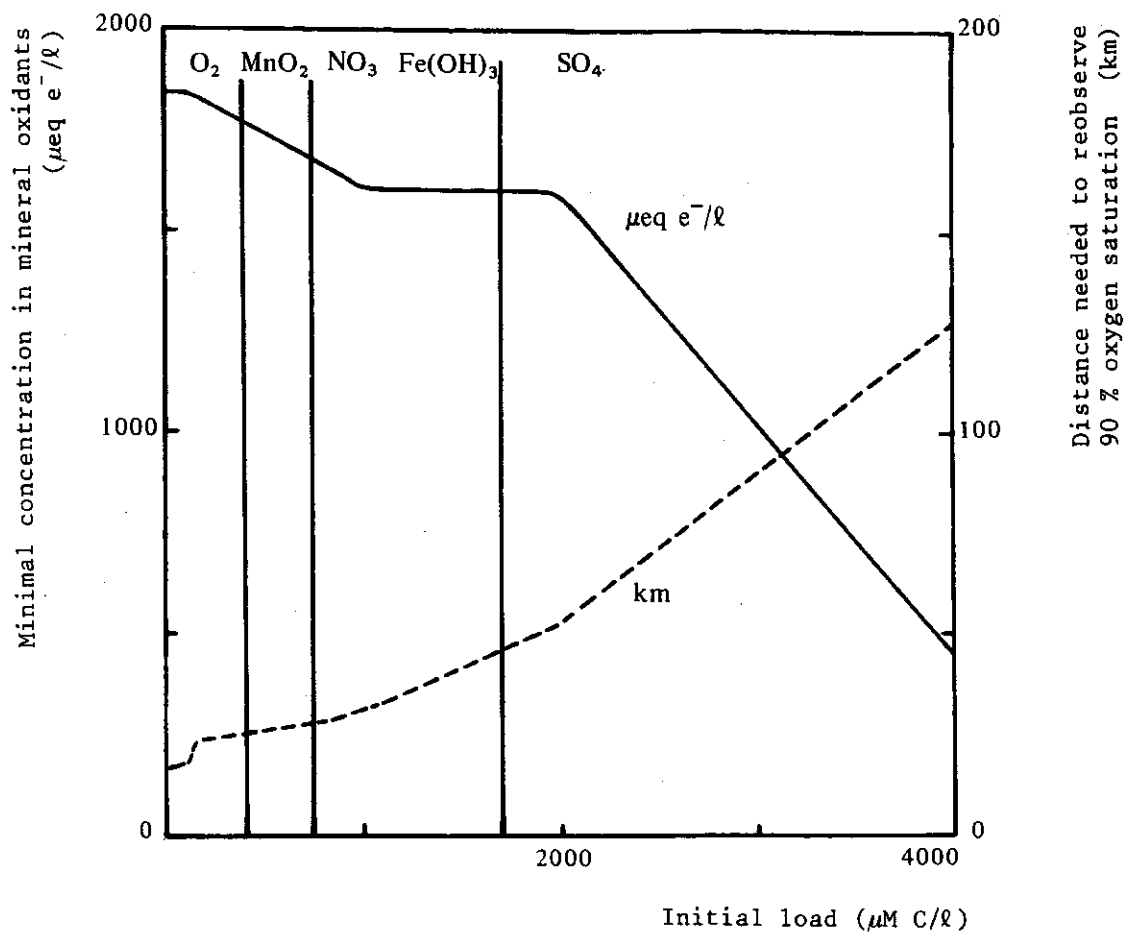


fig. 5.

Evolution of the minimal concentration of oxidants (—) and of the distance necessary to reobserve 90% of oxygen saturation (----) as a function of the initial organic load

up of oxygen,  $\text{MnO}_2$ ,  $\text{NO}_3^-$ . Sulfato-reduction occurs on a small reach of the river. This prediction is comparable with the observations in the upstream part of the Scheldt in summer (figure 2).

The model indicates (figure 5) that for organic loads in the range 1000 - 2000  $\mu\text{atg org C/l}$ , the most important deficit of oxidants does not change. This would further indicate if extrapolation of the ideal model to the Scheldt is correct, that an epuration of 50% of the load of the river, reducing the load to 1000  $\mu\text{atg org C/l}$ , would not improve the oxidants content of the river.

Dissolved oxygen would be regenerated sooner (more upstreams). In the Scheldt, however, regeneration of dissolved oxygen is chiefly governed by the mixing with aerated seawater.

#### 4. – Modelisation of nitrification process in the Scheldt.

##### 4.1. – Determination of ecophysiological parameters.

Two examples of experimental determination of the effect of an environmental parameter : *i.e.* substrate (ammonium) concentration and salinity on nitrifying activity will be described.

##### *Effect of substrate concentration.*

The relation between the potential nitrifying activity of an enrichment culture of nitrifiers and the ammonium concentration is shown on figure 6. This experimental relationship has been represented by a Michaelis-Menten-Monod function :

$$f_2 = \frac{[NH_4^+]}{[NH_4^+] + K_m}$$

with  $K_m$  equal to  $250 \mu M NH_4^+$ .

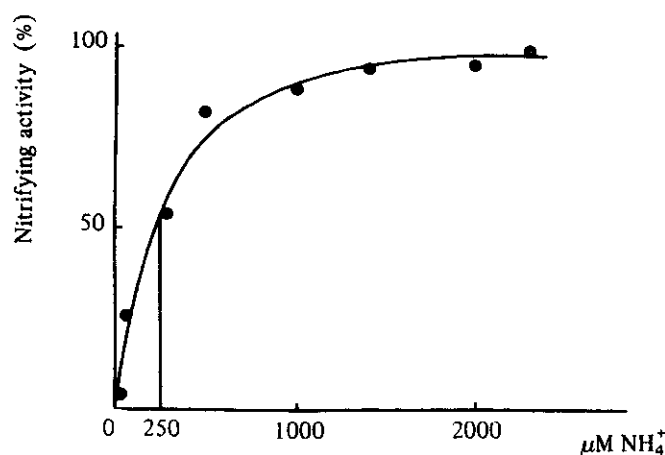


fig. 6.

Relation between the nitrifying activity and the ammonium concentration for an enrichment culture of nitrifiers

##### *Effect of salinity.*

Potential nitrifying activities measured on short term experiments by dark <sup>14</sup>C-incorporation (Somville, 1978) at different places in the estuary have shown that during progressive mixing of fresh into saline water masses, the *in situ* population of nitrifying bacteria tends to adapt itself to the prevailing chloride concentration, with, however, a definite delay (Somville, 1980).

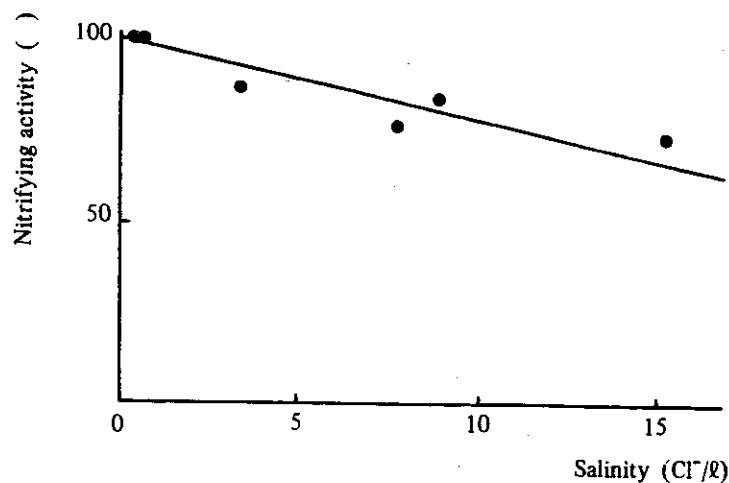


fig. 7.

Relation between the nitrifying activity at optimal salinity and the salinity of the original water mass

The relation found between the salinity of the sample and nitrifying activity at optimal salinity is presented on figure 7. This experimental relation will be modelated by the straight line drawn on figure 7.

#### 4.2.- *The model of nitrification.*

The model of nitrification described below has been realized in collaboration with G. Billen (U.L.B.) and J. Smitz (ULg - Sart Tilman, Liège, Belgium) and has been accepted for publication by Mathematical Modelling.

The hydrodynamics of the Scheldt is described by a simple one dimensional model. The longitudinal distribution of any cross-section-averaged concentration  $c$  can be described by an equation of the form (Nihoul and Ronday, 1976) :

$$\partial c \equiv \frac{\partial}{\partial t} (ac) + \frac{\partial}{\partial x} (auc) - \frac{\partial}{\partial x} [\Lambda \frac{\partial}{\partial x} (ac)] = P - D$$

where  $x$  is the longitudinal coordinate;  $a$  the mean cross-section (calculated as an exponential function of  $x$ , Wollast, 1973);  $u$  the cross-section-averaged residual velocity;  $\Lambda$  the global dispersion coefficient (including effects of tidal motions and other complex hydrodynamical phenomena typical of a partially stratified estuary);  $P$  and  $D$  are, respectively, the rates of production and destruction of  $c$  as a result of physical, chemical or biological reactions;  $c$  is the cross-section-averaged

concentration averaged over some period  $\tau$  larger than the tidal period and  $\mathcal{D}$  represents the hydrodynamical operator.

The computation of the residual velocity  $u$  and of the dispersion coefficient  $\Lambda$  is obtained by the hydrodynamical model of the estuary, the precise calibration being made on the chlorinity concentration profile (chlorinity is a conservative parameter which concentration depends on mixing between saline and fresh water).

In the Scheldt estuary, the upstream water discharge presents slow seasonal changes, and a steady-state assumption is valid for the description of concentrations variations.

The comparison of nitrate flux from Scheldt sediments (Somville, 1980) and of nitrate production by planktonic nitrification (Somville, 1978) has shown that the latter process, accounting for more than 90 % in the nitrate budget, was by far the most important.

These observations have led to consider in the model the nitrification process as the result of planktonic nitrification only.

Growth rate of nitrifiers ( $G$ ) and nitrifying activity ( $A$ ) are considered as proportional to the number of planktonic nitrifying bacteria ( $B$ ) :

$$G = K \times B$$

$$A = \alpha \times K \times B$$

where  $K$  ( $s^{-1}$ ) is the growth constant;  $\alpha$  the quantity of ammonium to be oxidized for duplicating one bacterium, *i.e.* the reciprocal of the yield constant  $Y$  ; and  $B$  the concentration of nitrifiers (bacteria/l).

The value of  $K$  is considered to depend on environmental parameters (namely salinity, ammonium concentration, temperature, redox potential).

The evolution of the nitrifying biomass  $B$  resulting from hydrodynamic processes, growth and mortality effect, can be expressed by :

$$(1) \quad B = KB - mB$$

and the distribution of ammonium and nitrate are then expressed by :

$$(2) \quad [NO_3^-] = \alpha KB$$

$$(3) \quad [NH_4^+] = - \alpha KB$$

$K$  can be expressed by :

$$K = k f_1(S) \times f_2([NH_4^+]) \times f_3(T) \times f_4(Eh)$$



where  $k$  is the optimal growth constant for nitrifying bacteria, and  $f_1, f_2, f_3, f_4$  are respectively functions of salinity, ammonium concentration, temperature, and redox potential; the value of these functions is 1 at optimal conditions.

#### *Solution of the differential equations.*

##### *Boundary conditions.*

For solving equations (1), (2) and (3), a set limit conditions (upstream and mouth water composition) has to be known. In the case of chemical species, ammonium and nitrate, these conditions are obviously the experimental concentrations. In the case of bacterial concentration, boundary conditions can be experimental MNP counts.

Owing to the poor reliability of this largely used numeration method (Tate, 1977; Belser, 1979), it appears necessary to check the accuracy of the nitrifier concentrations by comparing the computed activities ( $\alpha K[B]$ ), based on the possible range of  $\alpha$  and  $K$  values and the experimental bacterial concentration, with the *in situ* activities measured in the stream (Somville, 1978, 1980).

The comparison has shown that the MPN counts obtained in the Scheldt were several orders of magnitude lower than what could be expected from the direct activity measurements. It was therefore decided to evaluate nitrifiers numbers directly from the *in situ* measured activities.

##### *Solution of equations (1), (2), (3).*

Owing to the coupling of equation (1) and equation (3) by means of the ammonium concentration, the first step computes the solution of the bacteria equation (equation 1) using the experimental ammonium profile, previously smoothed.

The complete solution of the problem is calculated by an iterative process adjusting the constant  $\alpha$ . The convergence of the process is quadratic and is obtained after a few loops. The values of  $\alpha$  and  $k$  so determined are in perfect agreement with the literature.

The computed profiles of ammonium, nitrate bacteria and nitrifying activities are represented on figure 8 A and B, respectively, for the situations of February and July 1976 (values of  $\alpha$  and  $k$  used for these simulations are reported in table 1). The corresponding experimental profiles are represented on figure 8 C and D.

The unidimensional mathematical model of the nitrification exposed above describes quantitatively the nitrification process in the Scheldt estuary. With the aid of a limited number of ecophysiological relations, an accurate description of the *in situ* situation is possible.

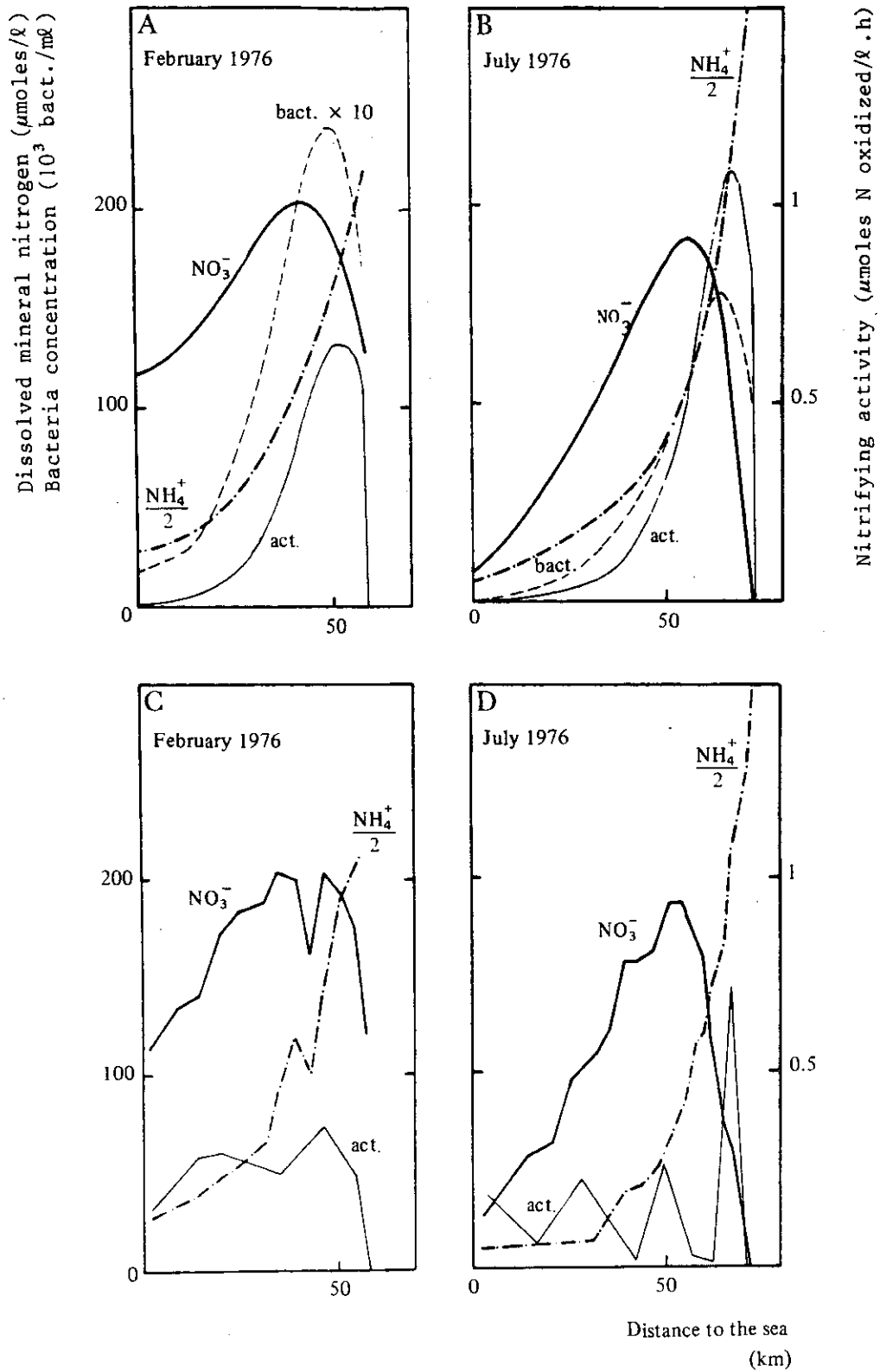


fig. 8.

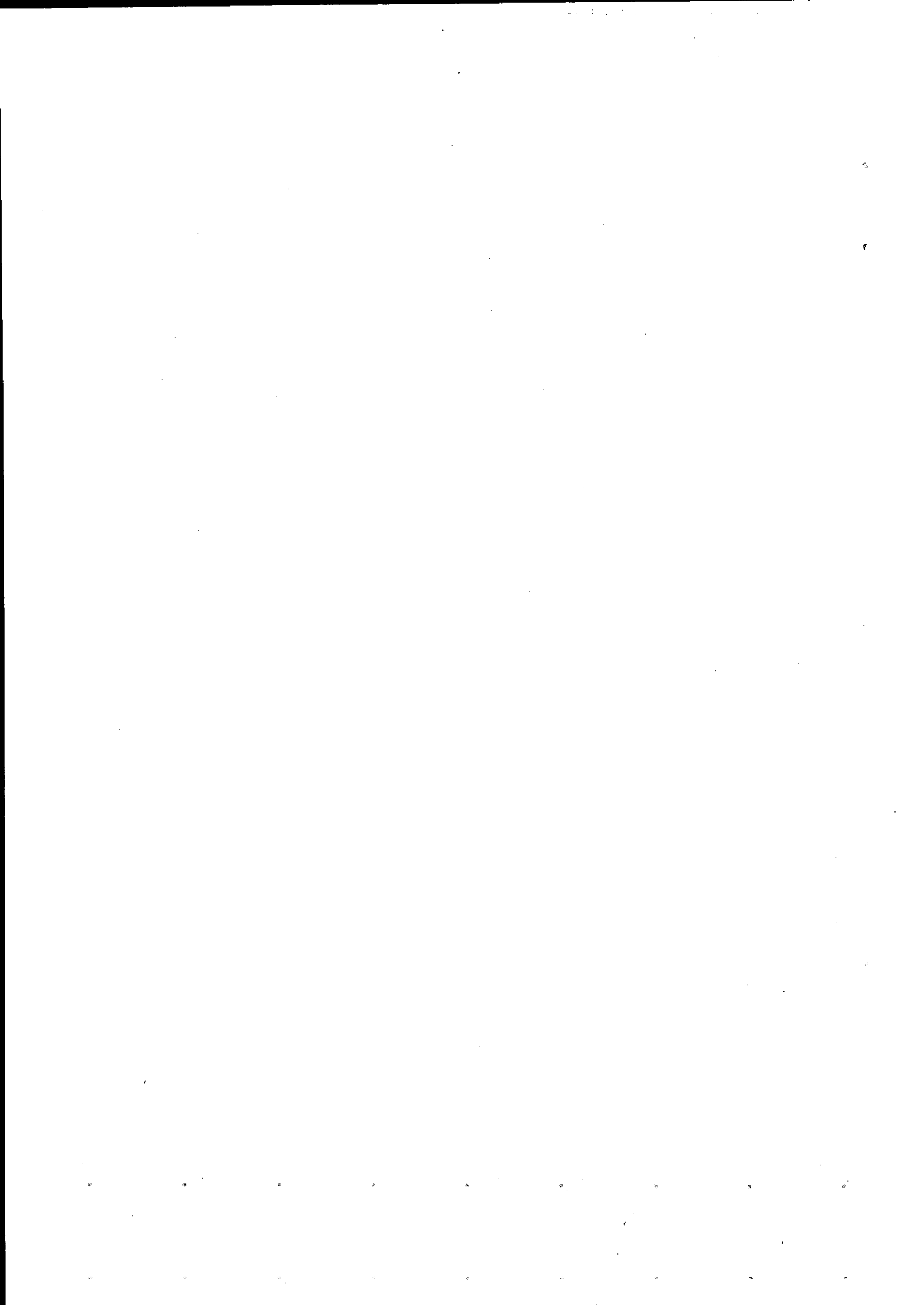
Calculated (A and B) and experimental profiles (C and D) of nitrate, ammonium, nitrifying germs and nitrifying activities as a function of the distance to the sea for February (A and C) and July 1976 (B and D)

Table 1  
 $\alpha$  and k values used in the simulation

Month	k	$\alpha$
	$10^{-6} \text{ s}^{-1}$	$10^{-6} \mu\text{M NH}_4^+/\text{bact.}$
February 1976	25	3
July 1976	7.5	0.74

#### References.

- BELSER, L.W., (1979). Population ecology of nitrifying bacteria, *Ann. Rev. Microbiol.*, **33**, 309-333.
- BERNER, R.A., (1971). *Principles of chemical sedimentology*, Mc Graw Hill, New York, 240 pp.
- BILLEN, G., (1975). Nitrification in the Scheldt estuary (Belgium and The Netherlands), *Est. Coast. Mar. Sci.*, **3**, 79-89.
- GARRELS, R.M. and CHRIST, C.L., (1965). *Solution, minerals and equilibria*, Harper & Row, New York.
- NIHOUL, J.C.J. and RONDAY, F.C., (1976). *Modèle d'un estuaire partiellement stratifié. Application à la circulation résiduelle et à l'étude de l'envasement de l'Escaut*, in *Modèle mathématique de la mer du Nord. Rapport de synthèse. Estuaire de l'Escaut*, vol. 10, J.C.J. Nihoul and R. Wollast (Eds.), Brussels.
- SOMVILLE, M., (1978). A method for the measurement of nitrification rates in water, *Wat. Res.*, **12**, 843-848.
- SOMVILLE, M., (1980). *Etude écophysiological des métabolismes bactériens dans l'estuaire de l'Escaut*, Thèse de doctorat, Faculté des Sciences, Université Libre de Bruxelles.
- SOMVILLE, M. and DE PAUW, N., (1982). Influence of temperature and river discharge on water quality of the Western Scheldt estuary, *Wat. Res.*, in press.
- TATE, R.L., (1977). Nitrification in histosols: a potential role for heterotrophic nitrifier, *Appl. Environm. Microbiol.*, **34**, 911-914.
- WOLLAST, R., (1973). *Origine et mécanisme de l'envasement de l'estuaire de l'Escaut. Rapport de synthèse. Recherches effectuées dans le cadre de l'étude de l'envasement de l'Escaut dirigée par le Laboratoire de Recherches hydrauliques de Borgerhout*, Ministère des Travaux publics.



Achévé d'imprimer le 20 avril 1983  
pour le compte de la  
Programmation de la Politique scientifique  
sur la presse offset d'é.t.a.b.é.t.y.p.  
à La Salle, B-4108 NEUPRÉ  
Tél.: (0)41/715810

D/1982/1191/8

